Technische Universität München
TUM School of Life Sciences

A porcine model of pancreatic ductal adenocarcinoma

Daniela Christine Kalla

Vollständiger Abdruck der von der TUM School of Life Sciences der Technischen Universität München zur Erlangung einer

Doktorin der Naturwissenschaften (Dr. rer. nat.)

genehmigten Dissertation.

Vorsitz: Prof. Dr. Benjamin Schusser

Prüfende der Dissertation:

1. Prof. Angelika Schnieke, Ph.D.
2. Prof. Dr. Friederike Ebner

Die Dissertation wurde am 19.09.2023 bei der Technischen Universität München eingereicht und durch die TUM School of Life Sciences am 06.05.2024 angenommen.

Table of contents

Abstract

Pancreatic ductal adenocarcinoma (PDAC) is a devastating disease characterised by late diagnosis and a very poor prognosis. Due to rising incidence rates, methods for early detection and progress in therapeutic interventions are urgently needed. As pigs exhibit many similarities to humans in anatomy and physiology, they represent a suitable translational model to complement the preclinical data gained from mouse studies and can thus advance the development of new detection and treatment strategies.

Therefore, this project focused on the generation of a porcine model for PDAC that recapitulates the human disease phenotype. Based on the murine PDAC model, the Chair of Livestock Biotechnology has generated pigs carrying latent *KRAS*^{G12D} and *TP53*^{R167H} mutations, equivalent to the most common mutations found in PDAC patients. In this work, different strategies were assessed to activate these mutations in the porcine pancreas. The first strategy focused on CRISPR/Cas9-mediated integration of the improved Cre (iCre) recombinase gene at the 5'end or 3'end of the porcine endogenous pancreas associated transcription factor 1a (*PTF1A*) gene locus followed by somatic cell nuclear transfer (SCNT) to generate gene edited pigs. The second approach used the piggyBac transposon system to generate transgenic pigs expressing iCre under the control of the murine pancreatic and duodenal homeobox 1 (*mPdx1*) promoter.

All three Cre driver lines successfully expressed iCre recombinase in a tissue-specific manner as shown by immune-histology and after cross breeding with dual fluorescent Cre reporter pigs. Up to now these are the only available organ-specific Cre-lines. Breeding them with pigs carrying the latent *KRAS*^{G12D} and *TP53*^{R167H} mutations resulted in efficient mutational activation. This in turn induced pancreatic abnormalities ranging from preneoplastic lesions to invasive PDAC. Severity and timeline depended on the presence or absence of mutant *TP53*.

PDAC is characterised by an accumulation of genetic alterations. As at the outset of the project the timeline for PDAC development in the pig was unknown, a method was established to enhance the mutational load if required, e.g. by multiplexed gene editing for simultaneous inactivation of the main tumour suppressor genes known from human PDAC. This multiplex CRISPR/Cas9 editing system was based on a polycistronic tRNA-gRNA (PTG) construct and accomplished high editing efficiencies in porcine cells, regardless of the position of the respective gRNA in the tRNA-gRNA array. To assess the tumour induction capacity of edited cells, autologous transplants were carried out.

The last part of this work describes the generation of a porcine *in vitro* model for acinar-to-ductal metaplasia (ADM), the earliest precursor lesion in human PDAC. Therefore, a protocol for the isolation and cultivation of pancreatic acinar cells was established. Different approaches for activating *KRAS*^{G12D} and *TP53*^{R167H} mutations were assessed. The best results were obtained for transduction with a Cre lentivirus. For transdifferentiation, different cytokines were evaluated. Both TGF-α and lL-17A were equally efficient in inducing ADM. This now enables species comparison of early neoplastic events *in vitro*.

In summary, this work supported the development of the first spontaneous swine model for PDAC, a most devastating disease, with no options for early diagnosis. For molecular and therapeutic assessments an ADM culture system was established. Finally, the multiplex editing tool enables efficient inactivation of multiple tumour suppressor genes and can be used to induce not only pancreatic but also other types of cancer.

Zusammenfassung

Das duktale Adenokarzinom des Pankreas (PDAC) ist eine verheerende Erkrankung, welche durch eine späte Diagnose und eine sehr schlechte Prognose gekennzeichnet ist. Aufgrund der steigenden Inzidenzraten sind Methoden zur Früherkennung und Fortschritte bei den therapeutischen Interventionen dringend erforderlich. Da Schweine in Anatomie und Physiologie viele Ähnlichkeiten mit dem Menschen aufweisen, stellen sie ein geeignetes translationales Modell dar, um die aus Mausstudien gewonnenen präklinischen Daten zu ergänzen und so die Entwicklung neuer Detektions- und Behandlungsstrategien voranzutreiben.

Daher konzentrierte sich dieses Projekt auf die Generierung eines Schweinemodells für PDAC, welches den menschlichen Krankheitsphänotyp rekapituliert. In Anlehnung an das murine PDAC-Modell, hat der Lehrstuhl für Biotechnologie der Nutztiere Schweine generiert, welche latente *KRAS*^{G12D}- und *TP53*^{R167H}-Mutationen tragen, die am häufigsten vorkommenden Mutationen bei PDAC-Patienten. In dieser Arbeit wurden verschiedene Strategien zur Aktivierung dieser Mutationen im porzinen Pankreas verfolgt. Die erste Strategie konzentrierte sich auf die CRISPR/Cas9-vermittelte Integration des verbesserten Cre (iCre)-Rekombinasegens am 5'- oder 3'-Ende des endogenen Pankreas-assoziierten Transkriptionsfaktor 1a (*PTF1A*) Genlokus des Schweins, gefolgt von somatischem Zellkerntransfer (SCNT), um gen-editierte Schweine zu erzeugen. Beim zweiten Ansatz wurde das PiggyBac-Transposon-System verwendet, um transgene Schweine zu generieren, die iCre unter der Kontrolle des murinen Pankreas- und Duodenal-Homeobox 1 (*mPdx1*)-Promotors exprimieren.

Alle drei Cre-Treiberlinien exprimierten die iCre-Rekombinase erfolgreich und gewebespezifisch, wie immunhistologisch und nach Kreuzung mit zweifach fluoreszierenden Cre-Reporter-Schweinen nachgewiesen werden konnte. Bislang sind dies die einzigen verfügbaren organspezifischen Cre-Linien. Ihre Verpaarung mit Schweinen, die die latenten Mutationen *KRAS*^{G12D} und *TP53*^{R167H} trugen, führte zu einer effizienten Mutationsaktivierung. Dies wiederum führte zu Anomalien der Bauchspeicheldrüse, die von präneoplastischen Läsionen bis hin zu invasivem PDAC reichten. Der Schweregrad und der zeitliche Ablauf hingen vom Vorhandensein oder Fehlen der *TP53*-Mutation ab.

PDAC ist durch eine Akkumulation von genetischen Veränderungen charakterisiert. Da zu Beginn des Projekts der zeitliche Ablauf der PDAC-Entwicklung beim Schwein nicht bekannt war, wurde eine Methode entwickelt, mit der die Mutationslast bei Bedarf erhöht werden kann, z. B. durch Multiplex-Gen-Editing zur gleichzeitigen Inaktivierung der wichtigsten Tumorsuppressorgene, die vom menschlichen PDAC bekannt sind. Dieses Multiplex-Gen-Editing-System basierte auf einem polyzistronischen tRNA-gRNA (PTG)-Konstrukt und erreichte hohe Editierungseffizienzen in porzinen Zellen, unabhängig von der Position der jeweiligen gRNA im tRNA-gRNA Array. Um die Tumorinduktionsfähigkeit der editierten Zellen zu beurteilen, wurden autologe Transplantationen durchgeführt.

Der letzte Teil dieser Arbeit beschreibt die Generierung eines porzinen *in vitro*-Modells für die azino-duktale Metaplasie (ADM), die früheste Vorläuferläsion bei menschlichem PDAC. Hierfür wurde ein Protokoll für die Isolierung und Kultivierung von Azinuszellen der Bauchspeicheldrüse etabliert. Es wurden verschiedene Ansätze zur Aktivierung von $KRAS^{G12D}$- und $TP53^{R167H}$-Mutationen bewertet. Die besten Ergebnisse wurden bei der Transduktion mit einem Cre-Lentivirus erzielt. Für die Transdifferenzierung wurden verschiedene Zytokine untersucht. Sowohl TGF-α als auch IL-17A waren bei der Induktion von ADM gleich effizient. Dies ermöglicht nun einen Artenvergleich der frühen neoplastischen Ereignisse *in vitro*.

Zusammenfassend lässt sich sagen, dass diese Arbeit die Entwicklung des ersten spontanen Schweinemodells für PDAC unterstützt hat, einer äußerst verheerenden Krankheit, für die es keine Möglichkeiten der Frühdiagnose gibt. Für molekulare und therapeutische Bewertungen wurde ein ADM-Kultursystem etabliert. Schließlich ermöglicht das Multiplex-Editing-Tool eine effiziente Inaktivierung mehrerer Tumorsuppressorgene und kann nicht nur für die Induktion von Bauchspeicheldrüsenkrebs, sondern auch bei anderen Krebsarten eingesetzt werden.

1 Introduction

The continually increasing human life expectancy and its resulting longevity are associated with rising expectations regarding health and well-being, drawing attention to age-related diseases including disorders of the circulatory system, diabetes and cancer [1].
In Germany, cardiovascular diseases (CVD) and cancer represent the major causes of death, with more than 340,619 and 229,068 deaths in 2021, respectively (Figure 1) [2].

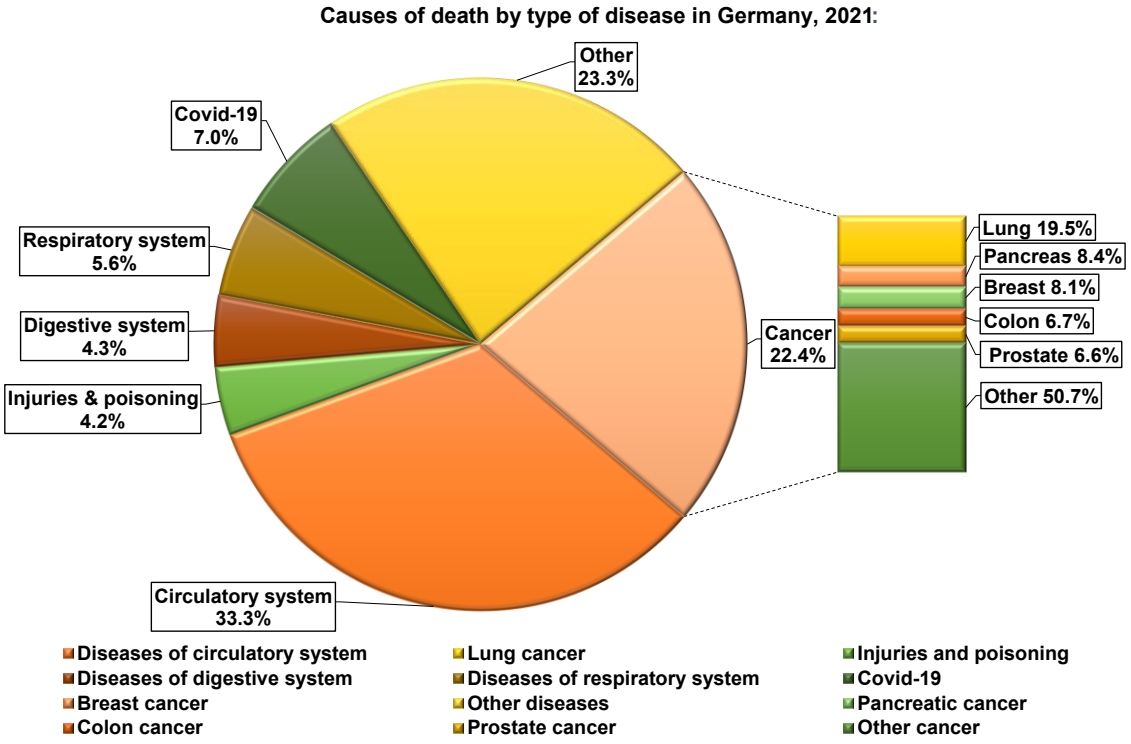

Figure 1. Causes of deaths in Germany in 2021. Illustration adapted from Statistisches Bundesamt (Destatis) [2, 3].

Over the past decades, CVD mortality rates have decreased significantly in Europe and the United States [4-6], due to improved prevention and treatment strategies [7]. In contrast, the number of newly approved cancer drugs between 2000 and 2015 was the lowest when compared to other diseases [8, 9]. Global cancer incidence has strongly increased [10], resulting in death rates superseding those of heart disease in some countries or states [11, 12]. Lung, breast, colon, and prostate cancer represent the four most common cancer types worldwide [13]. Although pancreatic cancer is one of the less frequently diagnosed cancers, it ranks worldwide as the 7th most common cause of cancer-related deaths with highest incidence in well-developed countries [14].

It is already the 4th leading cause of cancer deaths in Europe and the United States [15-18], and due to increasing incidence rates [19, 20], it is expected to become the 2nd by 2030 [21, 22]. In fact, pancreatic cancer has overtaken breast cancer and became the 2nd leading cause of cancer-related deaths in Germany in 2021 [3] (Figure 1).

1.1 Pancreatic cancer

1.1.1 The pancreas

The adult pancreas is a 12-25 cm long retroperitoneal organ located behind the stomach in the upper part of the abdomen. It has an elongated flattened J-form and can be divided into four parts: head, neck, body, and tail [23]. The head of the pancreas surrounds the superior mesenteric artery and vein and lies in the inner curve of the duodenum, while the pancreas tail extends to the spleen [24].

The pancreas can be further divided into an exocrine and endocrine portion. The exocrine part accounts for more than 80% of the pancreas mass and plays an important role in digestion by secreting digestive enzymes (e.g. proteases, lipases and amylases), water and sodium bicarbonate into the duodenum [25]. In order to protect the exocrine pancreatic cells from self-digestion, many of these enzymes such as trypsin, carboxypeptidase and elastase, are secreted as zymogens and are later activated in the duodenum [26].

Acinar cells are arranged in grape-like cell clusters called acini and constitute the functional unit of the exocrine pancreas. These cells produce, store and secrete the digestive enzymes into intercalated ducts, which then flow via intralobular ducts into the main pancreatic duct of Wirsung. In the pancreas head, the latter unites with the end of the common bile duct forming the hepatopancreatic duct, the so-called ampulla of Vater, which regulates the entry of bile and pancreatic juices into the duodenum and prevents duodenal reflux [27, 28]. This connection of gall bladder and pancreas explains why gall stones obstructing the biliary duct can trigger acute pancreatitis, while cancer located in the pancreas head often blocks the intrapancreatic part of the bile duct and causes jaundice [29, 30].

The endocrine part of the pancreas only accounts for a small percentage of the total pancreas mass and consists of the islets of Langerhans that are scattered among the exocrine structures [31]. Five cell types can be found in the islets of Langerhans: α-, β-, δ-, ε- and PP-cells [32]. These cells release hormones, such as insulin, glucagon, or somatostatin, into the blood stream in response to nutritional, neuronal or hormonal stimuli [33]. The well-known insulin-producing β-cells form the majority of the islet cell population, with more than 50% prevalence [34, 35]. Together with glucagon-producing α-cells, they regulate glucose homeostasis and their loss or dysfunction is thus involved in type 1 and 2 diabetes [36-38].

1.1.2 Types of pancreatic cancer

Pancreatic cancer development is associated with risk factors such as obesity, smoking and alcohol consumption, but also with familial predisposition, age, diabetes and chronic pancreatitis, the latter often caused by severe alcohol abuse [39]. The vast majority of cancers found in the pancreas develop from the exocrine part. Pancreatic ductal adenocarcinoma (PDAC) is the most common exocrine malignancy and accounts for more than 90% of all pancreatic cancers [40]. Since understanding of PDAC development is crucial in the fight against pancreatic cancer, this cancer type is discussed in detail in section 1.1.3.

Besides PDAC, other tumour types can also be found in the exocrine pancreas. Pancreatic acinar cell carcinoma (PACC) is a very rare disease, accounting for only 1% of all pancreatic cancers [41]. This cancer develops from acinar cells and is characterised by hypersecretion of digestive enzymes such as lipase, which can lead to clinical syndromes [42]. In the past, there have been case reports that PACC also occurs in children and adolescents [43-45]. Despite its relatively high malignancy, PACC has shown to be associated with higher survival rates than PDAC, especially for younger patients [46-49].

Other exocrine tumours are pancreatoblastoma and solid pseudopapillary neoplasms. Pancreatoblastoma is a malignant and heterogenous tumour that is often of embryonic origin and thus belongs to the most common pancreatic cancers in children between 1-10 years [50, 51]. This cancer is suspected to develop from persisting foetal origins of acinar cells and is usually found later as a slowly growing mass on the pancreas head [52]. In adults, pancreatoblastoma is very uncommon and associated with worse prognosis than in children [53].

Solid pseudopapillary neoplasm (SPN) is a tumour with unknown origin, primarily affecting young women between 20-30 years [54, 55]. The tumour is usually of low malignancy and grows as an encapsulated mass, thus favouring a good prognosis after surgical resection [56].

Less than 5% of all pancreatic cancers develop from endocrine tissue [57]. These pancreatic neuroendocrine tumours (PNETs) can be benign and tend to be slow growing [58, 59], but can also have malignant potential. Depending on their ability to produce hormones and cause clinical syndromes, PNETs can be divided into functional or non-functional tumours [60]. Functional PNETs are characterised by an increased release of hormones, such as insulin, gastrin or glucagon, leading to hormonal hypersecretion syndromes [61]. Insulinomas arising from β-cells are the most common form of functional PNETs, and their excessive insulin secretion results in hypoglycaemia, which can be a life-threatening condition if left untreated [62]. In contrast, non-functional PNETs are not associated with clinical syndromes as they do not produce hormones, secrete them in small quantities, or produce peptides not causing any symptoms [63]. These tumours are more common than functional PNETs, but due to their unspecific symptomatology they are often only diagnosed by accident or at advanced stage.

1.1.3 Pancreatic ductal adenocarcinoma

PDAC is one of the most malignant solid cancers and is associated with a very high mortality and an overall five-year survival rate of only 9% [64]. This poor prognosis is attributable to numerous characteristics of the disease. For example, patients are usually asymptomatic at disease onset with symptoms such as weight loss, abdominal pain and jaundice mostly occurring in late stages. In addition, PDAC progresses rapidly from low T1- to high T4-stage within only 14 months [65]. As a result, up to 80% of the patients are diagnosed with locally advanced or metastatic tumours that are unresectable [66, 67]. In the past, successful treatment of such locally advanced tumours have been reported using a combination of surgery and chemotherapy [68], however, these cases are rather rare. Another feature of PDAC tumours is their generally high intra-tumoral heterogeneity and plasticity, which promote drug-resistance and therefore make most conventional therapies ineffective [69-71].

PDAC mostly occurs in the head of the pancreas and can arise from five different pre-invasive precursor lesions: pancreatic intraepithelial neoplasia (PanIN), intraductal papillary mucinous neoplasm (IPMN), mucinous cystic neoplasm (MCN), intraductal tubulopapillary neoplasm (ITPN), and intraductal oncocytic papillary neoplasm (IOPN) [72]. Thereof, IPMNs, MCNs and IOPNs are macroscopic mucin-producing cystic lesions that are grossly visible (>1cm) [72].

Of all cystic lesions, IPMNs are the most common and develop, like IOPNs, in the pancreatic ductal system. IPMNs are characterised by papillary growth of neoplastic epithelium lining the main pancreatic duct or its branches, and its mucin production and intraluminal growth can result in duct dilatation [73, 74].

In contrast, MCNs are rare solitary lesions that usually grow large with no connection to the pancreatic duct and are mostly found in women [75, 76].

The macroscopic ITPN is a tubule-forming solid nodular mass that is hard to distinguish from IPMNs due to its intraductal appearance, but is mostly non-cystic with absent mucin production [77, 78].

PanINs are the most common precursors found in PDAC patients [79]. In contrast to the above mentioned lesions, PanINs are usually smaller than 0.5 cm and cannot be detected with conventional imaging methods [80]. These microscopic neoplastic lesions are suggested to arise from proliferating duct epithelium [81], however, the cell type of origin is still controversial and is discussed further in section 1.1.4.

The progression of PanINs to PDAC can be divided into three grades of increasing atypia, dysplasia and cytoarchitectural changes (Figure 2). PanIN-1 stage is characterised as flat (-1A) or papillary (-1B) lesion consisting of columnar epithelium with mucin production and basally located nuclei. In contrast, PanIN-2 lesions are mainly papillary showing nuclear abnormalities such as enlargement, crowding, pseudostratification, and loss of polarity.

Advanced PanIN-3 lesions, formerly called carcinoma *in situ*, are defined by serious nuclear atypia, mitotic abnormalities and budding of epithelial cell clusters into the ductal lumen. Although being non-invasive, PanIN-3 lesions are only rarely observed when cancer is absent. [82-84]

Besides cellular changes, the progression of PanINs to invasive PDAC is also associated with an accumulation of genetic alterations. As more than 90% of all PDAC tumours are sporadic, the most common somatic gene changes are addressed below. Mutation of the proto-oncogene kirsten rat sarcoma viral oncogene homologue (*KRAS*) is found in more than 90% of PDAC patients and is considered to be the main driver of PanIN formation [85] (Figure 2).

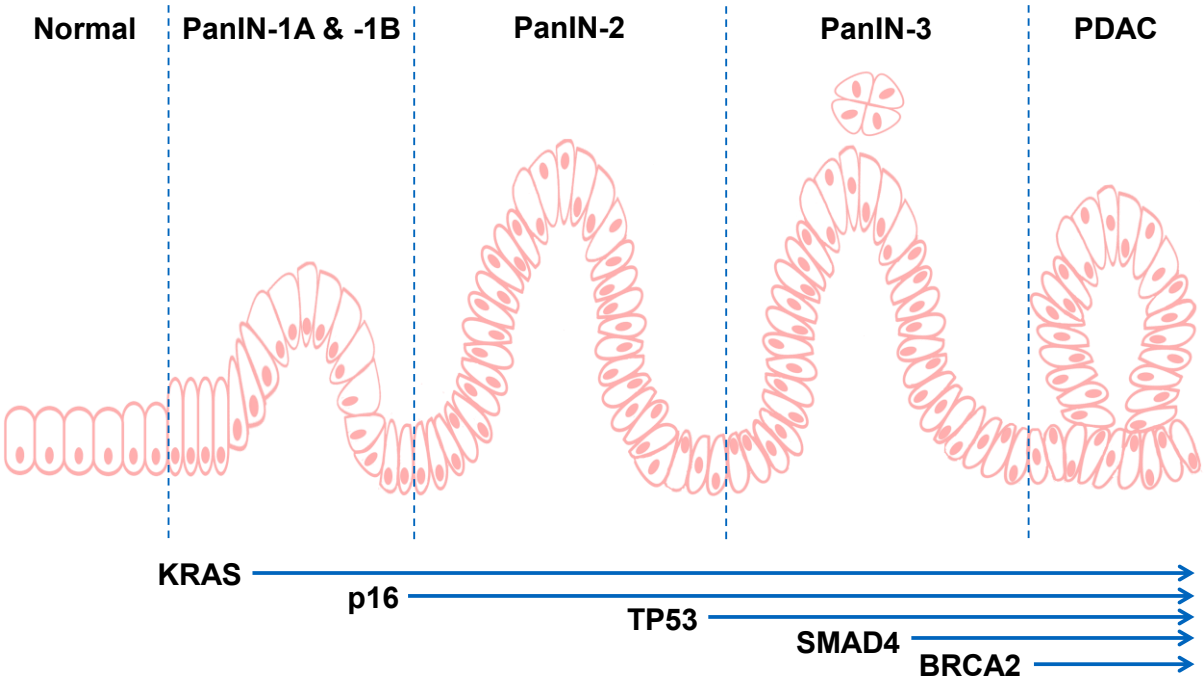

Figure 2. Progression of PanINs to PDAC. The progression of PDAC is accompanied by an accumulation of genetic alterations. Activating mutation of *KRAS* is sufficient to initiate PanIN formation. Further development into PDAC is accompanied by mutation of tumour suppressor genes, such as *p16*, *TP53*, *SMAD4* and *BRCA2*. Illustration adapted from Hruban et al. (2000) and Murtaugh (2013) [86, 87].

KRAS is a small 21 kDa GTPase that functions as molecular switch in signal transduction by cycling between a GTP-bound active and GDP-bound inactive state [88] (Figure 3). Regulation of KRAS activity is based on nucleotide exchange mediated by guanine nucleotide exchange-factors (GEFs) and GTPase-activating proteins (GAPs) which promote conversion to the active and inactive conformation, respectively [89]. *KRAS* mutations in PDAC affect codons 12, 13 and 61, with a G to D amino acid substitution at codon 12 (G12D) being the most prominent [90, 91]. Oncogenic mutations of KRAS affect its intrinsic GTPase activity and impair binding of GAPs, resulting in reduced GTP hydrolysis [92]. This continuously active form of KRAS leads to persistent activation of downstream signalling pathways, thus promoting tumour growth (Figure 3).

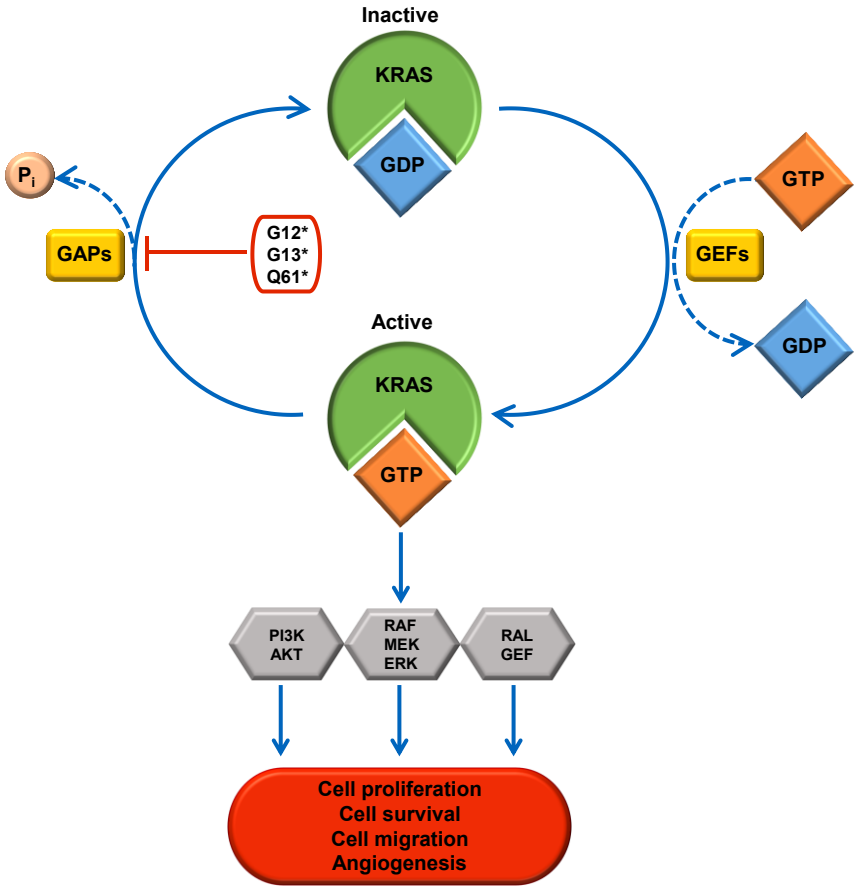

Figure 3. The KRAS cycle and its role in cancer development. KRAS activity is tightly regulated. GEFs promote the exchange of GDP by GTP and lead to conversion of KRAS to the active GTP-bound state mediating downstream effector signalling. Afterwards, signalling is switched off via GTP-hydrolysis and reversion of KRAS to its inactive GDP-bound form. Oncogenic mutations affecting codons 12, 13 and 61 impair GTP hydrolysis and result in continuously activated downstream signalling, that can lead to cell transformation. Illustration adapted from Vatansever et al. (2019) [92].

Apart from *KRAS*, most mutations found in PDAC affect tumour suppressors, with inactivation of cyclin-dependent kinase inhibitor 2A (*CDKN2A*) as earliest event following *KRAS* mutation. Loss of CDKN2A is detected in more than 90% of all PDAC tumours and is caused by intragenic mutation, homozygous deletion or epigenetic silencing [93, 94], mostly occurring at intermediate PanIN stage [95]. Due to an alternative reading frame, the *CDKN2A* locus encodes two proteins, $p16^{INK4A}$ and $p14^{ARF}$, both acting as tumour suppressors in different anti-cancer signalling pathways [96]. P14 prevents degradation of TP53 by inhibiting E3 ubiquitin ligases such as Mdm2, and therefore stabilizes TP53 activity [97]. In contrast, p16 preserves the tumour-suppressive retinoblastoma protein (Rb) pathway. It binds to cyclin-dependent kinases 4 and 6 preventing their complex formation with cyclin D and Rb phosphorylation [98]. Thus, Rb remains hypo-phosphorylated and associated with E2F resulting in G1/S transition blockade and cell cycle arrest [99]. In PDAC, *CDKN2A* mutation mainly affects p16 rather than p14 and is associated with uncontrolled cell proliferation and progression to high-grade PanIN-stage [57].

Tumour protein p53 (TP53) is the most frequently mutated gene in human cancers [100], and is mutated in more than 70% of all PDAC cases [90]. It is a transcription factor (TF) that plays a crucial role in maintaining genome integrity, also known as 'guardian of the genome'. TP53 is activated by cellular stress such as DNA damage, hypoxia and oncogene activation and in response leads to cell cycle arrest, DNA repair, senescence or apoptosis [101]. This cell response is initiated by binding of TP53 as a homo-tetramer to the response elements of its downstream target genes [102]. In PDAC, mutations of *TP53* mainly arise in high-grade PanINs and usually occur as missense mutations in the DNA binding domain with mutational hotspots at codons 175, 248, 273 and 282 [103-105]. As a result, binding and expression of TP53-regulated target genes is impaired and leads to survival of cells with damaged DNA and uncontrolled proliferation.

Inactivation of SMAD family member 4 (*SMAD4*), also called Mothers against decapentaplegic homolog 4, or deletion in pancreatic carcinoma locus 4 (*DPC4*), is detected in more than half of PDAC tumours and is often caused by homozygous deletions or an intragenic mutation followed by loss of the second allele (LOH) [106-109]. The TF SMAD4 is essential for signal transduction in the transforming growth factor beta (TGF-β) signalling pathway [110]. Upon binding of TGF-β to the cell surface receptor, SMAD2/3 are phosphorylated and form a complex with SMAD4 which then translocates into the nucleus where it interacts with other cofactors to regulate transcription of TGF-β target genes [111]. SMAD4-dependent TGF-β signalling mediates cell cycle arrest and apoptosis via expression of cyclin-dependent kinase (CDK) inhibitors and pro-apoptotic factors [112]. In PDAC, loss of SMAD4 occurs mainly in high-grade PanINs or invasive carcinoma and results in loss of growth inhibition [113, 114]. Interestingly, while TGF-β signalling is suppressive in early tumourigenesis, it can promote epithelial-mesenchymal transition (EMT), tumour invasion and metastasis in advanced cancer [115]. For example, if SMAD4 is lost, EMT can take place via SMAD4-independent pathways such as PI3K/Akt/mTOR [116]. However, the presence of intact SMAD4 in pancreatic tumours is suggested to promote EMT and tumour growth, thus highlighting the controversial role of SMAD4 in PDAC disease [117].

Mutations of the tumour suppressive breast cancer (*BRCA*) pathway are found in less than 10% of all PDAC tumours and are mainly of germline rather than somatic origin, with *BRCA2* being more frequently affected than *BRCA1* or *PALB2* (partner and localizer of BRCA2) [90]. BRCA1/2 and PALB2 play an essential role in DNA break repair by homologous recombination and their germline mutation is associated with the hereditary breast and ovarian cancer syndrome [118, 119], but also with an increased risk of developing pancreatic cancer [120, 121]. PDAC tumours harbouring mutations in such DNA maintenance genes have shown to be genomically instable with high numbers of structural variations [122].

BRCA1/2 are mostly inactivated by deletion followed by LOH [123], where it is assumed that the wild type allele in germline *BRCA2* mutation carriers is lost in high-grade PanIN stage [124]. Familial PDAC is also related to other germline mutations affecting cell cycle control and DNA repair genes such as *TP53* and its pathway members ATM Serine/Threonine Kinase (*ATM*) and checkpoint kinase 2 (*CHEK2*), as well as *CDKN2A-p16* [125]. Germline mutations in *TP53* and *CDKN2A* are associated with cancer predisposition disorders such as Li-Fraumeni and familial atypical multiple mole melanoma syndrome (FAMMM) and leads to an increased risk for PDAC development, with up to 60% for *CDKN2A* mutation carriers [126, 127].

1.1.4 Acinar-to-ductal metaplasia

Due to its ductal morphology, PDAC was initially thought to derive from epithelial cells lining the pancreatic duct. However, the cell type of origin is still controversial and recent evidence suggests that PDAC originates from pancreatic acinar cells that undergo a transdifferentiation process towards a ductal-like phenotype, called acinar-to-ductal metaplasia (ADM). In detail, this conversion involves dedifferentiation of acinar cells towards a progenitor-like state followed by transdifferentiation, and is characterised by a loss of acinar cell identity with concomitant increase of ductal marker expression [128]. It has been shown that PDAC can originate from both acinar and ductal cells, but acinar-derived PDAC develops via PanINs while ductal-derived PDAC mainly emerges in a PanIN-independent manner [129, 130]. Indeed, ADM has been shown to be a precursor of PanIN lesions in $KRAS^{G12D}$ mutant mice [131, 132]. However, besides oncogene expression, the development of acinar-derived PDAC in adult mice additionally required an inflammatory environment [133, 134].

Due to the above mentioned acinar plasticity, ADM also plays an important role in exocrine pancreas regeneration upon injury or chronic inflammation [135]. Chronic pancreatitis is a recognized risk factor for PDAC and certain pro- and anti-inflammatory cytokines, such as tumor necrosis factor (TNF), interleukins or TGFs, are known to be increased in PDAC initiation and progression [136]. In this context, the role of ADM in pancreatic tumourigenesis was first shown in transgenic mice in which acinar overexpression of TGF-α gave rise to metaplasia, pseudoductular structures and malignant pancreatic tumours with ductal phenotype [137, 138]. The establishment of 3D *in vitro* cultures from murine acinar cell clusters provided further insights into the development and progression of ADM including the interplay of KRAS hyperactivation, inflammation, oxidative stress, and increased epidermal growth factor (EGFR) signalling [139, 140].

In human acinar cells, ADM was shown to be induced *in vitro* by TGF-β1 in a SMAD-dependent manner, leading to the assumption that SMAD4 is crucial at disease onset while being lost at high-grade PanIN stage [141]. TGF-β1-induced ADM was characterised by the formation of duct-like spheres, an appearance that could be enhanced by oncogenic *KRAS* signalling [141].

This sphere formation is characteristic for ADM and can also be observed in TGF-α treated murine acinar explant cultures [142, 143]. Consistent with the findings from mouse experiments, ADM formation in human acinar cells was accompanied by a decrease of acinar cell markers, e.g. amylase alpha 2B *(AMY2B)* or pancreas associated transcription factor 1a (*PTF1A*), and increased expression of ductal markers such as cytokeratin 19 (*CK19*) or SRY-Box transcription Factor 9 (*SOX9*) [141]. Indeed, downregulation of *PTF1A* has been detected in human and murine PanIN lesions and its restoration reversed early pancreatic tumourigenesis in mice [144, 145], supporting the assumption of ADM being a precursor of PanIN lesions.

1.2 *PTF1A* locus

The *PTF1A* locus consists of two exons located in reverse orientation on chromosome 10 in pigs and in forward orientation on chromosomes 2 and 10 in mouse and human, respectively, and is highly conserved among these species [146-148] (Table 1).

Table 1. Similarity of porcine PTF1A in comparison to human and mouse [149].

Species	Porcine PTF1A nucleotide identity	Porcine PTF1A amino acid identity
Homo sapiens	85%	93%
Mus musculus	84%	88%

PTF1A is a 48kDa basic helix-loop-helix (bHLH) protein that acts as a DNA binding subunit of the trimeric PTF1 transcription factor complex and is therefore often referred to as PTF1-p48 [150]. In early murine embryogenesis, Ptf1a is expressed from day E9.5 in all progenitors of exocrine and endocrine cells in the pancreatic buds arising from foregut endoderm [151]. Ptf1a expression was shown to be regulated by three transcriptional domains comprising a ~2 kb distal 5'-enhancer, a proximal promoter region spanning more than 13 kb and a ~12 kb downstream 3'-control region, with the last two being more important for neural tube rather than pancreas development [152]. The 5'-enhancer is highly conserved and contains two bipartite binding sites for the trimeric PTF1 complex, each consisting of an E box and TC box motif separated by a helical DNA turn [152]. Following its first expression, Ptf1a forms a dimer with a class A bHLH protein (e.g. HEB) and joins the mammalian recombining binding protein suppressor of hairless (RBP-J) resulting in the trimeric PTF1-J transcription factor complex [153], which then binds to the 5'-enhancer of Ptf1a to autoregulate its own transcription and drive pancreatic development [152]. In this early embryogenesis, Ptf1a acts as an indispensable regulator of pancreatic cell fate and its inactivation has been shown to result in reversion of pancreatic progenitors towards duodenal fate in mice [154].

Thus, biallelic knockout led to a lethal condition of *Ptf1a*$^{-/-}$ mice, which lacked the exocrine pancreas and showed misallocation of endocrine cells [155]. Besides its crucial role in pancreatic development, *PTF1A* expression has also been shown to be essential for brainstem and cerebellum neurogenesis [156, 157].

Later in the mature pancreas, *PTF1A* expression becomes restricted to acinar cells and RBP-J is replaced by its paralogue RBP-L leading to the composition of the PTF1-L complex, which binds to the promoters of digestive enzymes, such as elastase or amylase, driving their high-level expression [152, 153, 158]. PTF1A also maintains acinar cell differentiation and homeostasis and its inactivation in adults can result in cellular stress and acinar cell apoptosis [159, 160]. As already described above, loss of *PTF1A* expression is associated with ADM, a progenitor state of PDAC. In this regard, Jakubison has shown that induced *PTF1A* expression in PDAC cell lines decreased their tumorigenic potential [161], which coincides with the previous findings of Krah et al. mentioned in section 1.1.4 [144, 145].

1.3 Mouse models for PDAC

Animal models represent an essential part of preclinical research as they enable a better understanding of human diseases. So far, biomedical research is mainly dominated by mice, due to their ease of husbandry, breeding and genetic modification. Especially in cancer research, genetically engineered mouse models (GEMMs) are an essential prerequisite to investigate disease development and treatment strategies.

Hingorani et al. have generated the first mouse model that fully recapitulates the features of human PDAC, thus defining the genetic requirements for disease development and progression. According to the most common mutation found in humans, they carried out targeted insertion of the oncogenic *Kras*^{G12D} mutation into the endogenous murine *Kras* gene. To avoid ubiquitous expression, *Kras*^{G12D} was silenced by a preceding lox-stop-lox (LSL) cassette and activated in pancreatic progenitor cells by interbreeding these *Kras*$^{LSLG12D/WT}$ animals with mice expressing Cre recombinase under the control of the pancreas-specific gene promoters pancreatic and duodenal homeobox 1 (*Pdx1*) or *Ptf1a*. Indeed, pancreatic expression of *Kras*^{G12D} was sufficient to initiate the formation of PanIN lesions, which then spontaneously developed into PDAC at low frequency. [162]

By including *Trp53*^{R172H}, an orthologue of human *TP53*^{R175H}, the group further showed that mutation of *Trp53* promotes the progression of *Kras*^{G12D} induced PanIN lesions towards cancer [163]. Triple genetically modified *Kras*$^{LSLG12D/WT}$*Trp53*$^{LSLR172H/WT}$*Pdx1-Cre* mice developed metastatic PDAC with severely shortened survival of ~5 months and replicated the human disease phenotype including sites of metastasis, genomic instability and high degree of heterogeneity [163].

As mentioned in chapter 1.1.3, inactivation of the tumour suppressor CDKN2A is the earliest event following *KRAS* mutation in human PDAC development. As with the mutation of tumour suppressor *Trp53*, deletion of Cdkn2a in *KRAS*^{G12D} mice also promotes the development of PDAC from preinvasive lesions. However, these *Kras*$^{LSLG12D/WT}$*Cdkn2a*$^{lox/lox}$*Pdx1-Cre* mice developed highly aggressive tumours that directly invaded other organs, such as duodenum and spleen [164]. As a consequence, these mice died at 11 weeks of age and therefore did not show the pronounced metastasis to liver and lung that is usually found in humans and *Kras*$^{LSLG12D/WT}$*Trp53*$^{LSLR172H/WT}$*Pdx1-Cre* mice [163, 164].

1.4 Pig models for PDAC

Despite the valuable insights that mice have provided in the past, their application in disease modelling is also associated with disadvantages. They show substantial differences to humans, e.g. in size, lifespan, organ anatomy, and immune responses [165-167]. In addition, their use in cancer research is limited, as murine cells are easier to immortalize than human cells and expression of human oncogenes sometimes fails to replicate the human disease phenotype in mice [168-170].

Therefore, non-rodent models are urgently needed to complement the preclinical data gained from mouse experiments and thus enhance their predictive value. Compared to other large animals such as dogs or non-human primates, pigs raise fewer ethical concerns as they have been domesticated as food animals for centuries [171]. Indeed, pigs represent a suitable translational model as they share many similarities with humans in body and organ size, physiology and drug metabolism [172-174]. Their long lifespan of 12-15 years enables the implementation of longitudinal studies to follow disease progression and evaluate imaging and treatment strategies [175].

In the past, pigs were engineered to model different types of cancer, such as osteosarcoma or colorectal cancer [176]. Based on the findings obtained from the above-mentioned mouse models, attempts were also made to generate PDAC in pigs. According to the mice of Hingorani et al., Schnieke and colleagues generated pigs carrying latent *KRAS*^{G12D} and *TP53*^{R167H} mutations (orthologue of human *TP53*^{R175H}) in exon 2 and 5 of their endogenous genes, respectively [177, 178]. Since these mutations are also silenced by an upstream LSL cassette, activation can be achieved by pancreas-specific Cre recombination using the pancreatic promoters *PTF1A* and *Pdx1*, which is part of this dissertation.

In contrast to these endogenous mutations, Schook et al. randomly introduced Cre-inducible *KRAS*^{G12D} and *TP53*^{R167H} mutations into the porcine genome and induced tumour formation by subcutaneous and intramuscular injection of Cre recombinase encoded by adenovirus (AdCre) [179]. AdCre delivery into the pancreatic main duct from these pigs resulted in tumours that were similar to human PDAC, but also showed neuroendocrine regions [180].

Besides, Berthelsen and colleagues generated a porcine model for PDAC which overexpresses an oncogene cassette consisting of *KRAS*^{G12D}, *c-MYC* (cellular myelocytomatosis) and *SV40LT* (Simian virus 40 large T antigen) [181]. None of the generated piglets survived long but the utilized murine *Pdx1* promoter (*mPdx1*) initiated oncogene expression early during embryogenesis and led to the formation of proliferative acinar hyperplastic foci at day 45 after birth [181].

1.5 Generation of genetically modified pigs

The era of generating genetically modified animals began with the development of pronuclear microinjection. This technique describes the injection of a transgenic DNA construct into the pronucleus of a fertilized oocyte followed by embryo transfer into a surrogate mother (Figure 4). First established in mice [182], pronuclear microinjection was soon expanded to larger animals and led to the generation of transgenic rabbits, sheep and pigs [183]. This relatively straightforward procedure was used for many years, but is far from ideal. Particularly with regard to livestock, the proportion of transgenic offspring obtained is very low, at only 1-5%, and the generation of excess non-transgenic animals is undesirable both ethically and in terms of expense [184]. In addition, pronuclear microinjection enables only random integration of the transgene into the host genome, which can damage the function of endogenous genes. Integration into host regulatory regions or heterochromatin can result in position effects, which in turn lead to substantially variable transgene expression levels and patterns among different animals [185]. Another drawback of microinjection is mosaicism, which is caused by delayed integration of the transgene and can also lead to differing expression profiles. In addition, the use of porcine oocytes is problematic as they are characterised by a high lipid content, which makes their pronuclei poorly visible and requires centrifugation prior to microinjection [186]. Therefore, recent attempts of generating transgenic pigs are based on cytoplasmic instead of pronuclear microinjection. This technique has been successfully used for the generation of simple porcine knockout models, e.g. by injection of the CRISPR/Cas9 system [187, 188]. However, especially with regard to transgene integration, this method is less efficient and associated with the same disadvantages mentioned above.

The drawbacks of microinjection prompted the search for a more efficient method of generating genetically modified mammals. In mice, the discovery of embryonic stem cells (ES cells), which are easily manipulated by gene targeting and subsequently populate the germline, led to the rapid production of a variety of genetically modified mouse lines [189-191]. In contrast, despite numerous efforts, the isolation and cultivation of functional ES cells from livestock species was so far unsuccessful [192]. This led to the development of somatic cell nuclear transfer (SCNT) as a suitable alternative for the generation of modified farm animals.

SCNT describes the transfer of a nucleus from a diploid somatic cell, that can be cultured and modified *in vitro*, into an enucleated metaphase II arrested (MII) oocyte. Following electrofusion and oocyte activation, the developing embryo is transferred into a surrogate mother and thus enables the generation of cloned animals with modified genotypes (Figure 4).

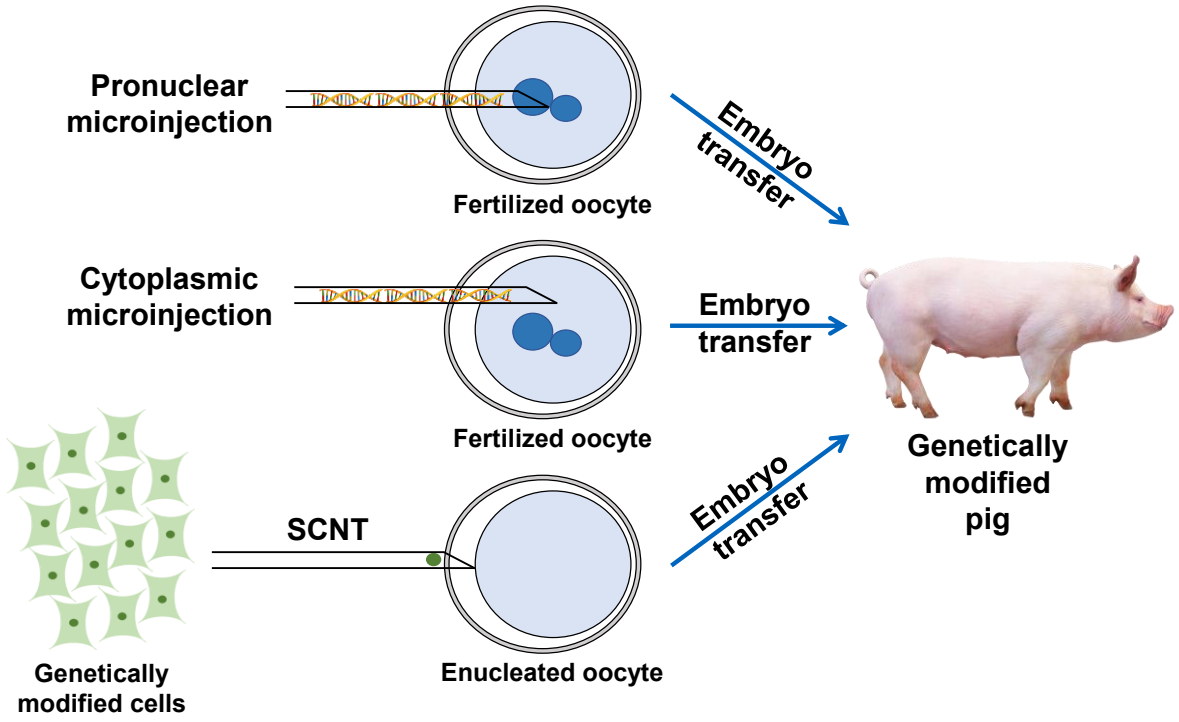

Figure 4. Methods to generate genetically modified pigs. Genetically engineered pigs can be generated in three different ways: pronuclear microinjection, cytoplasmic microinjection and SCNT. Pronuclear and cytoplasmic microinjection result in random integration of the transgene, while the latter is mainly used for gene knockouts via CRISPR/Cas9-mediated genome editing. In contrast, SCNT enables the generation of gene-targeted pigs from somatic cells that have been previously modified and analysed *in vitro*.

Cloning by SCNT was first established in sheep, where the usage of embryonic, foetal and adult cells resulted in viable offspring that were identical to the respective cell donor [193, 194]. Shortly afterwards, the use of genetically modified cells for SCNT led to the generation of the first transgenic sheep produced by random integration and gene targeting [195, 196]. Thus, this technique was soon expanded to other livestock species and gave rise to the first random transgenic and gene-targeted knockout pigs [197, 198].

Compared to microinjection, SCNT has numerous advantages for the production of transgenic pigs. Besides random integration, it also enables precise genetic modification and detailed analysis of the cultured cells prior to SCNT. Furthermore, unlike microinjection, the proportion of transgenic offspring derived from SCNT is virtually 100%. In addition, depending on the choice of the cell donor, the gender of the resulting piglets can be predetermined, which can have substantial advantages for further breeding.

However, despite the many advances it has brought, SCNT is also characterised by numerous drawbacks. Unlike ES cells, primary somatic cells have a relatively short lifespan in culture, which severely limits the time available for genetic modification, selection and characterisation of cell clones.

In addition, homologous recombination (HR) is less frequent in somatic cells when compared to ES cells, which preferentially use HR as repair pathway [199], thus making gene targeting in differentiated cells more difficult. Furthermore, SCNT is technically challenging and marked by a very low cloning efficiency, as the percentage of live-born animals is far below 5% [200, 201]. This is mainly caused by incomplete or inaccurate reprogramming, which often results in abnormalities in the cloned animals and thus leads to high morbidity and mortality rates [202]. In fact, only few lines of healthy and viable genetically modified pigs were generated within the last years.

1.6 Genetic engineering

1.6.1 The Cre-loxP recombination system

In the early 1980s, Sternberg and Hamilton discovered a site-specific recombination machinery in bacteriophage P1, comprising Cre protein (*causes recombination*) and its recognition sequences, the so called loxP sites (*locus of crossing-over in P1*) [203]. This Cre-loxP system was shown to play an important role in P1 life cycle, most likely by cyclization of the linear phage genome upon injection into the host and resolution of dimeric P1 DNA molecules [204, 205].

A DNA sequence flanked by two loxP sites is said to be “floxed” and the 34 bp loxP sites each consist of two 13 bp inverted repeats that are separated by an 8 bp core region [206] (Figure 5A). Cre is a 38 kDa tyrosine recombinase that binds as a monomer to each of those inverted repeats [207, 208]. In the presence of two loxP sites, Cre dimers form a synaptic tetramer which then mediates the site-specific recombination reaction: conserved tyrosine residues from two of the four subunits cleave the DNA leading to the formation of 3’-phosphotyrosine linkages (Figure 5B). The released 5’-hydroxyl groups then perform nucleophilic attack on the partner phosphotyrosine bonds leading to the formation of a Holliday-junction intermediate as a result of the first strand exchange. Afterwards, a second round of cleavage mediated by the other two subunits completes the recombination reaction and yields the recombined DNA products. [209, 210]

The outcome of the recombination reaction depends on the orientation and location of the loxP sites. If located on the same chromosome, equal orientation will result in excision of the floxed DNA sequence, while oppositely directed loxP sites will lead to sequence inversion. In contrast, two loxP sites present on different chromosomes induce translocation of the genomic sequence (Figure 5C).

As excision is accompanied by the loss of one loxP site, this reaction is primarily non-reversible, whereas inversion and translocation can be reversed as long as Cre recombinase is active. However, this reversibility if often undesirable in genome engineering.

Reaction between asymmetric loxP sites, each carrying a mutation in either the left or right inverted repeat, results in the generation of one loxP site with two mutated Cre binding regions and one wild type loxP site, rendering the recombination reaction irreversible [211, 212]. While mutated inverted repeats convey unidirectionality by reducing the binding ability of Cre, mutations in the core region have an impact on the reaction specificity as Cre cleaves the DNA within the spacer sequence [213, 214].
The usage of such heterospecific loxP sites enables efficient insertion of DNA sequences into predefined locations without the integration of plasmid backbone in a mechanism called recombinase-mediated cassette exchange (RMCE) (Figure 5D) [215].

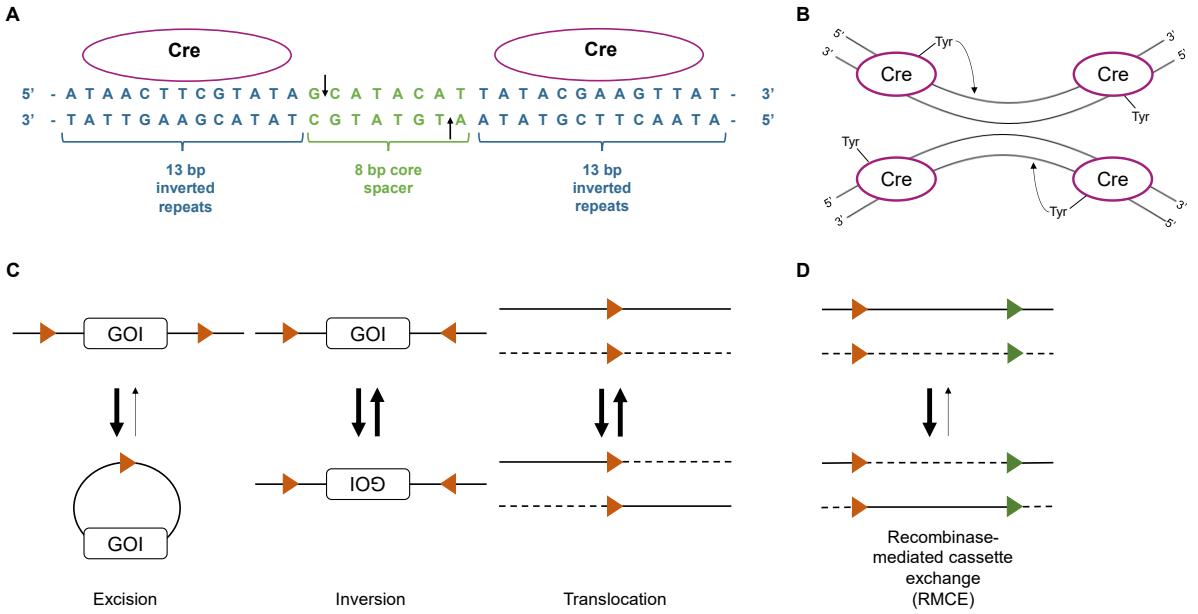

Figure 5. Schematic overview of site-specific Cre-loxP recombination. (A) Binding of Cre dimer to the inverted repeats of one loxP site. Cleavage occurs in the core spacer region at the positions indicated by arrows. (B) Nucleophilic attack by conserved Tyr-324 residues results in strand cleavage and 3'-phosphotyrosine linkage formation and presents the first step in the Cre-loxP recombination reaction. (C) The type of recombination reaction is determined by the orientation and location of the loxP sites. (D) RMCE: heterospecific loxP sites allow for integration of desired DNA sequences without plasmid backbone. GOI=Gene of interest. Illustration adapted from Guo et al. (1997) and Bouhassira et al. (1997) [209, 215].

The Cre-loxP system has been optimised for targeted modification of mammals and led to the development of numerous GEMMs. Of these, many are conditional models that locally and temporally restrict the recombination reaction and thus enable tissue-specific modification of genes, which are crucial for development. This spatiotemporality is achieved by using tissue-specific promoters in combination with inducible systems to drive Cre protein expression.

A well-known inducible system is based on the fusion of Cre recombinase to the binding domain of the human oestrogen receptor (Cre-ER^T). Due to a mutation, this ligand binding domain (LBD) responds to synthetic ligands such as tamoxifen or 4-hydroxytamoxifen (4-OHT) but is unresponsive to endogenous oestrogen [216, 217]. In the absence of tamoxifen, Cre-ER^T is bound to heat shock protein 90 (HSP90) and remains in the cytoplasm. Upon administration and binding of tamoxifen, HSP90 dissociates from the complex and Cre-ER^T translocates into the nucleus where it executes recombination between the loxP sites [218]. In order to reduce side effects of tamoxifen treatment, the Cre-ER^T system was replaced by the Cre-ER^{T2} system, which carries a triple-mutant of LBD and has up to 10-fold higher sensitivity for 4-OHT when compared to Cre-ER^T [219, 220].

Another inducible system relies on the tetracycline (Tet) resistance operon from *Escherichia coli* (*E.coli*) and is available as Tet-On and Tet-Off variant regulating Cre expression upon doxycycline (Dox) administration. More specifically, the Tet-Off system consists of a Tet-Repressor fused to the VP16-activator protein from *herpes simplex virus*, resulting in the formation of the tetracycline transactivator (tTa). In the absence of Dox, tTa binds to the Tet-operon and drives Cre expression, while administration of Dox inhibits this binding and prevents expression. In contrast, the Tet-On system uses a reversed transactivator (rtTa), which leads to Cre expression in the presence of Dox, whereas Tet-operon binding and Cre activation is inhibited when Dox is absent. [218, 221, 222]

Efficient expression of Cre recombinase is crucial for the successful generation of animal models. However, as Cre recombinase originates from bacteriophage, it is characterised by prokaryotic codon usage which can affect expression in eukaryotes. Application of mammalian codon usage with reduction of the high CpG-content resulted in an improved Cre (iCre) recombinase which enables efficient expression in mammals and reduces the risk of epigenetic silencing [223].

1.6.2 Transposon systems

Transposable elements (TEs) were first described in 1950 by Barbara McClintock, after she discovered a variegation of pigmentation in maize [224]. These elements, also known as “jumping genes”, are repetitive DNA sequences that can move within the genome and can be found in every organism [225]. In humans, up to 45% of the genome was shown to be derived from TEs [226].

Depending on their mode of transposition, TEs can be divided in two classes (Figure 6). Class I transposons move in a replicative manner, via reverse transcription of an RNA intermediate of themselves, also known as “copy and paste”-mechanism [227]. As they encode their own reverse transcriptase, they are also called retrotransposons and can be further classified by the presence or absence of flanking long terminal repeats (LTRs).

LTR-Retrotransposons are usually 5-7 kb long and possess genes which have a high equivalence to *gag* and *pol* from retrovirus [228]. They are able to form non-infectious virus-like particles which in turn perform replicative transposition in the genome within a cell [226].

Non-LTR retrotransposons consist of two main groups, composed *of long* and *short interspersed nucleotide elements* (LINEs and SINEs), respectively [229]. LINEs represent the most common TEs in the human genome and have a length of ~6 kb harbouring a 5'-untranslated region (UTR) containing their own promoter followed by two open reading frames (ORFs) and 3'UTR [226, 229]. LINEs encode their own RNA-binding protein, endonuclease and reverse transcriptase, and amplify in the genome by reimport of their mRNA into the nucleus as ribonucleoprotein particles (RNPs) followed by reverse transcription and integration [230, 231]. Unlike the above-mentioned TEs, SINEs are very short (100-500 bp) and possess an RNA-polymerase III promoter [232]. In addition, they are non-protein coding and thus non-autonomous, requiring the endonuclease and reverse transcriptase function from LINEs for propagation within the genome [233].

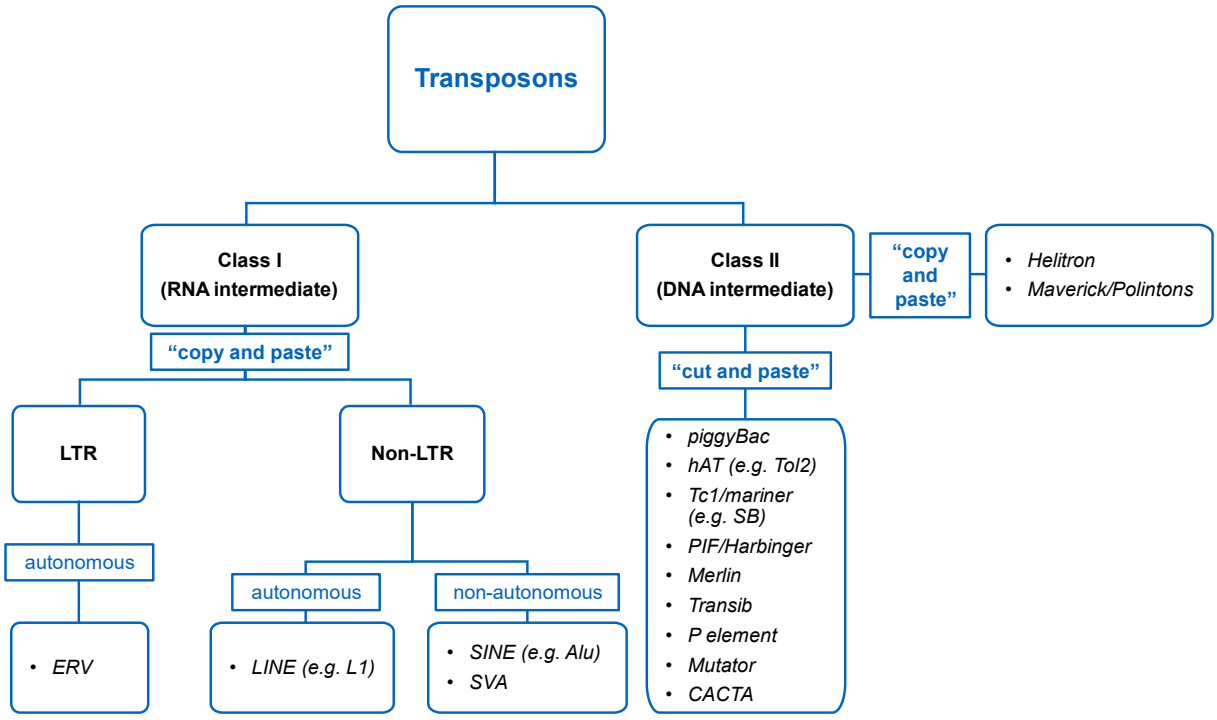

Figure 6. Eukaryotic transposon systems. Illustration adapted from Finnegan (2012) and Feschotte & Pritham (2007) [228, 234].

Class II transposons account for 3% of the human genome [226]. They encode a transposase gene which is flanked by two inverted terminal repeats (ITRs). Upon expression, the transposase binds to these ITRs and performs excision and reinsertion of the intervening DNA into another site of the genome [227].

The last step is performed on a staggered DNA break at the new genomic location and successful integration results in duplication of the target site sequence [235] (Figure 7). Therefore, unlike their class I counterparts, class II TEs move in a non-replicative “cut and paste”-mechanism through a DNA intermediate and are thus called DNA transposons [225].

Eukaryotic DNA transposons comprise several families which can be distinguished, for example, by the sequence of their ITRs or target site duplication, with *piggyBac*, *hAT* and *Tc1/mariner* being the most commonly used DNA transposons for genetic engineering [225]. A small subgroup of DNA transposons is formed by *Helitron* and *Maverick/Polintons*, which move in a replicative manner via single strand cleavage [236]. Although not using the "cut and paste”-mechanism for movement, they still belong to class II transposons due to the absence of an RNA intermediate.

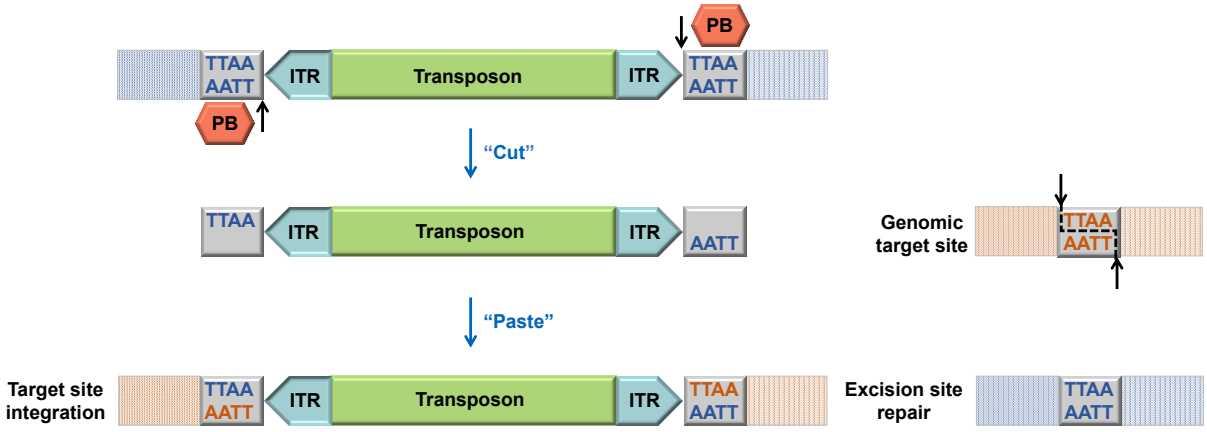

Figure 7. Mechanism of piggyBac-mediated DNA transposition. Most DNA transposons function in a “cut and paste” mechanism: PB-Transposase binds to its recognition sequences at the end of the flanking ITRs and generates DNA nicks to release the intervening sequence. The excised transposon is then integrated into a staggered DNA break at the new genomic location which harbours the TTAA recognition sequence. This mechanism leads to target site duplication. Illustration adapted from Woodard & Wilson (2015) and Kim & Pyykko (2011) [237, 238].

Based on the simplicity of their “cut and paste”-mechanism, DNA transposons have become a widely used tool for non-viral gene delivery. For this purpose, the gene of interest (GOI) is flanked by ITRs and transferred simultaneously with the transposase into the cell. Transmission can be performed in *cis* or *trans*, with transposon and transposase located on the same plasmid or separately from each other [239]. As already mentioned above, *piggyBac* (PB), *Sleeping Beauty* (SB) from *Tc1/mariner* and *Tol2* from *hAT* are the most commonly used transposon systems for gene delivery. They all differ in origin, cargo size capacity and transposition efficiency and have been subject to numerous optimizations in the past, such as the generation of hyperactive transposase variants [240, 241].

The SB transposon belongs to the *Tc1/mariner* superfamily and has been artificially constructed using phylogenetic information from salmonid fish [242]. It performs efficient integration into TA-sites within the genome and has found successful application in the generation of transgenic mammalian models and in gene therapy studies [243, 244]. However, it has been shown that SB transposition efficiency decreases by 50% for cargo size > 6 kb and that high transposase concentrations result in a phenomenon called overproduction inhibition (OPI) [245].

PB was identified in cabbage looper moth (*Trichoplusia ni*), as a naturally active transposon that integrates specifically into genomic TTAA-sites [246, 247] (Figure 7). The PB transposon system owns a higher cargo capacity compared to SB and even movements of transgenes larger than 100 kb have been reported [248]. In addition, it is less sensitive to OPI in the presence of higher transposase concentrations [249]. Therefore, the PB system has been used for numerous scientific applications, such as for the generation of transgenic mice and induced pluripotent stem (iPS) cells or for the modification of T cells [250-252].

Tol2 was identified in the genome of *Oryzias latipes*, the Japanese rice fish, and belongs to the *hAT* family of transposons [253]. It is commonly used for studies in zebrafish (*Danio rerio*) [254-256], but also works successfully in human and murine cells [257, 258]. Like PB, *Tol2* is also characterised by a high cargo capacity and low sensitivity to OPI, but shows however less efficient transposition in human cells [249, 259, 260].

1.6.3 CRISPR/Cas9 systems

For a long time, gene targeting was the method of choice for targeted integration of transgenes and mutations. However, due to the absence of ES cells in mammals other than mice, this classical approach is less efficient as it solely relies on homologous recombination, an event that occurs only rarely in mammalian somatic cells [261, 262].

The development of artificial nucleases enabled the introduction of targeted DNA double-strand breaks (DSBs) and thus opened the era of precise genome editing. Such nucleases can be classified into three groups: Zinc Finger Nucleases (ZFNs), Transcription Activator-like Effector Nucleases (TALENs) and Clustered Regularly Interspaced Short Palindromic Repeats (CRISPR) with their CRISPR-associated protein 9 (Cas9).

In eukaryotes, nuclease-induced genomic DSBs are mainly repaired by two distinct mechanisms: non-homologous end joining (NHEJ) and homology-directed repair (HDR) (Figure 8) [263]. NHEJ describes the direct ligation of both DSB ends without the need for a DNA template [264]. Rejoining is mediated by the DNA-dependent protein kinase (DNA-PK) complex, which consists of the DNA-PK catalytic subunit (DNA-PK_{CS}) and the proteins Ku70 and Ku80 that form the Ku heterodimer [265].

Binding of Ku70/80 to the DSB leads to recruitment and activation of DNA-PK_{CS}, which in turn promotes binding of nuclease, polymerase and ligase to fulfil the joining reaction [266]. NHEJ-mediated repair is highly efficient, but also error-prone and often leads to the introduction of insertion or deletion mutations (InDels), which can result in a shift of the reading frame and thus in the generation of premature stop codons [263]. Therefore, this pathway is often employed for inactivation of particular genes.

In contrast, HDR enables error-free DSB repair for which it requires an homologous template, either provided by the sister chromatid or by an exogenous DNA sequence. During HDR, the ends of the DSB are shortened towards 3'-overhangs, followed by BRCA1/2- and PALB2-assisted binding of recombinase RAD51 which performs strand invasion of the homologous sequence that serves as a template for DNA synthesis [267]. As a result, an exogenous DNA sequence can be used to insert specific mutations or sequences into desired genomic locations. Nevertheless, upon DSB, NHEJ is more frequent than HDR, as it is active throughout the cell cycle while HDR is mainly restricted to S/G2 phase, when sister chromatids are available [268].

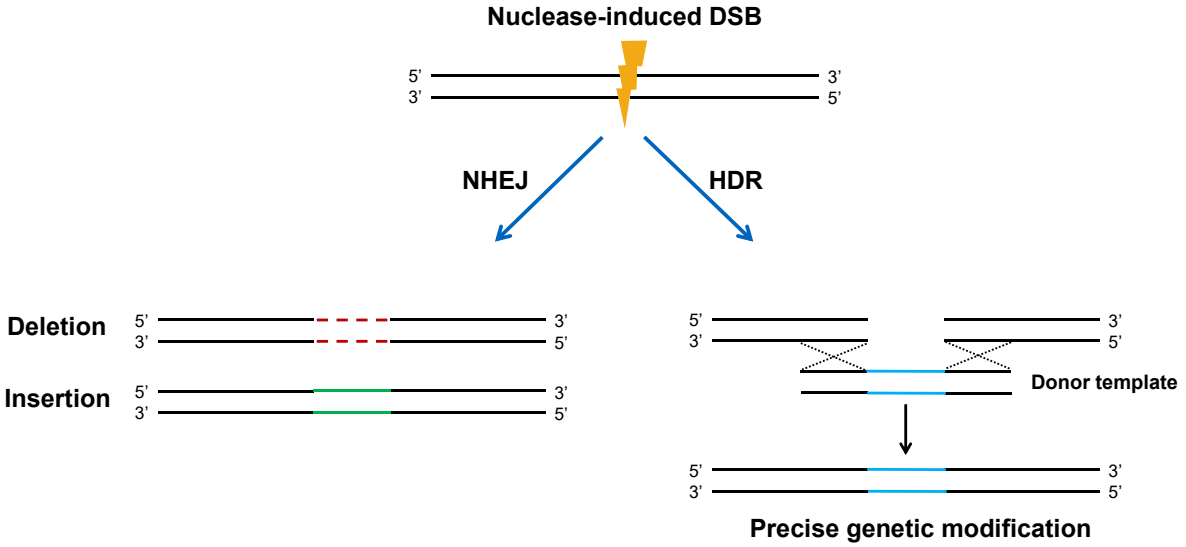

Figure 8. DSB-repair in eukaryotes. Eukaryotic cells use two distinct mechanisms for DSB-repair: NHEJ and HDR. NHEJ is an error-prone mechanism which leads to the introduction of InDel mutations. In contrast, HDR relies on homologous recombination with a donor template and can be used to insert specific sequences or point mutations. Illustration adapted from Sander & Joung (2014) [263].

Genome editing was initially based on ZFNs and TALENs. They consist of engineered DNA-binding motifs fused to the cleavage domain of FokI restriction enzyme and bind to the genomic target region as a protein pair, resulting in dimerization of FokI and generation of a DSB [269]. However, the generation of ZFNs and TALENs is labour- and cost-intensive and the discovery of CRISPR/Cas9 soon provided a faster and more efficient system for genome editing.

The CRISPR/Cas system was originally identified as an adaptable immune system in bacteria and archaea. This defence system integrates stretches of invading DNA, e.g. from plasmids or viruses, between CRISPR repeats [270]. Upon repeated infection, the transcripts of these spacer sequences help the Cas proteins to recognize and cleave the foreign DNA, thus leading to host immunity [271]. The type II CRISPR/Cas9 system from *Streptococcus pyogenes* represents the most studied tool for genome editing.

In this system, transcription of the repeat-spacer unit yields the precursor CRISPR RNA (pre-crRNA), which is then bound by transactivating crRNA (tracrRNA) that mediates crRNA maturation by recruiting RNaseIII [272]. Afterwards, the tracrRNA-crRNA duplex directs Cas9 to the target site, whereby site-specific recognition is determined by a ~20 bp crRNA encoded guide RNA (gRNA) sequence, which binds complementary to the foreign DNA [273]. However, DNA cleavage occurs only in the presence of a protospacer adjacent motif (PAM), that consists of a 5'-NGG-3' sequence and lies immediately downstream of the DNA target site [274]. The RNA-guided endonuclease Cas9 consists of two nuclease domains: HNH and RuvC. These domains cleave the DNA by generating site-specific nicks on the complementary and noncomplementary target strand, respectively, and thus generate a blunt-ended DSB 3-4 bp upstream of PAM [274] (Figure 9).

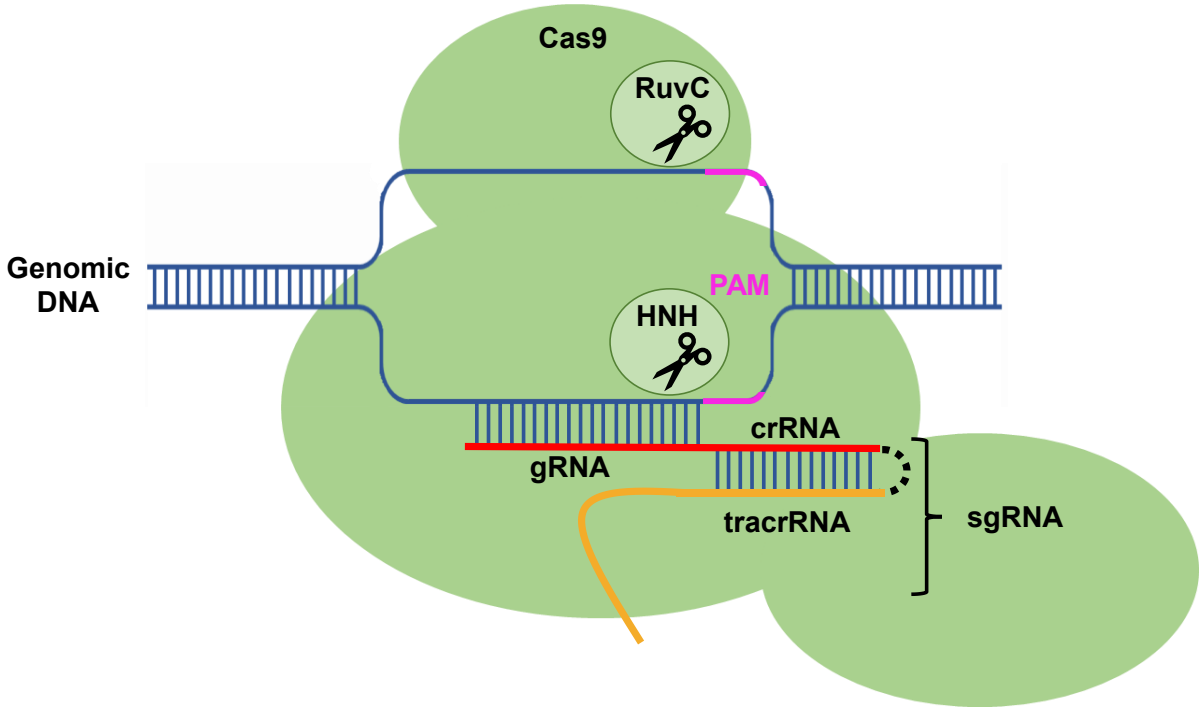

Figure 9. Overview of Cas9-mediated DNA cleavage for genome editing. The gRNA directs Cas9 to the complementary target sequence in the genome which is followed by PAM. The two nuclease domains of Cas9, HNH and RuvC, cleave the double-stranded DNA 3-4 bp upstream of the PAM sequence, leading to a DSB that can be repaired by either NHEJ or HDR. Illustration adapted from Redman et al. (2016) [275].

Based on these findings, the CRISPR/Cas9 system was optimized for its use in targeted genome editing. Fusion of the crRNA 3'-end with the 5'-part of the tracrRNA led to the generation of a single chimeric RNA, called single gRNA (sgRNA), which imitates the secondary structure of the tracrRNA-crRNA complex and still efficiently guides Cas9 to the genomic target site [273] (Figure 9). This enables the use of CRISPR/Cas9 as a two-component system for targeting any DNA sequence of the 5'-N20-NGG-3' type, only by altering the 20 bp gRNA sequence. Hence, the CRISPR/Cas9 system evolved as a cost-effective and straightforward tool for gene editing, which has found numerous applications in different species, such as mouse, human and pig [276-278].

Due to its ease of use, this system also allows for the simultaneous manipulation of several genes. Multiplexed editing can be achieved, for example, by delivering a polycistronic tRNA-gRNA (PTG) gene that gives rise to one single transcript which is cleaved by endogenous RNases for releasing the individual sgRNAs in the target cell [279] (Figure 10).

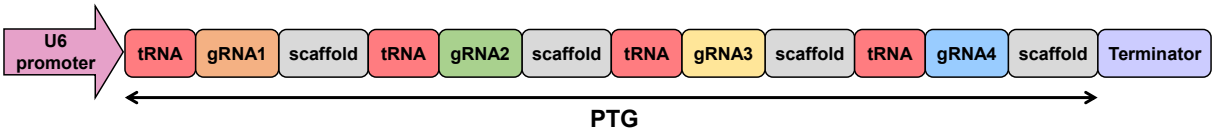

Figure 10. PTG construct for multiplexed genome editing. Illustration adapted from Xie et al. (2015) [279].

Furthermore, different experimental requirements led to the development of several Cas9 variants, such as Cas9 nickase (Cas9n). Cas9n has only one active nuclease domain due to a D10A or H840A mutation in the RuvC or HNH domain, respectively, and thus generates a DNA single-strand break [273]. Application of Cas9n together with two sgRNAs in a "paired nickase" system results in the generation of a DSB with increased reaction specificity and can therefore lead to a reduction of potential off-targets [280].

1.7 Objectives

The overall objective of this work was to generate a porcine model for PDAC, which recapitulates the human disease phenotype. These pigs could then enable the validation and complementation of research findings gained from *in vitro* and mouse studies and thus serve as a translational model for preclinical studies with high predictive value.

The established *KRAS*$^{LSLG12D/WT}$ and *TP53*$^{LSLR167H/WT}$ pigs carry orthologues of the most common mutations found in human PDAC disease. The main goal of this thesis was to activate these mutations in the porcine pancreas by Cre recombination and characterise the aspects of tumour formation. Based on the mouse models from Hingorani et al., the remit of this project was to generate pigs that express Cre recombinase under the control of the murine *Pdx1* (*mPdx1*) and porcine *PTF1A* promoter. If successful, the next aim would then be the characterisation of the generated Cre-pigs followed by crossbreeding with *KRAS*$^{LSLG12D/WT}$*TP53*$^{LSLR167H/WT}$ pigs and analysis of their progeny.

Besides *KRAS* and *TP53* mutations, PDAC is also characterised by an accumulation of other genetic changes. Therefore, another objective was to establish and test a PTG construct for *KRAS*^{G12D} and *TP53*^{R167H} activation and multiplexed CRISPR/Cas9-mediated gene editing of the porcine tumour suppressor genes (TSGs) *TP53*, *p16*, *SMAD4* and *BRCA2* and the porcine class I major histocompatibility subunit Beta-2-microglobulin (B2M) in pig cells. If successfully modified, the tumour induction capacity of these cells should be validated by transplantation.

As ADM is suggested to be the earliest precursor of human PDAC, a final aim was to establish the isolation and culture of porcine pancreatic acinar cells in order to model ADM *in vitro*. Upon successful establishment of the porcine *in vitro* ADM model, methods of mutational activation and the influence of different cytokines on the transdifferentiation rate should be investigated.

2 Materials and methods

2.1 Materials

2.1.1 Chemicals

Table 2. Chemicals.

Chemical type	Source
Acetic acid ($C_2H_4O_2$)	AppliChem, Darmstadt, GER
Agarose	Sigma-Aldrich, Steinheim, GER
Boric acid (H_3BO_3)	AppliChem, Darmstadt, GER
Bovine serum albumin (BSA) Fraction V	Roche Diagnostics, Mannheim, GER
Chloroform ($CHCl_3$)	AppliChem, Darmstadt, GER
Citric acid ($C_6H_8O_7$)	Sigma-Aldrich, Steinheim, GER
Deoxynucleotide (dNTP) solution mix	New England Biolabs, Frankfurt, GER
Disodium hydrogen phosphate heptahydrate (Na_2HPO_4 x $7H_2O$)	Sigma-Aldrich, Steinheim, GER
Droplet generation oil for probes	Bio-Rad Laboratories, Hercules, CA, USA
EDTA	Sigma-Aldrich, Steinheim, GER
Eosin solution	Waldeck GmbH, Münster, GER
Ethanol absolute (EtOH)	VWR International GmbH, Ismaning, GER
Ethanol denatured (EtOH)	CLN GmbH, Niederhummel, GER
Formaldehyde solution (37%) (CH_2O)	AppliChem, Darmstadt, GER
Gel loading dye purple (6x)	New England Biolabs, Frankfurt, GER
Goat serum	Sigma-Aldrich, Steinheim, GER
Hem alum solution acid (Hematoxylin)	Carl Roth, Karlsruhe, GER
Hydrochloric acid (37%) (HCl)	Sigma-Aldrich, Steinheim, GER
Hydrogen peroxide (30%) (H_2O_2)	Riedel-de Haen, Seelze, GER
Magnesium chloride hexahydrate ($MgCl_2$ x6 H_2O)	Carl Roth, Karlsruhe, GER
Mayer's Hemalum solution, acidic	Carl Roth, Karlsruhe, GER
Methanol (CH_3OH)	Sigma-Aldrich, Steinheim, GER
Paraplast	Carl Roth, Karlsruhe, GER
peqGreen DNA/RNA Dye	Peqlab Biotechnologie, Erlangen, GER
Phenol:Chloroform:Isoamyl alcohol (25:24:1)	AppliChem, Darmstadt, GER
Potassium chloride (KCl)	Carl Roth, Karlsruhe, GER
Potassium dihydrogen phosphate (KH_2PO_4)	Carl Roth, Karlsruhe, GER
Propan-2-ol (C_3H_8O)	Thermo Fisher Scientific, Waltham, MA, USA
ROTI® Histol (= xylene substitute)	Carl Roth, Karlsruhe, GER
ROTI® Histokitt	Carl Roth, Karlsruhe, GER
Silicon grease	Kurt Obermeier, Bad Berleburg, GER
Sodium bicarbonate ($NaHCO_3$)	Sigma-Aldrich, Steinheim, GER
Sodium chloride (NaCl)	AppliChem, Darmstadt, GER
Sodium Citrate tribasic dihydrate	Sigma-Aldrich, Steinheim, GER
Sodium dihydrogen phosphate monohydrate (NaH_2PO_4 x H_2O)	Merck, Darmstadt, GER
Sodium dodecyl sulfate (SDS)	Sigma-Aldrich, Steinheim, GER
Sodium hydroxide (NaOH)	Sigma-Aldrich, Steinheim, GER
Sucrose ($C_{12}H_{22}O_{11}$)	Riedel-de Haen, Seelze, GER
Tissue-Tek® O.C.T. Compound	Sakura Finetek Germany, Umkirch, GER
Tris-HCl ($C_4H_{11}NO_3$ x HCl)	Sigma-Aldrich, Steinheim, GER

Tris ultrapure ($C_4H_{11}NO_3$)	AppliChem, Darmstadt, GER
Triton X-100	Sigma-Aldrich, Steinheim, GER
TRIzol Reagent	Ambion, Austin, TX, USA
Tween-20	Sigma-Aldrich, Steinheim, GER
VECTASHIELD® Antifade Mounting Medium with DAPI	Vector Laboratories, Burlingame, CA, USA
(Z)-4-Hydroxytamoxifen (4-OHT)	Sigma-Aldrich, Steinheim, GER

2.1.2 Buffers

Table 3. Buffers.

Buffer type	Ingredients	Quantity
1x PBS (pH=7.2)	NaCl KCl Na_2HPO_4 KH_2PO_4 H_2O	8 g 0.2 g 1.44 g 0.24 g Up to 1 l
1x PBST (pH=7.2)	NaCl KCl Na_2HPO_4 KH_2PO_4 Tween-20 H_2O	8 g 0.2 g 1.44 g 0.24 g 1 ml Up to 1 l
10x PBS (pH=7.4)	NaCl KCl Na_2HPO_4 KH_2PO_4 H_2O	80 g 2 g 14.4 g 2.4 g Up to 1 l
Blocking buffer (2%)	Goat serum PBS	100 µl Up to 5 ml
Cell lysis buffer	1 M Tris 0.5 M EDTA SDS (10%) 5 M NaCl H_2O	2 ml 0.2 ml 0.4 ml 0.8 ml 16.6 ml
0.5 M EDTA (pH=8))	EDTA NaOH H_2O	93.05 g 10 g 400 ml
Low-EDTA-Tris buffer	1 M Tris-HCl 0.5 M EDTA H_2O	0.5 ml 10 µl 49.49 ml
Permeabilization buffer	Goat serum Tween-20 Triton-X-100 PBS	200 µl 10 µl 80 µl Up to 20 ml
Sodium citrate buffer (pH=6)	Sodium citrate $C_6H_8O_7$ Millipore dH_2O	3 g 0.4 g Up to 1 l
TAE (50x)	Tris 0.5 M EDTA $C_2H_4O_2$ H_2O	242 g 100 ml 57.1 ml Up to 1 l

TBE (10x)	Tris H_3BO_3 0.5 M EDTA dH_2O	545 g 275 g 200 ml Up to 5 l
TE buffer	Tris-HCl EDTA H_2O	158 mg 29 mg 100 ml
TTE buffer	Tris Triton X-100 EDTA H_2O	242 mg 1 ml 584 mg 100 ml

2.1.3 Tissue culture reagents

Table 4. Tissue culture reagents.

Reagent	Source
Accutase	Sigma-Aldrich, Steinheim, GER
Ala-Gln (GlutaMax)	Sigma-Aldrich, Steinheim, GER
Amphotericin B	Sigma-Aldrich, Steinheim, GER
Blasticidin S (10 mg/ml)	InvivoGen, San Diego, CA, USA
Bovine pituitary extract (BPE) (2.5 mg/ml)	Corning Inc., Corning, NY, USA
Collagen Type I, Rat tail	Corning Inc., Corning, NY, USA
Collagenase from clostridium histolyticum, Type IA	Sigma-Aldrich, Steinheim, GER
Collagenase from clostridium histolyticum, Type VIII	Sigma-Aldrich, Steinheim, GER
Dulbecco's Modified Eagle Medium (DMEM) - high glucose	Sigma-Aldrich, Steinheim, GER
Dulbecco′s Phosphate Buffered Saline (PBS) (1x)	Sigma-Aldrich, Steinheim, GER
Fetal bovine serum (FBS) superior	Merck, Darmstadt, GER
Geneticin (G418) (50 mg/ml)	Genaxxon bioscience, Ulm, GER
HEPES (1M)	Thermo Fisher Scientific, Waltham, MA, USA
Insulin-Transferrin-Selenium (ITS) (100x)	Gibco
Lipofectamine 2000	Thermo Fisher Scientific, Waltham, MA, USA
McCoy’s 5A medium modified with sodium	Sigma-Aldrich, Steinheim, GER
MEM non-essential amino acid (NEAA) solution (100x)	Sigma-Aldrich, Steinheim, GER
Opti-MEM reduced serum medium	Life Technologies GmbH, Darmstadt, GER
Penicillin-Streptomycin (P/S)	Sigma-Aldrich, Steinheim, GER
Primocin (50 mg/ml)	InvivoGen, San Diego, CA, USA
Puromycin (10 mg/ml)	InvivoGen, San Diego, CA, USA
Recombinant human IL-17A	PeproTech GmbH, Hamburg, GER
Recombinant human TGF-α	PeproTech GmbH, Hamburg, GER
Recombinant human TGF-β1	PeproTech GmbH, Hamburg, GER
Sodium pyruvate solution (100mM)	Sigma-Aldrich, Steinheim, GER
TransDux virus transduction reagent (200x)	System Biosciences, Palo Alto, CA, USA
Trypan blue (0.4%)	Invitrogen, Darmstadt, GER
Trypsin inhibitor from Glycine max (soybean) solution	Sigma-Aldrich, Steinheim, GER

Ulex Europaeus Agglutinin I (UEA I), Fluorescein labelled	Vector Laboratories, Burlingame, CA, USA
Water (H_2O), cell culture grade	Sigma-Aldrich, Steinheim, GER
Waymouth MB 752/1 medium	Sigma-Aldrich, Steinheim, GER

2.1.4 Tissue culture media and solutions

Table 5. Tissue culture media and solutions.

Reagent type	Ingredient	Quantity
Acinar cell culture medium	Waymouth 752/1 medium BSA (10%) Typsin inhibitor Primocin FBS ITS BPE HEPES $NaHCO_3$	23,425 µl 250 µl 250 µl 50 µl 25 µl 250 µl 500 µl 250 µl 65 mg Final: 25 ml
Acinar cell recovery medium	Acinar cell culture medium FBS	3.5 ml 1.5 ml Final: 5 ml
Cell culture medium	DMEM FBS GlutaMax NEAA Sodium pyruvate	500 ml 100 ml 6 ml 6 ml 6 ml Final: 618 ml
PBS+P/S	PBS P/S	500 ml 5 ml Final: 505 ml
Electroporation solution	KCl $MgCl_2$ Na_2HPO_4 NaH_2PO_4	5 mM 10 mM 70 mM 70 mM
Solution 1 (SOL1)	McCoy's 5A medium BSA (10%) P/S Trypsin inhibitor (10 mg/ml)	288 ml 3 ml 3 ml 6 ml Final: 300 ml
Solution 2 (SOL2)	SOL1 Collagenase, Type VIII	30 ml 30 mg Final: 30 ml
Wash solution	SOL1 FBS	70 ml 30 ml Final: 100 ml

2.1.5 Bacterial culture reagents

Table 6. Bacterial culture reagents.

Type	Source
Ampicillin ($C_{16}H_{19}N_3O_4S$)	Carl Roth, Karlsruhe, GER
LB agar, Miller (Luria-Bertani)	Difco BD, Sparks, MD, USA
Luria Broth Base (Miller)	Difco BD, Sparks, MD, USA

2.1.6 Enzymes

Table 7. Enzymes.

Enzyme type	Source
ddPCR™ Supermix for Probes (no dUTP) (2x)	Bio-Rad Laboratories, Hercules, CA, USA
GoTaq® G2 DNA Polymerase 5x Green GoTaq reaction buffer	Promega GmbH, Mannheim, GER
NEBuilder® HiFi DNA Assembly Mastermix	New England Biolabs, Frankfurt, GER
Phire Hot Start II DNA Polymerase 5x Phire reaction buffer	Thermo Fisher Scientific, Waltham, MA, USA
Proteinase K (20 mg/ml)	Macherey-Nagel, Düren, GER
Q5® High-Fidelity DNA Polymerase, 5x Q5 reaction buffer, 5x Q5 high GC enhancer	New England Biolabs, Frankfurt, GER
Restriction endonucleases	New England Biolabs, Frankfurt, GER
Restriction endonuclease buffers: CutSmart® Buffer NEBuffer™ 1.1, NEBuffer™ 2.1, NEBuffer™ 3.1	New England Biolabs, Frankfurt, GER
RNase A	Sigma-Aldrich, Steinheim, GER
T4 DNA ligase T4 DNA ligase buffer (10x)	New England Biolabs, Frankfurt, GER

2.1.7 Antibodies

Table 8. Antibodies.

Name	Utilized dilution for IHC	Source
Cre Recombinase (D7L7L) XP® Rabbit mAb #15036	1:50-1:100	Cell Signaling Technology, Danvers, MA, USA
Goat anti-mouse IgG-HRP	1:200	Santa Cruz Biotechnology, Dallas, TX, USA
Goat Anti-Rabbit IgG-HRP	1:150-1:200	SouthernBiotech, Birmingham, AL, USA
Pdx1 (D59H3) XP® Rabbit mAb #5679	1:200	Cell Signaling Technology, Danvers, MA, USA

2.1.8 Kits

Table 9. Kits.

Kit	Source
Avidin/Biotin Blocking Kit	Vector Laboratories, Burlingame, CA, USA
DAB Substrate Kit	Vector Laboratories, Burlingame, CA, USA
CloneJET PCR Cloning Kit	Thermo Fisher Scientific, Waltham, MA, USA
FastGene Scriptase II cDNA Kit	Nippon Genetics Europe GmbH, Düren, GER
GenElute™ Mammalian Genomic DNA Miniprep Kit	Sigma-Aldrich, Steinheim, GER
InnuSPEED Tissue RNA Kit	Analytic Jena, Jena, GER
MEGAclear™ Transcription Clean-Up Kit	Invitrogen, Darmstadt, GER
Mix2Seq kit	Eurofins Genomics, Ebersberg, GER
mMESSAGE mMACHINE™ T7 Transcription Kit	Ambion, Austin, TX, USA
NucleoBond® Xtra Midi kit	Macherey-Nagel, Düren, GER
Poly(A) Tailing Kit	Ambion, Austin, TX, USA
PyroMark PCR Kit (200)	Qiagen, Hilden, GER
PyroMark Q48 Advanced CpG Reagents (4 x 48)	Qiagen, Hilden, GER
SurePrep™ RNA/DNA/Protein Purification Kit	Thermo Fisher Scientific, Waltham, MA, USA
Turbo DNA-free™ Kit	Invitrogen, Darmstadt, GER
Vectastain Elite ABC Kit	Vector Laboratories, Burlingame, CA, USA
Wizard® SV Gel and PCR Clean-Up System	Promega GmbH, Mannheim, GER

2.1.9 Mammalian cells

Table 10. Mammalian cells.

Name	Genotype	Source
Porcine adipose-derived mesenchymal stem cells (PADMSCs 110111)	Wild type	Chair of livestock biotechnology, TUM, Freising, GER
Porcine ear fibroblasts (PEFs #2094)	*KRAS*$^{LSLG12D/WT}$-*TP53*$^{LSLR167H/WT}$	Chair of livestock biotechnology, TUM, Freising, GER
Porcine ear fibroblasts (PEFs #2097)	*KRAS*$^{LSLG12D/WT}$-*TP53*$^{LSLR167H/WT}$	Chair of livestock biotechnology, TUM, Freising, GER
Porcine kidney fibroblasts (PKFs 120419-7)	Wild type	Slaughterhouse
Porcine kidney fibroblasts (PKF #270)	*R26*$^{mT-mG/WT}$	Chair of livestock biotechnology, TUM, Freising, GER
Porcine kidney fibroblasts (PKF #232)	*KRAS*$^{LSLG12D/WT}$-*R26*$^{mT-mG/WT}$	Chair of livestock biotechnology, TUM, Freising, GER

2.1.10 Bacterial strains

Table 11. Bacterial strains.

Name	Genotype	Source
Escherichia coli ElectroMAX DH10B (DH10B *E. coli*)	F- *mcr*A Δ(*mrr-hsd*RMS-*mcr*BC) φ80*lac*ZΔM15 Δ*lac*X74 *rec*A1 *end*A1 *ara*D139Δ(*ara*, *leu*)7697 *gal*U *gal*K λ-*rps*L *nup*G	Invitrogen, Karlsruhe, GER

2.1.11 Oligonucleotides

2.1.11.1 Primers

Table 12. Primers.

Name	Sequence
PTF1A screening	
#229 PTF1a-5'-Screen-F	5'-ctctctggagcctggctttta-3'
#138 KpnI-LHA-OE-F1	5'-ctgcacgagtactgctaccg-3'
#37 iCre-seq-R1	5'-agagtcatccttggcaccat-3'
#36 iCre-seq-F1	5'-caagctggtggagagatgga-3'
#20 PTF1a-3'-PCR R2	5'-ctggccagagttgttccaac-3'
#113 PTF1a-PCR_for_KpnI-R	5'-gctgaaagggatgagagggt-3'
mPdx1 screening	
#62 Rosa26 I1 F2	5'-tatgggcgggattcttttgc-3'
#67 R26-SA-R	5'-gaaagaccgcgaagagtttg-3'
#22 mPDX-loxP-Removal-R1	5'-aatgttctctctggtgggct-3'
#64 Rosa26 I1 R3	5'-gtttgcacaggaaacccaag-3'
#239-mPdx1-screen-F	5'-acagcgctgagttctgcaag-3'
#37 iCre-seq-R1	5'-agagtcatccttggcaccat-3'
#36 iCre-seq-F1	5'-caagctggtggagagatgga-3'
#245-mPdx1-F2	5'-tgagggtacggacacatgaa-3'
#255-iCre-R2	5'-agggacacagcattggagtc-3'
#20g-AAV8_F20	5'-ttccgcgcacatttccccga-3'
#145 T2A-iCre-cloning-R1	5'-cgcagcgagtcagtgagcga-3'
RT-PCR	
InDel-F	5'-ctctcagcttcagcacatcg-3'
iCre_rev	5'-ggtcaaagtcagtgcgttca-3'
LEA F	5'-tgacagccaggtgactgaag-3'
LEAexpr2R	5'-atgagctccaccttgcagat-3'
#42 PTF1a-RTPCR-F	5'-gaaggtcatcatctgccacc-3'
#43 PTF1a-RTPCR-R	5'-ttgagtttcctggggtcctc-3'
#44 PDX-1-RTPCR-F	5'-cacctccaccaccacctc-3'
#45 PDX-1-RTPCR-R	5'-gcttgttctcctcgggct-3'
F.GAPDH S.scrofa	5'-ttccacggcacagtcaaggc-3'
R.GAPDH S.scrofa	5'-gcaggtcagatccacaac-3'
RPS28_1F	5'-gttaccaaggttctgggcag-3'
RPS28_1R	5'-cagatatccaggacccagcc-3'
ddPCR	
ddGAPDH F1	5'-ctcaacgaccacttcgtcaa-3'
ddGAPDH R1	5'-ccctgttgctgtagccaaat-3'
ddGAPDH-HEX	5'-HEX-tgtgatcaagtctggtgccc-BHQ-3'

ddiCre F1	5’-gtgcaagctgaacaacagga-3’
ddiCre R1	5’-gactccaatgctgtgtccct-3’
ddiCre-FAM	5’-FAM-cagaggcctggctgtgaaga-BHQ-3’
#269-Lac-ddPCR-test-F2	5’-cacagccggtaagagtaacc-3’
#270-Lac-ddPCR-test-R2	5’-caccccaggctttacacttt-3’
Lac-FAM-ddPCR-Probe	5’-FAM-tccacacaacatacgagccgga-BHQ-3’
Pyrosequencing	
#177 KRAS-Pyro-F (Ex1)	5’-ccatttcggactgggagcta-3’
#181 KRAS-Pyro-R1-biotin (Ex2)	5’-BIO-gctgtattgtcaaggcactcttgc-3’
#276-KRAS-Seq-F1 (Ex2)	5’-gcctgctgaaaatgactga-3’
#280-KRAS-Pyroseq-R1-Bio (Ex3)	5’-BIO-catgtactggtccctcatt-3’
#182 KRAS-Pyro-Seq	5’-tgtggtagttggagctg-3’
p53 SNP 1F	5’-tgtccgcgccatggccatct-3’
p53 SNP 1R	5’-BIO-cagagccgacctcgggcg-3’
p53 SNP 1S	5’-accgaggtggtga-3’
LSL-excision PCR & genotyping	
KRAS_loxP_F	5’-aaagcggtacttgcctttaat-3’
KRAS_loxP_R	5’-tgaggaaaagaacagtgcaaa-3’
TP53_int1F	5’-tgaggaatttgtatgccaagg-3’
TP53_int1R	5’-ttccaccagtgaatccacaa-3’
R26-Targ-F	5’-tctgctgcctcctttccta-3’
R26 targ_SA_R	5’-gaaagaccgcgaagagtttg-3’
Neo-KF R	5’-agcccctgatgctcttcgtc-3’
Multiplexing of gRNAs	
gRNA_scaff-R	5’-taggtctccaaacggatgagcgacagcaaacaaa aaaaaaagcaccgactcg-3’
PCRolap_3 (LSL_TP53_R)	5’-tcaataagctgttttgccaggtcccaccgagat-3’
PCRolap_6 (LSL_TP53_F)	5’-ggcaaaacagcttattgagttttagagctagaaa-3’
#211 PCRolap_7 (p16-3-R)	5‘-tcggccgactggctagcctcaggtcccaccgagat-3‘
#212 PCRolap_7 (p16-3-F)	5‘-gaggctagccagtcggccgagttttagagctagaaa-3‘
#213 PCRolap_7 (Smad4-2R)	5‘-gtctgagcattgtacatagtcaggtcccaccgagat-3‘
#214 PCRolap_7 (Smad4-2F)	5‘-gactatgtacaatgctcagacgttttagagctagaaa-3‘
#215 tRNA-BbsI-Fok-R1	5’-ggcaggatgagcgacagcaaactcgtcttct cgaagactcgcaccgactcg-3’
#216 BbsI-tRNA-F	5’-gaagacctgtgcgcagcaggtcccat-3’
#217 BbsI-gRNA-p16-R	5‘-gaagactcaaactcggccgactggctagcctc-3‘
#226 Smad4-BbsI-R	5’-gaagactcaaacgtctgagcattgtacatagtcag gtcccaccgagat-3‘
#227 BRCA2-gRNA1-Rolap-R	5’-attggatgcaaagagagaccaggtcccaccgagat-3’
#228 BRCA2-gRNA1-Rolap-F	5’-ggtctctctttgcatccaatgttttagagctagaaa-3’
#230 BRCA2-BbsI-R	5’-gaagactcaaacattggatgcaaagagagacc aggtcccaccgagat-3’
#233 gRNA-scaffold-F1	5’-gttttagagctagaaatagc-3’
#234 gRNA-scaffold-F2	5’-ggctagtccgttatcaacttg-3’
#248-FokI-BbsIx2-pIDT-F1	5’-ggatgggcagtctgcaccgggtcttcgagaagac gagttttagagctaga-3’
#249-FokI-BbsIx2-pIDT-R1	5’-ggatgagcgacagcaaaccgaggggagc catcgctaaggtcccaccgaga-3’
#250-BbsI-Pentaplex-F1	5’-gaagactgcaccgcagcaggtcccatgg-3’
#251-BbsI-Pentaplex-R1	5’-gaagacgaaaacattggatgcaaagagagacc-3’
#256-B2M-R1	5’-cgaggggagccatcgcta-3’
#257-B2M-Scaffold-F1	5’-tagcgatggctcccctcggttttagagctagaaatagc-3’
tRNA BsaI-FokI-F	5’-cgggtctcaggcaggatgggca-3’

Screening of gRNA target sites	
porP16_TIDE_F1	5’-ctccgggtggaaagataccg-3’
porP16_TIDE_R1	5’-tgtcctccgacggatttctg-3’
porSMAD4_TIDE_F1	5’-agcaatttcatcttttcccaagt-3’
porSMAD4_TIDE_R1	5’-gactaacctgaagcctccca-3’
porTP53_TIDE_F1	5’-accctggtcccaaagttgaa-3’
porTP53_TIDE_R1	5’-gcccactcaccatcgctata-3’
#158 BRCA1-gRNA1TIDE-F1	5’-ggcaacaccggatccttaac-3’
#159 BRCA1-gRNA1TIDE-R1	5’-acccctaacctggaaacctc-3’
#160 BRCA1-gRNA2TIDE-F1	5’-tcaggatccgagctgtgttt-3’
#161 BRCA1-gRNA2TIDE-R1	5’-tgcaccattattttctgtaccac-3’
#162 BRCA2-gRNA1TIDE-F1	5’-gcggaatcttgctcttttgga-3’
#163 BRCA2-gRNA1TIDE-R1	5’-gccagtctcctctttgtcca-3’
pB2M Scr 5’UTR F1	5’-ccacccagtccaacctttgcc-3’
pB2M Scr I1 R1	5’-ccagagttagcgcccggagt-3’
#23 3'-control-gDNA-F1	5’-atgaagcctaagacgcctgt-3’
#24 3'-control-gDNA-R1	5’-tccactccctttcagctcaa-3’

2.1.11.2 gRNA oligonucleotides

Table 13. gRNA oligonucleotides.

gRNA target site	Oligonucleotide name	Sequence
B2M gRNA (Beate Rieblinger)	B2M-F1	5’-cacctagcgatggctcccctcg-3’
	B2M-R1	5’-aaaccgaggggagccatcgcta-3’
BRCA1 gRNA 1	porBRCA1-gRNA1-F1	5’-caccgaaatatgtggtcacactttg-3’
	porBRCA1-gRNA1-R1	5’-aaaccaaagtgtgaccacatatttc-3’
BRCA1 gRNA 2	porBRCA1-gRNA2-F1	5’-caccgtaaatcttgtactttcttgt-3’
	porBRCA1-gRNA2-R1	5’-aaacacaagaaagtacaagatttac-3’
BRCA2 gRNA 1	porBRCA2-gRNA1-F1	5’-caccggtctctctttgcatccaat-3’
	porBRCA2-gRNA1-R1	5’-aaacattggatgcaaagagagacc-3’
p16 gRNA 3	porp16-gRNA3-F1	5’-caccgaggctagccagtcggccga-3’
	porp16-gRNA3-R1	5’-aactcggccgactggctagcctc-3’
p16 gRNA 4	porp16-gRNA4-F1	5’-caccgtgcggcggaggctagccagt-3’
	porp16-gRNA4-R1	5’-aaacactggctagcctccgccgcac-3’
PTF1A-Ex1-gRNA 4 (Alessandro Grodziecki)	PTF1A-gRNA4-F	5’-caccgtcctcttactttgacgagg-3’
	PTF1A-gRNA4-R	5’-aaaccctcgtcaaagtaagaggac-3’
PTF1A-3’UTR gRNA 1	gRNA1_3'UTR-F1	5’-caccgaccagatcctcaggagggtc-3’
	gRNA1_3'UTR-R1	5’-aaacgaccctcctgaggatctggtc-3’
PTF1A-3’UTR gRNA 2	gRNA2_3'UTR-F1	5’-caccgacataaccagatcctcagg-3’
	gRNA2_3'UTR-R1	5’-aaaccctgaggatctggttatgtc-3’
PTF1A-3’UTR gRNA 3	gRNA3_3'UTR-F1	5’-caccgacataaccagatcctcagga-3’
	gRNA3_3'UTR-R1	5’-aaactcctgaggatctggttatgtc-3’
R26-gRNA	R26-gRNA-F1	5’-caccattgaacctacaacctcg-3’
	R26-gRNA-R1	5’-aaaccgaggttgtaggttcaat-3’
SMAD4 gRNA 2 (Alessandro Grodziecki)	SMAD4-sus scrofa-gRNA2-F1	5’-caccgactatgtacaatgctcagac-3’
	SMAD4-sus scrofa-gRNA2-R1	5’-aaacgtctgagcattgtacatagtc-3’
TP53 gRNA (Carolin Perleberg)	CRISPR_TP53_Ex5_1A	5’-caccggcaaaacagcttattga-3’
	CRISPR_TP53_Ex5_1B	5’-aaactcaataagctgttttgcc-3’

gRNAs for KRAS/TP53 mutational activation (multiplexed)		
SA gRNA 1	#173 PCRolap_2 (LSL-G1R)	5'-taacttcgtataatgtatgcaggtcccaccg agat-3'
	#175 PCRolap_4 (LSL-G1F)	5'-gcatacattatacgaagttagttttagagct agaaa-3'
SA gRNA 2	#174 PCRolap_3 (LSL-G2R)	5'-tcgatccccactggaaagacaggtcccac cgagat-3'
	#176 PCRolap_6 (LSL-G2F)	5'-gtctttccagtggggatcgagttttagagcta gaaa-3'
SA gRNA 3	#218 SA-Remov-gRNA-New-R	5'-gtggggatcgacggtatcgacaggtccca ccgagat-3'
	#219 SA-Remov-gRNA-New-F	5'-gtcgataccgtcgatccccacgttttagagc tagaaa-3'
Neo gRNA 1	#220 SA-Neo-Remov-gRNA2-R	5'-cggcacttcgcccaatagcacaggtccca ccgagat-3'
	#221 SA-Neo-Remov-gRNA2-F	5'-gtgctattgggcgaagtgccggttttagagc tagaaa-3'

2.1.12 Nucleic acid ladders

Table 14. Nucleic acid ladders.

Name	Range	Source
2-log DNA ladder	0.1-10 kb	New England Biolabs, Frankfurt, GER
RiboRuler High Range RNA Ladder & RNA loading dye (2x)	0.2-6 kb	Thermo Fisher Scientific, Waltham, MA, USA
Quick-Load® 1 kb Extend DNA Ladder	0.5-48.5 kb	New England Biolabs, Frankfurt, GER

2.1.13 Vectors and DNA constructs

Table 15. Vectors and DNA constructs.

Name	Source
1044_pBS-CMV-gag-pol plasmid (Addgene plasmid #35614)	Addgene, Watertown, MA, USA
990_GAG-CRErec plasmid (Addgene plasmid #119971)	Addgene, Watertown, MA, USA
CAG-LEA29Y plasmid	Kindly provided by Nikolai Klymiuk, Institute of Molecular Animal Breeding and Biotechnology, LMU, Munich, GER
CMV-VSV-G plasmid (Addgene plasmid #8454)	Addgene, Watertown, MA, USA
hyPB-Transposase-T2A-mCherry-WPRE plasmid	Kindly provided by Prof. Dr. Roland Rad, Institute of Molecular Oncology and Functional Genomics, Klinikum rechts der Isar, TUM, Munich, GER
hyPB-Transposase-T2A-mCherry-bGH_pA plasmid	Daniela Kalla, Chair of livestock biotechnology, TUM, Freising, GER
iCre-pA plasmid	Chair of Livestock Biotechnology, TUM, Freising, GER

mPdx1-iCre-PGK-Neo plasmid for random integration	Daniela Kalla, Chair of livestock biotechnology, TUM, Freising, GER
Multiplexed PTG constructs	Daniela Kalla, Chair of livestock biotechnology, TUM, Freising, GER
PB/SB-DNA transposon plasmid	Kindly provided by Prof. Dr. Roland Rad, Institute of Molecular Oncology and Functional Genomics, Klinikum rechts der Isar, TUM, Munich, GER
PB-mPdx1-iCre-DNA transposon plasmid	Daniela Kalla, Chair of livestock biotechnology, TUM, Freising, GER
pcDNA3.1-Hygro-CAG plasmid	Konrad Fischer, Chair of livestock biotechnology, TUM, Freising, GER
pcDNA3.1-Hygro-CAG-LEA29Y plasmid	Daniela Kalla, Chair of livestock biotechnology, TUM, Freising, GER
Pdx1-mTQ2-P2A-FlpO-PA (Addgene plasmid #67279)	Addgene, Watertown, MA, USA
PGK-ER^{T2}-Cre-ER^{T2} plasmid (plasmid #814)	Chair of Livestock Biotechnology, TUM, Freising, GER
pJET1.2/blunt cloning vector	Thermo Fisher Scientific, Waltham, MA, USA
pSL1180 cloning vector	Amersham Biosciences, Amersham, UK
PTF1A double cut donor templates	Daniela Kalla, Chair of livestock biotechnology, TUM, Freising, GER
PTG template construct	Tatiana Flisikowska, Chair of Livestock Biotechnology, TUM, Freising, GER
pX330-U6-Chimeric_BB-CBh-hSpCas9 (Addgene plasmid #42230)	Addgene, Watertown, MA, USA
pX330-U6-Chimeric_BB-CBh-hSpCas9-T2A-Puro_MCS (plasmid #841)	Daniela Huber, Chair of livestock biotechnology, TUM, Freising, GER
pX330-hSpCas9-PTF1A_Ex1_gRNA4	Alessandro Grodziecki, Chair of livestock biotechnology, TUM, Freising, GER
pX330-hSpCas9-PTF1A_3'UTR_gRNA3	Daniela Kalla, Chair of livestock biotechnology, TUM, Freising, GER
pX330-hSpCas9-R26-gRNA	Chair of Livestock Biotechnology, TUM, Freising, GER
pX462-U6-BB-hSpCas9n(D10A)-T2A-Puro (Addgene plasmid #62987)	Addgene, Watertown, MA, USA
pX462-hSpCas9n(D10A)-PTF1A_Ex1_gRNA4	Daniela Kalla, Chair of livestock biotechnology, TUM, Freising, GER
R26-SA-BS-mPdx1-iCre targeting vector	Daniela Kalla, Chair of livestock biotechnology, TUM, Freising, GER
R26-SA-Neo-Pdx1-Cre targeting vector (plasmid #792)	Chair of Livestock Biotechnology, TUM, Freising, GER
R26-SA-Neo-mPdx1-iCre targeting vector	Daniela Kalla, Chair of livestock biotechnology, TUM, Freising, GER

2.1.14 Consumables

Table 16. Consumables.

Name	Source
Cell strainer (200 µm)	PluriSelect Life Science, Leipzig, GER
C-Chip Neubauer improved cell counting chamber	Carl Roth, Karlsruhe, GER
Cloning rings: reaction tubes	Brand, Wertheim, GER
Countess™ Cell Counting Chamber Slides	Invitrogen, Karlsruhe, GER
Cryovials	Corning Incorporated, Corning, NY, USA
ddPCR™ 96-Well Plates	Bio-Rad Laboratories, Hercules, CA, USA
DG8™ Cartridges for QX200™/QX100™ Droplet Generator	Bio-Rad Laboratories, Hercules, CA, USA
DG8™ Gaskets for QX200™/QX100™ Droplet Generator	Bio-Rad Laboratories, Hercules, CA, USA
Electroporation cuvettes (2 mm)	VWR International GmbH, Ismaning, GER
Embedding cassettes, Q Path® MicroStar V	VWR International GmbH, Ismaning, GER
Falcon tubes (15 ml, 50 ml)	Greiner Bio-One, Frickenhausen, GER
Glass pasteur pipettes	Brand, Wertheim, GER
Microscope slides	VWR International GmbH, Ismaning, GER
Microtome Blades R35	FEATHER® Safety Razor, Osaka, JPN
Parafilm	Bemis, Neenah, WI, USA
PCR reaction tubes (8-strip, 0.2 ml)	Starlab, Hamburg, GER
Petri dishes	Greiner Bio-One, Frickenhausen, GER
Pipette tips (2 µl, 20 µl, 200 µl, 1000 µl)	Mettler-Toledo, Columbus, OH, USA
Pierceable foil heat seal	Bio-Rad Laboratories, Hercules, CA, USA
PyroMark Q48 Absorber Strips	Qiagen, Hilden, GER
PyroMark Q48 Discs	Qiagen, Hilden, GER
Reaction tubes (1.5 ml, 2 ml)	Zefa Laborservice, Harthause, GER
Scalpels	Braun, Melsungen, GER
Serological pipettes Costar® stripettes (1 ml, 2 ml, 5 ml, 10 ml, 25 ml, 50 ml)	Corning Incorporated, Corning, NY, USA
StarGuard® nitril gloves (S, M, L, XL)	Starlab, Hamburg, GER
Sterile filter (0.22 µm)	Berrytec, Grünwald, GER
Syringes (2 ml, 5 ml, 25 ml)	Becton Dickinson, Franklin Lakes, NJ, USA
Tissue culture flask (T25, T75, T150)	Corning Incorporated, Corning, NY, USA
Tissue culture plates (10 cm, 15 cm, 6-well, 12-well, 24-well, 48-well, 96-well)	Corning Incorporated, Corning, NY, USA
Tissue-Tek® Cryomold® Standard (25 x 20 x 5 mm)	Sakura Finetek Germany, Umkirch, GER

2.1.15 Laboratory equipment

Table 17. Laboratory equipment.

Device	Source
BlueLight table	Serva, Heidelberg, GER
BTX ECM 830 Electro Square Porator	BTX Harvard Apparatus, Holliston, MA, USA
Bacterial incubator	Thermo Fisher Scientific, Waltham, MA, USA
Centrifuges: Sigma 3-16; Sigma 1-15; Sigma 1-15K; Sigma 4K15	Sigma, Osterode, GER
CO_2 incubator “Forma Steri-Cycle”	Thermo Fisher Scientific, Waltham, MA, USA

Countess™ Automated Cell Counter	Invitrogen, Karlsruhe, GER
CryoStar™ NX70 Cryostat	Thermo Fisher Scientific, Waltham, MA, USA
Electroporator “Multiporator”	Eppendorf, Hamburg, GER
Freezer -20°C	Liebherr International, Bulle, Switzerland
Freezer -80°C	Thermo Fisher Scientific, Waltham, MA, USA
Fridge +4°C	Beko, Neu-Isenburg, GER
Gel electrophoresis system	Peqlab Biotechnologie, Erlangen, GER
Heating block	Thermo Fisher Scientific, Waltham, MA, USA
HERAsafe safety cabinet	Heraeus, Hanau, GER
Hot plate magnetic stirrer AREC.X	VELP Scientifica, Usmate, IT
Ice machine	Eurfrigor, Lainate, IT
Leica ST5020 Multistainer	Leica Mikrosysteme Vertrieb GmbH Mikroskopie und Histologie, Wetzlar, GER
Leica TCS SP8 HyVolution 2 confocal microscope	Leica Mikrosysteme Vertrieb GmbH Mikroskopie und Histologie, Wetzlar, GER
Leica TP1020 tissue processor	Leica Mikrosysteme Vertrieb GmbH Mikroskopie und Histologie, Wetzlar, GER
M8 digital microscope & slide scanner	PreciPoint, Freising, GER
Microscopes: Axiovert 40CLF, Axiovert 200 M, Primo Star	Carl Zeiss, Jena, GER
Microwave	MHA, Barsbüttel, Germany
Mr. Frosty Freezing Container	Thermo Fisher Scientific, Waltham, MA, USA
MS2 Minishaker IKA®	IKA®-Werke GmbH, Staufen, GER
Nanodrop Lite Spectrophotometer	Thermo Fisher Scientific, Waltham, MA, USA
Orbital shaker	Thermo Fisher Scientific, Waltham, MA, USA
PCR cycler: PeqStar 2x Thermocycler	Peqlab Biotechnologie, Erlangen, GER
PCR cycler: DNS Engine DYAD	Bio-Rad Laboratories, Hercules, CA, USA
Perfect Spin Mini Centrifuge	Peqlab Biotechnologie, Erlangen, GER
Pipettes: Gilson pipetman (0.2-2 µl, 2-20 µl, 20-200 µl, 100-1000 µl, multichannel)	Gilson, Middleton, WI, USA
Pipette controller: Pipettus® reddot	Hirschmann Laborgeräte, Eberstadt, GER
Pipetting controller: accu-jet pro®	Brand, Wertheim, GER
Power supply EPS 301	Thermo Fisher Scientific, Waltham, MA, USA
Power supply Owl™ EC-105	Owl™ EC-105 Compact Power Supply
Power supply PeqPOWER	Peqlab Biotechnologie, Erlangen, GER
PX1™ PCR Plate Sealer	Bio-Rad Laboratories, Hercules, CA, USA
PyroMark® Q48 Autoprep Instrument	Qiagen, Hilden, GER
Quantum ST5 gel documentation system	Vilber Lourmat, Eberhardzell, GER
QX 200™ Droplet Generator	Bio-Rad Laboratories, Hercules, CA, USA
QX 200™ Droplet Reader	Bio-Rad Laboratories, Hercules, CA, USA
Rotary microtome “Microm 355”	Microm International, Walldorf, GER
Rotary oven	Thermo Fisher Scientific, Waltham, MA, USA
Slide staining system M920-StainTray	Simport Scientific, Saint-Mathieu-de-Beloeil, Québec, CA
SpeedMill PLUS	Analytic Jena, Jena, GER
Water bath	Memmert GmbH, Schwabach, GER

2.1.16 Software and online tools

Table 18. Software and online tools.

Software/tool	Source
“Axio Vision” Microscope software	Carl Zeiss, Göttingen, GER
“Benchling” biotechnology software	https://www.benchling.com/
“CRISPOR” gRNA design tool	http://crispor.tefor.net/ Santa Cruz Genomics Institute, Santa Cruz, CA, USA
Digital microscope software	PreciPoint, Freising, GER
“Endmemo” DNA/RNA GC Content Calculator	http://www.endmemo.com/bio/gc.php/ EMBL-EBI, Hinxton, UK
“Ensembl” genome browser	https://www.ensembl.org/index.html
“Finch TV” chromatogram viewer	Geospiza Inc., Seattle, WA, USA
“ICE v2 CRISPR Analysis Tool”	https://ice.synthego.com/ Synthego, Menlo Park, CA, USA
“miRBase” MicroRNA target prediction software	http://www.mirbase.org University of Manchester, Manchester, UK
Microsoft Office 365	https://www.microsoft.com
“NCBI” Genome database	https://www.ncbi.nlm.nih.gov National Center for Biotechnology Information, Bethesda, MD, USA
“NEBuilder® Assembly Tool”	https://nebuilder.neb.com
“Primer3” Primer design tool	https://primer3.ut.ee/ Whitehead Institute for Biomedical Research, Cambridge, MA, USA
“PyroMark Q48 Autoprep Software”	Qiagen, Hilden, GER
“QuantaSoft™ software” ddPCR software	Bio-Rad Laboratories, Hercules, CA, USA
“TIDE: Tracking of Indels by Decomposition”	https://tide.deskgen.com/ Desktop Genetics, London, UK

2.2 Methods

2.2.1 Molecular biological methods

2.2.1.1 Isolation of nucleic acids

2.2.1.1.1 Isolation of genomic DNA by phenol-chloroform extraction

Phenol-Chloroform extraction was used to obtain mammalian tissue DNA with high yield and purity. The cells were detached from the cell culture vessel and depending on the size, the cell pellet was resuspended in 0.5-3 ml cell lysis buffer containing 0.4 mg/ml proteinase K. Cell lysis was performed overnight at 37°C. The next day, 20 µl RNase A was added, followed by incubation for 5 min at room temperature (RT). After mixing with one volume of phenol-chloroform-isoamyl alcohol (25:24:1), the samples were shaken by hand and incubated at RT for 10 min, followed by centrifugation for 10 min at 14,000 rpm. For precipitation, the upper phase was transferred into a new tube and then mixed with 1/10 volume of 3M NaCl and 0.7 volumes of isopropyl alcohol by shaking. Precipitated DNA was pelletized by centrifugation for 10 min at 14,000 rpm. After removing the supernatant, the cell pellet was washed with 1 ml 70% EtOH and centrifuged for 5 min at 14,000 rpm. The DNA pellet was air-dried and dissolved in 30-50 µl Low-EDTA-Tris buffer at 50°C for 30 min.

2.2.1.1.2 Isolation of genomic DNA using QuickExtract

For rapid isolation of genomic DNA (gDNA) from mammalian cells, QuickExtract DNA extraction solution was used. Cells were detached from a half of 12-well or 6-well and centrifuged at 300 x g for 5 min. The supernatant was aspirated and the cell pellet was resuspended in 30 µl of QuickExtract solution. Extraction was performed by heating the sample at 68°C for 15 min, followed by 98°C for 8 min in a thermal cycler.

2.2.1.1.3 Isolation of plasmid DNA using NaCl purification

NaCl purification was used to recover large amounts of plasmid DNA in high purity after restriction digest. Therefore, the restriction digest was mixed with 1/10 volume of NaCl and 2 volumes of ice-cold 100% EtOH. The sample was shaken until precipitation and then incubated for 2 h at -80°C. After centrifugation for 15 min at 14,000 rpm, the supernatant was removed and the DNA pellet was washed with 1 ml 70% EtOH, followed by another centrifugation step. The supernatant was discarded and the pellet was dissolved in 30-50 µl Low-EDTA-Tris buffer for 15 min at 50°C.

2.2.1.1.4 Isolation of plasmid DNA from bacteria

Plasmid DNA was isolated from bacterial cells using the NucleoBond® Xtra Midi kit. For this, a 100 ml bacterial overnight culture was prepared as described in section 2.2.2.3.

On the next day, the bacterial suspension was divided onto two 50 ml falcons and centrifuged for 20 min at 5000 x g and 4°C. The supernatant was discarded and the pellets were each resuspended in 4 ml Resuspension buffer and combined. Further plasmid isolation was performed as described in the manufacturer's instructions. Finally, the pellet was dissolved in 100 µl nuclease-free H_2O or Low-EDTA-Tris buffer.

2.2.1.1.5 Genomic DNA/RNA isolation using SurePrep™ Purification Kit

The SurePrep™ RNA/DNA/Protein Purification Kit was used to isolate DNA and RNA of porcine cells grown in monolayer and pancreatic acinar cells from 3D culture. Cells were harvested as described in sections 2.2.3.3 and 2.2.3.13.4, respectively. RNA and DNA was isolated according to the manufacturer's protocol for lifted cells. Elution was performed using 30 µl RNA elution buffer or 50 µl DNA elution buffer.

2.2.1.1.6 Isolation of RNA using TRIzol

RNA from cells grown in monolayer and pancreatic acinar 3D culture was isolated using TRIzol reagent. For monolayer culture grown in a T150 flask, growth medium was removed and 2 ml of TRIzol were directly added onto the cells. After numerous pipetting up and down, the lysed cells were transferred to a tube. For pancreatic acinar 3D culture, cells were harvested as described in section 2.2.3.13.4 and resuspended in 1 ml TRIzol. RNA isolation was performed according to the manufacturer's protocol and the RNA pellets were solved in 50 µl and 28 µl nuclease-free H_2O for monolayer cells and pancreatic acinar cells, respectively.

2.2.1.1.7 Isolation of RNA using innuPREP RNA kit

RNA from tissues was isolated using innuPREP RNA Mini Kit 2.0. A small piece of 1-3 mm was cut from the tissue and transferred into a homogenizer reaction vessel containing 450 µl Lysis Solution RL. The tissue was homogenized for 30 s using the SpeedMill Plus machine. RNA isolation was performed according to the manufacturer's instructions. An additional washing step with 70% EtOH was included at the end to improve RNA purity and elution was performed using 50 µl nuclease-free H_2O.

2.2.1.2 DNase digest

After RNA isolation, digestion of remaining DNA was performed using the Turbo DNA-free™ Kit according to the manufacturer's instructions.

2.2.1.3 Determination of DNA/RNA concentration

Concentrations of DNA and RNA were determined using the NanoDrop™ Lite Spectrophotometer, which measures the absorbance of nucleic acids at 260 nm. Measurement was performed as described in the manufacturer's manual and concentrations were calculated using the respective conversion factor (Table 19) and a pathlength of 1 cm:

$$Concentration = \frac{A_{260} \; x \; conversion \; factor}{1 \; cm} = ng/\mu l$$

Table 19. Conversion factors for nucleic acid concentration determination.

Nucleic acid type	Conversion factor in $\frac{ng \; x \; cm}{\mu l}$
Double-stranded DNA (dsDNA)	50
Single-stranded DNA (ssDNA)	33
RNA	40

The purity was calculated as A_{260}/A_{280} ratio.

2.2.1.4 Polymerase chain reaction

Amplification of DNA fragments from gDNA, cDNA or plasmids was performed by polymerase chain reaction (PCR). Depending on the template and the experimental design, different polymerases were used. Colony PCR and PCRs for simple gDNA and cDNA targets were performed using GoTaq® G2 DNA Polymerase (Table 20).

Table 20. GoTaq® G2 DNA Polymerase reaction and cycling protocol.

Pipetting scheme		Cycling conditions			
Component	**Volume**	**Step**	**Temperature**	**Duration**	**Cycles**
DNA	< 200 ng	Initial denaturation	95°C	3 min	1
GoTaq® Reaction Buffer Green(5x)	5 µl	Denaturation	95°C	45 s	35
dNTPs (10 µM)	0.5 µl	Annealing	58-60°C	45 s	
Primer forward (10 µM)	0.5 µl	Elongation	72°C	60 s/kb	
Primer reverse (10 µM)	0.5 µl	Final elongation	72°C	5 min	1
GoTaq® G2 DNA Polymerase	0.15 µl	Hold	8°C	infinite	1
H_2O	Up to 25 µl				

For cloning purposes, DNA fragments from plasmids were amplified using Q5® High-Fidelity DNA Polymerase that has a high proofreading capability (Table 21).

Table 21. Q5® High-Fidelity DNA Polymerase reaction and cycling protocol.

Pipetting scheme		Cycling conditions			
Component	**Amount/ Volume**	**Step**	**Temperature**	**Duration**	**Cycles**
DNA	100 ng	Initial denaturation	98°C	30 s	1
Q5® Reaction Buffer (5x)	10 µl	Denaturation	98°C	10 s	35
dNTPs (10 µM)	1 µl	Annealing	59-62°C	30 s	
Primer forward (10 µM)	2.5 µl	Elongation	72°C	30 s/kb	
Primer reverse (10 µM)	2.5 µl	Final elongation	72°C	2 min	1
Q5® GC Enhancer (5x)	10 µl	Hold	8°C	infinite	1
Q5® High-Fidelity DNA Polymerase	0.5 µl				
H_2O	Up to 50 µl				

Difficult templates with high GC content were amplified by Phire Hot Start II DNA Polymerase in combination with 1.4 M Betaine, which was added for the reduction of secondary structures (Table 22).

Table 22. Phire Hot Start II DNA Polymerase reaction and cycling protocol.

Pipetting scheme		Cycling conditions			
Component	**Volume**	**Step**	**Temperature**	**Duration**	**Cycles**
DNA	100 ng	Initial denaturation	98°C	4 min	1
Phire II Reaction Buffer (5x)	5 µl	Denaturation	98°C	20 s	35-40
Betaine (5M)	7 µl	Annealing	64-66°C	20 s	
dNTPs (10 µM)	1 µl	Elongation	72°C	20 s/kb	
Primer forward (10 µM)	2.5 µl	Final elongation	72°C	3 min	1
Primer reverse (10 µM)	2.5 µl	Hold	8°C	infinite	1
Phire Hot Start II DNA Polymerase	0.5 µl				
H_2O	Up to 25 µl				

Amplification for pyrosequencing was performed by GoTaq or PyroMark PCR (Table 23).

Table 23. PyroMark PCR reaction and cycling protocol.

Pipetting scheme		Cycling conditions			
Component	**Volume**	**Step**	**Temperature**	**Duration**	**Cycles**
cDNA	1-2 µl	Initial denaturation	95°C	15 min	1
PyroMark PCR master mix (2x)	12.5 µl	Denaturation	95°C	30 s	45
CoralLoad concentrate (10x)	2.5 µl	Annealing	59°C	30 s	
25 mM $MgCl_2$	0.5 µl	Elongation	72°C	30	
Primer forward (10 µM)	0.5 µl	Final elongation	72°C	10 min	1
Primer reverse biotinylated (10 µM)	0.5 µl	Hold	8°C	infinite	1
H_2O	Up to 25 µl				

2.2.1.5 Agarose gel electrophoresis

DNA fragments were separated by size using agarose gel electrophoresis. 1x TAE buffer and 1x TBE buffer were used for preparative and analytical purposes, respectively. Depending on the expected fragment size, gels were prepared containing 0.8-2% agarose. 4 µl pegGreen DNA/RNA dye were added per 100 ml of agarose gel. PCR reactions containing loading dye in their reaction buffer were directly applied onto the gel, while other samples were mixed with loading dye first. Separation was performed for at least 1 h at 90-120 V and the DNA fragments were visualized with UV light at 366 nm using the Quantum ST5 gel documentation system.
Agarose gels for RNA fragments contained 800 µl formaldehyde and 6 µl peqGreen per 100 ml of 1% TBE gel. The samples were mixed with 2x RNA loading dye, heated for 10 min at 70°C and then cooled for 5 min at 4°C. Afterwards, the samples were immediately stored on ice until they were applied on the gel.

2.2.1.6 Purification of DNA fragments and PCR products

Purification of agarose gel fragments containing DNA fragments and PCR products as well as of PCR amplifications and DNA ligations was performed using Wizard® SV Gel and PCR Clean-Up System. For gel fragments, 10 µl Membrane Binding Solution was added per 10 mg of gel slice and the mixture was incubated at 65°C until the gel slice completely dissolved. For PCR amplifications and ligation reactions, the PCR reaction was mixed with an equal volume of Membrane Binding Solution. Binding of DNA to the column and washing were performed according to the manufacturer's protocol.

Elution was carried out using 35 µl and 20 µl of nuclease-free H_2O preheated to 65°C for gel fragments and PCR or ligation products, respectively.

2.2.1.7 Restriction digest

Analytical and preparative restriction digest was performed with 1 µg and 10-30 µg DNA, respectively. Buffers and supplements were used according to the manufacturer's instructions. The reaction was set up as described in Table 24 and was incubated at 37°C for 1.5-2 h.
To prevent enzyme star activity, the proportion of enzyme in the total reaction volume was always kept below 5%.

Table 24. DNA restriction digest reaction.

Component	Amount/Concentration
DNA	Analytical digest: 1 µg Preparative digest: 10-30 µg
Reaction Buffer (10x)	1/10 of total volume
Restriction enzyme	3 Units/µg
H_2O	Depending on enzyme volume

2.2.1.8 Generation of CRISPR/Cas9 plasmids

Suitable gRNAs with high editing efficiencies and low off-target effects were identified using the "CRISPOR" gRNA design tool. The respective oligonucleotides were designed to contain overhangs compatible with BbsI digested pX330-U6-Chimeric_BB-CBh-hSpCas9-T2A-Puro_MCS (plasmid #841) and pX462-U6-BB-hSpCas9n(D10A)-T2A-Puro vectors. Per each gRNA, the single stranded DNA oligonucleotides (forward and reverse) were diluted in TE buffer to a concentration of 1 µg/µl. Subsequently, the oligonucleotides were diluted to 10 ng/µl by adding 1 µl of each to 100 µl TE buffer. Oligo annealing was performed by heating the mixture for 5 min at 100°C, followed by slow cooling down to RT. After annealing, 1.5 µl (≙ 15 ng) were used for ligation into the above mentioned BbsI digested Cas9 plasmids.

2.2.1.9 Multiplexing of gRNAs

As described in section 1.6.3, the application of PTG constructs enables the simultaneous modification of several genes. For gRNA multiplexing, a PTG template construct containing the pig specific pre-tRNA sequence was used. The strategy for multiplexing two gRNAs is depicted in Figure 11A. Furthermore, up to five gRNAs were multiplexed according to the strategies shown in Figure 11B and C. As plasmid #841-pX330-U6-Chimeric_BB-CBh-hSpCas9-T2A-Puro_MCS already included one scaffold and U6 terminator, it was not mandatory to add these after the last gRNA during the cloning procedure (Figure 11B+C).

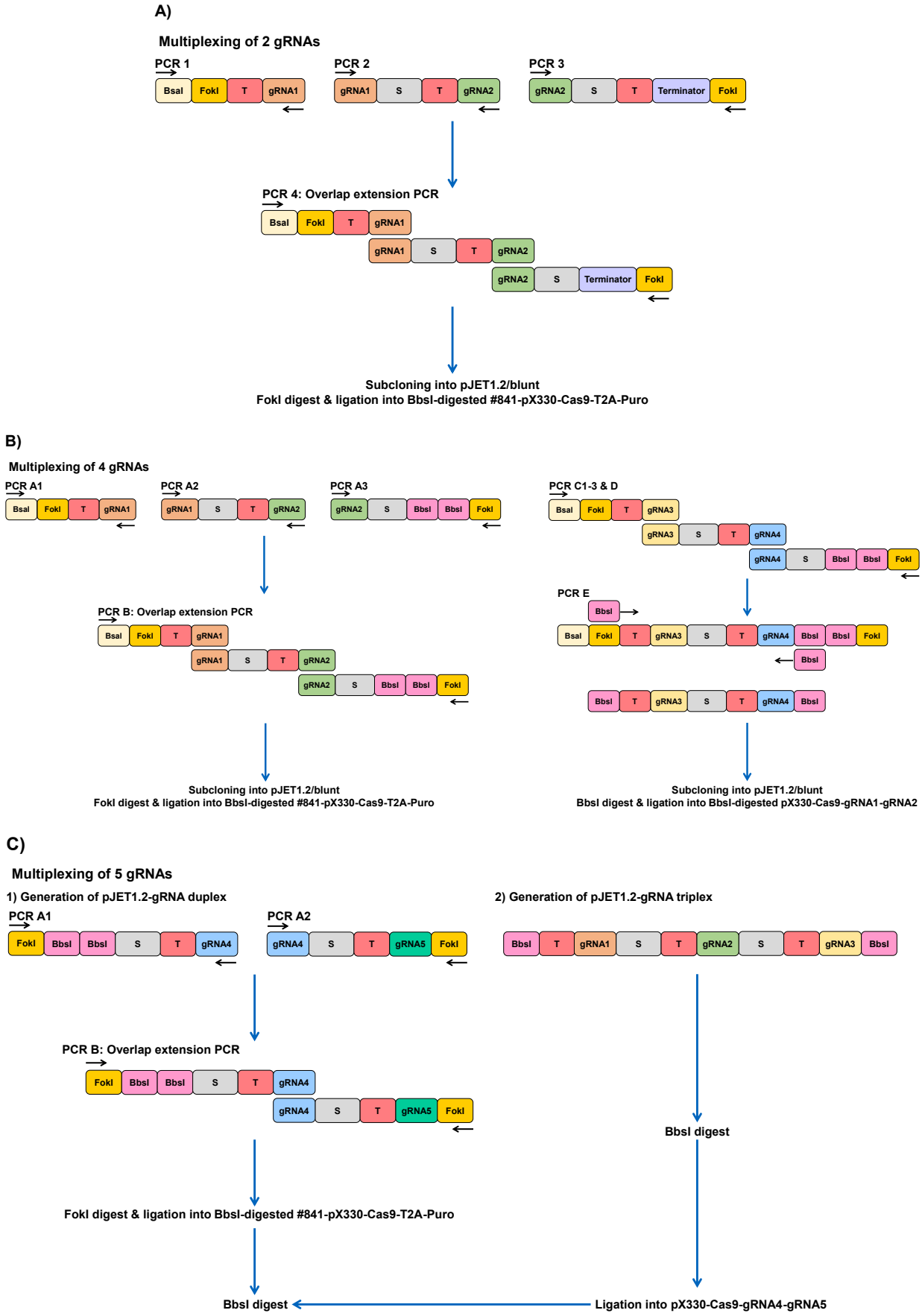

Figure 11. Cloning strategy for gRNA multiplexing. (A) Multiplexing of two gRNAs. (B) Multiplexing of four gRNAs. (C) Multiplexing of five gRNAs. T: tRNA, S: scaffold

The multiplexing procedure was based on annealing of multiple sequence segments that had overlapping regions. These sequence parts were amplified from plasmids using Q5® High-Fidelity DNA Polymerase with the help of primers containing the respective overlap sequences as overhangs. Following overhang PCR, the generated PCR products were annealed at the corresponding overlapping sequences by overlap extension PCR (Table 25). Overlap extension PCR included annealing of two PCR products in a short cycling step. Afterwards, annealing of the third PCR segment and amplification of the final end product was carried out.

Table 25. Overlap extension PCR reaction and cycling protocol.

Pipetting scheme		**Cycling conditions**			
Component	**Volume**	**Step**	**Temperature**	**Duration**	**Cycles**
Q5® Reaction Buffer (5x)	8 µl	Initial denaturation	98°C	30 s	1
dNTPs (10 µM)	2 µl	Denaturation	98°C	5 s	5
Purified PCR product 1	2 µl	Annealing	48°C	15 s	
Purified PCR product 2	2 µl	Elongation	72°C	15 s	
Q5® GC Enhancer (5x)	8 µl	Final elongation	72°C	2 min	1
Q5® High-Fidelity DNA Polymerase	0.5 µl	Hold	8°C	infinite	1
H_2O	17.5 µl				
Addition of the following components and further cycling protocol:					
Component	**Volume**	**Step**	**Temperature**	**Duration**	**Cycles**
Q5® Reaction Buffer (5x)	2 µl	Initial denaturation	98°C	30 s	1
Purified PCR product 3	2 µl	Denaturation	98°C	5 s	5
Q5® GC Enhancer (5x)	2 µl	Annealing	48°C	15 s	
Primer forward (10 µM)	2 µl	Elongation	72°C	15 s	
Primer reverse (10 µM)	2 µl	Denaturation	98°C	5 s	35
		Annealing	58°C	15 s	
		Elongation	72°C	15 s	
		Final elongation	72°C	2 min	1
		Hold	8°C	infinite	1

Following overhang and overlap extension PCR, the final multiplexed constructs were completed by further subcloning and cloning steps using the generated PCR products.

2.2.1.10 Determination of gRNA efficiencies

To evaluate the efficiencies of cloned gRNAs, porcine cells were transfected with the generated CRISPR-Cas9 constructs, followed by puromycin selection for 48 h. After isolation of genomic DNA from the cell pool, the respective genomic gRNA target sites were screened by PCR and the PCR products were sent for sequencing. Correct analysis also required amplification and sequencing of the unedited wild type region. For analysis, the obtained .ab1 files and the respective gRNA sequence were uploaded to the "TIDE: Tracking of Indels by Decomposition" or "ICE v2 CRISPR Analysis Tool" websites, which calculated the total mutational rate as well as InDel identity and frequency using specific algorithms.

The goodness of fit was determined using the statistical R^2 value ranging from zero to one and reliable results were obtained with $R^2>0.9$ [281].

2.2.1.11 Ligation

Ligation of DNA fragments was performed using T4 DNA ligase. The reaction was prepared in a molar ratio of 3:1 of insert to backbone as described below.

$$Mass_{Insert} = \frac{Size_{Insert}}{Size_{Backbone}} x\ Mass_{Backbone}\ x\ 3$$

Table 26. DNA ligation reaction.

Component	Amount/Volume
Backbone	50 or 100 ng
Insert	Calculated mass (3:1)
T4 DNA Ligase Buffer (10x)	2 µl
T4 DNA Ligase	1.5 µl
H_2O	Up to 20 µl

The ligation mix was incubated overnight at 16°C and was then purified using Wizard® SV Gel and PCR Clean-Up System prior to bacterial transformation.

2.2.1.12 Cloning via DNA assembly

In the absence of suitable restriction sites, cloning was performed using NEBuilder® DNA assembly. The backbone plasmid was linearized by restriction digest and the desired insert sequence was amplified by PCR with primers previously generated using the NEBuilder® Assembly Tool. These primers generate overhangs complementary to the backbone restriction site. PCR product and linearized plasmid were purified from the gel and used for DNA assembly in a molar ratio of 2:1 (Table 27).

$$Mass_{Insert} = \frac{Size_{Insert}}{Size_{Backbone}} x\ Mass_{Backbone}\ x\ 2$$

Table 27. NEBuilder DNA assembly reaction.

Component	Amount/Volume
Backbone	100 ng
Insert	Calculated mass (2:1)
NEBuilder® HiFi DNA Assembly Mastermix	10 µl
H_2O	Up to 20 µl

The reaction was incubated for 1 h at 50°C and then 2 µl were used for transformation into *E.coli*.

2.2.1.13 DNA sequencing

Sequencing of DNA samples was performed using the Mix2SeqKit from Eurofins Genomics. The samples were prepared according to the manufacturer's instructions and the sequencing results were obtained on the next day.

2.2.1.14 Droplet digital PCR

Copy numbers of transgenes were determined using droplet digital PCR (ddPCR). For this purpose, 0.25-1 µg genomic DNA was digested with the restriction enzyme HindIII according to the protocol described in section 2.2.1.7. Incubation was performed for 2 h at 37°C, followed by inactivation at 65°C for 20 min.

The PCR reaction was set up as described in Table 28. The housekeeping gene Glyceraldehyde 3-phosphate dehydrogenase (GAPDH) was used as reference gene for normalization of copy numbers.

Table 28. DdPCR reaction.

Primer/probe mix (20 µl) For ~17 reactions		**ddPCR mastermix (23 µl) For 1 reaction**	
Component	Volume	Component	Volume
ddPrimer F	3.6 µl	Digested DNA	2 µl (≙ 25-100 ng)
ddPrimer R	3.6 µl	2x ddPCR supermix for probes (no dUTP)	11.5 µl
ddProbe (FAM/HEX)	1 µl	20x target primer/probe mix (FAM)	1.15 µl
H_2O	11.8 µl	20x reference primer/probe mix (HEX)	1.15 µl
		H_2O	7.2 µl

20 µl of the ddPCR mastermix was pipetted into the respective wells of the cartridge shown in Figure 12 and 70 µl droplet generator oil was filled into the wells below.

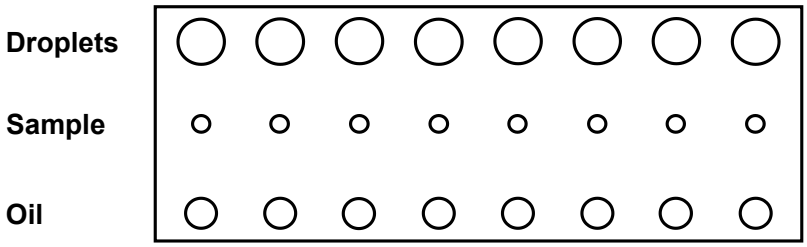

Figure 12. Cartridge filling at ddPCR.

Droplet generation was performed using the QX 200™ Droplet Generator. Afterwards, the droplets were carefully transferred to a 96-well plate and the plate was sealed with pierceable foil for 5 s at 180°C. The PCR was performed according to the cycling protocol depicted in Table 29. Droplet and copy number analysis was performed using the QX 200™ Droplet Reader and QuantaSoft™ software.

Table 29. DdPCR cycling protocol.

Step	Temperature	Duration	Cycles
Enzyme activation	95°C	10 min	1
Denaturation	94°C	30 s	40
Annealing/extension	60°C	1 min	40
Enzyme deactivation	98°C	10 min	1
Hold	4°C	infinite	1

2.2.1.15 Pyrosequencing

Activation and expression of *KRAS*^{G12D} and *TP53*^{R167H} mutations was analysed by pyrosequencing at the cDNA level. Pyrosequencing describes a method of DNA sequencing that uses single-stranded DNA to enzymatically generate the complementary strand. Each incorporated nucleotide leads to the release of pyrophosphate and generates a light reaction, which enables the analysis of point mutations or Single Nucleotide Polymorphisms (SNPs).

A certain stretch of cDNA for porcine *KRAS* or *TP53* was amplified by GoTaq or Pyromark PCR as described in section 2.2.1.4. As pyrosequencing requires the addition of biotin to the PCR product, PCR was performed using a biotinylated reverse primer. Before use, the PyroMark device was cleaned according to the machine's instructions. A new absorber strip was placed into the device and injector priming was performed. A PyroMark Q48 disc was inserted and the cavities were each loaded with 3 µl magnetic beads and 10 µl PCR product. Sequencing was performed according to the preinstalled program derived from the PyroMark Q48 Advanced and PyroMark Q48 Advanced CpG Reagents Handbook.

Afterwards, the data were analysed using the PyroMark Q48 Autoprep Software which assessed run quality (Figure 13) and calculated allele frequencies as percentage values.

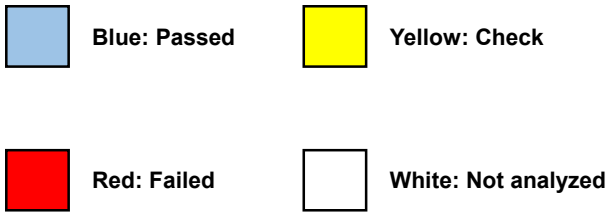

Figure 13. Pyrosequencing run quality assessment.

2.2.1.16 cDNA synthesis

For cDNA synthesis, the FastGene Scriptase II cDNA Kit was used. 30-500 ng of total RNA were reverse transcribed using random hexamer primers according to the manufacturer's protocol.

2.2.1.17 *In vitro* transcription

In vitro transcription of DNA template encoding PB transposase was performed using the mMESSAGE mMACHINE™ T7 Transcription Kit. Before transcription, 15 µg of plasmid was linearized with a single-cutter restriction enzyme. The restriction digest was then purified by NaCl purification. The *in vitro* transcription reaction was assembled according to the protocol shown in Table 30, which deviated slightly from the manufacturer's instructions, and was incubated for 4 h at 37°C.

Table 30. *In vitro* transcription reaction.

Component	Amount/Volume
NTP/CAP (2x)	10 µl
Reaction Buffer (10x)	2 µl
GTP	0.5 µl
Purified linear DNA	5 µg
Enzyme mix	2 µl
H_2O	Up to 20 µl

Afterwards, 2 µl of RNA transcript were retained for an RNA agarose control gel.

2.2.1.18 Poly(A) tailing

Polyadenylation of RNA transcripts generated by the mMESSAGE mMACHINE™ T7 Transcription Kit was performed according to the manufacturer's instructions of the Poly(A) Tailing Kit. 0.5 µl of the reaction was then taken to perform an RNA agarose control gel together with the retained sample from *in vitro* transcription.

2.2.1.19 Purification of RNA

After polyadenylation, the *in vitro* transcribed RNA was purified using the MEGAclear™ Transcription Clean-Up Kit according to the manufacturer's instructions. The purified RNA was eluted twice with 50 µl Low-EDTA-Tris buffer each and then stored at -80°C for further use.

2.2.1.20 Immunohistochemistry (IHC)

Tissues were fixed in 4% formaldehyde solution for 48 h and stored in 70% ethanol until dehydration, which was performed using Leica TP1020 tissue processor and the following protocol:

Table 31.Tissue dehydration protocol.

Step	Reagent	Duration
1	EtOH 70%	60 min
2	EtOH 70%	60 min
3	EtOH 80%	60 min
4	EtOH 96%	60 min
5	EtOH 96%	60 min
6	EtOH 100%	60 min
7	EtOH 100%	60 min
8	EtOH 100%	60 min
9	Xylene	60 min
10	Xylene	60 min
11	Paraplast	90 min
12	Paraplast	90 min

Afterwards, the samples were embedded into paraffin and sections with 2 µm thickness were prepared. Deparaffinization was performed by heating the slides at 55°C for 10 min followed by washing twice for 5 minutes in ROTI® Histol. The sections were rehydrated by washing twice in 100% ethanol, 95% ethanol, 70% ethanol, 50% ethanol and H_2O for 5 min each. For antigen demasking, the slides were boiled in 1L of citrate buffer (pH=6) for 25 min in the microwave and cooled down at RT for 30-45 min.

The slides were washed twice for 5 min in PBS and endogenous peroxidases were inactivated by 15 min incubation with 3% H_2O_2 in methanol. After washing three times for 5 min in PBS, the slides were carefully dried with a paper towel and the tissues were circled with a hydrophobic barrier pen. Permeabilization was performed by 10 min incubation with permeabilization buffer. Unspecific signals were blocked by incubation in blocking buffer for 1 h at room temperature in the dark. Afterwards, the sections were incubated with primary antibody in dilutions ranging from 1:50 to 1:200 overnight at 4°C in the dark. The next day, the slides were washed three times for 5 min in PBS and incubated with secondary antibody in 1:200 dilution for 1 h at RT in the dark. Sections were washed three times for 5 min in PBS and stained using the DAB substrate kit according to the manufacturer's instructions.

Counterstaining was performed by incubating for 1-2 min in hematoxylin followed by 5 min under flushing tap water. Samples were dehydrated at 70% ethanol, 96% ethanol, 100% ethanol and ROTI® Histol for 2 min each. Then, the slides were mounted with ROTI® Histokitt, covered with cover slips and dried overnight.

For the generation and analysis of cryo sections, the standard operating procedure of the Institute of Diabetes and Regeneration Research (IDR) at the Helmholtz Diabetes Center Munich was adapted to porcine tissue samples.

Tissues were cut into pieces of 0.5 cm and fixed in 4% formaldehyde solution at 4°C overnight. After washing with PBS, the tissue was incubated at room temperature for 4 h in PBS with 7.5% sucrose on a roller. Subsequently, the specimen was incubated at room temperature for 4-6 h in PBS containing 15% sucrose and then in 30% sucrose at 4°C overnight. The next day, the sample was transferred into a petri dish containing Tissue-Tek® O.C.T. Compound and cleaned from remaining sucrose. Afterwards, the specimen was put into a Tissue-Tek® Cryomold® and frozen on dry ice. Then, the tissue blocks were wrapped into parafilm and stored at -80°C. Sections with 12 µm thickness were prepared using the CryoStar™ NX70 Cryostat and transferred onto cryo glass slides. The sections were incubated in PBS for 30-60 min and then washed twice in PBST. Subsequently, the specimen was covered with a drop of VECTASHIELD® Antifade Mounting Medium with DAPI and the sections were analysed using the Leica TCS SP8 HyVolution 2 confocal microscope.

2.2.1.21 Hematoxylin and Eosin (H&E) staining

After embedding into paraffin, tissues were sectioned and the tissue slides were automatically stained with H&E using the Leica ST5020 Multistainer and the following protocol:

Table 32. H&E staining protocol.

Step	Reagent	Duration
1	Xylene	5 min
2	Xylene	5 min
3	EtOH 100%	5 min
4	EtOH 100%	5 min
5	EtOH 96%	2 min
6	EtOH 96%	2 min
7	EtOH 70%	2 min
8	EtOH 70%	2 min
9	Aqua distilled	30 s
10	Hematoxylin	2 min
11	Aqua distilled	15 s
12	Bluing Agent	30 s
13	Aqua distilled	30 s
14	EtOH 96%	30 s

15	Eosin	2 min
16	EtOH 96%	30 s
17	EtOH 96%	30 s
18	EtOH 100%	30 s
19	EtOH 100%	30 s
20	Xylene	1,5 min
21	Xylene	1,5 min
22	Xylene	infinite

Afterwards the tissue slides were mounted with ROTI® Histokitt, covered with cover slips and dried overnight.

2.2.2 Microbiological methods

2.2.2.1 Transformation of electrocompetent bacteria

For the introduction of plasmids into bacterial cells, electroporation was used. An aliquot containing 50 µl electrocompetent E.coli DH10B cells was thawed on ice before it was mixed with the plasmid or ligation product. For cloning, 5 µl and 2 µl were used for purified and non-purified ligation products. Retransformation of already existing plasmids was carried out with 1 µl of a 1:10,000 dilution. The respective amount of plasmid was added to the bacteria and the suspension was transferred into a precooled electroporation cuvette with 2 mm gap width. The bacteria were electroporated for 5 ms at 2500 V and then immediately mixed with 1 ml LB medium. The bacterial suspension was transferred into a 2 ml tube and incubated for 45-60 min at 37°C and 210 rpm. Subsequently, 50-200 µl of the bacterial suspension was plated onto LB agar plates containing 100 µg/ml ampicillin. The plates were incubated overnight at 37°C and checked the next day for growth of bacterial colonies.

2.2.2.2 Colony PCR

Bacterial colonies carrying the correct plasmid were identified by Colony PCR. Single bacterial colonies were picked with a pipette tip and spread out on a new agar plate containing the respective antibiotic and resuspended in 30 µl TTE buffer. The mixture was then heated for 5 min at 95°C for bacterial lysis. Colony PCR was performed using GoTaq® G2 DNA Polymerase according to the protocol described in Table 20 with primers binding in the insert and plasmid backbone and 2 µl of the lysed TTE-bacterial mixture as DNA template.

2.2.2.3 Cultivation of bacteria

Besides incubation on LB agar plates containing ampicillin, bacterial cells were also cultivated as liquid overnight cultures for plasmid isolation via midiprep. Therefore, 100 ml LB medium containing 100 µg/ml ampicillin were prepared in a 500 ml or 1000 ml flask.

Then, the cells were transferred into the flask by dropping a pipette tip into it, that was either used to pick one single bacterial colony from the LB agar plate or to dip into a glycerol stock of previously preserved bacteria. The liquid bacterial culture was incubated overnight at 37°C and 210 rpm.

2.2.2.4 Preservation of bacteria

Long-term storage of bacterial cultures that contain a plasmid of interest was performed by cryoconservation. Therefore, 500 µl bacterial culture were mixed with 500 µl 99% glycerine and stored at -80°C.

2.2.3 Cell culture methods

2.2.3.1 Isolation of porcine cells

Porcine kidney fibroblasts (PKFs) were isolated from kidneys of German Landrace pigs from the TUM experimental facility in Thalhausen or a slaughterhouse. Porcine ear fibroblasts (PEFs) were isolated from a piece of porcine ear tissue. After removal of fat and blood, a 1 cm piece of tissue was cut from the inside of the kidney and washed twice with 80% EtOH and PBS. The piece was cut into small pieces using sterile scissors and washed with PBS until the supernatant became clear. The pieces were then transferred into an Erlenmeyer flask containing 10 ml collagenase Type IA (10 mg/ml) and incubated for 30 min at 37°C while stirring. Afterwards, medium was added and the cells were centrifuged for 5 min at 300 x g. The supernatant was discarded and the cell pellet was resuspended in an appropriate amount of medium and distributed onto three to five T-150 flasks. During the first week after isolation, the cultivation medium contained P/S and amphotericin B and was exchanged every day. The cells were then cultured in antibiotic-free medium and tested for mycoplasma.

2.2.3.2 Cultivation of porcine cells

PKFs, PEFs and PADMSCs were cultured in DMEM containing 20% FBS, 1x NEAA, 2 mM Ala-Gln and 1 mM sodium pyruvate solution at 37°C and 5% CO_2 in a humidified Steri-Cycle CO_2 incubator. All cell culture works were performed in a sterile class 2 laminar flow hood. The cell culture medium was exchanged every 2-3 days.

2.2.3.3 Passaging of porcine cells

The cells were passaged when reaching 80-90% confluence. The medium was aspirated, cells were washed with PBS and then incubated with accutase at 37°C for 5-10 min. The detachment reaction was stopped by adding at least the same volume of cell culture medium. The cells were separated by pipetting up and down and were either transferred to a new culture vessel or used for cell counting, transfection, freezing or DNA/RNA isolation.

2.2.3.4 Counting of porcine cells

After detachment, 10 µl of cell suspension was mixed with 10 µl of trypan blue stain (0.4%). Of this mixture, 10 µl were transferred into a Countess™ Cell Counting Chamber Slides for automatic cell counting using the Countess™ Automated Cell Counter, which determined the total cell density, concentration of dead and living cells and cell viability. Alternatively, cells were counted manually with the help of a C-Chip Neubauer improved cell counting chamber.

2.2.3.5 DNA transfection

DNA transfection of PKFs and PADMSCs was performed by electroporation. Therefore, 4-6 µg of DNA was mixed with 100 µl of electroporation solution. After detachment, 0.5-1 million cells were centrifuged for 5 min at 300 x g. The supernatant was aspirated, the cell pellet was resuspended in the electroporation mixture and transferred into an electroporation cuvette with 2 mm gap width. Cells were transfected using the BTX ECM 830 Electro Square Porator at 300 V with two pulses and a pulse length of 1 ms each. Afterwards, the cuvette was flushed with 500 µl cell culture medium to transfer all cells into a T-25 flask containing 4.5 ml of medium. The next day, cells were washed with PBS and puromycin selection was started for 48 h.

PEFs were transfected by lipofection. The day before lipofection, the cells were seeded on 6-well plates at 30% density. The next day, the cell culture medium was removed, cells were washed with PBS and 1 ml of Opti-MEM was added to the respective wells. For each reaction, two mixtures were prepared, containing 50 µl Opti-MEM with 1 µl Lipofectamine 2000 and 50 µl Opti-MEM with 1 µg DNA, respectively. The mixtures were incubated for 5 min at RT and then the lipofection mix was added dropwise to the DNA mixture followed by incubation for 25 min at RT. Afterwards, the complete mixture was dropped onto the cells by holding the 6-well plate transversely. After 4-5 h cultivation in the incubator, 1 ml of cell culture medium was added. The next day, cells were washed with PBS and puromycin selection was started for 48 h.

2.2.3.6 Cre protein transduction

Cre protein was produced by Érica Schulze. For efficient Cre recombination, cells were transduced with 2 µM Cre protein using Lipofectamine 2000 as described in section 2.2.3.5.

2.2.3.7 Selection of stable transfected cells

Cell clones with stable transgene integration were identified by selecting for the presence of the neomycin and blasticidin resistance genes using the antibiotics geneticin (G418) and blasticidin S, respectively. The selection was started 24 h after transfection with an antibiotic concentration that had previously been determined for the respective cell type in a killing curve.

Media change was performed every second day and the selection was stopped after 21-28 days.

2.2.3.8 Isolation of single cell clones

For isolation of single cell clones, $1x10^3$ cells were seeded per 150 mm cell culture dish containing 20 ml of cell culture medium. After 7-10 days, well separated single cell clones were marked with the help of the microscope and the cells were washed with PBS.
Self-made cloning rings were dipped into silicone grease, placed onto the marked cell clones and lightly pressed on using sterile tweezers. Accutase was added into the cloning rings and the cells were incubated for 5-10 min at 37°C until they had detached. The reaction was stopped by adding cell culture medium and the cell suspension was pipetted up and down before being transferred to a 24-well plate containing 500 µl of cell culture medium in each well. Isolated cell clones were incubated at 37°C and 5% CO_2 until they reached confluence and were then used for cell clone analysis and expansion.

2.2.3.9 Cryopreservation of porcine cells

For cryopreservation, the cells were detached and centrifuged for 5 min at 300 x g. The cell pellet was resuspended in 1 ml cold cryomedium containing 70% FBS, 20% cell culture medium and 10% DMSO, transferred into a cryovial and slowly frozen to -80°C using a Mr. Frosty Freezing Container. Long-term storage was performed in liquid nitrogen tanks.

2.2.3.10 Thawing of cryopreserved porcine cells

Cryopreserved cells were thawed in a water bath at 37°C and then transferred into a 15 ml falcon containing 5 ml cell culture medium. After centrifugation for 5 min at 300 x g, the supernatant was aspirated and the cell pellet was resuspended in 2 ml cell culture medium and transferred into an appropriate cell culture vessel.

2.2.3.11 Preparation of porcine cells for SCNT

One week before embryo transfer, the cells were seeded on a 96-well plate at densities of 6.25%, 12%, 25%, 35% and 50% and cultivated in standard cell culture medium. Two days before SCNT, the cells were washed twice with PBS and starvation medium containing 0.5% FBS was added to induce cell cycle synchronization. Then, the cell clones were sent for SCNT, which was performed by Prof. Dr. Valeri Zakhartchenko and Dr. Mayuko Kurome (Chair of Molecular Animal Breeding and Biotechnology, Munich). Embryo transfer into recipient sows was performed by Dr. Barbara Kessler (Chair of Molecular Animal Breeding and Biotechnology, Munich).

2.2.3.12 Microinjection

Oocytes were isolated from porcine ovaries and *in vitro* maturation (IVM) and fertilisation (IVF) was performed. Prior to microinjection, hyPB-Transposase-T2A-mCherry mRNA and mPdx1-iCre transposon plasmid DNA were freshly mixed in sterile low tris EDTA buffer at concentrations of 5 ng/µl and 7.5 ng/µl, respectively. Subsequently, ~10 picoliter (pl) of the transposon mixture were injected into the cytoplasm of the porcine zygotes. Injected zygotes were incubated in a triple gas incubator (5% O_2, 5% CO_2, 90% N_2) at 38.5°C for 12-36 h before being transferred into synchronised recipient sows. Oocyte collection, IVM, IVF and microinjection was performed by Dr. Bernhard Klinger, Thomas Winogrodzki, Liang Wei and Alexander Carrapeiro. Embryo transfer was performed by Dr. Bernhard Klinger or Dr. Barbara Kessler (Chair of Molecular Animal Breeding and Biotechnology, Munich).

2.2.3.13 Porcine pancreatic acinar cell culture

2.2.3.13.1 Isolation of porcine pancreatic acinar cells

The protocol for the isolation of porcine pancreatic acinar cells was based on the isolation protocol for mice by Lubeseder et al. [282], and was kindly provided by Thorsten Neuß (Klinikum rechts der Isar, TUM, Munich). Initial adjustments to the pig were made by Kirsten Goijvaerts as part of her master's thesis and were then further optimised by Alexander Carrapeiro and Daniela Kalla. The optimal yield of acinar cells was achieved by using pancreata from 4-5 weeks old pigs. The pancreas was removed immediately after the death of the piglet and transferred to a petri dish, where a ~1.5 cm piece was cut off. The piece was briefly washed in 80% EtOH and then twice in PBS+1%P/S. Afterwards, the piece was transferred into a beaker glass containing 7 ml SOL2. The solution was taken up using a sterile 5 ml syringe and injected several times into the tissue until bubbles formed. The piece was cut into 1-2 mm small pieces using sterile scissors, transferred into a 10 cm cell culture dish and incubated for 5 min at 37°C and 5% CO_2 with occasional shaking. The content was then transferred into a 50 ml falcon and pipetted up and down several times using a serological 10 ml pipette. The dish was washed with a volume of 12 ml, which was then added to the suspension in the falcon. The falcon was centrifuged for 5 min at 20 x g and 18°C and the supernatant was carefully removed using a serological 25 ml pipette. The pellet was resuspended in 7 ml SOL2 and pipetted up and down several times, before it was transferred to a fresh 10 cm cell culture dish and incubated for 10 min at 37°C and 5% CO_2 with occasional shaking. In the meantime, a mesh filter with 200 µm mesh size was placed onto a 50 ml falcon and wetted with 1 ml SOL1. After incubation, the cell suspension was pipetted onto the mesh filter. The mesh filter was washed twice with 5 ml SOL1 and in between, the tissue was pressed through the filter using a syringe piston. The falcon was centrifuged for 5 min at 20 x g and 18°C and the supernatant was removed with a serological 25 ml pipette.

The cell pellet was carefully aspirated in 20 ml wash solution and transferred into a fresh 50 ml falcon, which was then centrifuged for 5 min at 20 x g and 18°C. This washing step was repeated three times. After centrifugation and removal of the supernatant, the pellet was resuspended in 1 ml acinar cell recovery medium and transferred into the well of a 6-well plate. The falcon was washed with a volume of 1 ml, which was then added to the well. Pancreatic acinar cell clusters where checked under the microscope and the plate was incubated for 60 min at 37°C and 5% CO_2 for cell recovery. During this recovery step, the first collagen layer for the 3D acinar cell culture was prepared according to the following protocol shown in Table 33.

Table 33. Pipetting scheme for 1st and 3rd collagen layer of the 3D collagen system.

Pipetting order	Reagent	Stock	Volume	Final concentration
1.	Cell culture grade H_2O	Not specified	Up to total volume	Not specified
2.	PBS	10x	1/10 of total volume	1x
3.	NaOH	1 M	$\mu l_{Collagen}$ x 0.023	Not specified
4.	Collagen Type I, Rat tail	Depends on LOT	X µl	2.5 mg/ml

After rapid mixing on ice, 150 µl of the solution was pipetted into each well of a 48-well plate using a 200 µl pipette and distributed over the entire bottom of the well using the pipette tip. To harden the collagen, the plate was incubated at for 45 min at 37°C and 5% CO_2. After acinar cell recovery, the cell suspension was collected from the 6-well plate and transferred into a 15 ml falcon. The well was flushed with 1 ml acinar cell recovery medium to collect all remaining cells. The falcon was centrifuged for 5 min at 20 x g and 18°C and the supernatant was carefully removed using a 1000 µl pipette. The cell pellet was then resuspended in an appropriate volume of acinar cell culture medium so that the pipette tip was easily visible in the cell suspension. A certain volume of cell suspension was saved for nucleic acid isolation of day 0 sample. For the second collagen layer, the same volume (vol) of collagen and the corresponding amount of NaOH was added to the cell suspension according to the following protocol:

2^{nd} collagen layer = 1 vol cell suspension + 1 vol collagen + $\mu l_{Collagen}$ x 0.023 1M NaOH

150 µl was pipetted into each pre-coated well and the cell-collagen mixture was carefully distributed over the entire surface of the well with the pipette tip without destroying the 1st collagen layer. The second layer was cured for 45-60 min at 37°C and 5% CO_2. The 3rd collagen layer was then mixed according to the protocol in Table 33 and carefully spread over the second layer. After another hardening step, the wells were covered with 350 µl acinar cell culture medium each.

2.2.3.13.2 Culture of pancreatic acinar cells

Porcine pancreatic acinar cells were cultured up to one week. The effect on transdifferentiation was tested for four different culture conditions: 100 ng/ml TGF-α, 50 ng/ml TGF-β1, 20 ng/ml IL-17A and untreated. Media change was performed on the first, third and fifth day after isolation. Old medium was carefully removed from the well using a 1000 µl pipette and fresh medium was added by slow pipetting against the wall of the well.

The transdifferentiation rate was evaluated mainly on day two by manual counting of acinar cell clusters and ADM structures within selected facial fields:

$$ADM\ in\ \% = \frac{Number\ of\ acinar\ cell\ clusters}{Number\ of\ transdifferentiated\ structures}\ x\ 100\%$$

2.2.3.13.3 Transduction of pancreatic acinar cells

Transduction with Cre virus-like particles (VLPs) or Cre lentivirus (LV) was performed during the acinar cell recovery step. Cre VLPs were produced by Dr. Tatiana Flisikowska from the chair of livestock biotechnology (TUM). For transduction with VLPs, the cells were either incubated in 1 ml Cre VLP supernatant or in 2 ml cell culture medium+30% FBS containing 20 µl concentrated Cre VLP. In addition, the cells were embedded into the 2nd collagen layer containing 30 µl of concentrated Cre VLP.

A non-integrating LV expressing Cre recombinase under the control of the spleen focus forming virus (SFFV) promoter was kindly provided by Dr. Marcel Rommel from Paul-Ehrlich-Institute (viral titer: 2.3x10^4 TU/µl). For transduction with Cre LV, 15 µl TransDux virus transduction reagent were mixed with 15 µl of non-integrating Cre LV and added to the acinar cells residing in 1 ml acinar cell recovery medium during the recovery step. Afterwards, the cells were embedded into the 2nd collagen layer containing an additional mixture of 15 µl TransDux virus transduction reagent and 15 µl Cre LV.

2.2.3.13.4 Recovery of pancreatic acinar cells from collagen discs

The collagen discs were usually recovered for nucleic acid isolation on the second, third and sixth day after isolation. Medium from the 48-well plate was removed and the collagen discs were carefully removed from the wells using a small spoon. Collagen discs from 3 wells of a 48-well plate were combined into one 15 ml falcon, which were then filled with 1 ml SOL2. The falcons were fixed horizontally on a shaker and shaken for 10-15 min at 37°C and 60 rpm. After addition of 2 ml PBS per tube, the falcons were centrifuged for 5 min at 300 x g. The supernatant was aspirated and the cell pellets were used for nucleic acid isolation via SurePrep™ RNA/DNA/Protein Purification Kit or TRIzol reagent.

3 Results

Pancreatic cancer is a devastating disease characterised by late diagnosis and very poor prognosis, thus requiring improvements in early detection and treatment strategies. Based on the murine model from Hingorani et al. [163], Schnieke and colleagues have generated pigs carrying latent *KRAS*^{G12D} and *TP53*^{R167H} mutations, which are orthologues of the most common mutations found in human PDAC disease [177, 178]. As shown in Figure 14, the mutations were targeted into exons 2 and 5 of the endogenous porcine *KRAS* and *TP53* genes, respectively, and have been silenced by a preceding lox-stop-lox (LSL) cassette. Activation of these mutations can be achieved by Cre recombination, which leads to excision of the LSL cassette und thus to expression of the downstream mutations.

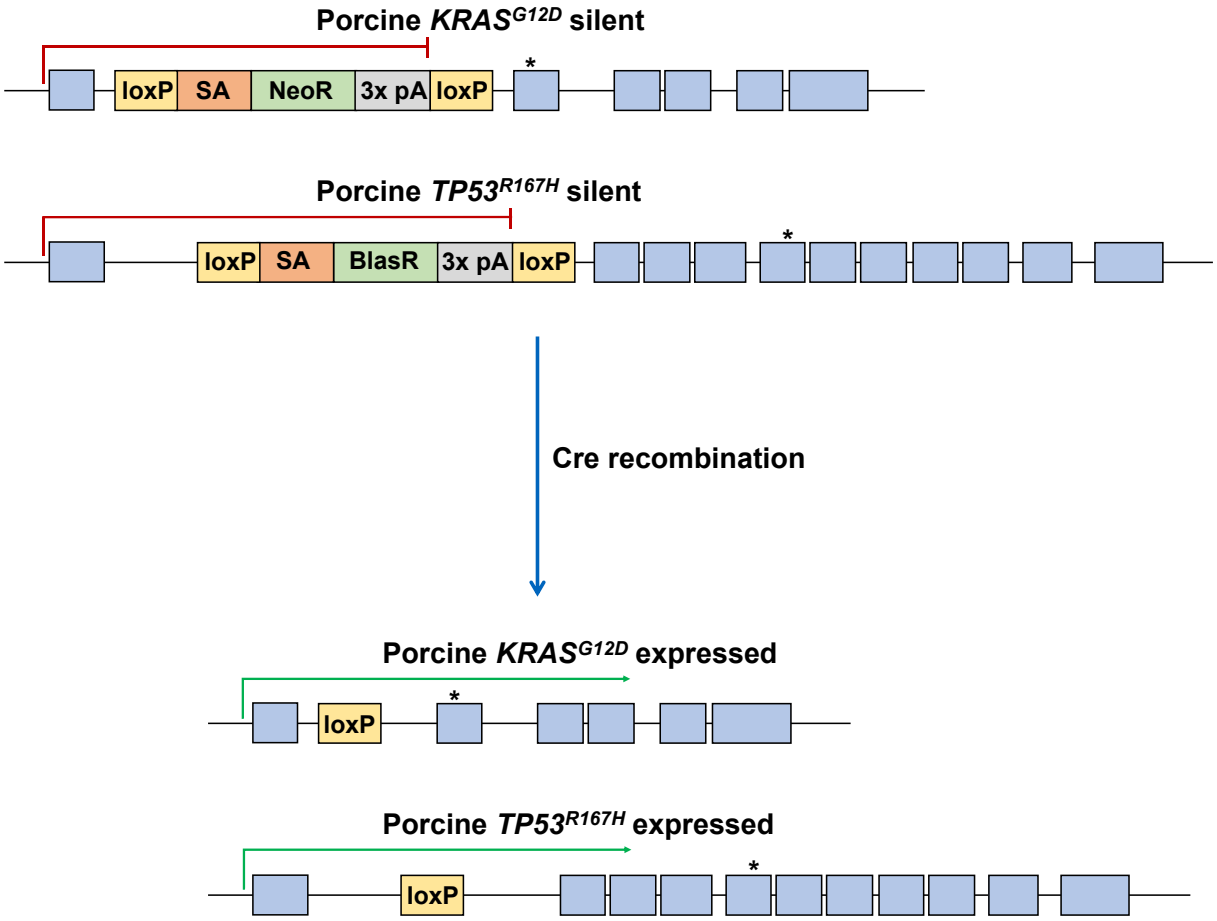

Figure 14. Activation of porcine *KRAS*^{G12D} and *TP53*^{R167H} by Cre recombination. Blue box: exon; loxP: loxP site; SA: splice acceptor; NeoR: neomycin resistance gene; BlasR: blasticidin resistance gene; pA: polyA; *: mutation

But so far, no tissue-specific porcine Cre-driver line existed. The main objective of this thesis was therefore to generate transgenic pigs with pancreas-specific Cre expression. This would then allow the generation of a porcine model for pancreatic ductal adenocarcinoma (PDAC), which should recapitulate the human disease phenotype.

The generation of Cre driver lines for PDAC modelling requires the expression of Cre recombinase from a pancreas-specific promoter. In mice, the transcription factors Pdx1 and Ptf1a are expressed from embryonic day 8.5 and 9.5 in all developing cells of the murine pancreas and become later restricted to islet and acinar cells, respectively [151, 283] (Figure 15). Thus, expression of Cre recombinase driven by *Pdx1* or *Ptf1a* promoters will result in recombination of mutated *Kras* and *Trp53* alleles in all pancreatic cell types. Indeed, it has been shown that crossing mice carrying latent $Kras^{LSLG12D}$ with *Pdx1-Cre* or *Ptf1a-Cre* mice leads to activation of $Kras^{G12D}$ mutation in the pancreas [162].

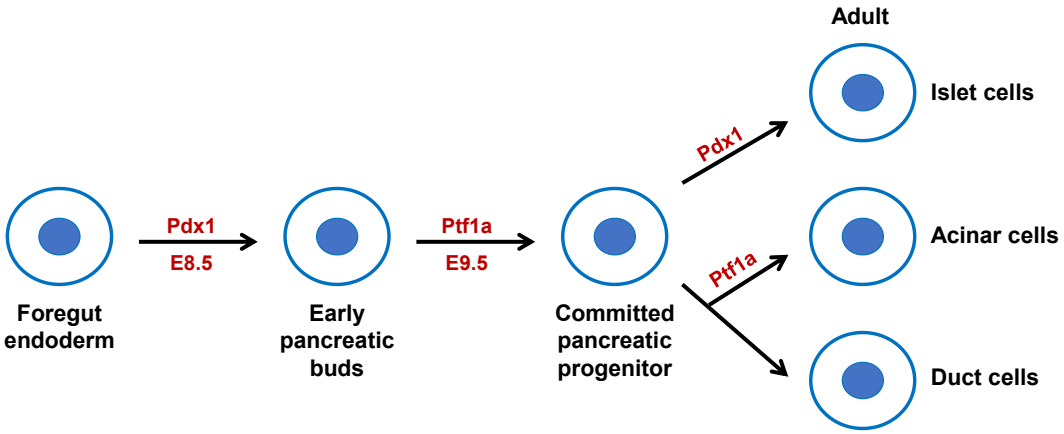

Figure 15. The developing mouse pancreas. Illustration adapted from Hingorani et al. (2003) and Ijichi (2011) [162, 284].

Based on these findings, sections 3.1 and 3.2 describe the generation of porcine Cre driver lines using either the endogenous porcine *PTF1A* or the murine *Pdx1* promoter for pancreas-specific expression of iCre recombinase. Founder animals were characterised by expression analysis and were then used for crossbreeding with dual-fluorescent reporter pigs and $KRAS^{LSLG12D}$ and $TP53^{LSLR167H}$ pigs to assess tissue-specificity of Cre recombination as well as mutational activation and tumour formation.

As an alternative to developing Cre driver lines to model tumour formation in the pig, section 3.3 focuses on the transformation and retransplantation of porcine cells. Therefore, polycistronic tRNA-gRNA (PTG) constructs were generated and evaluated for multiplexed CRISPR/Cas9-mediated activation of $KRAS^{G12D}$ and $TP53^{R167H}$ and inactivation of porcine *TP53*, *p16*, *SMAD4*, *BRCA2* and *B2M* genes.

Another aim of this work was to mimic the transdifferentiation of acinar cells towards a ductal-like phenotype via acinar-to-ductal metaplasia (ADM) *in vitro*. Therefore, section 3.4 describes the establishment of porcine pancreatic acinar cell isolation and culture. In this process, a 3D cell culture system was used to study the effects of different cytokines on the transdifferentiation rate of acinar cells.

3.1 Generation of a porcine PDAC model using *PTF1A^{iCre}* pigs

As mentioned above, the major goal of this work was to generate a porcine model for human PDAC. Therefore, Schnieke and colleagues have generated pigs carrying latent *KRAS^{G12D}* and *TP53^{R167H}* mutations [177, 178], which can be activated by breeding with pigs expressing Cre recombinase in the porcine pancreas. Thus, one of the main objectives was the generation of porcine Cre driver lines. As the transcription factor Ptf1a was shown to be expressed during early pancreatic organogenesis in all pancreatic cell types in mice [151], a part of this project was to generate pigs expressing iCre recombinase from the endogenous *PTF1A* promoter. The resulting Cre driver pigs can then be bred with *KRAS^{LSLG12D}* and *TP53^{LSLR167H}* mutant animals to model PDAC.

3.1.1 Generation of *PTF1A^{iCre}* pigs

To generate *PTF1A^{iCre}* driver pig lines, the iCre recombinase gene was targeted into the endogenous porcine *PTF1A* locus using CRISPR/Cas9 systems. The first strategy aimed at targeting of iCre recombinase into the 5'end of *PTF1A* to achieve expression at endogenous levels. However, targeting into the 5'end leads to disruption of the respective *PTF1A* allele and thus had to be strictly limited to one allele due to the importance of *PTF1A* expression for development. Since possible detrimental effects of reduced *PTF1A* expression on pig development could not be completely excluded, a second strategy aimed at targeting of iCre into the 3'end of *PTF1A* to preserve the function of the targeted *PTF1A* allele. Some of the data described in sections 3.1.1.4, 3.1.2.1 and 3.1.2.2 have already been published during the completion of this thesis (The missing link: Cre pigs for cancer research; frontiers in Oncology; Kalla et al. [285]) and are shown here in adapted form.

3.1.1.1 *PTF1A* 5'end targeting

For targeting into the 5'end of porcine *PTF1A*, different gRNAs binding in exon 1 were designed and tested by Alessandro Grodziecki [286]. The most efficient gRNA, binding 47 bp after the start codon, was then selected for CRISPR/Cas9-mediated homology-directed repair (HDR). As mentioned in section 1.2, expression of *PTF1A* is essential for pancreatic cell fate and development. As targeting of exon 1 leads to disruption of the respective *PTF1A* allele, it was crucial that only one allele was modified. However, as shown in my master thesis [287], in addition to monoallelic integration of iCre, transfection of pX330-hSpCas9-PTF1A_Ex1_gRNA4 plasmid in combination with a conventional targeting vector also led to InDel mutations of the second *PTF1A* allele. This introduced premature stop codons resulting in an inactivation of both alleles. In order to maintain the integrity of the second *PTF1A* allele, targeting of iCre into the first exon was now performed by using Cas9 nickase (Cas9n).

Cas9n generates only single-strand breaks and in turn causes less mutagenic end-joining than DNA double-strand breaks (DSBs) [288, 289]. Regarding iCre integration, the efficiency of Cas9n-mediated HDR can be increased with the help of a double cut donor template [290, 291]. Therefore, a vector was generated, consisting of two exon 1 gRNA target sites (gRNA+PAM) flanking the *PTF1A* homology arms and iCre-polyA (Figure 16).

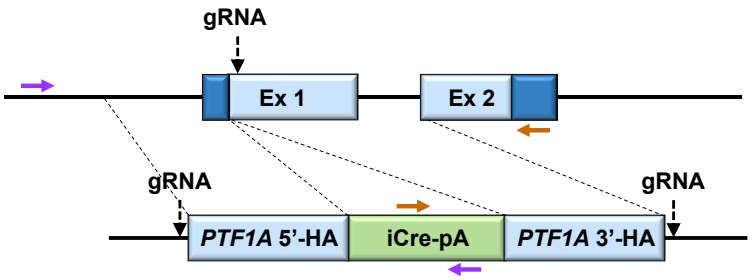

Figure 16. *PTF1A* 5'end targeting using Cas9n and double cut donor template. Targeting into the first exon of porcine *PTF1A* was achieved by using Cas9n in combination with a double cut donor template containing exon 1 gRNA target sites flanking the two homology arms. Primer positions for 5' and 3'screening PCRs are indicated as purple and brown arrows, respectively. Ex: exon; HA: homology arm; pA: polyA

For the generation of *PTF1A*$^{5'iCre}$ pigs, male porcine kidney fibroblast (PKF) 120419-7 cells were transfected with pX462-hSpCas9n(D10A)-PTF1A_Ex1_gRNA4 plasmid and the double cut donor template shown in Figure 16. Afterwards, correct iCre placement into *PTF1A* was determined by 5' and 3'junction PCRs (Supplementary figure 11A+B). The PCRs revealed that 25% of all screened single cell clones were positive for 5'targeting, of which 89% also showed correct 3'targeting. Monoallelic integration was confirmed by combination of endogenous PCR and ddPCR for iCre copy number determination (Supplementary figure 11C+D).

3.1.1.2 *PTF1A* 3'end targeting

In addition to integration into the first exon, a second strategy aimed at integrating iCre into the 3'end of porcine *PTF1A*. In contrast to 5'end targeting, integration into the 3'UTR does not lead to a loss of the targeted *PTF1A* allele but instead allows simultaneous expression of both *PTF1A* alleles together with iCre recombinase. For targeting into the 3'UTR of *PTF1A*, three different gRNAs were selected for efficiency testing, all of which bind in the 3'UTR between 29-35 bp downstream of the stop codon (Figure 17).

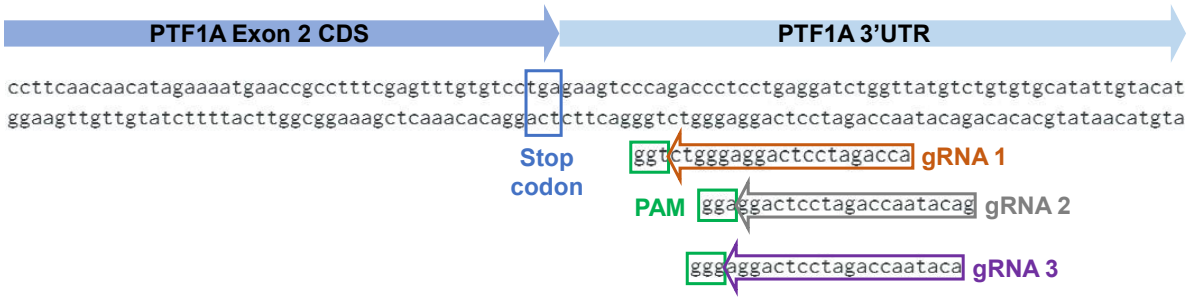

Figure 17. Binding sites of *PTF1A* 3'UTR gRNAs.

All three tested gRNAs showed similar efficiencies, with the highest score for PTF1A gRNA 3 (Table 34). As NHEJ-induced InDel mutations in the 3'UTR should not result in a loss of expression of the functional protein from the second allele, conventional Cas9 nuclease could be used for cleavage and a pX330-hSpCas9-PTF1A_3'UTR_gRNA3 plasmid was generated.

Table 34. gRNA efficiency results for *PTF1A* 3'UTR editing.

gRNA	gRNA target site	InDel efficiency	R^2 value
PTF1A gRNA 1	PTF1A 3'UTR	71.8%	0.97
	PTF1A 3'UTR	68.2%	0.94
PTF1A gRNA 2	PTF1A 3'UTR	76.4%	0.87
	PTF1A 3'UTR	79.0%	0.89
PTF1A gRNA 3	PTF1A 3'UTR	92.2%	0.99
	PTF1A 3'UTR	85.4%	0.9

In order to achieve expression of iCre from the 3'end of *PTF1A*, targeting vector generation required the removal of the stop codon after the second *PTF1A* exon. In addition, a "self-cleaving" peptide from thosea asigna virus 2A (T2A) was introduced upstream of iCre to allow polycistronic expression of iCre recombinase from the porcine *PTF1A* locus [292] (Figure 18). As with 5'end targeting, HDR efficiency for integrating iCre into the 3'end should also be increased by using a double cut donor template [291].

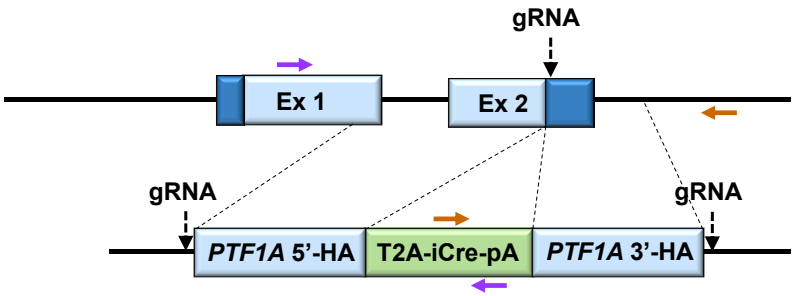

Figure 18. *PTF1A* 3'end targeting using Cas9 and double cut donor template. Targeting into the 3'UTR of porcine *PTF1A* was achieved by using conventional Cas9 nuclease in combination with a double cut donor template containing 3'UTR gRNA target sites flanking the two homology arms and a T2A peptide sequence in front of iCre. Primer positions for 5' and 3'screening PCRs are indicated as purple and brown arrows, respectively. Ex: exon; HA: homology arm; pA: polyA

Targeting of iCre-pA into *PTF1A* 3'UTR was performed by transfecting male porcine adipose-derived mesenchymal stem cells (PADMSCs) 110111 with pX330-hSpCas9-PTF1A_3'UTR_gRNA3 plasmid and the double cut donor construct depicted in Figure 18. Afterwards, correct iCre placement into *PTF1A* was determined by 5' and 3'junction PCRs (Supplementary figure 12A+B). Precise 5'targeting was only found in 11% of all cell clones examined, of which solely 40% were also correctly 3'targeted. The positive cell clones were further analysed by endogenous PCR and ddPCR (Supplementary figure 12C+D).

3.1.1.2.1 Inducible Cre recombinase for *PTF1A* 3'end targeting

The *PTF1A* 3'end targeting strategy was also used to generate an inducible Cre driver pig line for spatiotemporal control of iCre expression. For this, iCre recombinase was fused to the ligand binding domain of the triple mutant human oestrogen receptor (iCre-ER^{T2}). As described in section 1.6.1, this mutated binding domain only responds to synthetic ligands like 4-hydroxytamoxifen (4-OHT) but not to endogenous oestrogen and can therefore be used to switch on iCre expression by administration of 4-OHT. However, Cre-ER^{T2} has been repeatedly reported to be leaky in mice [293, 294].

Hence, two different constructs, fusion of iCre to one or two ER^{T2} domains, were generated and compared (Figure 19). Prior to the possible generation of genetically modified pigs the iCre-ER^{T2} and ER^{T2}-iCre-ER^{T2} systems were first tested for efficiency and leakiness *in vitro*. For this purpose, PKF #270 cells (*R26*$^{mT\text{-}mG/WT}$) were transfected with the PGK-iCre-ER^{T2}-pA and PGK-ER^{T2}-iCre-ER^{T2}-pA plasmids shown below (Figure 19).

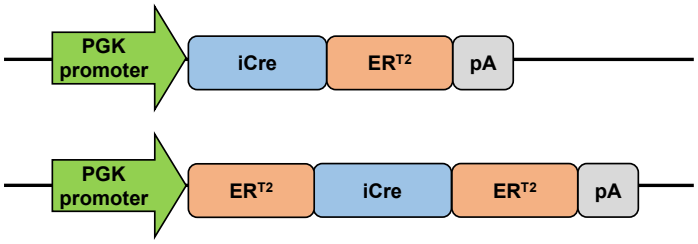

Figure 19. Structure of the iCre-ER^{T2} and ER^{T2}-iCre-ER^{T2} expression vectors.

PKF #270 cells were isolated from a dual-fluorescent reporter pig carrying a floxed membrane-targeted Tomato fluorescence cassette (mTomato) followed by membrane-targeted GFP (mGFP) placed at the porcine *ROSA26* (R26) gene locus [295]. In the absence of Cre recombination the cells show red fluorescence. Recombination leads to an excision of the mTomato cassette and thus to a switch to green fluorescence (Figure 20A).

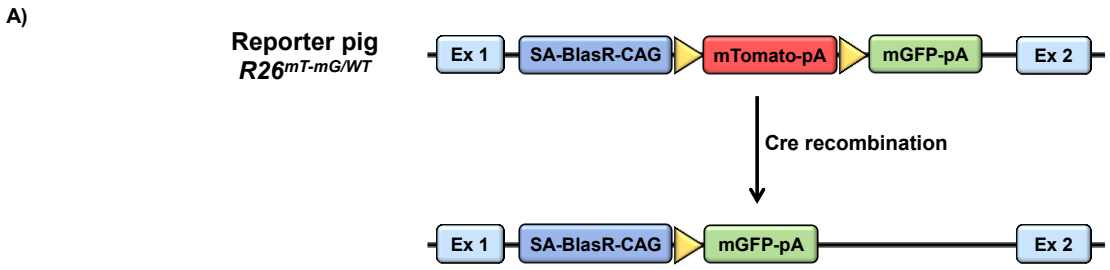

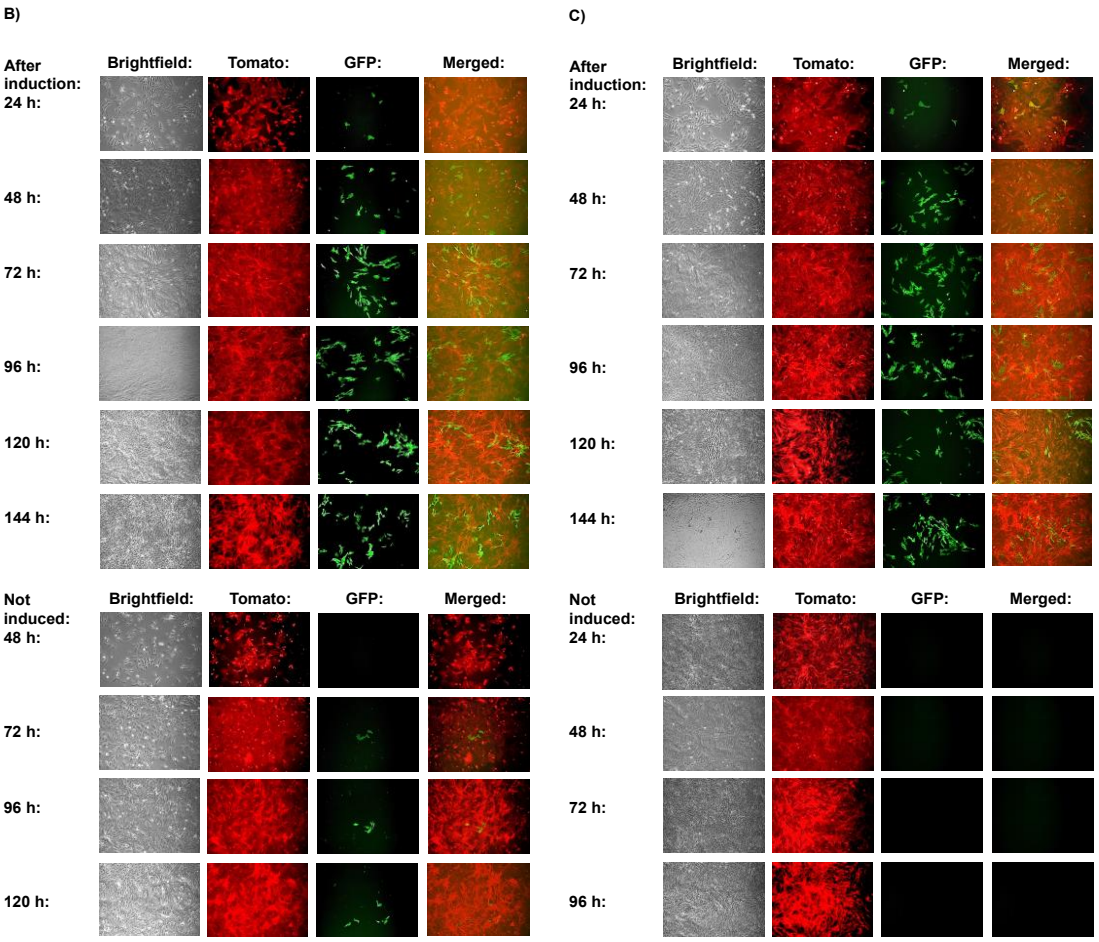

Figure 20. Fluorescence microscopy results of 4-OHT induction experiment. (A) Dual fluorescence reporter cassette placed at the porcine *R26* locus. Cre recombination results in excision of the floxed mTomato sequence leading to a switch from red to green fluorescence. The efficiencies of the tamoxifen-inducible iCre systems were assessed by induction with 4-OHT. (B) Fluorescence microscopy of PKF #270 cells transfected with PGK-iCre-ER^{T2}-pA plasmid. (C) Fluorescence microscopy of PKF #270 cells transfected with PGK-ER^{T2}-iCre-ER^{T2}-pA plasmid. Ex: exon, SA: splice acceptor, BlasR: blasticidin resistance gene, CAG: CAG promoter, pA. polyA, triangle: loxP site

In order to test the efficiency and leakiness of the above mentioned tamoxifen-inducible systems, the cells were induced with 1 µM 4-OHT 24 h after transfection and the fluorescence was evaluated by microscopy for a time period of 6 days (Figure 20B+C). Switching to green fluorescence for both PGK-iCre-ER^{T2}-pA and PGK-ER^{T2}-iCre-ER^{T2}-pA transfected cells was observed from 24 h after induction. As expected, the recombined cells were dually labelled, as it has been reported that red fluorescence persists for up to 8 and 9.2 days in dual-fluorescent pig and mouse cells, respectively [295, 296]. The leakiness of both systems was tested using control cells that were transfected with the respective plasmid but not induced with 4-OHT (Figure 20B+C, lower panels). In fact, the presence of only one ER^{T2} site was found to be slightly leaky (Figure 20B, lower panel), while the presence of two ER^{T2} sites efficiently prevented recombination in the absence of 4-OHT (Figure 20C, lower panel).

Since the size of the targeting vector could be minimised by using only one ER^{T2} site, a T2A-iCre-ER^{T2} double cut donor template was generated for targeting into *PTF1A* 3'UTR (Figure 21).

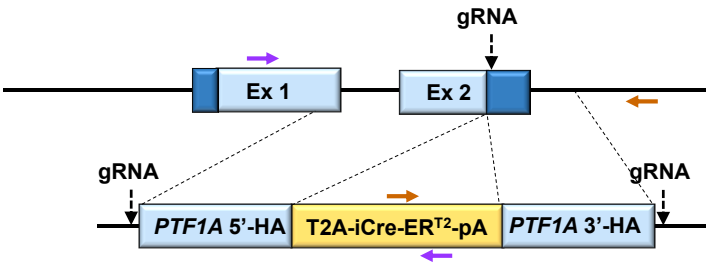

Figure 21. *PTF1A* 3'end targeting for inducible Cre driver line generation. Primer positions for 5' and 3'screening PCRs are indicated as purple and brown arrows, respectively.

For the generation of a 4-OHT inducible Cre driver pig line for spatiotemporal control of iCre expression, male PKF #270 cells were transfected with pX330-hSpCas9-PTF1A_3'UTR_gRNA3 plasmid and T2A-iCre-ER^{T2} double cut donor template (Figure 21). Of all screened cell clones, 20% revealed correct 5'targeting, of which 80% were also precisely 3'targeted (Supplementary figure 13A+B). Further analysis of the cell clones was performed by endogenous PCR and ddPCR (Supplementary figure 13C+D).

3.1.1.3 Generation of *PTF1A^{iCre}* pigs by SCNT

For the generation of *PTF1A^{iCre}* pigs, two PKF 120419-7 cell clones for *PTF1A* 5'end targeting with one copy of iCre each, and three PADMSC 110111 cell clones for *PTF1A* 3'UTR targeting with two, four and seven iCre copies, were selected. The cell clones were mixed and sent for SCNT, which was performed by Prof. Dr. Valeri Zakhartchenko and Dr. Mayuko Kurome (Chair of Molecular Animal Breeding and Biotechnology, Munich). 111 reconstituted embryos were generated and transferred into two recipient sows (performed by Dr. Barbara Kessler, Chair of Molecular Animal Breeding and Biotechnology, Munich). After a gestation period of 115 days, both sows gave birth to a total of nine male piglets, three of which were stillborn (Table 35). PKF #270 cell clones with T2A-iCre-ER^{T2} targeting into the 3'end of *PTF1A* were not used for SCNT due to cell incompatibility reasons, which are described in more detail in section 3.2.1.2.

3.1.1.4 Genotypic analysis of *PTF1A^{iCre}* founder animals

All live-born founders were healthy and viable. DNA was isolated from earclip tissue of both stillborn and viable piglets and used for genotyping via screening PCRs and for copy number determination. Furthermore, tissue samples from stillborn piglets were used for expression analysis. Genotyping identified four *PTF1A$^{5'iCre}$* and five *PTF1A$^{3'iCre}$* piglets, of which two and one were stillborn, respectively (Figure 22A+B). In addition, monoallelic integration of iCre into *PTF1A* was confirmed by endogenous PCR for all nine piglets (Figure 22C).

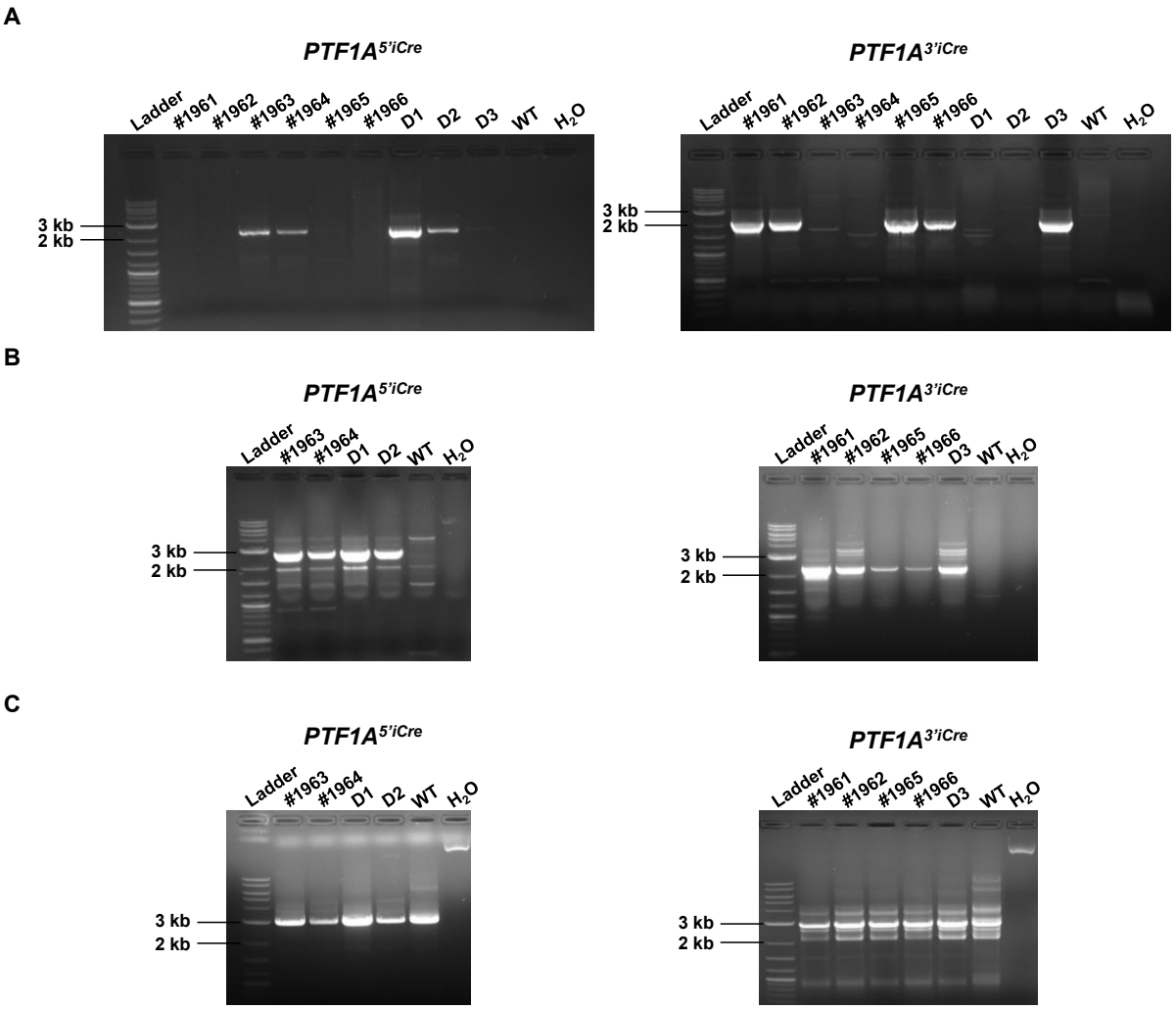

Figure 22. Genotyping of *PTF1A*^{iCre} founders. Left panel: *PTF1A*$^{5'iCre}$ screening PCRs. Right panel: *PTF1A*$^{3'iCre}$ screening PCRs. (A) 5'junction PCRs: correct *PTF1A* 5'end and 3'end targeting resulted in 2233 bp and 2127 bp PCR products, respectively. (B) 3'junction PCR revealed a 2346 bp product for correct 5'end targeting and a 2300 bp product for 3'end targeting. (C) Endogenous PCR for the non-targeted allele resulted in amplification of 3020 bp and 2887 bp PCR products for *PTF1A*$^{5'iCre}$ and *PTF1A*$^{3'iCre}$ founders, respectively. Illustration adapted from Kalla et al. (2021) [285].

Determination of iCre copy numbers by ddPCR revealed the presence of one copy of the iCre transgene in all *PTF1A*$^{5'iCre}$ founders (Figure 23A), which is consistent with the genotype of the cell clones used for SCNT (Figure 23B). In contrast, *PTF1A*$^{3'iCre}$ founders were shown to carry iCre copy numbers between two and seven, indicating that they were derived from all three cell clones used for SCNT. However, as the screening PCRs and the endogenous PCR of the three utilized cell clones showed only single insertion of iCre at *PTF1A* with simultaneous integrity of the second allele, the extra copies are suggested to be non-functional due to the absence of a promoter.

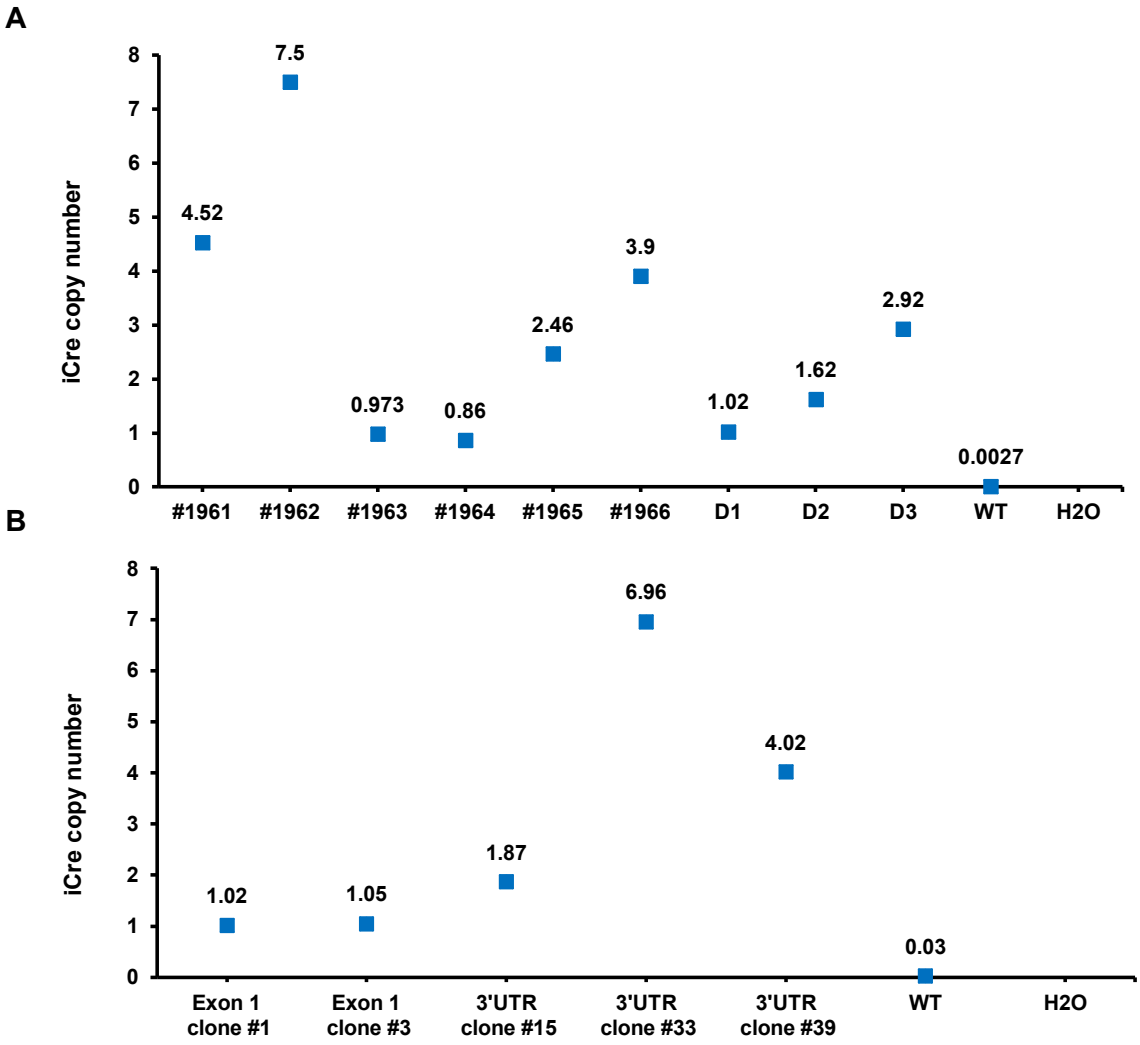

Figure 23. iCre copy number determination. (A) DdPCR results of *PTF1A*^{iCre} founder piglets. (B) DdPCR results of cell clones used for *PTF1A*^{iCre} pig generation.

The genotyping results shown above are summarized in Table 35. Out of nine piglets, three were stillborn (grey), two were positive for 5'end targeting (blue) and four were positive for placement of iCre into the 3'end of *PTF1A* (green).

Table 35. Summarised genotyping analysis of *PTF1A*^{iCre} founders.

Piglet	Live-born	Gender	Generation	Genotype	iCre copy number
#1961	Yes	Male	G0	*PTF1A*$^{3'iCre}$	4
#1962	Yes	Male	G0	*PTF1A*$^{3'iCre}$	7
#1963	Yes	Male	G0	*PTF1A*$^{5'iCre}$	1
#1964	Yes	Male	G0	*PTF1A*$^{5'iCre}$	1
#1965	Yes	Male	G0	*PTF1A*$^{3'iCre}$	2
#1966	Yes	Male	G0	*PTF1A*$^{3'iCre}$	4
D1	No	Male	G0	*PTF1A*$^{5'iCre}$	1
D2	No	Male	G0	*PTF1A*$^{5'iCre}$	1
D3	No	Male	G0	*PTF1A*$^{3'iCre}$	2

3.1.2 Functionality of iCre recombinase

3.1.2.1 Expression analysis of *PTF1A*^{iCre} pigs

In a next step, tissue samples from stillborn piglets D1 and D3 were used for expression analysis of iCre, PTF1A and GAPDH on RNA level using reverse transcription-polymerase chain reaction (RT-PCR) (Figure 24).

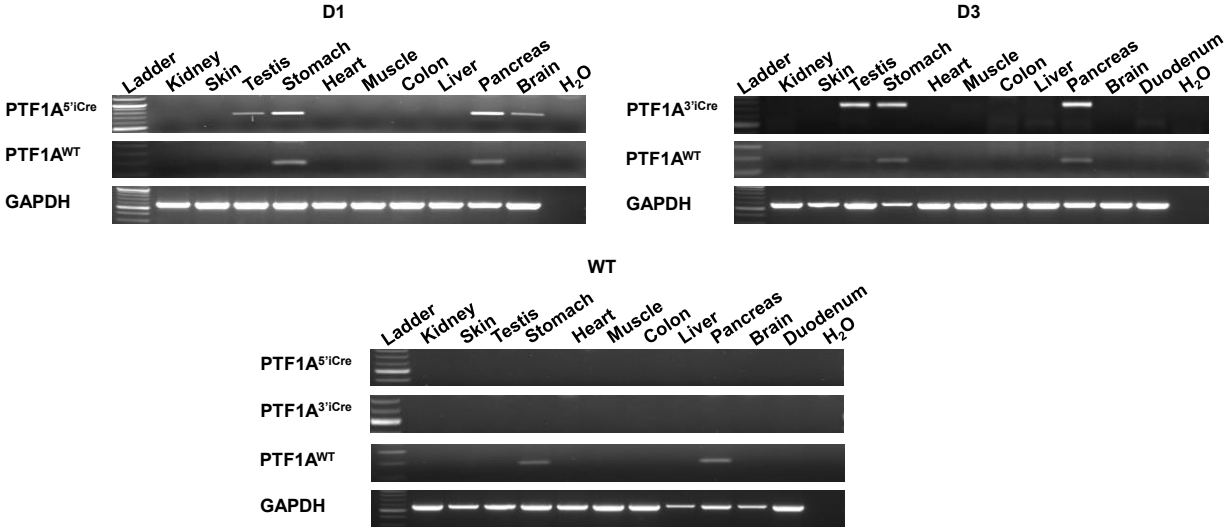

Figure 24. RT-PCR analysis of stillborn *PTF1A*^{iCre} piglets D1 and D3. Wild type piglet RNA was used as a control.

For both stillborn *PTF1A*^{iCre} piglets, iCre recombinase expression was detected in testis, stomach and pancreas, while *PTF1A*$^{5'iCre}$ piglet D1 also expressed iCre in the brain, albeit at the same weak intensity as in the testis. The difference between the two animals in the brain expression pattern may be due to the fact that the samples were possibly obtained from different brain regions. Furthermore, despite targeting of one *PTF1A* allele, the maintenance of endogenous PTF1A expression could be demonstrated, as expression of PTF1A was detected in the stomach and pancreas of both animals, with additional weak expression in the testis of *PTF1A*$^{3'iCre}$ piglet D3. Consistent with this, the wild type piglet that served as a control expressed PTF1A in stomach and pancreas, while expression of iCre was absent.

Figure 25. *PTF1A*^{iCre} boars #1961, #1963 and #1965 at age of 5.5 weeks. Illustration adapted from Kalla et al. (2021) [285].

Boars #1964 and #1962 were terminated at age of 6.5 weeks and 9 months, respectively. Tissue samples isolated from those animals were used to compare the RNA expression patterns with the stillborn animals analysed above (Figure 26). Due to the inconsistent results of brain expression in the piglets shown above, care was taken this time to distinguish between cerebrum and cerebellum when sampling the brain. For *PTF1A*$^{5'iCre}$ pig #1964, expression of iCre was detected in the pancreas and stomach. Expression of *PTF1A* was detected in pancreas and stomach, and to a lesser extent in the cerebellum. *PTF1A*$^{3'iCre}$ pig #1962 showed the same expression pattern as *PTF1A*$^{5'iCre}$ boar #1964. However, it should be mentioned that GAPDH expression was very weak for testis of pig #1962 and thus did not allow to make conclusions regarding no or low Cre expression in the testis of this pig. In summary, the results for pigs #1964 and #1962 corresponded to the *PTF1A* expression pattern of the wild type pig that served as a control.

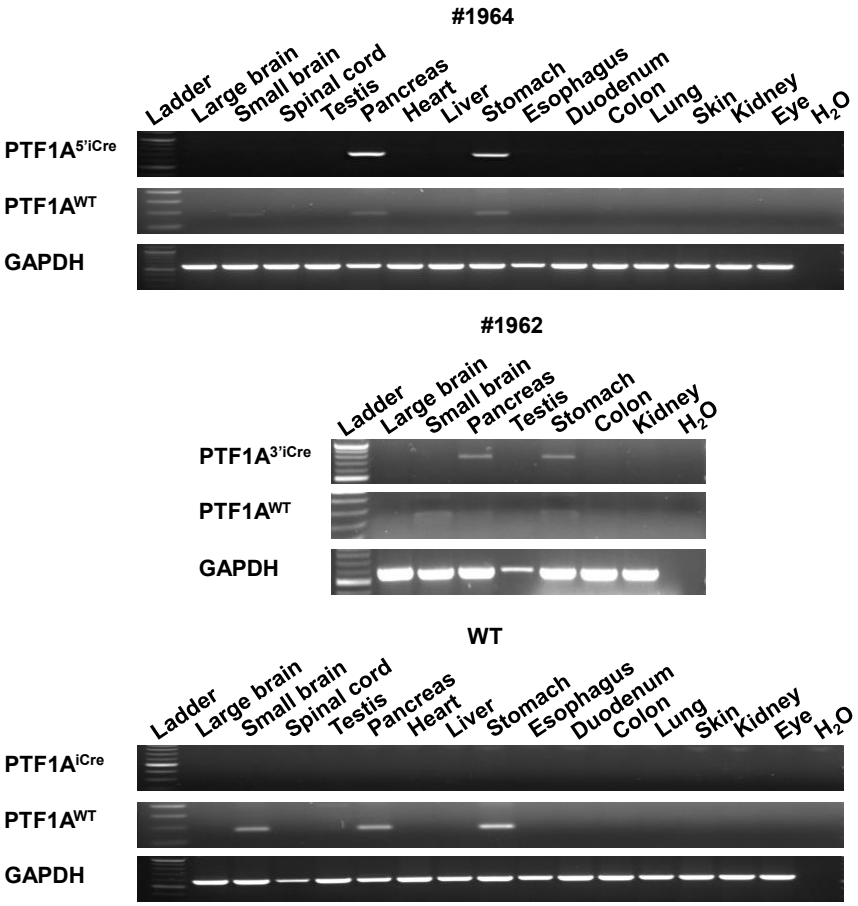

Figure 26. RT-PCR analysis of *PTF1A*^{iCre} boars #1964 and #1962. RNA from a wild type pig was used as a control.

Next, iCre expression was validated on protein level by immunohistochemistry (IHC). In both *PTF1A*$^{5'iCre}$ and *PTF1A*$^{3'iCre}$ piglets, the expression of iCre recombinase in the pancreas was restricted to acinar cells, while ductal cells remained negative (Figure 27A). Isolated expression was also found in the stomach, but was absent in other organs such as the cerebellum and kidney (Figure 27B).

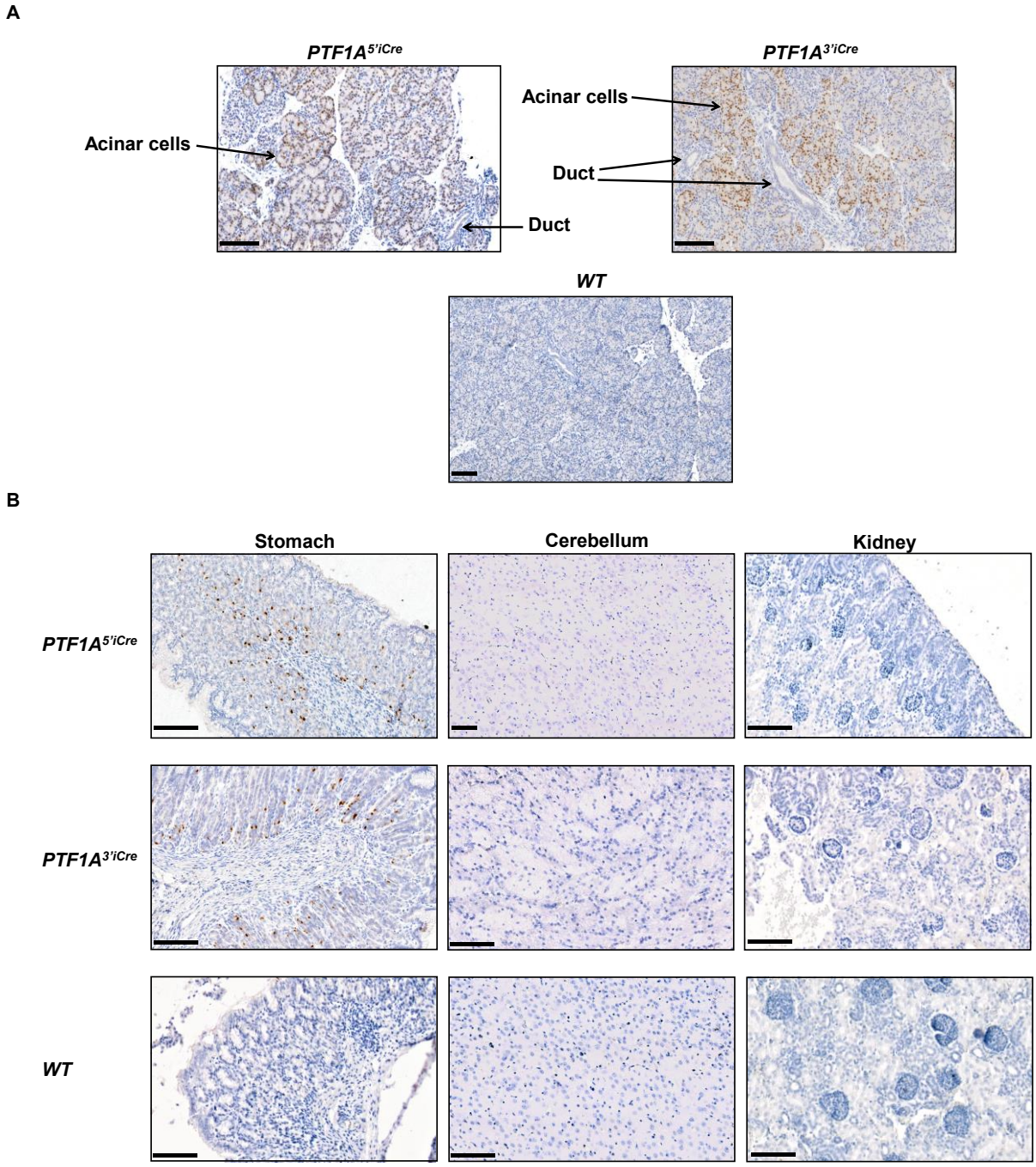

Figure 27. Cre protein expression in stillborn *PTF1A*^{iCre} piglets D1 and D3. (A) IHC staining of *PTF1A*$^{5'iCre}$ and *PTF1A*$^{3'iCre}$ pancreata. (B) IHC staining of *PTF1A*$^{5'iCre}$ and *PTF1A*$^{3'iCre}$ stomach, cerebellum and kidney. Wild type samples serves as control. Scale bar represents 100 µm. Illustration adapted from Kalla et al. (2021) [285].

3.1.2.2 Analysis of *Reporter-PTF1A*^{iCre} pigs

For functional analysis, the generated *PTF1A*^{iCre} founders were crossed with the dual fluorescent reporter pig line *R26*$^{mT\text{-}mG/WT}$. The F1 animals were healthy and viable and showed an inheritance of iCre recombinase according to the Mendelian rules. Two of the piglets were selected for functional analysis by fluorescence imaging. As expected, the numbers of iCre copies of the F1 piglets corresponded to those of the founder animals used for breeding, which had one and four copies of iCre, respectively (Table 36).

Table 36. *Reporter-PTF1A^{iCre}* piglets used for fluorescence analysis.

Sow (F4 generation)	Boar (G0 generation)	Genotype of piglet used for fluorescence analysis	Generation	Gender	iCre copies
#1838 *R26$^{mT\text{-}mG/WT}$-KRAS$^{LSLG12D/WT}$-TP53$^{LSLR167H/WT}$*	#1963 *PTF1A$^{5'iCre/WT}$*	*R26$^{mT\text{-}mG/WT}$-KRAS$^{LSLG12D/WT}$-PTFA$^{5'iCre/WT}$*	F1	Male	1
#1842 *R26$^{mT\text{-}mG/WT}$-KRAS$^{LSLG12D/WT}$*	#1961 *PTF1A$^{3'iCre/WT}$*	*R26$^{mT\text{-}mG/WT}$-KRAS$^{LSLG12D/WT}$-PTFA$^{3'iCre/WT}$*	F1	Female	4

In order to verify the functionality and tissue specificity of iCre, the selected *R26$^{mT\text{-}mG/WT}$PTF1A$^{5'iCre}$* and *R26$^{mT\text{-}mG/WT}$PTF1A$^{3'iCre}$* piglets and one *R26$^{mT\text{-}mG/WT}$* piglet were sacrificed on postnatal day one for fluorescent imaging of four different tissues (Figure 28). In contrast to the expression analysis of the *PTF1A^{iCre}* founder pigs, which showed iCre expression at the time of analysis, the *Reporter-PTF1A^{iCre}* pigs showed the marking of expression during development by means of a fluorescence switch from red to green fluorescence. Therefore, it was expected that the results of the fluorescence analysis of the *Reporter-PTF1A^{iCre}* pigs would differ from the expression patterns of the founder animals detected by RT-PCR and IHC. Indeed, while tissues from *R26$^{mT\text{-}mG/WT}$* piglet were red fluorescent, imaging revealed extensive green fluorescence in the pancreata and small brains of *Reporter-PTF1A^{iCre}* piglets. In addition, stomach tissues of those animals showed single green fluorescent cells, while all other tissues such as the kidney were negative.

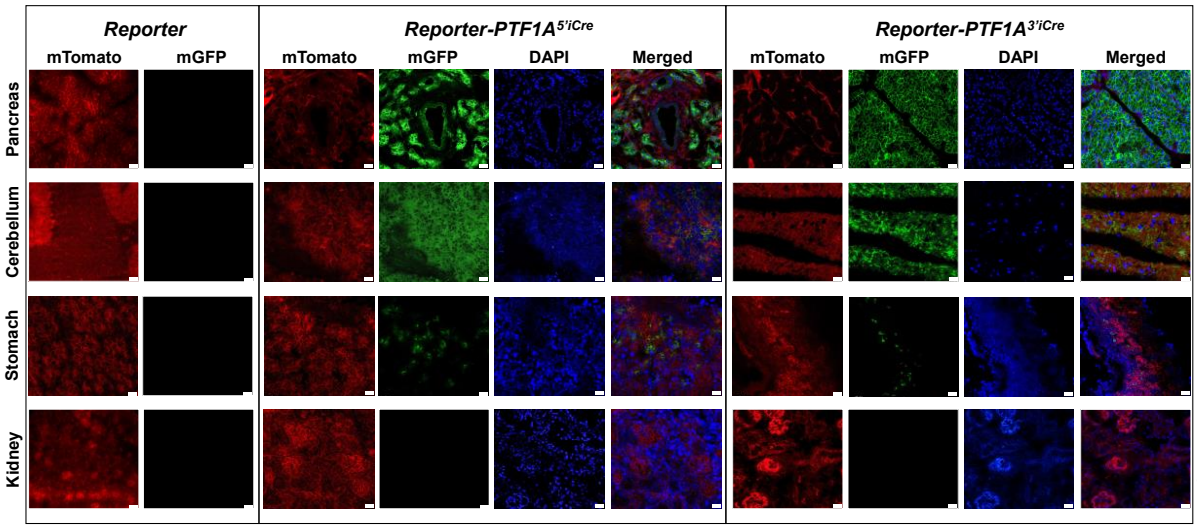

Figure 28. Fluorescent imaging for functional analysis of iCre in *Reporter-PTF1A^{iCre}* pigs. Detection of mTomato and mGFP fluorescence in tissues from one day old *R26$^{mT\text{-}mG/WT}$*, *R26$^{mT\text{-}mG/WT}$PTF1A$^{5'iCre}$* and *R26$^{mT\text{-}mG/WT}$PTF1A$^{3'iCre}$* piglets. Scale bar represents 20 µm. Illustration adapted from Kalla et al. (2021) [285].

3.1.3 Modelling PDAC in *PTF1A^{iCre}* pigs

After the functionality of iCre recombinase was proven, the next step was to model PDAC in pigs. This was to be achieved by mutational activation in the porcine pancreas by breeding of the *PTF1A^{iCre}* pigs with *KRAS$^{LSLG12D/WT}$* and *TP53$^{LSLR167H/WT}$* pigs. The *PTF1A^{iCre}* offspring all appeared physically healthy, but in contrast to *Reporter-PTF1A^{iCre}* animals, the *KRAS$^{LSLG12D/WT}$PTF1A^{iCre}* or *KRAS$^{LSLG12D/WT}$TP53$^{LSLR167H/WT}$PTF1A^{iCre}* piglets showed varying degrees of leg problems, the so-called splay leg syndrome.

Tissues from one day old *KRAS$^{LSLG12D/WT}$PTF1A^{iCre}* and *TP53$^{LSLR167H/WT}$PTF1A^{iCre}* piglets were examined for Cre recombination and mutational activation. Excision of the LSL cassette in front of the *KRAS^{G12D}* and *TP53^{R167H}* mutations was verified by LSL-excision PCR using gDNA from seven different porcine tissues (Figure 29). PCR revealed recombination and thus excision of the LSL cassette in pancreas and cerebellum for both *KRAS$^{LSLG12D/WT}$PTF1A^{iCre}* and *TP53$^{LSLR167H/WT}$PTF1A^{iCre}* pigs regardless of whether they were generated by breeding with *PTF1A* 5' or 3'end targeted pigs. In contrast, other tissues of those animals, such as large brain, colon or kidney, showed only PCR products for the wild type and unrecombined allele. As expected, PCR of tissue samples from wild type pig only gave rise to 167 bp and 198 bp *KRAS^{WT}* and *TP53^{WT}* bands, respectively.

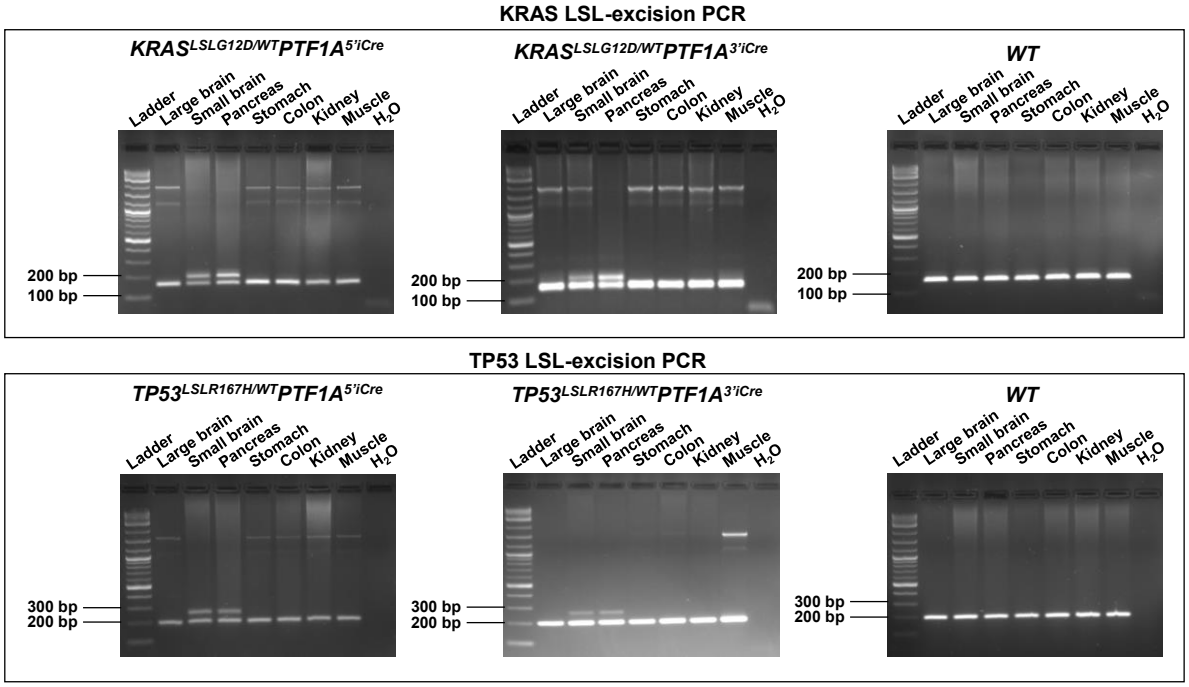

Figure 29. LSL-excision PCR results for *KRAS-PTF1A^{iCre}* and *TP53-PTF1A^{iCre}* piglets. KRAS LSL-excision PCR revealed recombination in cerebellum and pancreas of one day old *KRAS$^{LSLG12D/WT}$PTF1A$^{5'iCre}$* and *KRAS$^{LSLG12D/WT}$PTF1A$^{3'iCre}$* piglets, leading to bands at 167 bp and 203 bp for the wild type and recombined allele, respectively, and a weak band of 1878 bp band for the unrecombined allele. All other tissues showed PCR products at 1878 bp for the unrecombined allele and 167 bp for the wild type allele. TP53 LSL-excision PCR revealed recombination in cerebellum and pancreas of *TP53$^{LSLR167H/WT}$PTF1A$^{5'iCre}$* and *TP53$^{LSLR167H/WT}$PTF1A$^{3'iCre}$* piglets, leading to bands at 198 bp and 238 bp for the wild type and recombined allele and a weak band of 1520 bp for the unrecombined allele. All other tissues showed PCR products at 1520 bp for the unrecombined allele and 198 bp for the wild type allele. Tissues from a wild type piglet served as a control and showed the wild type bands of 167 bp and 198 bp for *KRAS^{WT}* and *TP53^{WT}*, respectively.

As mentioned above, excision of the LSL cassette leads to expression of the downstream *KRAS*^{G12D} and *TP53*^{R167H} mutations, which are characterised by a G to A base mutation (G→A) at the DNA level. For KRAS, this single-base missense mutation results in Glycine→Aspartic acid amino acid substitution (G→D) and thus leads to expression of *KRAS*^{G12D}.
For TP53, the G→A mutation leads to Arginine→Histidine amino acid substitution (R→H) and to expression of *TP53*^{R167H} (Figure 30).

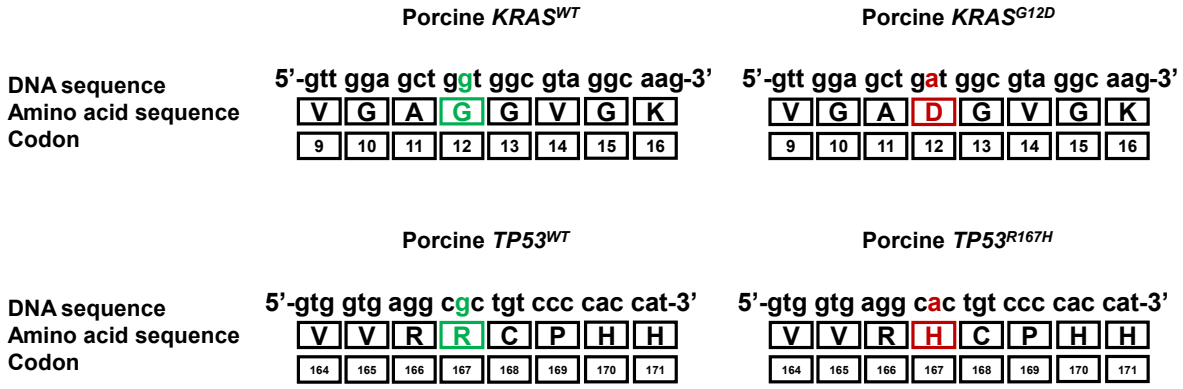

Figure 30. Representation of *KRAS*^{G12D} and *TP53*^{R167H} mutations.

RNA isolated from different tissues was used to analyse the presence and frequency of a G→A mutation at the cDNA level at *KRAS* codon 12 and *TP53* codon 167 by pyrosequencing (Table 37). As the analysed piglets were heterozygous for *KRAS*^{LSLG12D} or *TP53*^{LSLR167H}, the expected maximum frequency of a G→A mutation was 50%.

Table 37. Pyrosequencing results for *KRAS* and *TP53* mutations in *PTF1A*^{iCre} progeny. SB: stillborn

KRAS				
Genotype	**Age**	**Tissue**	**Nucleobase G**	**Nucleobase A**
***KRAS*$^{LSLG12D/WT}$*PTF1A*$^{5'iCre}$**	3 days	Small brain	57%	43%
		Pancreas	65%	35%
		Stomach	94%	6%
		Kidney	98%	2%
***Reporter-KRAS*$^{LSLG12D/WT}$*PTF1A*$^{5'iCre}$**	SB	Small brain	53%	47%
		Pancreas	51%	49%
		Stomach	92%	8%
		Kidney	98%	2%
***KRAS*$^{LSLG12D/WT}$*TP53*$^{LSLR167H/WT}$ *PTF1A*$^{5'iCre}$**	2 days	Small brain	53%	47%
		Pancreas	63%	37%
		Stomach	96%	4%
		Kidney	97%	3%
***KRAS*$^{LSLG12D/WT}$*PTF1A*$^{3'iCre}$**	SB	Small brain	46%	54%
		Pancreas	65%	35%
		Stomach	96%	4%
		Kidney	88%	13%

Reporter-KRAS$^{LSLG12D/WT}$PTF1A$^{3'iCre}$	SB	Small brain	66%	34%
		Pancreas	39%	61%
		Stomach	95%	5%
		Kidney	94%	6%
WT	SB	Small brain	98%	2%
		Pancreas	96%	4%
		Stomach	99%	1%
		Kidney	98%	2%
TP53				
Genotype	**Age**	**Tissue**	**Nucleobase G**	**Nucleobase A**
TP53$^{LSLR167H/WT}$PTF1A$^{5'iCre}$	SB	Small brain	60%	40%
		Pancreas	85%	15%
		Stomach	97%	3%
		Kidney	98%	2%
KRAS$^{LSLG12D/WT}$TP53$^{LSLR167H/WT}$ PTF1A$^{5'iCre}$	2 days	Small brain	67%	33%
		Pancreas	77%	23%
		Stomach	97%	3%
		Kidney	97%	3%
TP53$^{LSLR167H/WT}$PTF1A$^{3'iCre}$	3 weeks	Small brain	55%	45%
		Pancreas	73%	27%
		Stomach	97%	3%
		Kidney	97%	3%
WT	SB	Small brain	97%	3%
		Pancreas	96%	4%
		Stomach	98%	2%
		Kidney	97%	3%

Indeed, pyrosequencing of four different tissues revealed conversion of nucleobase G to nucleobase A in small brain and pancreas of all tested mutant *PTF1A^{iCre}* genotypes (Table 37). In these two tissues, frequency of the G→A mutation ranked between 34% and 61% for *KRAS*, while *TP53* mutations were less frequent, ranging between 15% and 45%. However, the low value of 15% for the pancreas of the *TP53$^{LSLR167H/WT}$PTF1A$^{5'iCre}$* piglet was most likely due to poor quality or too late collection of the sample. In contrast, stomach and kidney were negative for G→A conversion. The original pyrosequencing results are shown in Supplementary figures 14-23.

Since the ability of PTF1A-iCre to excise the LSL cassette and thus activate the *KRAS* and *TP53* mutations was proven, pancreatic tissue samples from different genotypes of one-day-old piglets were analysed by H&E staining (Figure 31). As shown in Figure 31, activation of *TP53^{R167H}* alone did not lead to pancreatic abnormalities in *PTF1A$^{5'iCre}$* piglets, resulting in the same pancreatic phenotype as in wild type piglets. In contrast, pancreatic activation of *KRAS^{G12D}* led to the development of widespread ADM accompanied by the onset of fibrosis, as shown in *Reporter-KRAS$^{LSLG12D/WT}$PTF1A^{iCre}* piglets. Pancreata from triple mutant piglets revealed higher-grade lesions, which were caused by the simultaneous activation of *KRAS^{G12D}* and *TP53^{R167H}* in these newborn animals.

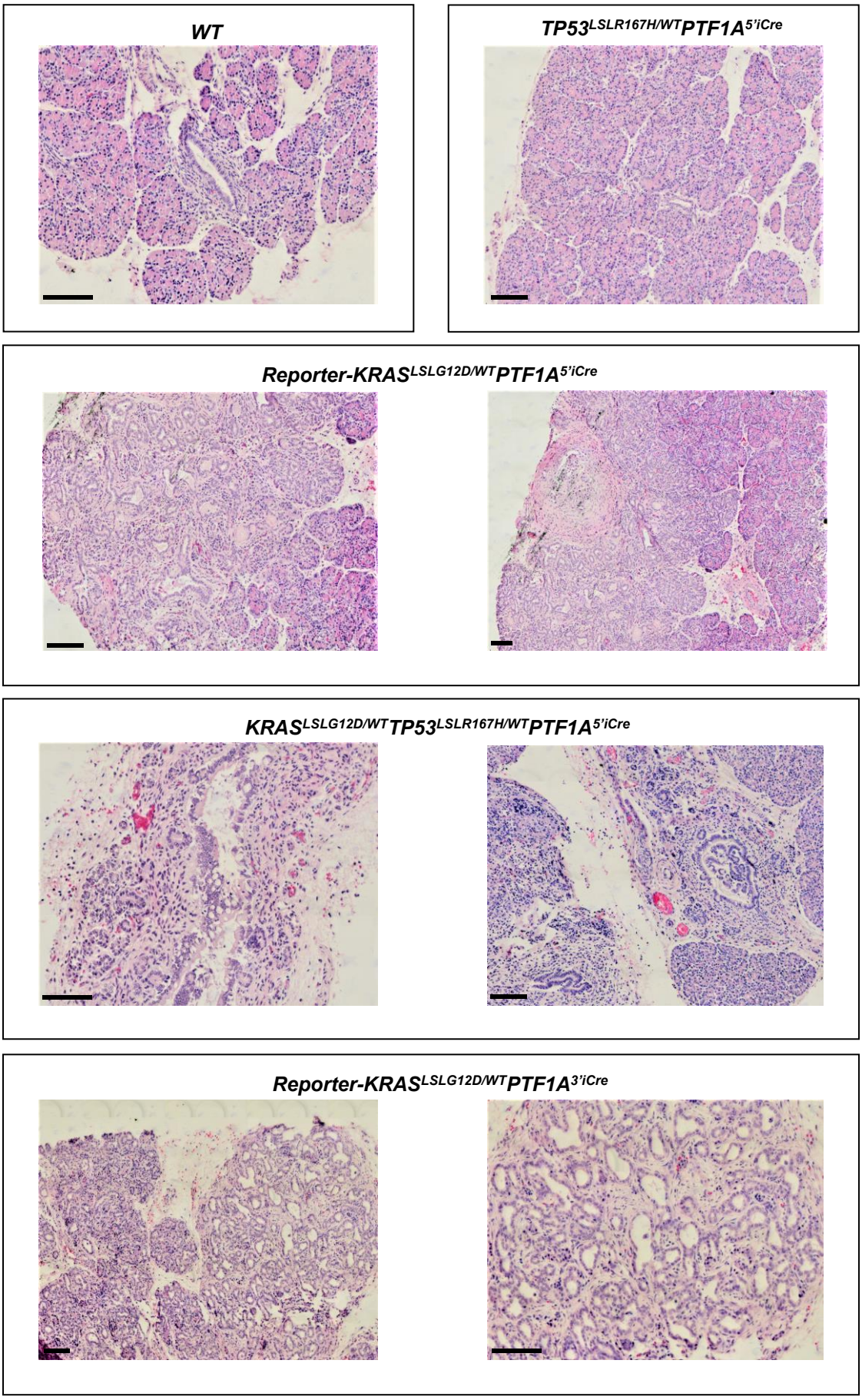

Figure 31. H&E staining of pancreata from *KRAS* and *TP53* mutant *PTF1A*^{iCre} piglets. Scale bar represents 100 µm.

To analyse the PDAC development and timeline, 4-5 week old piglets were terminated. Apart from splay legs, these animals showed no physical abnormalities such as slow growth or insufficient weight gain, which could indicate a pancreatic problem. However, the dissection of 4-5 week old *KRAS*$^{LSLG12D/WT}$*TP53*$^{LSLR167H/WT}$*PTF1A*$^{5'iCre}$ and *KRAS*$^{LSLG12D/WT}$*PTF1A*$^{5'iCre}$ animals revealed severely altered pancreata, ranging from single (Figure 32A, lower panels) to multiple tumours (Figure 32A, upper panel). Interestingly, the disease severity varied between animals of the same genotype that originated from one litter, as shown for piglets #2237 and #2238. These differences between individual animals were also confirmed by histological analysis, which showed a mixture of ADM, PanIN lesions and PDAC with severe connective tissue deposition (Figure 32B). Simultaneous activation of *KRAS*^{G12D} and *TP53*^{R167H} in 10 weeks old *PTF1A*$^{3'iCre}$ piglet also resulted in altered pancreas histology with ADM and PanIN lesions with fibrosis (Figure 32B). Activation of only *KRAS*^{G12D} resulted in the development of ADM and PanIN lesions in the pancreata of 5-week-old *KRAS*$^{LSLG12D/WT}$*PTF1A*$^{5'iCre}$ and *KRAS*$^{LSLG12D/WT}$*PTF1A*$^{3'iCre}$ piglets. With regard to the Cre-driver lines, no differences in the disease phenotype have been found when oncogenic mutations were induced by *PTF1A*$^{5'iCre}$ or *PTF1A*$^{3'iCre}$.

A

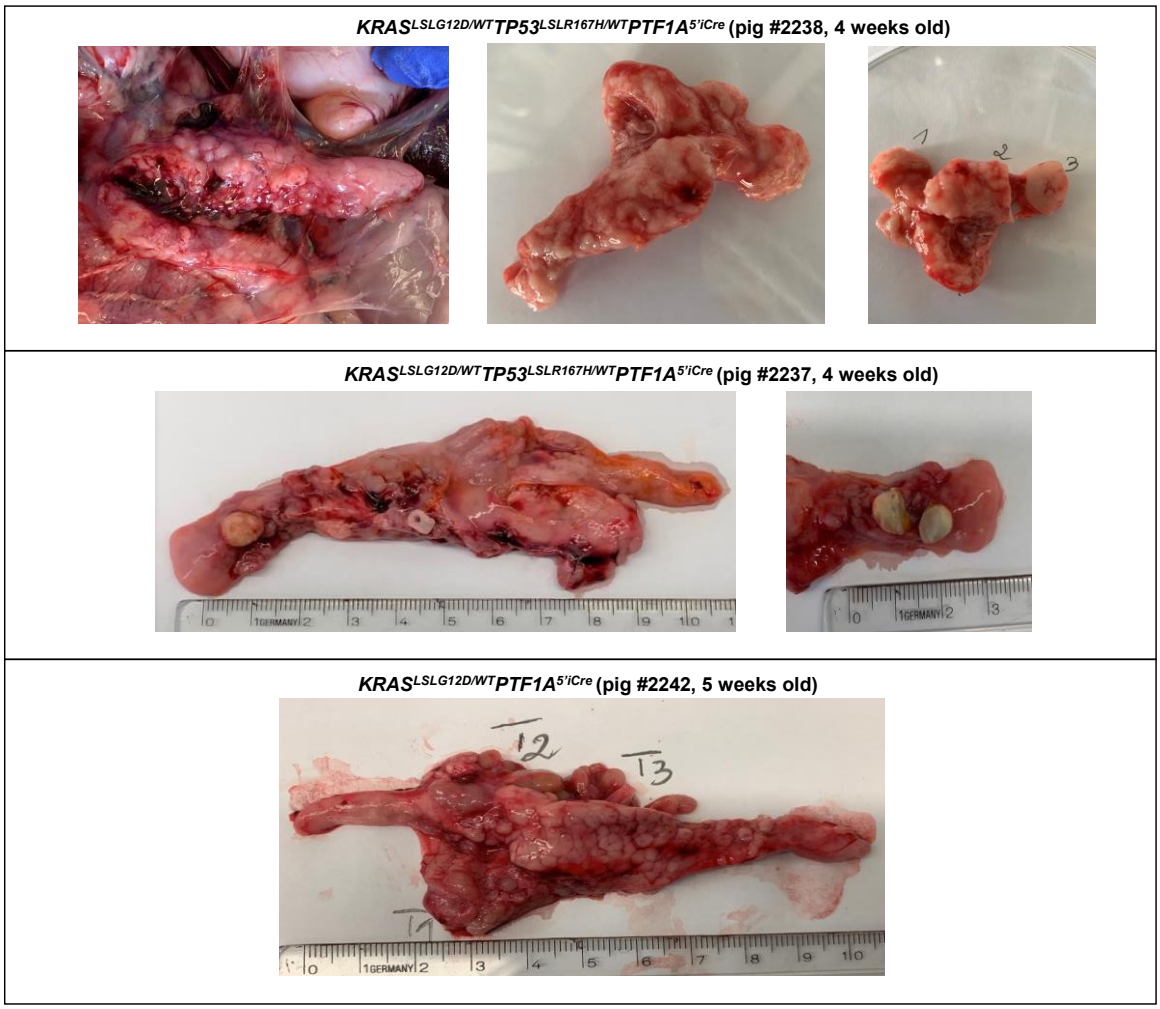

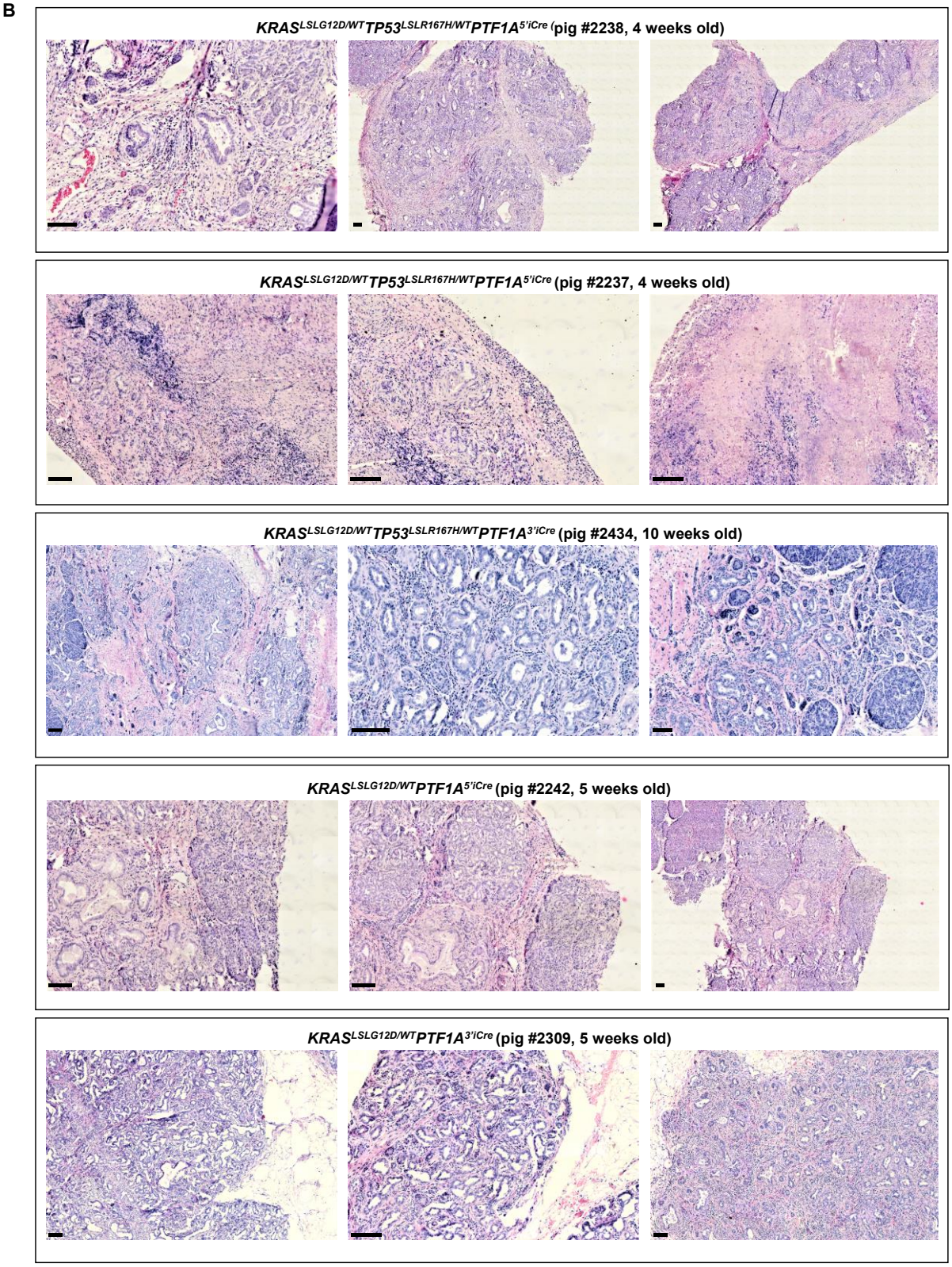

Figure 32. Analysis of pancreatic tissues from *KRAS* and *TP53* mutant *PTF1A*^{iCre} pigs. (A) Pictures of pancreata from 4-5 week old *KRAS*$^{LSLG12D/WT}$*TP53*$^{LSLR167H/WT}$*PTF1A*$^{5'iCre}$ and *KRAS*$^{LSLG12D/WT}$*PTF1A*$^{5'iCre}$ pigs. (B) H&E staining of pancreatic samples from *KRAS*$^{LSLG12D/WT}$*TP53*$^{LSLR167H/WT}$*PTF1A*^{iCre} and *KRAS*$^{LSLG12D/WT}$*PTF1A*^{iCre} pigs. Scale bar represents 100 µm.

In summary, the above results describe the generation of *PTF1A*^{iCre} pigs by 5'end or 3'end targeting of iCre recombinase into the endogenous porcine *PTF1A* locus with the help of CRISPR/Cas9 systems. Expression analysis of the founder animals and Reporter-*PTF1A*^{iCre} pigs revealed concordant iCre expression and recombination patterns for both targeting approaches. In addition, crossbreeding of *PTF1A*^{iCre} with *KRAS*$^{LSLG12D/WT}$ and *TP53*$^{LSLR167H/WT}$ pigs allowed successful modelling of PDAC, as the offspring showed efficient mutational activation and various pancreatic alterations ranging from ADM, PanINs to multiple tumours.

3.2 Generation of a porcine PDAC model using *mPdx1-iCre* pigs

In addition to Ptf1a, the transcription factor Pdx1 is another important player in the development of the pancreas, which Hingorani and colleagues also used to model PDAC in mice [163]. Therefore, a second approach for the creation of a porcine PDAC model was based on the generation of pigs expressing iCre recombinase from the *Pdx1* promoter to enable mutational activation in the porcine pancreas by breeding with *KRAS* and *TP53* mutant pigs.

3.2.1 Generation of *mPdx1-iCre* pigs

However, targeting of iCre into the endogenous porcine *PDX1* gene, as applied for *PTF1A*, would most likely result in maturity-onset diabetes of the young (MODY), as is the case in humans [297, 298] and in heterozygous knockout mice [299, 300]. To avoid possible adverse effects it was decided to use a Cre expression vector for random or targeted insertion into the porcine genome. A previous experiment (by PhD student Érica Schulze) using the human *PDX1* promoter to drive Cre resulted in piglets with insufficient expression to induce excision of the LSL cassette [301]. However, others had shown that the mouse *Pdx1* promoter (*mPdx1*) in combination with part of the rabbit β-globin gene, which comprises a sequence from part of the second exon through to the third exon, allows efficient pancreas-specific expression of transgenes in pigs [181, 302]. Therefore, an equivalent construct was generated in order to produce genetically modified pigs with pancreas-specific expression of iCre recombinase (Figure 33).

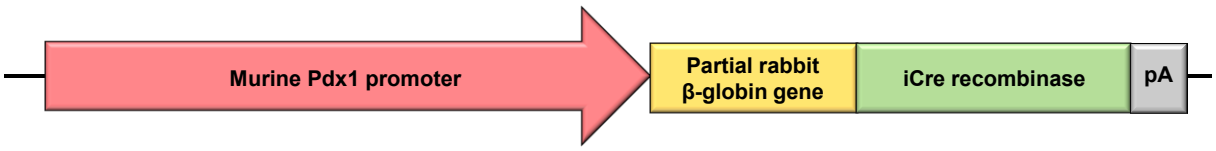

Figure 33. Structure of the *mPdx1-iCre* transgene. The transgene consists of the 6.3 kb murine *Pdx1* promoter fused to a part of the rabbit β-globin gene followed by iCre recombinase and polyA.

Three different strategies for the generation of *mPdx1-iCre* pigs were pursued: targeting into the ubiquitously expressed porcine *ROSA26* locus and random transgene integration using linearized gene constructs or piggyBac transposon systems.

3.2.1.1 Generation of *mPdx1-iCre* pigs by *ROSA26* targeting

The non-coding *Rosa26* (reverse orientation splice acceptor β-geo 26) locus was first discovered in mice in gene trapping experiments in embryonic stem cells [303]. Since gene targeting into murine *Rosa26* is characterised by a high frequency of homologous recombination and ubiquitous transgene expression without effects on viability or fertility, this strategy has been used to generate numerous murine knock-in strains such as Cre reporter mice [296, 304-306]. The subsequently identified human and rat orthologues showed similar properties in terms of successful gene targeting and widespread transgene expression [307, 308], and the high conservation between the three species allowed the identification of the porcine *ROSA26* gene [295].

The ubiquitously expressed *ROSA26* locus is located on porcine chromosome 13 and consists of four exons that give rise to two non-coding transcripts, allowing for transgene expression in several porcine tissues without detrimental effects on physiology and reproduction [295].

As porcine *ROSA26* has been identified as permissive for gene targeting, the first strategy was targeted placement of *mPdx1-iCre* into the first intron of the porcine *ROSA26* gene (Figure 34).

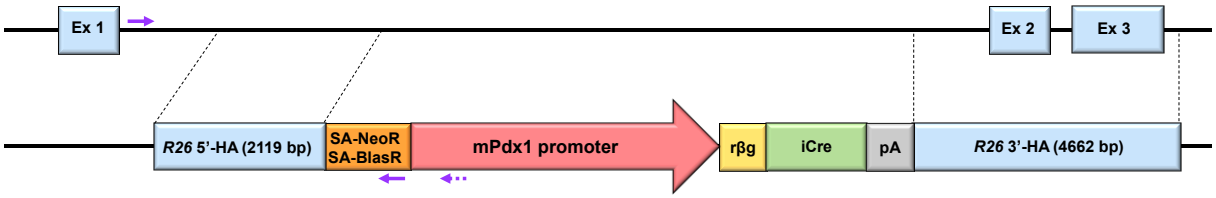

Figure 34. *ROSA26* targeting strategy. Primer positions for 5'screening PCRs are indicated as purple arrows. Ex: exon; HA: homology arm; SA: splice acceptor; NeoR: neomycin resistance gene; BlasR: blasticidin resistance gene; rβg: rabbit β-globin; pA: polyA

However, conventional gene targeting did not result in correctly targeted cell clones. In order to increase the efficiency, the CRISPR/Cas9-mediated HDR strategy was applied using linearized R26-SA-BS-mPdx1-iCre or R26-SA-Neo-mPdx1-iCre targeting vectors in combination with a pX330-hSpCas9-R26-gRNA plasmid. The sgRNA recognized a site in the first *ROSA26* intron between the two homology arms. Screening of transfected PADMSC 110111 cells revealed that ~19% of all screened cell clones were positive for 5'junction PCR (Supplementary figure 24A). Furthermore, the presence of *mPdx1-iCre* and monoallelic integration into *ROSA26* was proven by PCR (Supplementary figures 24B+C). It was not possible to confirm the correct 3'junction, as the PCR across the long arm of homology was unsuccessful. Next, ddPCR analysis revealed that among 20 screened cell clones only one carried single copy integration of iCre (Supplementary figure 24D).

3.2.1.2 Generation of *mPdx1-iCre* pigs by random integration

Besides targeting into porcine *ROSA26*, another strategy was based on random transgene integration. Since it has been reported in the past that Pdx1 is also expressed in organs other than the pancreas [309-311], it was unclear whether the *mPdx1* promoter is active in porcine kidney cells. In order to monitor *mPdx1* promoter activity, PKF #270 cells isolated from a dual-fluorescent reporter pig were used for transfection with a linearized *mPdx1-iCre* gene construct from which the bacterial plasmid backbone had previously been removed. Subsequently, the transfected cells were selected for stable transgene integration using G418.

Activity of the *mPdx1* promoter in PKF #270 cells results in expression of iCre recombinase, which in turn leads to excision of the floxed mTomato sequence and thus to a switch from red to green fluorescence as shown in Figure 20A in section 3.1.1.2.1.

In most cases selection with G418 resulted in mixed cell clones consisting of red and green fluorescent cells. Only green fluorescent cell clones, with proven mPdx1-iCre functionality, were further analysed by ddPCR. Cell clones #1, #4, #5 and #17 with iCre copy numbers between three and 18 were sent for SCNT (performed by Prof. Dr. Valeri Zakhartchenko and Dr. Mayuko Kurome, Chair of Molecular Animal Breeding and Biotechnology, Munich). Afterwards, embryo transfer was performed by Dr. Barbara Kessler (Chair of Molecular Animal Breeding and Biotechnology, Munich). Two sows gave birth to five *mPdx1-iCre* piglets, one of which was stillborn. However, the live-born piglets only survived for a maximum of two days, as they showed severe abnormalities such as enlarged tongue and splay legs and had to be humanly killed. As SCNT with PKF #270 cells resulted in animal defects, these cells were no longer used. However, tissues from the five *mPdx1-iCre* piglets were isolated for analysis (Figure 35). Genotyping revealed the presence of three copies of the *mPdx1-iCre* transgene in all five piglets (Figure 35A+B). As green fluorescent cells were used for SCNT, the piglets and cells isolated from them showed green fluorescence (Figure 35C).

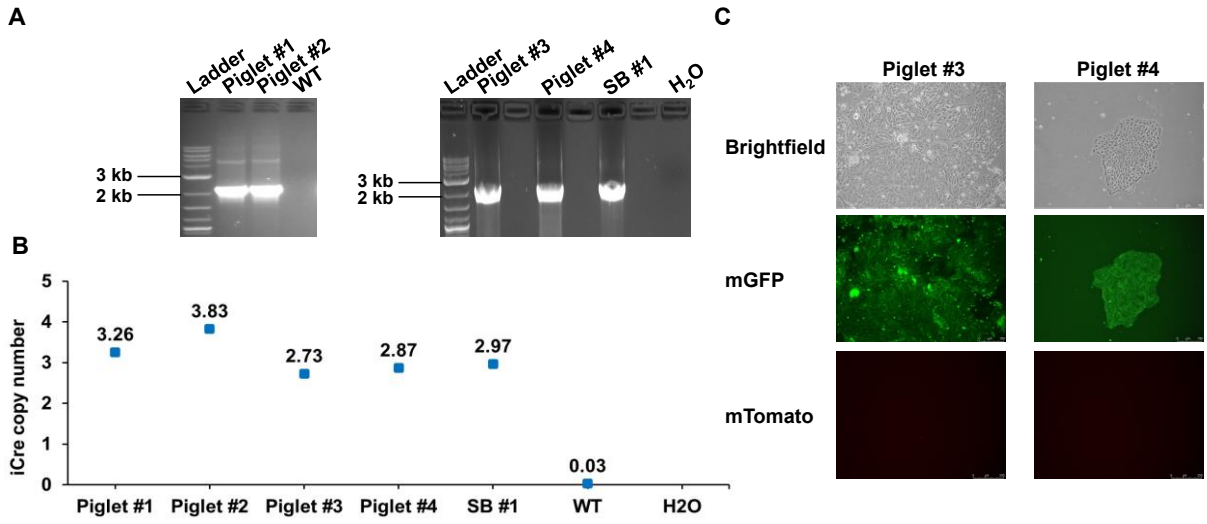

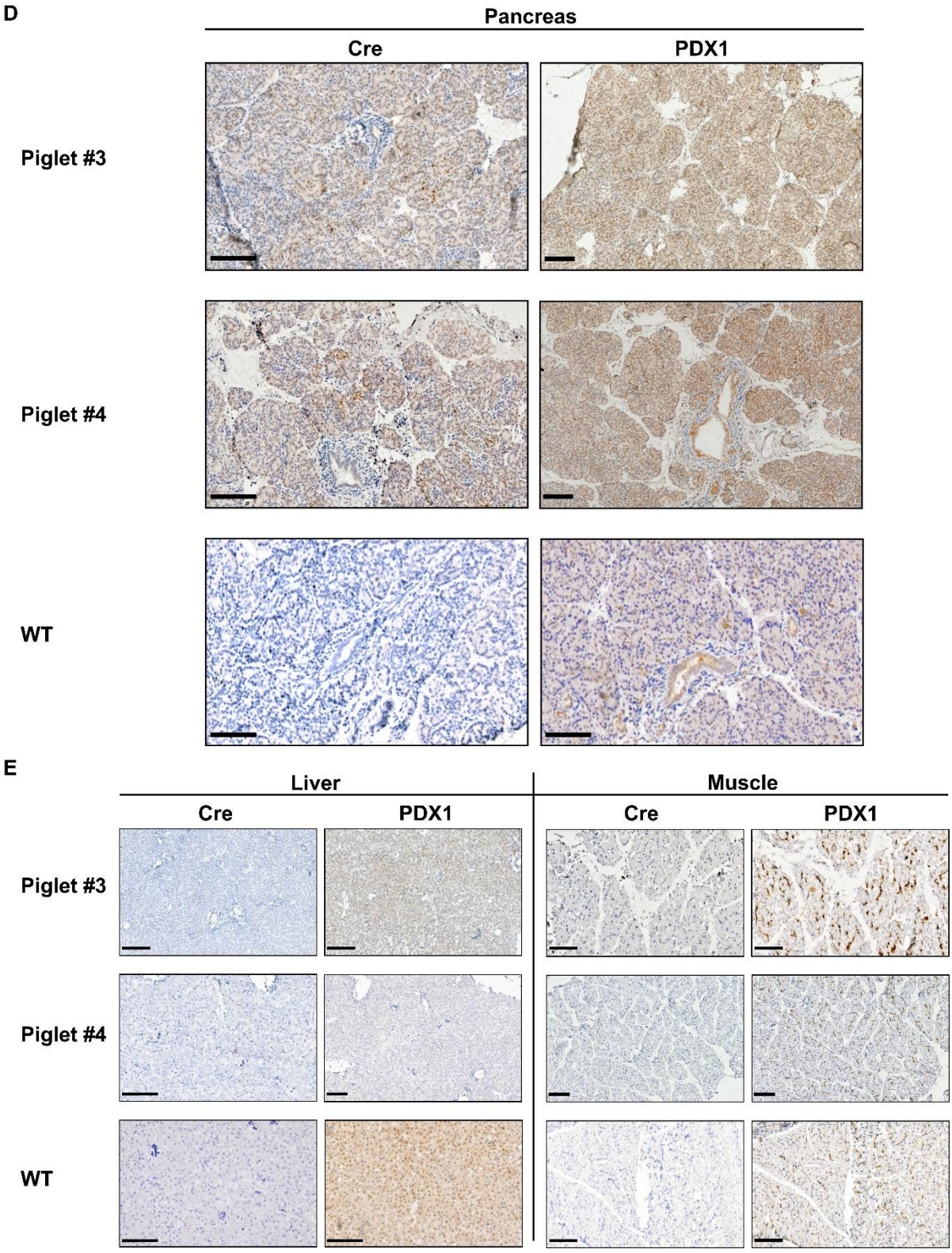

Figure 35. Analysis of *mPdx1-iCre* piglets generated by random integration. (A) Genotyping PCR showed a 2226 bp band for *mPdx1-iCre* piglets. (B) iCre copy number determination by ddPCR. (C) Fluorescence microscopy of PKF cells isolated from *mPdx1-iCre* piglets #3 and #4. (D) IHC staining for Cre protein and PDX1 in pancreata of *mPdx1-iCre* piglets #3, #4 and wild type piglet. (E) IHC staining for Cre protein and PDX1 in liver and muscle of *mPdx1-iCre* piglets #3, #4 and wild type piglet. Scale bar represents 100 µm. WT: wild type, SB: stillborn

Furthermore, the isolated pancreata from piglets #3 and #4 showed a widely distributed expression of iCre recombinase with different intensity levels (Figure 35D+E). Liver and muscle were negative for iCre expression. In contrast, IHC for PDX1 revealed widespread expression in pancreas, liver and muscle, which was probably due to unspecific binding of the utilized antibody as it was produced based on human residues.

3.2.1.3 Generation of *mPdx1-iCre* pigs by piggyBac-mediated transposition

Since the generation of a *mPdx1-iCre* driver pig line via SCNT was unsuccessful, a different approach was chosen. It was decided to use transposon-mediated integration of the *mPdx1-iCre* transgene into the porcine genome via microinjection of *in vitro* produced fertilized oocytes.

The work on porcine embryo culture, which included oocyte collection, *in vitro* maturation, *in vitro* fertilization and microinjection was carried out by Dr. Bernhard Klinger, Thomas Winogrodzki, Liang Wei and Alexander Carrapeiro. The hyperactive PB transposase and transposon plasmids were kindly provided by Prof. Dr. Roland Rad (Institute of Molecular Oncology and Functional Genomics, Munich) and were further modified.

For the generation of *mPdx1-iCre* pigs, the *mPdx1-rβg-iCre-pA* sequence was inserted into the transposon plasmid by cloning and the hyperactive piggyBac (PB) transposase plasmid was used to produce hyperactive PB transposase mRNA.

The components of the transposon system, hyperactive PB transposase mRNA and *mPdx1-iCre* transposon plasmid DNA (Figure 36A) were co-injected into the cytoplasm of fertilized oocytes (Figure 36B). In a first round of microinjection, the toxicity and efficiency of the transposon system was assessed by co-injection of PB transposase mRNA and *mPdx1-iCre* transposon plasmid DNA into 100 oocytes. Following parthenogenetic activation, 42% of parthenotes developed to blastocyst stage (Figure 36C), compared to 50% for the non-injected control group (data not shown). As the PB transposase gene was linked to a red fluorescence marker (mCherry), it was also possible to assess the efficiency of microinjection (Figure 36E). In total, 43% of parthenogenetic blastocysts revealed the presence of the *mPdx1-iCre* transgene as indicated by PCR (Figure 36D).

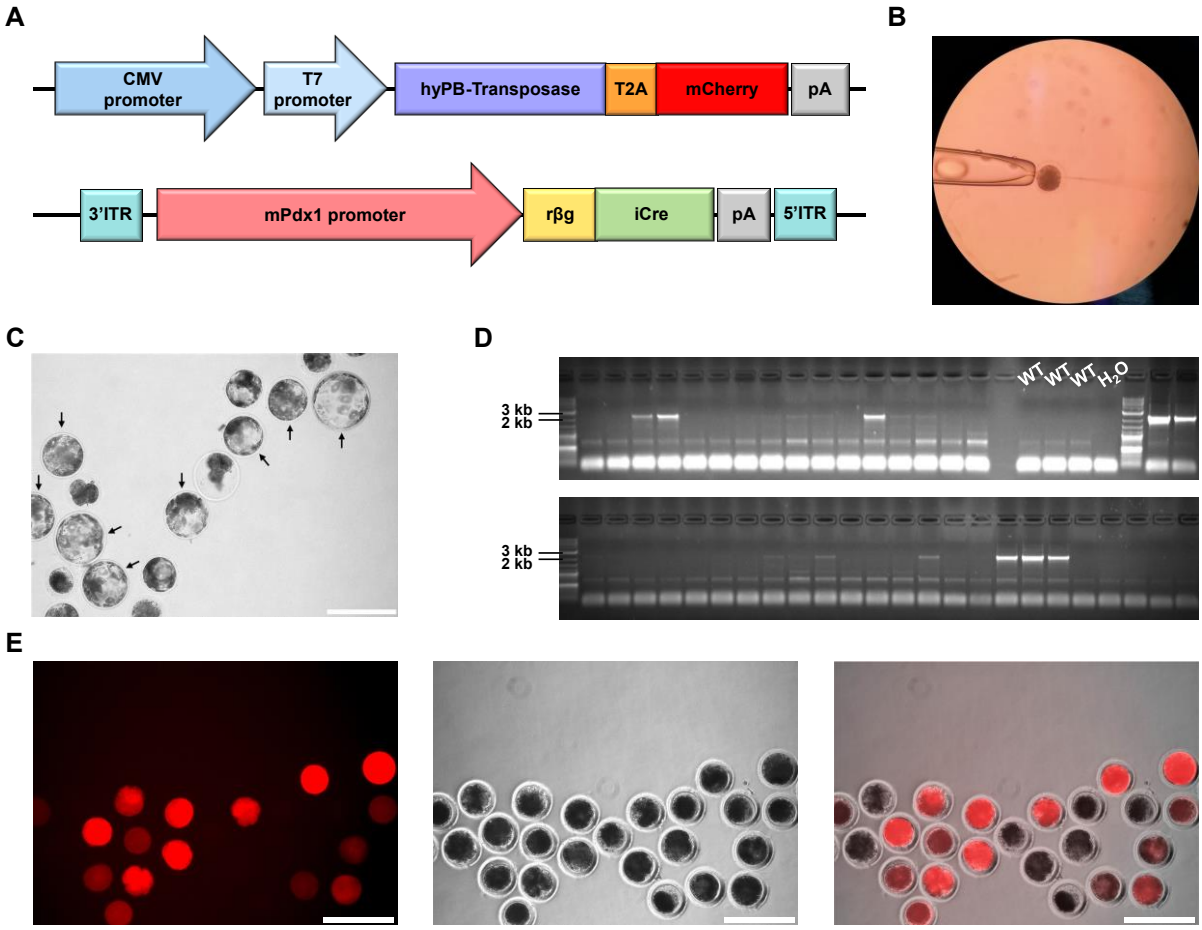

Figure 36. Generation of *mPdx1-iCre* pigs using the piggyBac transposon system. (A) Genetic constructs for porcine oocyte injection of Transposase-T2A-mCherry mRNA and *mPdx1-iCre* transposon plasmid DNA. (B) Cytoplasmic injection of porcine zygotes. (C) Development of injected oocytes to blastocyst stage. Early and late blastocysts are marked by black arrows. (D) Screening PCR for *mPdx1-iCre* showed the expected band at 2226 bp for 43% of the blastocysts. (E) Fluorescence microscopy of porcine zygotes 24 h after injection. Scale bar represents 250 µm.

Based on these promising results, two days after the second round of microinjection a total of 320 embryos were transferred into a recipient sow. After a gestation period of 114 days, the sow gave birth to ten piglets, two males and eight females.

3.2.2 Genotypic analysis of *mPdx1-iCre* founder animals

The born piglets were first analysed by PCR for the presence of the *mPdx1-iCre* transgene. Genotyping PCRs amplifying either 184 bp, 2226 bp or 6064 bp of the transposon vector, identified three female piglets carrying the *mPdx1-iCre* transgene (Figure 37A+C). Piglets #2017 and #2022 showed strong bands for all three genotyping PCRs, while the signal for piglet #2024 was of very low intensity (Figure 37A). DdPCR analysis indicated the presence of eleven and four iCre recombinase copies for piglets #2017 and #2022, respectively, and below level of detection for piglet #2024 (Figure 37B), which could be indicative of low mosaicism.

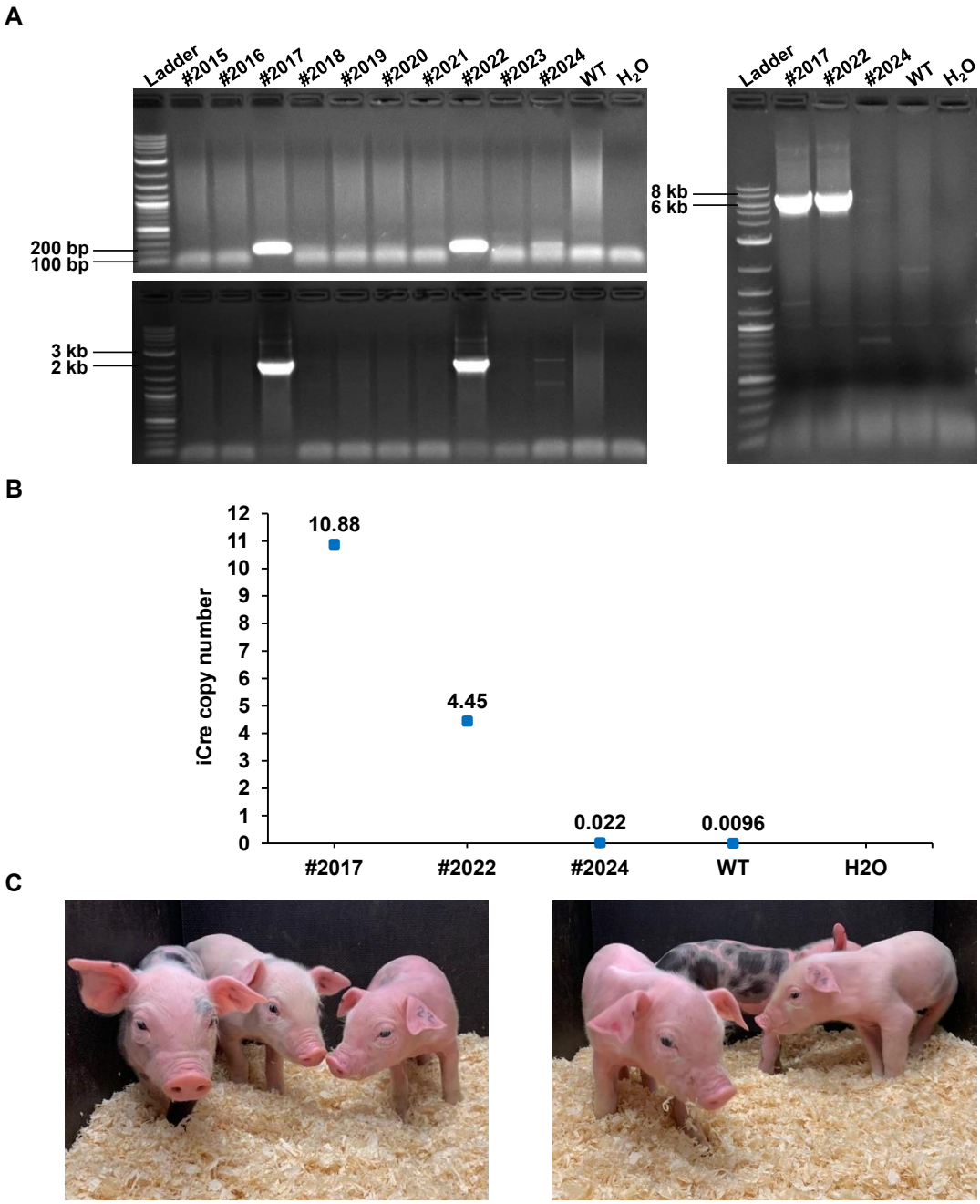

Figure 37. Analysis of *mPdx1-iCre* founders. (A) Genotyping PCRs. Piglets #2017 and #2022 showed bands at 184 bp (upper left image), 2226 bp (lower left image) and 6064 bp (right image) for the presence of the *mPdx1-iCre* sequence. Piglet #2024 showed the same result, but with very weak band intensity. (B) iCre copy number determination by ddPCR. (C) *mPdx1-iCre* piglets at age of 3 days.

To determine if transgenesis was caused by either piggyBac-mediated transposition or simple integration of the transposon plasmid, the *mPdx1-iCre* piglets were tested for the presence of the plasmid backbone. Two sets of primers, binding within the plasmid backbone and in the *mPdx1-iCre* transgene, were used for PCR analysis (Figure 38A). Transposon plasmid backbone was detected in piglet #2017, while piglets #2022 and #2024 were negative (Figure 38B+C). Subsequent ddPCR determined a single plasmid backbone copy for piglet #2017 (Figure 38D).

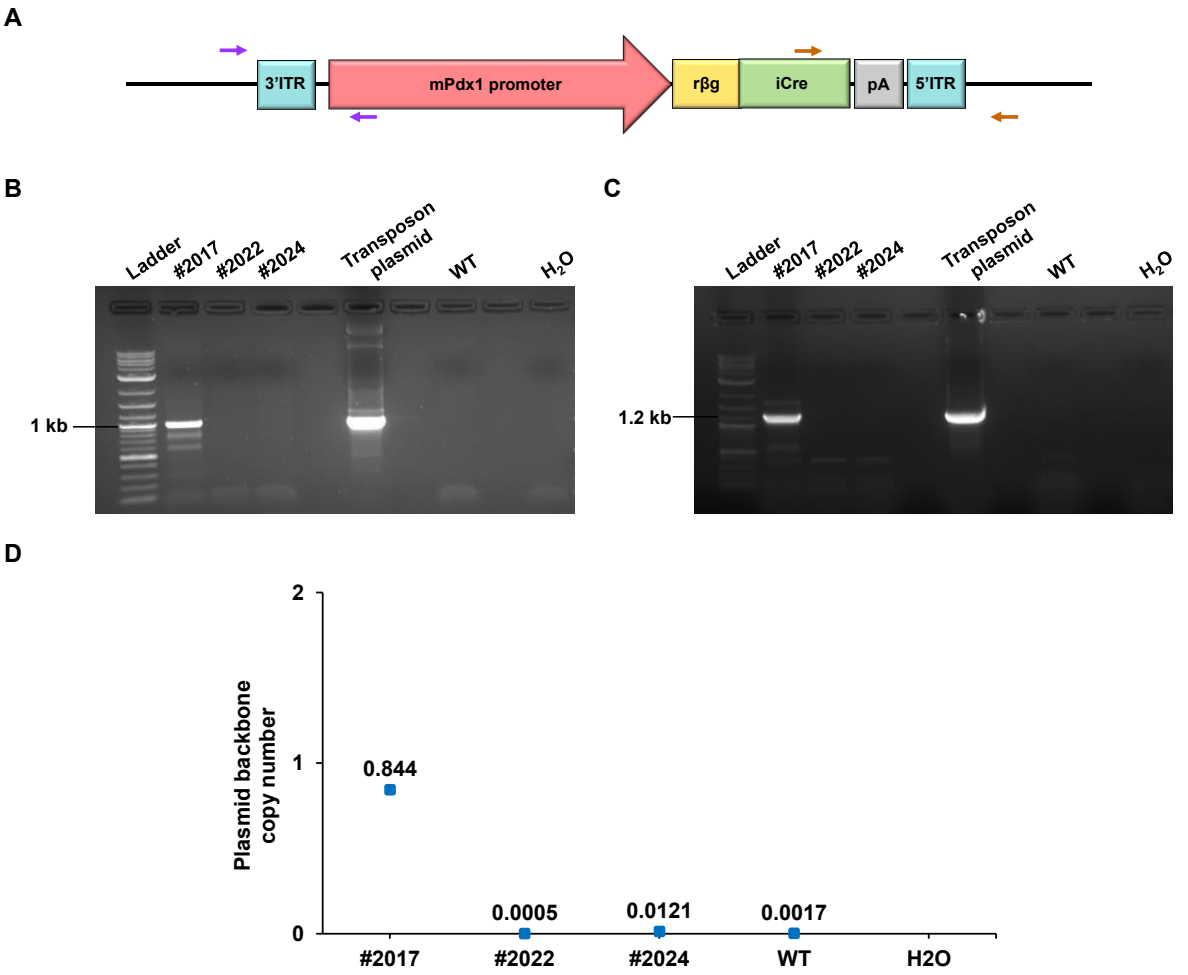

Figure 38. Examination for residual transposon plasmid backbone in *mPdx1-iCre* piglets. (A) Plasmid backbone detection by PCR using two primer pairs binding upstream of 3'ITR and in *mPdx1* promoter (purple arrows) or in iCre and upstream of the 5'ITR sequence (brown arrows). (B) PCR with primer pair one (purple arrows) revealed a band of 1026 bp for piglet #2017. (C) PCR with primer pair two (brown arrows) showed a band of 1273 bp for piglet #2017. (D) Plasmid backbone copy number determination by ddPCR.

After reaching reproductive fertility, sow #2017 was used for breeding, as this animal carried the highest copy number of iCre recombinase. Pig #2017 was mated with an *APC*$^{1311/WT}$*TP53*$^{LSLR167H/LSLR167H}$ boar and gave birth to one stillborn and six live-born piglets. In this case, *APC*$^{1311/WT}$ was included in order to generate the broadest possible spectrum of genotypes that can be used for future breeding, also for other projects.

A segregation of the transposon copies was expected in the offspring, and accordingly the live-born piglets showed different iCre copy numbers as determined by ddPCR.

The genotypes and iCre copy numbers are listed in Table 38. Further breeding was performed with the F1 animals marked in blue.

Table 38. *mPdx1-iCre* F1 generation.

Piglet number	Gender	Generation	Genotype	iCre copy number	Used for further breeding
2329	Male	F1	$APC^{1311/WT}mPdx1^{iCre}$	1	No
2330	Male	F1	$mPdx1^{iCre}$	6	Yes
2331	Male	F1	$mPdx1^{iCre}$	4	No
2332	Male	F1	$TP53^{LSLR167H/WT}mPdx1^{iCre}$	11	Yes
2333	Female	F1	$APC^{1311/WT}mPdx1^{iCre}$	7	Yes
2334	Female	F1	$mPdx1^{iCre}$	10	No

3.2.3 Expression analysis of *mPdx1-iCre* founder animals

After establishing the *mPdx1-iCre* pig line, the founder animals were sacrificed and used for expression analysis. Pancreatic tissues of the founder animals were examined for expression of iCre recombinase (Figure 39). IHC analysis showed localised expression of iCre recombinase in the islets of Langerhans.

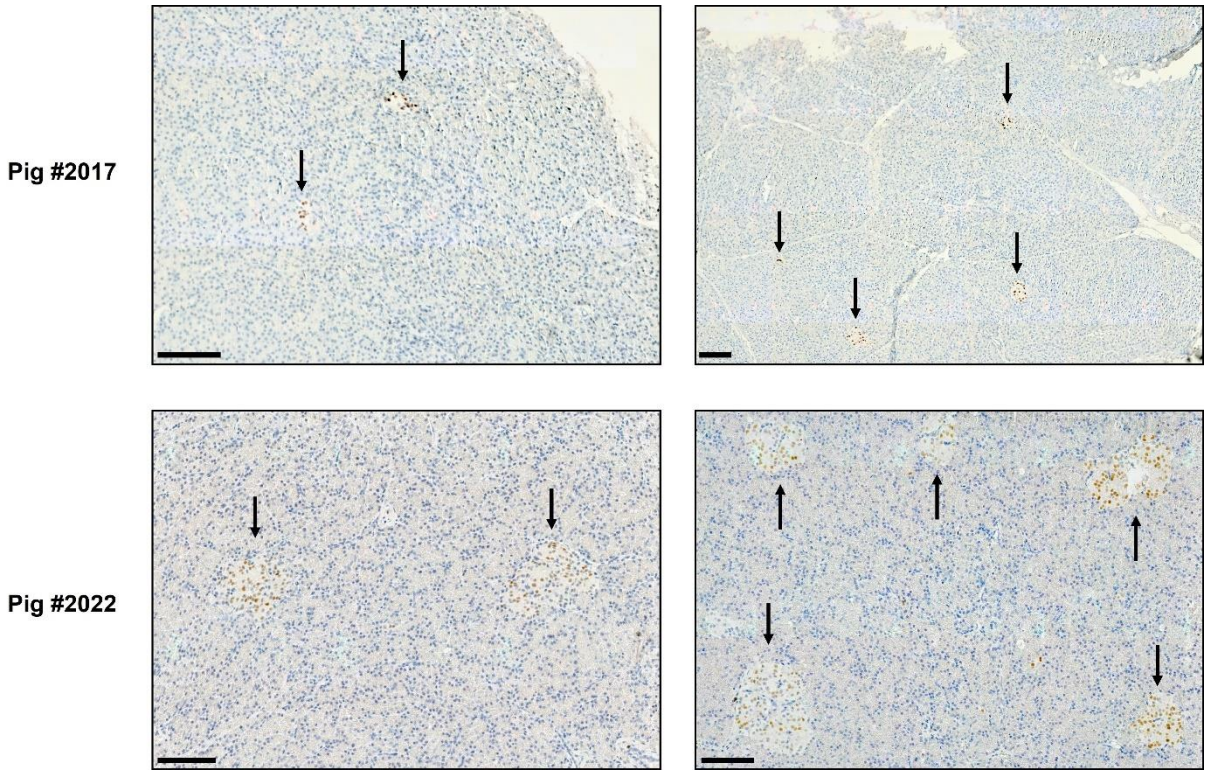

Figure 39. Cre protein expression in the pancreas of *mPdx1-iCre* founders. IHC revealed localised Cre recombinase expression in circularly arranged cell clusters (black arrows) in the pancreata of pigs #2017 and #2022 at 14 and 12 months of age, respectively. Scale bar represents 100 µm. Staining was performed by Laura Beltrán Sangüesa.

3.2.4 Modelling PDAC in *mPdx1-iCre* pigs

In order to model PDAC in *mPdx1-iCre* pigs, F1 boar #2332, carrying 11 copies of the *mPdx1-iCre* transgene was bred with a *TP53*$^{LSLR167H/LSLR167H}$*KRAS*$^{LSLG12D/WT}$ sow. Breeding resulted in birth of nine live-born piglets with iCre copy numbers varying from one to six (Table 39).

Table 39. *mPdx1-iCre* F2 generation.

Piglet number	Gender	Generation	Genotype	iCre copy number
2653	Female	F2	*TP53*$^{LSLR167H/WT}$*mPdx1*^{iCre}	2
2654	Female	F2	*TP53*$^{LSLR167H/WT}$*mPdx1*^{iCre}	1
2655	Female	F2	*KRAS*$^{LSLG12D/WT}$*mPdx1*^{iCre}	5
2656	Female	F2	*KRAS*$^{LSLG12D/WT}$*TP53*$^{LSLR167H/WT}$*mPdx1*^{iCre}	2
2657	Female	F2	*TP53*$^{LSLR167H/WT}$*mPdx1*^{iCre}	2
2658	Female	F2	*KRAS*$^{LSLG12D/WT}$*mPdx1*^{iCre}	3
2659	Male	F2	*TP53*$^{LSLR167H/WT}$*mPdx1*^{iCre}	4
2660	Male	F2	*TP53*$^{LSLR167H/WT}$*mPdx1*^{iCre}	5
2661	Male	F2	*TP53*$^{LSLR167H/WT}$	1

One animal (piglet #2658) was sacrificed at day 4 post partum to determine iCre function. This animal was genotyped as *KRAS*$^{LSLG12D/WT}$*mPdx1*^{iCre} with three copies of iCre. KRAS LSL-excision PCR for nine different tissues detected recombination in pancreas and duodenum (Figure 40A). Most importantly, analysis of pancreatic tissue revealed the presence of widespread ADM and PanIN regions with strong expression of Cre recombinase localised to these areas (Figure 40B+C), indicating a pronounced Pdx1 expression in these regions.

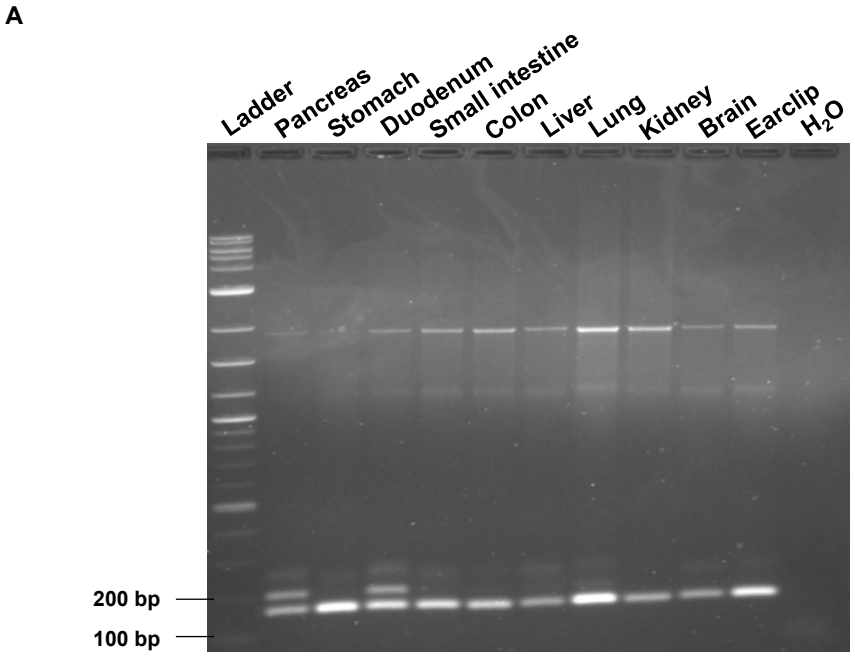

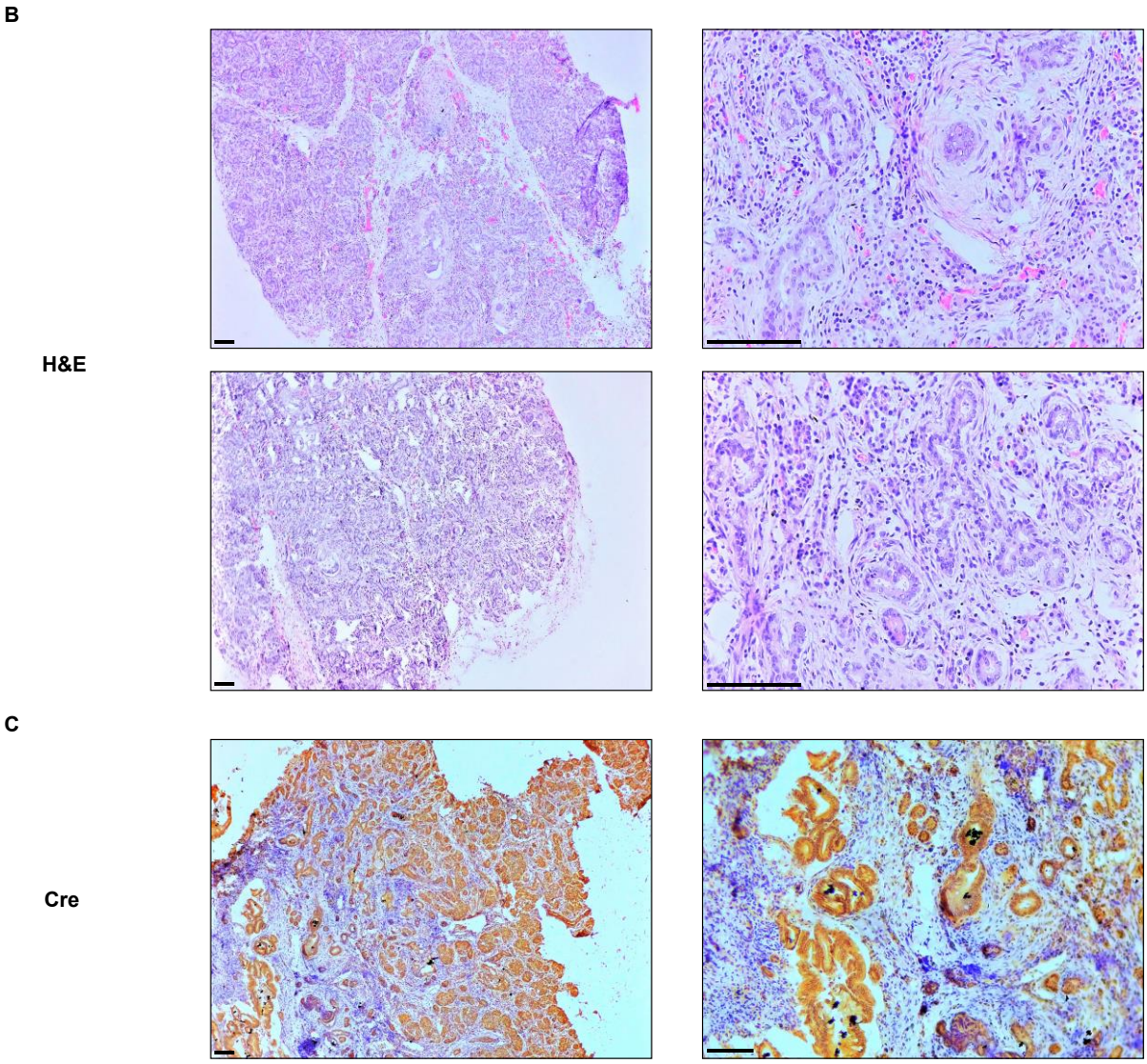

Figure 40. Analysis of *KRAS*$^{LSLG12D/WT}$*mPdx1*^{iCre} piglet. (A) KRAS LSL-excision PCR of tissues from 4 day old *KRAS*$^{LSLG12D/WT}$*mPdx1*^{iCre} piglet #2658 showed recombination in pancreas and duodenum, leading to three bands of 167 bp and 203 bp for the wild type and recombined allele, respectively, and the 1878 bp band for the unrecombined allele. (B) H&E staining of pancreatic tissue from piglet #2658. (C) IHC for expression of Cre recombinase in pancreatic tissue of piglet #2658. Scale bar represents 100 µm. Staining was performed by Laura Beltrán Sangüesa.

In summary, the results demonstrate the successful use of the PB transposon system to generate *mPdx1-iCre* pigs. The *mPdx1-iCre* pigs expressed iCre recombinase in the porcine pancreas, with restriction to pancreatic islet cells. In addition, analysis of a *KRAS*$^{LSLG12D/WT}$*mPdx1*^{iCre} piglet of the F2 generation revealed iCre recombination in the pancreas and duodenum as well as extensive ADM and PanIN lesions in the porcine pancreas. These findings show that the generated *mPdx1-iCre* pigs, like the *PTF1A*^{iCre} pigs, enable the generation of a porcine PDAC model.

3.3 Transformation and retransplantation of porcine cells

As described above, the main objective of this work was to activate *KRAS*^{G12D} and *TP53*^{R167H} mutations in *KRAS*$^{LSLG12D/WT}$ and *TP53*$^{LSLR167H/WT}$ pigs by crossing with pigs expressing Cre recombinase in the pancreas. As creating Cre driver pig lines was challenging, it was decided to use a parallel approach for the activation of *KRAS*^{G12D} and *TP53*^{R167H} mutations and the induction of tumour formation in the pig. Here the aim was to activate the porcine *KRAS*^{G12D} and *TP53*^{R167H} mutations with the help of the CRISPR/Cas9 system. Since progression of PDAC is accompanied by an accumulation of genetic alterations, a multiplex gene editing strategy was developed to manipulate the tumour suppressor genes (TSGs) most affected in PDAC development. Following activation of *KRAS*^{G12D} and *TP53*^{R167H} and the introduction of additional TSG mutations, the cells could then be used for retransplantation into the pig to assess their ability to induce tumour formation.

3.3.1 Activation of porcine *KRAS*^{G12D} and *TP53*^{R167H} by gene editing

As an alternative to activating the *KRAS*^{G12D} and *TP53*^{R167H} mutations via Cre recombinase, the option to excise the splice acceptor (SA) of the LSL cassette, using the CRISPR/Cas9 system, was assessed. Therefore, four gRNAs were designed (Table 40). SA gRNA 1 is specific for the loxP sequence, but only leads to cleavage of the 5' loxP site, due to the absence of a PAM sequence downstream of the 3' loxP site (Figure 41A). SA gRNAs 2 and 3 target the 3'end of the SA sequence of both the mutant *KRAS* and *TP53* alleles, while Neo gRNA 1 binds to the neomycin resistance gene only in the *KRAS* targeted allele (Figure 41B).

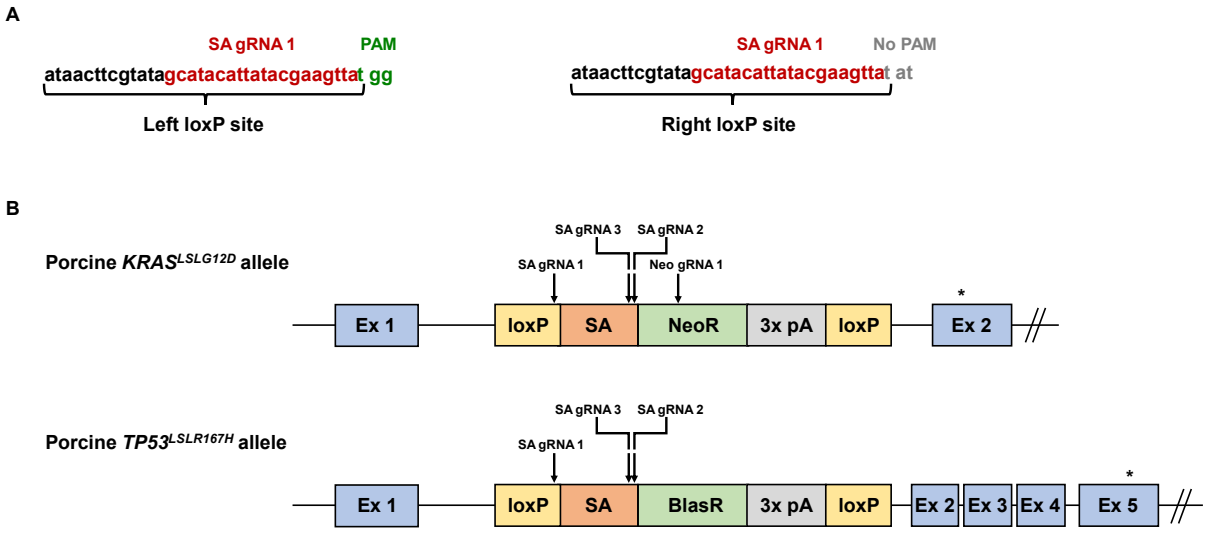

Figure 41. Application of gRNAs for *KRAS*^{G12D} and *TP53*^{R167H} activation. (A) SA gRNA 1 binds in both loxP sites, but only leads to cleavage of the left loxP site due to the absence of PAM following the gRNA binding site in the right loxP site. (B) Schematic representation of the gRNA binding sites in the porcine *KRAS*^{LSLG12D} and *TP53*^{LSLR167H} alleles. Ex: exon; loxP: loxP site; SA: splice acceptor; NeoR: neomycin resistance gene; BlasR: blasticidin resistance gene; pA: polyA; *: mutation

Table 40. gRNA sequences for SA excision.

Target	gRNA	gRNA sequence
Left loxP site	SA gRNA 1	5'-gcatacattatacgaagtta-3'
Splice acceptor	SA gRNA 2	5'-tctttccagtggggatcga-3'
Splice acceptor	SA gRNA 3	5'-tcgataccgtcgatccccac-3'
Neomycin resistance gene	Neo gRNA 1	5'-tgctattgggcgaagtgccg-3'

As sequence excision required the simultaneous application of two gRNAs, the following three Cas9-polycistronic tRNA-gRNA (PTG) multiplex-constructs were generated (Figure 42).

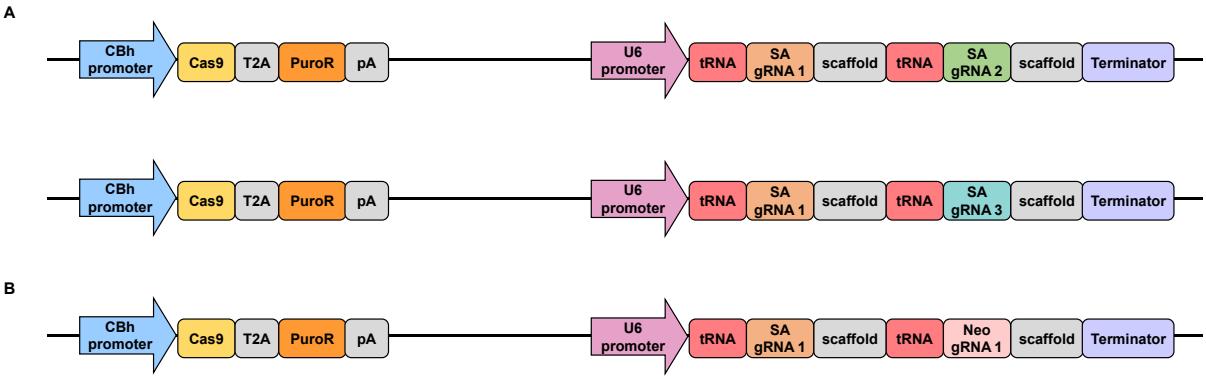

Figure 42. Cas9-PTG constructs for *KRAS*^{G12D} and *TP53*^{R167H} activation. (A) Cas9-PTG1/2 constructs for SA excision and activation of *KRAS*^{G12D} and *TP53*^{R167H}. (B) Cas9-PTG3 construct for removal of SA and part of the neomycin resistance cassette for *KRAS*^{G12D} activation.

SA gRNA 1 in combination with SA gRNA 2 (Cas9-PTG1) or SA gRNA 3 (Cas9-PTG2) should lead to removal of the SA sequence and thus to activation of both latent *KRAS*^{G12D} or *TP53*^{R167H} mutations (Figures 41B+42A). Since the *TP53*^{LSLR167H} allele does not contain a neomycin resistance gene (Figure 41B), activation of only *KRAS*^{G12D}, if desired, can be achieved by using SA gRNA 1 together with Neo gRNA 1 (Cas9-PTG3) (Figures 41B+42B).

Since the analysis of the porcine *KRAS*^{LSLG12D} allele allowed the evaluation of all three Cas9-PTG constructs, only PKF #232 cells (*KRAS*$^{LSLG12D/WT}$-*R26*$^{mT\text{-}mG/WT}$) were used for the determination of gene editing and mutational activation efficiencies. Therefore, PKF #232 cells were transfected with the generated Cas9-PTG constructs and genomic DNA and RNA was isolated for further analysis. PCR showed sequence excision upstream of porcine *KRAS* exon 2 for all three constructs compared to untransfected PKF #232 cells (Figure 43). The bachelor student Melissa Thalhammer participated in performing excision PCR.

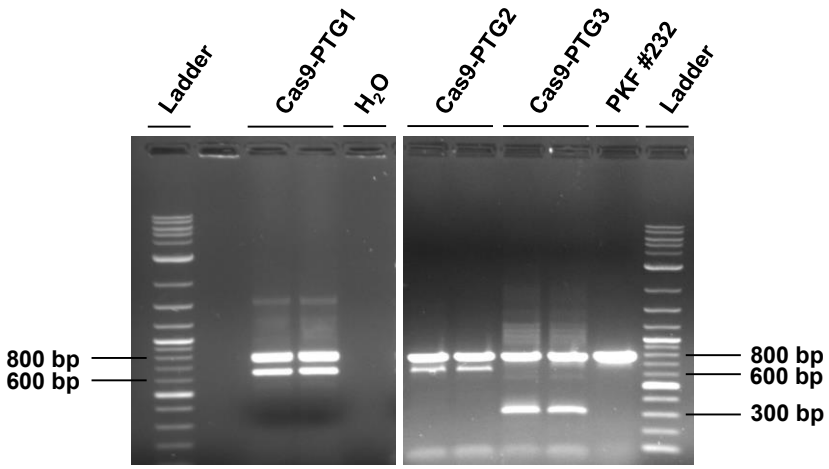

Figure 43. PCR for SA excision. PCR of PKF #232 cells transfected with Cas9-PTG1 showed an excision of approximately 148 bp, resulting in bands of 787 bp and 639 bp. Transfection with Cas9-PTG2 resulted in excision of about 143 bp, leading to bands of 787 bp and 644 bp. In contrast, gDNA from cells transfected with Cas9-PTG3 led to excision of a larger fragment of 467 bp and thus resulted in two bands of 787 bp and 320 bp on the agarose gel. PCR of untransfected PKF #232 cells showed no sequence excision and only one band of 787 bp.

Next, the efficiency of *KRAS*^{G12D} allele activation by CRISPR/Cas9-mediated SA excision was determined by pyrosequencing as described in section 3.1.3 (performed by the bachelor student Melissa Thalhammer). As pig #232 was heterozygous for *KRAS*^{LSLG12D}, the maximum frequency of a G→A mutation could be 50%. The frequency of an A variant in the *KRAS* gene was 26% for both Cas9-PTG1 and Cas9-PTG3, and 17% for Cas9-PTG2. Untransfected PKF #232 cells served as a control and showed a G→A prevalence of 2%, which was caused by background noise (Table 41) (Supplementary figures 25+26).

Table 41. Pyrosequencing results for G→A mutation at *KRAS* codon 12.

Condition	Nucleobase A	Nucleobase G
Cas9-PTG1 (SA gRNA 1 & SA gRNA 2)	26%	74%
Cas9-PTG2 (SA gRNA 1 & SA gRNA 3)	17%	83%
Cas9-PTG3 (SA gRNA 1 & Neo gRNA 1)	26%	74%
PKF #232 control	2%	98%

3.3.2 Inactivation of porcine tumour suppressor genes by multiplexed gene editing

The development and progression of PDAC is characterised by an accumulation of genetic alterations. As already mentioned in section 1.1.3, most affected genes are the proto-oncogene *KRAS* and the TSG *TP53*, but also TSGs *p16*, *SMAD4* and *BRCA1/2* [86, 87, 312]. In the context of pancreatic cancer, TSG alterations are largely of an inactivating or truncating nature. The CRISPR/Cas9 system allows efficient and straightforward manipulation of genes and therefore offers a suitable tool for the mutation of TSGs.

Using the “CRISPOR” gRNA design tool, different gRNAs were generated to target the coding DNA sequence (CDS) of porcine *p16* and *BRCA1/2*. Guide RNAs for inactivation of porcine *SMAD4* and *TP53* were designed and tested by Alessandro Grodziecki and Carolin Perleberg, respectively. As mentioned in section 1.1.3, the tumour suppressor $p16^{INK4A}$ is encoded by the *CDKN2A* locus, which also produces $p14^{ARF}$ due to an alternative reading frame. Both genes have their own promoter and first exons, but share parts of a common second exon [96, 313] (Figure 44). Therefore, gRNAs targeting porcine p16 were designed to bind in the CDS of its unique first exon, named exon 1A.

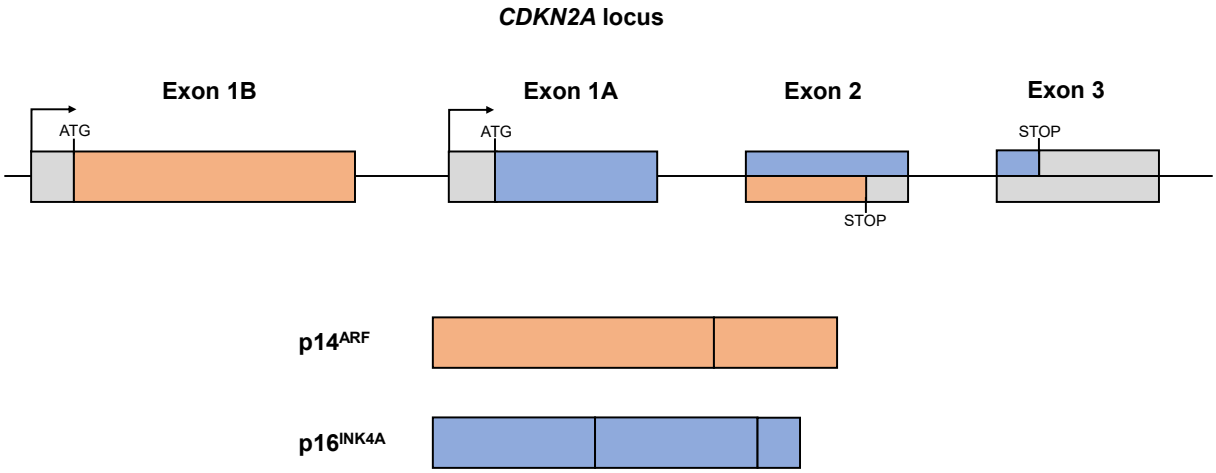

Figure 44. Alternative splicing at the *CDKN2A* locus. Illustration adapted from Sharpless (2005) and Fontana et al. (2019) [96, 313].

Due to the presence of eight splice variants, gRNAs targeting porcine *BRCA1* were selected to bind in exons three or four and exons five or six. For *BRCA2*, a gRNA binding in the first exon (3 bp downstream to the start codon) was chosen. Efficient gRNAs were identified by transfection of PKF cells followed by puromycin selection, isolation of gDNA from the cell pool and PCR analysis. InDel frequency was determined using “TIDE: Tracking of Indels by Decomposition” or “ICE v2 CRISPR” analysis tools. Analysis revealed high editing efficiencies for all tested gRNAs, ranging from 59% to 94% (Table 42). The most frequent mutation was 1 bp deletion or insertion, which led to the occurrence of a premature stop codon for porcine *p16*, *BRCA1* and *BRCA2*.

Table 42. gRNA efficiency results for TSG editing.

TSG	gRNA	gRNA target site	InDel efficiency	R^2 value	Most frequent alteration
Porcine p16	gRNA 3	Exon 1A (CDS)	94.2%	0.96	1 bp deletion
	gRNA 4	Exon 1A (CDS)	88.3%	0.9	1 bp deletion
Porcine BRCA1	gRNA 1	Exon 3/4 (CDS)	59%	0.9	1 bp insertion
	gRNA 2	Exon 5/6 (CDS)	82.8%	0.9	1 bp deletion
Porcine BRCA2	gRNA 1	Exon 1 (CDS)	80.3%	0.94	1 bp deletion

Since it was unclear at this stage whether inactivation of *TP53* and *BRCA2* was desired in all future experiments, the most efficient gRNAs were selected to generate three different PTG constructs that varied in the number and composition of gRNAs (Figure 45). Cloning was performed by the bachelor student Melissa Thalhammer. As mutations in *BRCA1* occur less frequently in PDAC, and the tested *BRCA1* gRNAs had the lowest editing efficiency it was not used for multiplexing.

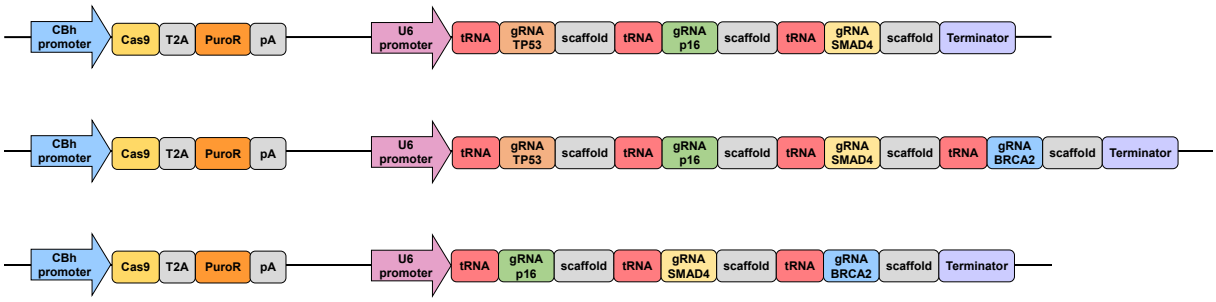

Figure 45. Cas9-PTG constructs for TSG knockouts.

Editing activity of the PTG constructs was evaluated after transfection into PKF #232 cells using “TIDE” or “ICE v2 CRISPR” analysis tools. As shown in Table 43, analysis revealed high editing efficiencies for all four gRNAs, regardless of their respective position in the tRNA-gRNA array:

Table 43. gRNA efficiency results for multiplexed TSG editing.

PTG construct	gRNA/ exon binding	InDel efficiency	R^2 value	Most frequent alteration	Premature stop codon
TP53-p16-SMAD4	TP53 Exon 5	57.3%	0.96	1 bp insertion	✓
	p16 gRNA 3 Exon 1A	80.1%	0.96	1 bp deletion	✓
	SMAD4 gRNA 2 Exon 3	93.2%	0.99	1 bp insertion	✓
TP53-p16-SMAD4-BRCA2	TP53 Exon 5	50.8%	0.92	1 bp insertion	✓
	p16 gRNA 3 Exon 1A	69.3%	0.95	1 bp deletion	✓
	SMAD4 gRNA 2 Exon 3	86.2%	0.99	1 bp insertion	✓
	BRCA2 gRNA 1 Exon 1	51.6%	0.99	1 bp deletion	✓
p16-SMAD4-BRCA2	p16 gRNA 3 Exon 1A	65.4%	0.96	1 bp deletion	✓
	SMAD4 gRNA 2 Exon 3	83.8%	0.98	1 bp insertion	✓
	BRCA2 gRNA 1 Exon 1	41.8%	0.98	1 bp deletion	✓

3.3.3 Retransplantation of transformed porcine cells

After establishing the multiplexing system, *in vitro* transformed porcine cells were to be tested for their ability to induce tumours after transplantation into pigs. Therefore, it was planned to inactivate the porcine TSGs *TP53*, *p16*, *SMAD4* and *BRCA2* and activate $KRAS^{G12D}$ and $TP53^{R167H}$ mutations. In order to enable not only autologous retransplantation of the transformed cells but also allotransplantation, the risk of cell rejection needed to be reduced. Options would be to carry out immune suppression, reduce immunogenicity of the transplanted cells or express immune regulatory genes in the cells. To test the latter two approaches, porcine Beta-2-microglobulin (B2M) was to be inactivated and/or LEA29Y expressed in the porcine cells. Since B2M is an essential subunit of porcine MHC class I, knockout of B2M leads to a lack of antigen presentation and thus prevents T cell activation. LEA29Y is a high affinity variant of the T cell co-stimulation inhibitor cytotoxic T-lymphocyte antigen 4 (CTLA4-Ig) that also inhibits T cell activation (Figure 46).

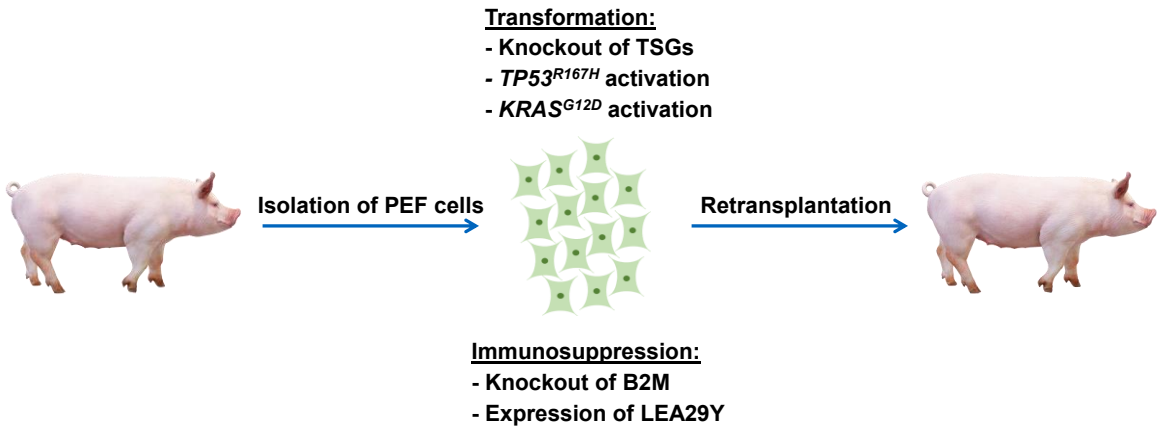

Figure 46. Transformation and retransplantation of porcine cells.

Inactivation of the above mentioned TSGs and B2M required the generation of a pentaplex Cas9-PTG construct using the following previously tested gRNAs:

Table 44. gRNAs used for pentaplexing.

Target	gRNA	gRNA sequence
Porcine TP53, exon 5	TP53 gRNA	5'-ggcaaaacagcttattga-3'
Porcine p16, exon 1A	p16 gRNA 3	5'-gaggctagccagtcggccga-3'
Porcine SMAD4, exon 3	SMAD4 gRNA 2	5'-actatgtacaatgctcagac-3'
Porcine BRCA2, exon 1	BRCA2 gRNA 1	5'-ggtctctctttgcatccaat-3'
Porcine B2M, exon 2	B2M gRNA	5'-tagcgatggctcccctcg-3'

To simplify the cloning strategy, the B2M gRNA was not added to the 3' end of the existing TP53-p16-SMAD4-BRCA2 construct, but was instead introduced together with TP53 gRNA into the p16-SMAD4-BRCA2 plasmid (Figure 47).

Figure 47. Cas9-PTG construct for transformation and retransplantation of porcine cells.

In addition, a LEA29Y overexpression plasmid for immunosuppression was generated:

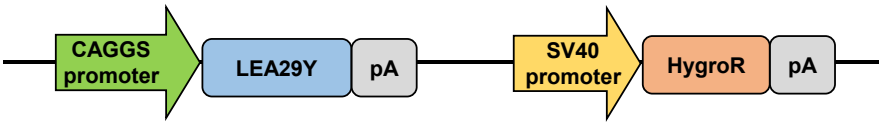

Figure 48. Structure of the pcDNA3.1-Hygro-CAG-LEA29Y overexpression vector.

Porcine ear fibroblast (PEF) cells isolated from 13 days old piglets #2094 and #2097 (*KRAS*$^{LSLG12D/WT}$-*TP53*$^{LSLR167H/WT}$) were co-transfected with the generated pentaplex and pcDNA3.1-Hygro-CAG-LEA29Y constructs. Because the puromycin selection was already harmful to the cells, the selection for LEA29Y expression with hygromycin was omitted to maximise cell viability following transfection. Nevertheless, LEA29Y expression was detected in both transfected #2094 and #2097 PEF cells (Figure 49).

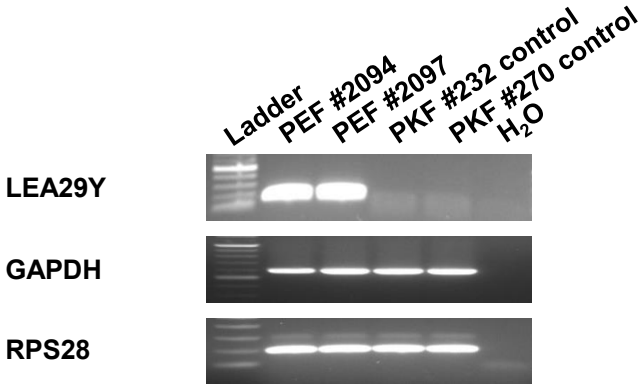

Figure 49. RT-PCR for LEA29Y expression. Expression of LEA29Y was detected at 171 bp for transfected #2094 and #2097 PEF cells. GAPDH and 40S ribosomal protein S28 (RPS28) served as controls for RNA quality and gave rise to bands at 576 bp and 186 bp, respectively.

Transfection with the pentaplex PTG construct resulted in high editing efficiencies for *p16*, *SMAD4* and *B2M*, medium efficiency for *TP53*, and low or no editing for *BRCA2* (Table 45).

Table 45. gRNA efficiency results for pentaplexed gene editing.

Cell isolate #2094					
	p16	**SMAD4**	**BRCA2**	**B2M**	**TP53**
InDel efficiency	90%	99%	5%	82%	36%
R^2 value	0.93	0.99	0.98	0.97	0.98
Cell isolate #2097					
InDel efficiency	96%	98%	8%	96%	61%
R^2 value	0.96	0.98	0.97	0.96	0.91

In the next step, *KRAS*^{G12D} and *TP53*^{R167H} mutations were activated in gene edited PEF cells by Cre protein transduction. Efficiency of Cre recombination was verified by LSL-excision PCR (Figure 50). Indeed, Cre protein transduction of gene-edited #2094 and #2097 PEF cells led to efficient excision of the LSL cassette for the *KRAS*^{LSLG12D} and *TP53*^{LSLR167H} alleles. However, while LSL cassette excision resulted in bands of equal intensity for the wild type (198 bp) and recombined (238 bp) *TP53* alleles, PCR for *KRAS* showed that the band for the recombined allele (203 bp) was of much higher intensity compared to the almost invisible wild type band (167 bp), suggesting a loss of wild type *KRAS* (Figure 50).

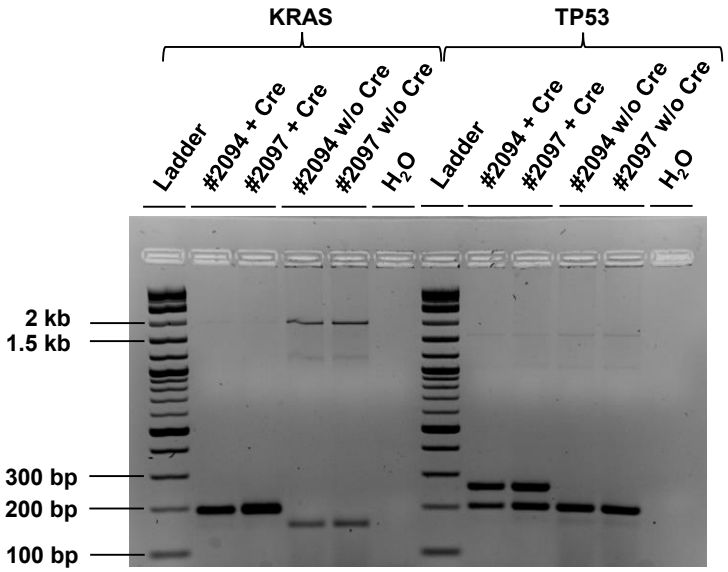

Figure 50. PCR for LSL excision after Cre protein transduction. KRAS PCR revealed two bands for untransduced #2094 and #2097 cells: A band of 1878 bp for the unrecombined LSL allele and a band at 167 bp for the wild type allele. Cre protein transduced cells showed a strong band for the recombined allele at 203 bp and only weak bands for the wild type and unrecombined allele at 167 bp and 1878 bp, respectively. TP53 PCR of untransduced #2094 and #2097 cells revealed two bands of 198 bp and 1520 bp for the wild type and unrecombined LSL allele, while transduction with Cre protein resulted in three bands at 198 bp, 238 bp and 1520 bp for the wild type allele, the recombined allele and the unrecombined LSL allele, respectively.

The expression of mutated *KRAS* and *TP53* was verified by RT-PCR followed by sequencing of the RT-PCR products. Sequencing revealed that Cre recombination resulted in successful G→A conversion for both *KRAS* and *TP53*, when compared to the unrecombined control samples (#232-*KRAS*$^{LSLG12D/WT}$-*R26*$^{mT\text{-}mG/WT}$ and #270-*R26*$^{mT\text{-}mG/WT}$ PKF cells) (Figure 51A+B).

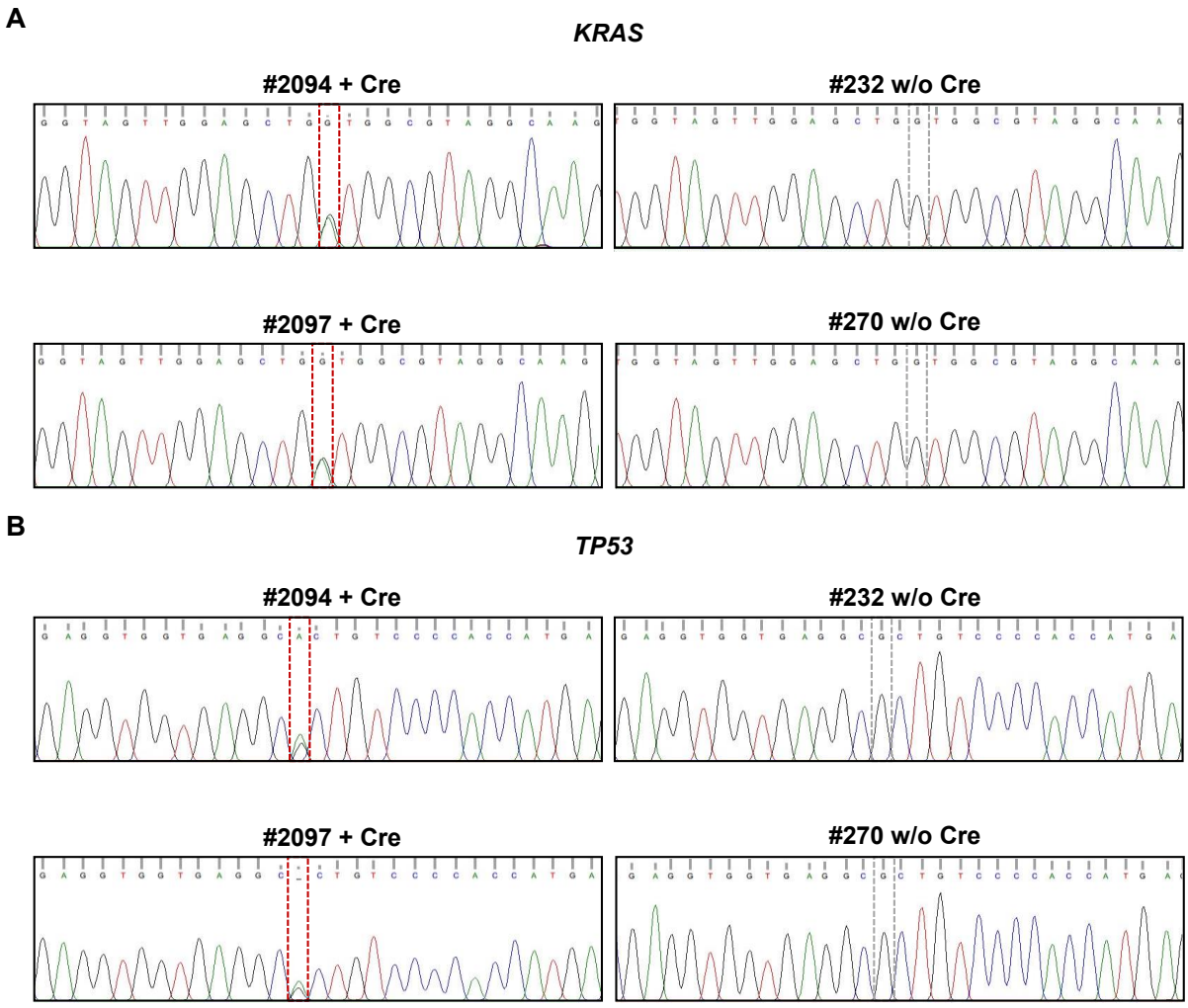

Figure 51. Sequencing of *KRAS* and *TP53* RT-PCRs. (A) Heterozygous G→A conversion at *KRAS* codon 12, resulting in G→D amino acid substitution. (B) Heterozygous G→A conversion at *TP53* codon 167, resulting in R→H amino acid substitution. Controls #232 and #270 only showed the presence of guanine at the respective positions.

Indeed, the modified cells showed an increased growth rate compared to the untransfected #2094 and #2097 control cells. Thus, after validating successful gene editing and Cre recombination, the modified cells were resuspended in PBS and autologously transplanted into pigs #2094 and #2097 at the age of 60 days. Although this was an autologous transplant, cells with B2M knockout and LEA29Y expression were used because it was unclear whether the cells would also be used for the other individual or other pigs in the near future. For pig #2094, 2 million cells were injected subcutaneously into the ear and flank site while pig #2097 was injected with 5 million cells each into and behind the ear as well as into the flank site (Figure 52). After injection, the pigs were monitored for tumour development, but no tumour growth was detected within the following 3.5 months.

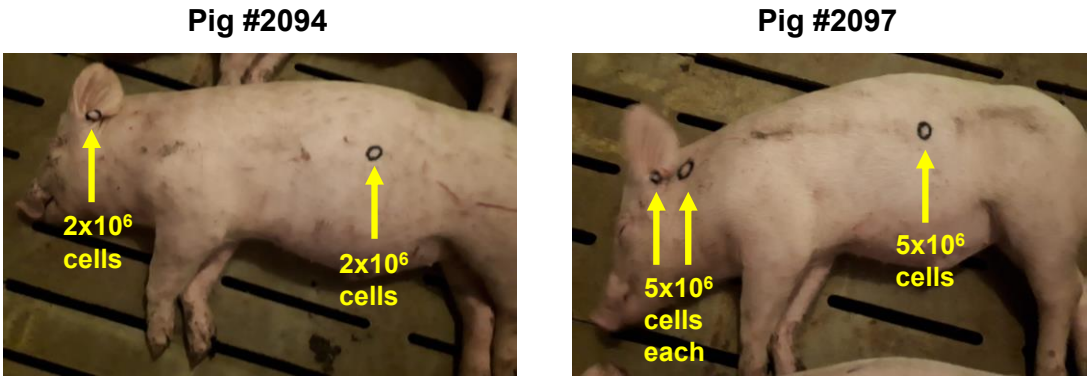

Figure 52. Retransplantation of modified PEF cells into pigs #2094 and #2097.

In summary, the above results described the establishment of a multiplexed gene editing strategy to achieve *KRAS*^{G12D} and *TP53*^{R167H} activation and inactivation of TSGs that are commonly mutated in human PDAC. The generated Cas9-PTG constructs achieved high editing efficiencies in porcine cells and therefore the capacity of the cells to form tumours was tested in a first attempt of autologous transplantation.

3.4 Porcine ADM modelling

ADM represents the first step in pancreatic carcinogenesis and is therefore of great interest for preclinical PDAC research with regard to early diagnosis and the development of effective treatment strategies. *In vitro* models for the cultivation and transdifferentiation of murine and human pancreatic acinar cells already exist and have provided a better understanding of the ADM process. As a porcine ADM model could allow validation and complementation of the data obtained so far from mouse and human cells, the isolation, cultivation and transdifferentiation of porcine acinar cells was established.

3.4.1 Establishment of porcine acinar cell culture

The first attempts to isolate and culture porcine pancreatic acinar cells were based on the protocols of De Waele et al. and Akanuma as a two-dimensional (2D) monolayer culture system with different media compositions (data not shown) [314, 315]. However, 2D systems do not mimic the conditions experienced by cells *in vivo*. As a consequence, it was decided to establish a three-dimensional (3D) culture instead. Therefore, the isolation procedure for porcine acinar cells was developed based on a modified version of the protocol for the isolation of mouse acinar cells established by Lubeseder-Martellato [282] (kindly provided by Thorsten Neuß, Klinikum rechts der Isar, TUM, Munich).

This protocol describes the isolation of pancreatic acinar cell clusters from 3-6 week old mice and their embedding in a 3D collagen system, thus allowing the investigation of the effect of transdifferentiating agents such as TGF-α on the acinar cells.

The first adaptations of the protocol to the pig were made by Kirsten Goijvaerts as part of her Master's thesis and were then further optimised as part of this project. After isolation, the porcine pancreatic tissue was processed by repeated digestion with collagenase, filtration and centrifugation before being embedded in a 3D collagen system (Figure 53A). If desired, Cre recombination was performed during the acinar cell recovery step as well as during embedding into collagen (Figure 53A). Piglets of 4-7 weeks of age were tested for acinar cell isolation and the best results in terms of quality and yield of acinar cell clusters were obtained when using 4-5 weeks old piglets (Table 46). To best mimic the natural environment, it was essential to maintain the grape-like acinar cell cluster structure during and after isolation. The optimal yield after successful isolation of porcine acinar cells and the preservation of their cell cluster structure before and after embedding in collagen is shown in Figure 53B.

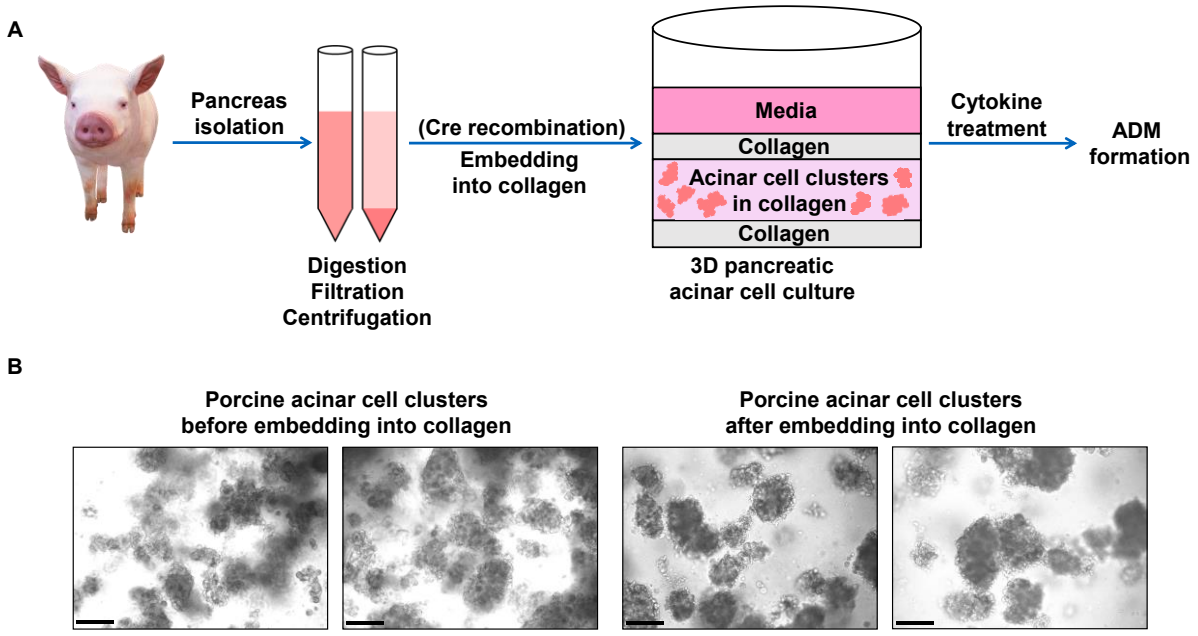

Figure 53. Porcine ADM modelling. (A) Pancreata isolated from young piglets were processed by digestion, filtration and centrifugation and the obtained acinar cell clusters were embedded into a 3D collagen system. If desired, Cre recombination was performed by transduction with Cre-VLPs or Cre-LV before and during embedding. Addition of cytokines such as TGF-α and IL-17A to the medium induced transdifferentiation of acinar cells towards ADM. (B) Porcine cell clusters during the recovery step and after embedding in collagen. Scale bar represents 100 µm.

Following isolation, the cytokines TGF-α (100 ng/ml) and IL-17A (20 ng/ml) were used for the induction of acinar cell transdifferentiation. In previous experiments, the cytokine TGF-β1 was also tested for the induction of ADM. As it resulted in very low ADM efficiency (data not shown), it was omitted from further experiments.

3.4.2 Transdifferentiation of porcine acinar cells

Once the isolation of porcine acinar cells and their 3D culture was fully established, the effect of cytokines on the transdifferentiation rates was studied and compared using cells isolated from animals representing different genotypes (Table 46). Due to the limited availability of 4-5 weeks old piglets with both mutant *KRAS* and *TP53*, also pigs with a *TP53* and *APC* mutant genotype were used to establish the method.

Table 46. Pigs used for the generation of the ADM data shown below.

Pig ID	Genotype	Gender	Age (in weeks w and days d)
#2071	$TP53^{LSLR167H/WT}$	Male	5w2d
#2059	$KRAS^{LSLG12D/WT}TP53^{LSLR167H/WT}$	Male	7w5d
#2084	$TP53^{LSLR167H/LSLR167H}$	Male	4w3d
#2093	$TP53^{LSLR167H/LSLR167H}$	Male	5w5d
#2107	$TP53^{LSLR167H/LSLR167H}$	Male	4w5d
#2125	$TP53^{LSLR167H/LSLR167H}$	Male	5w3d
#2108	$APC^{1311/WT}TP53^{LSLR167H/LSLR167H}$	Male	5w5d
#2109	$APC^{1311/WT}TP53^{LSLR167H/LSLR167H}$	Male	4w
#2122	$APC^{1311/WT}TP53^{LSLR167H/LSLR167H}$	Male	5w2d
#2210	$KRAS^{LSLG12D/WT}TP53^{LSLR167H/WT}R26^{Cas9/WT}$	Male	4w4d
#2242	$KRAS^{LSLG12D/WT}PTF1A^{5'iCre/WT}$	Male	5w2d

While establishing the 3D culture, only the effect of the cytokine TGF-α (100 ng/ml) on the transdifferentiation rate of pancreatic acinar cells was investigated. For this purpose, $TP53^{LSLR167H/WT}$ and $KRAS^{LSLG12D/WT}TP53^{LSLR167H/WT}$ pigs were used for acinar cell isolation (referred to as TP53 and KRAS/TP53 acinar cells), both with non-activated mutations. The cells developed duct-like structure with or without addition of TGF-α, but TGF-α increased the overall number of acinar clusters showing sphere formation (Figure 54A+B). Transdifferentiation was assessed by microscopy and manual counting of ADM structures per number of acinar cell clusters in the visual field on day two and four, respectively. The transdifferentiation rate of TP53 acinar cells treated with TGF-α was 14.67% compared to 7.83% for the untreated control on day 2 after isolation (Figure 54C). In contrast, KRAS/TP53 acinar cells showed a transdifferentiation of 29.4% at culture day 4 versus 9.98% for the control sample (Figure 54C). Since transdifferentiation was already visible on day 2, all future counts were carried out 2 days after isolation, except for sample #2242 which, for organisational reasons, was counted on day 3.

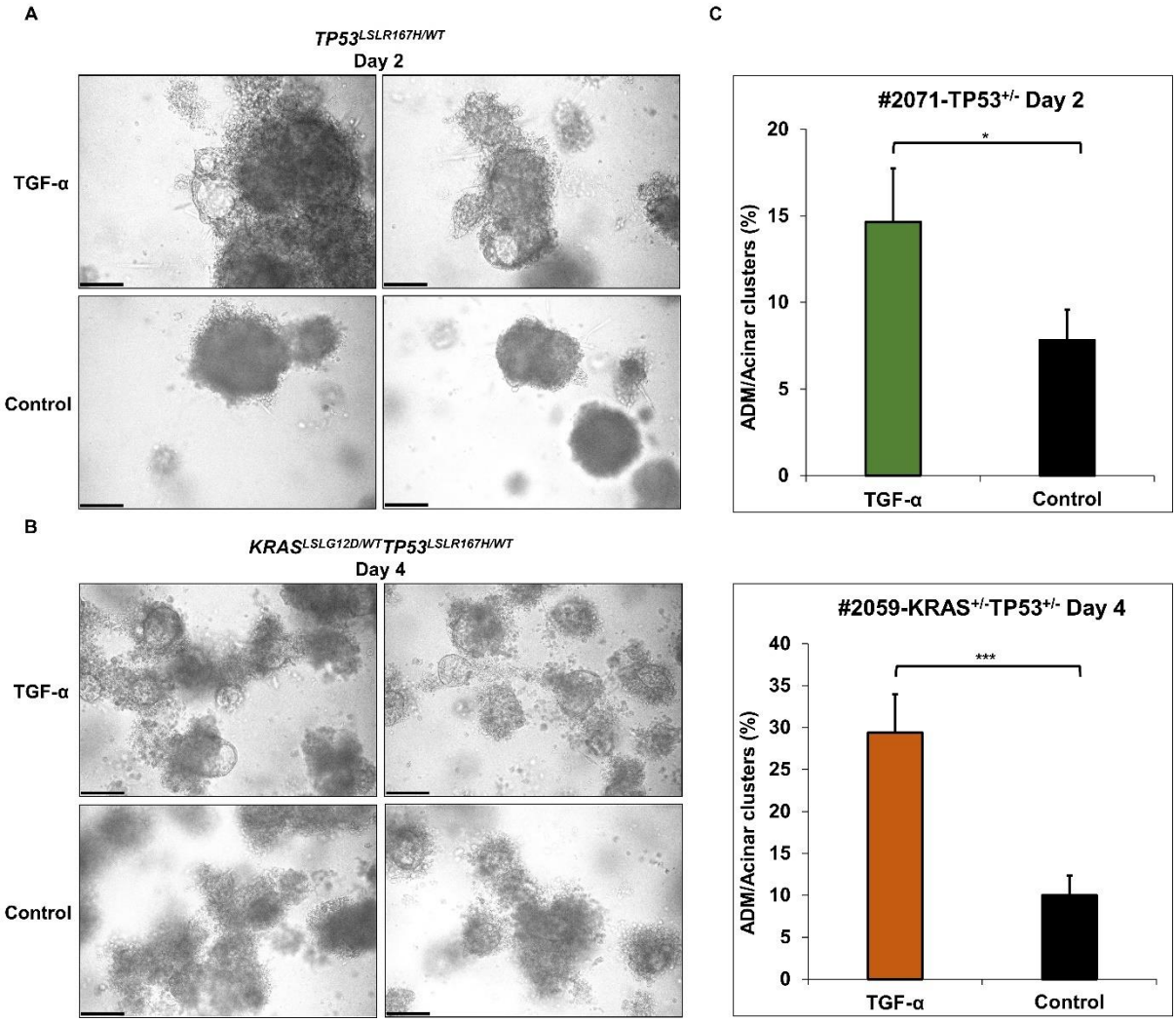

Figure 54. ADM modelling in *TP53* and *KRAS* mutant piglets. Porcine 3D acinar cell culture isolated from 5 week old $TP53^{LSLR167H/WT}$ and 7 week old $KRAS^{LSLG12D/WT}TP53^{LSLR167H/WT}$ piglets using two different culture conditions (100 ng/ml TGF-α or control). (A) Microscopy of a two-day-old acinar cell culture from $TP53^{LSLR167H/WT}$ piglet. (B) Microscopy of a four-day-old acinar cell culture from $KRAS^{LSLG12D/WT}TP53^{LSLR167H/WT}$ piglet. (C) Transdifferentiation rates indicated as percentage of ADM events per counted number of acinar cell clusters. Scale bar represents 100 µm. $TP53^{+/-}$: $TP53^{WT/LSLR167H}$, $KRAS^{+/-}TP53^{+/-}$: $KRAS^{WT/LSLG12D}TP53^{WT/LSLR167H}$, *p<0.05, **p<0.01, ***p<0.001

In the next step, the transdifferentiation of $TP53^{LSLR167H/LSLR167H}$ (TP53-hom) and $APC^{1311/WT}TP53^{LSLR167H/LSLR167H}$ (APC/TP53-hom) pancreatic acinar cells with non-activated mutant *TP53* allele was investigated. Since IL-17A has also been shown to mediate ADM induction in mice [316], both TGF-α and IL-17A were assessed for porcine ADM. Acinar cells from three pigs per genotype at 4-5 weeks of age, all with non-activated mutations, were used for the analysis. Cytokines TGF-α and IL-17A both led to successful transdifferentiation of the cells (Figure 55A). In detail, the average transdifferentiation rate of TP53-hom cells was 28.53% and 28.63% for TGF-α and IL-17A, respectively, with only 10.93% for the control sample (Figure 55B). Similarly, APC/TP53-hom cells demonstrated a transdifferentiation efficiency of 25.86% following TGF-α treatment and 24.36% after IL-17A administration compared to 11.6% duct-like cells in the control (Figure 55B).

In summary, the two cytokines did not differ significantly in the transdifferentiation rate they induced (Figure 55C). However, treatment with IL-17A was associated with the appearance of larger duct-like spheres (Figure 55A).

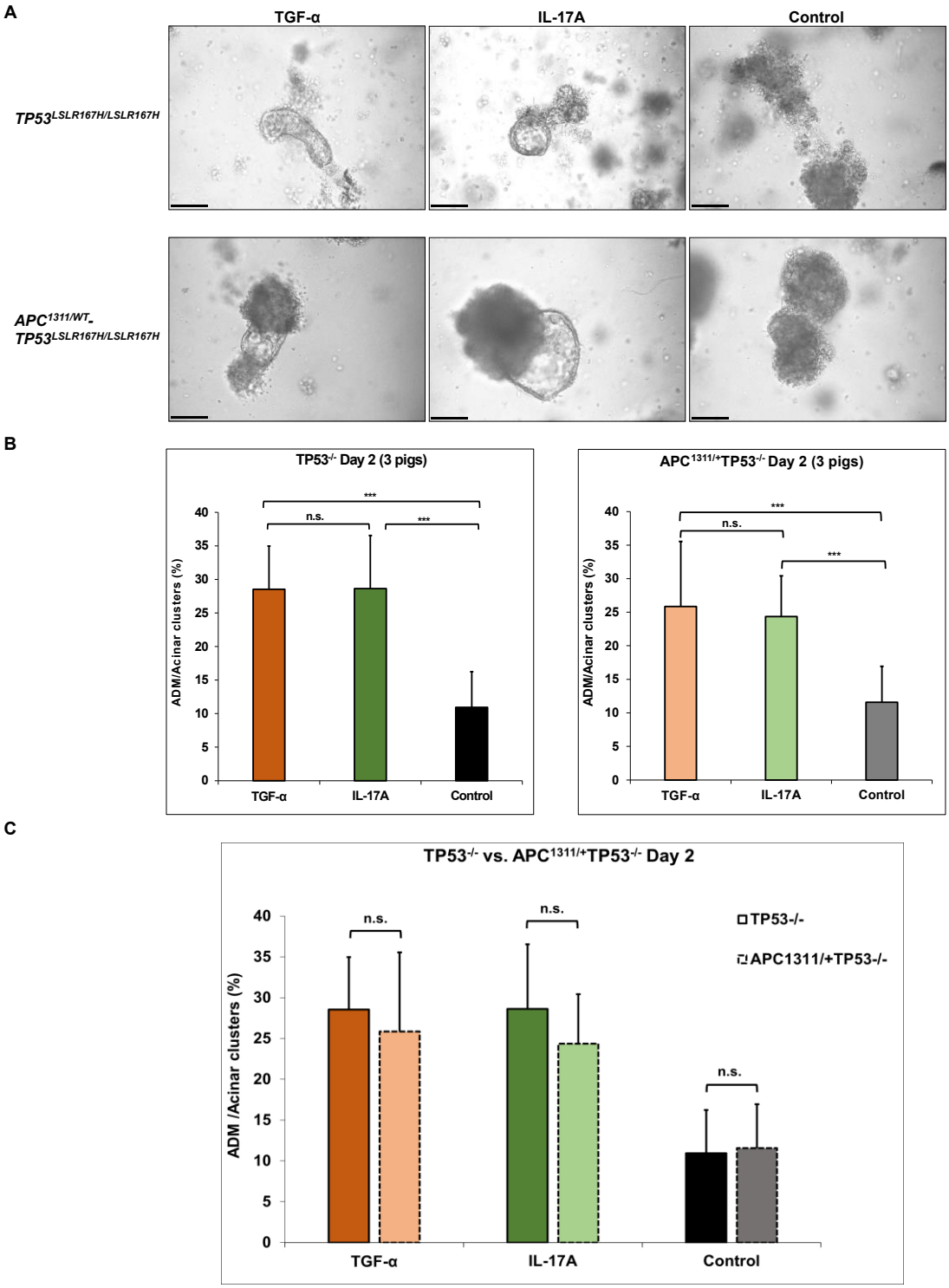

Figure 55. ADM modelling in *TP53* and *APC-TP53* mutant piglets. Porcine 3D acinar cell culture isolated from 4-5 week old *TP53*$^{LSLR167H/LSLR167H}$ and *APC*$^{1311/WT}$*TP53*$^{LSLR167H/LSLR167H}$ mutant piglets using three different conditions (100 ng/ml TGF-α, 20 ng/ml IL-17A or control). (A) Microscopy of two-day-old acinar cell cultures. (B) Transdifferentiation rates indicated as percentage of ADM events per counted number of acinar cell clusters. (C) Comparison of the transdifferentiation rates. Scale bar represents 100 µm. TP53$^{-/-}$: *TP53*$^{LSLR167H/LSLR167H}$, APC$^{1311/+}$TP53$^{-/-}$: *APC*$^{1311/WT}$*TP53*$^{LSLR167H/LSLR167H}$, *p<0.05, **p<0.01, ***p<0.001, n.s.: not significant

3.4.3 The effect of mutational activation on porcine acinar cell transdifferentiation

After the ADM-inducing effect of TGF-α and IL-17A was proven for the TP53-hom and APC/TP53-hom cells, the next step was to investigate whether an activated *TP53*^{R167H} mutation leads to increased transdifferentiation. For activation two approaches were tested, transduction of acinar cells, using either Cre lentivirus (LV) or Cre virus-like particles (VLPs) (Figure 56). The Co-cultivation with LV or VLPs was carried out both prior to embedding in collagen and concomitant with the addition of collagen.

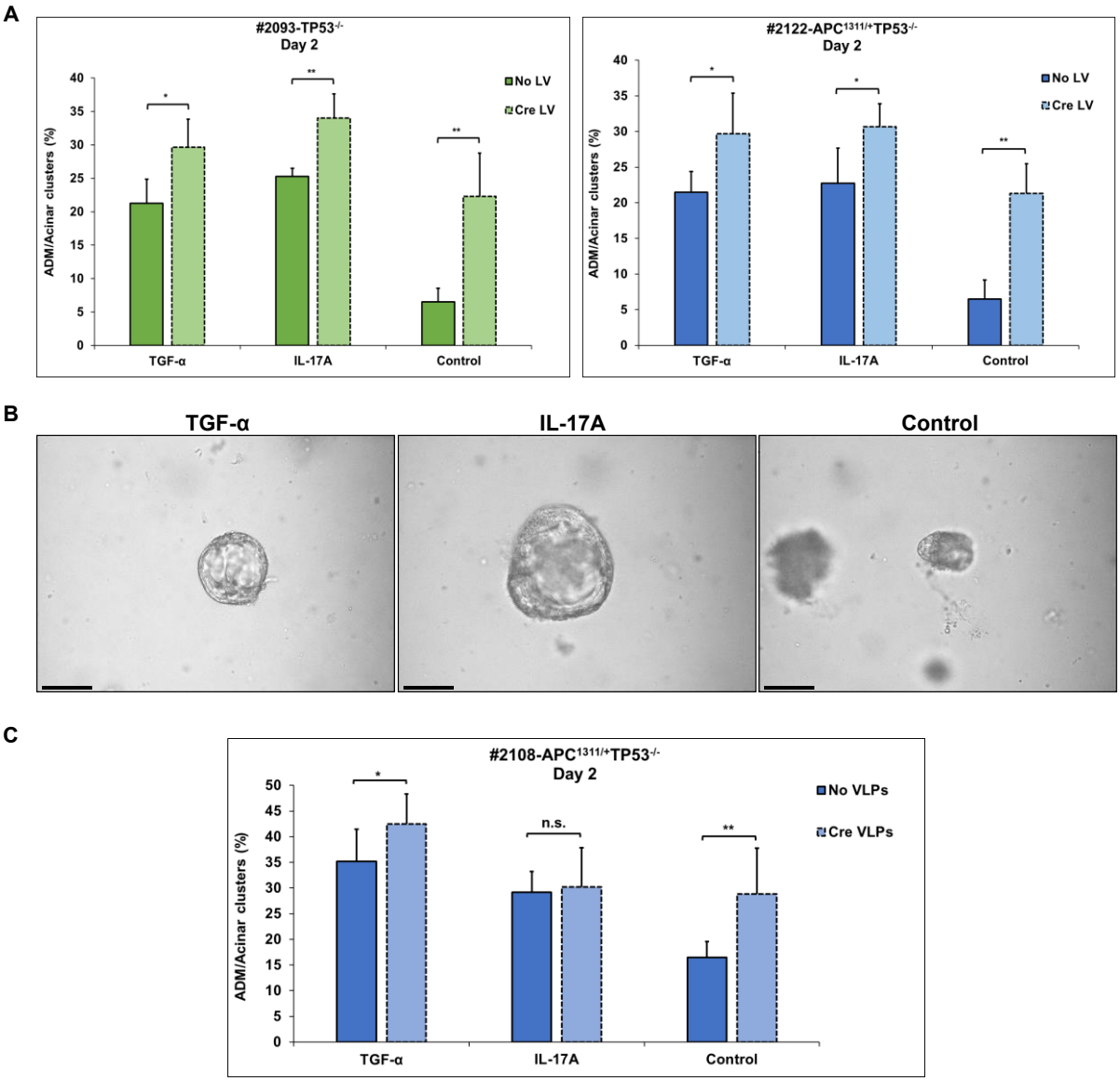

Figure 56. Method evaluation for Cre recombination in porcine acinar cells. Porcine 3D acinar cultures isolated from 5 week old *TP53*$^{LSLR167H/LSLR167H}$ and *APC*$^{1311/WT}$*TP53*$^{LSLR167H/LSLR167H}$ piglets, treated with Cre LV or Cre VLPs and cultured under three different conditions (100 ng/ml TGF-α, 20 ng/ml IL-17A or control). (A) Transdifferentiation rates of 2-day-old Cre LV transduced acinar cells from both genotypes indicated as percentage of ADM events per counted number of acinar cell clusters. (B) Two-day-old Cre LV acinar culture of piglet #2093. (C) Transdifferentiation rates of Cre VLP treated *APC*$^{1311/WT}$*TP53*$^{LSLR167H/LSLR167H}$ acinar cells cultured under three different conditions (100 ng/ml TGF-α, 20 ng/ml IL-17A or control). Scale bar represents 100 µm. TP53$^{-/-}$: *TP53*$^{LSLR167H/LSLR167H}$, APC$^{1311/+}$TP53$^{-/-}$: *APC*$^{1311/WT}$*TP53*$^{LSLR167H/LSLR167H}$, *p<0.05, **p<0.01, ***p<0.001, n.s.: not significant

Transdifferentiation was more prominent for both TP53-hom and APC/TP53-hom cells after Cre LV transduction in comparison to control cells (without Cre LV). For TP53-hom acinar cells, the transdifferentiation of control cells compared to Cre LV transduced cells was 21.25% vs. 29.67% for TGF-α, 25.25% vs. 34% for IL-17A and 6.5% vs. 22.3% for the control sample (Figure 56A, left panel). The ADM rate for APC/TP53-hom non-LV treated cells compared to Cre LV transduced cells was 21.5% vs. 29.67% for TGF-α, 22.75% vs. 30.67% for IL-17A and 6.5% vs. 21.3% for the control sample (Figure 56A, right panel). Microscopy also revealed that the ADM structures of the virus-transduced cells increased in size more quickly (Figure 56B), although they did not differ in shape from the duct-like spheres of non-LV treated cells shown previously. Transduction with VLPs only slightly increased the transdifferentiation rate of APC/TP53-hom cells compared to non-VLP treated cells, with 35.16% vs. 42.5% for TGF-α, 29.17% vs. 30.17% for IL-17A and 16.5% vs. 28.83% for the control (Figure 56C).

Besides a quantitative assessment of transdifferentiation, the expression analysis of acinar and ductal cell markers was attempted. Isolation of qualitatively sufficient RNA from the collagen discs proved to be difficult and required optimisation of the RNA isolation protocol. While this was achieved as proven by RT-PCR amplification of GAPDH (Supplementary figure 27), analysis of lineage markers is still outstanding.

After establishing both the ADM culture and Cre transduction protocol, these were applied to acinar cells isolated from a pig carrying latent $KRAS^{G12D}$ and $TP53^{R167H}$ mutations to mimic ADM in human patients. For reasons of availability, a 4 week-old $KRAS^{LSLG12D/WT}TP53^{LSLR167H/WT}R26^{Cas9/WT}$ piglet was used for this experiment, which also had the Cas9 transgene placed at the *ROSA26* locus. Without Cre-induction of mutant oncogenes the transdifferentiation rates were 38.56% for TGF-α treatment, 32.67% for IL-17A, and 13.88% for the control sample (Figure 57A, left panel). In order to later obtain a sufficient amount of nucleic acids from the acinar cells for recombination analysis by PCR and sequencing, the available number of acinar cell clusters did not allow treatment with Cre and comparison of all culture conditions. Therefore, only the control sample was treated with Cre recombinase to check whether activation of $KRAS^{G12D}$ and $TP53^{R167H}$ leads to an increase in the transdifferentiation rate. Transduction of the untreated control sample with Cre LV resulted in an increase in ADM prevalence from 13.88% to 27.38%. In contrast, no increase was observed after transduction with Cre VLPs (12.25%) (Figure 57A, right panel). The efficiency of recombination was investigated by LSL-excision PCR using gDNA isolated from day 3 culture of Cre LV and Cre VLP transduced and untransduced control cells (Figure 57B).

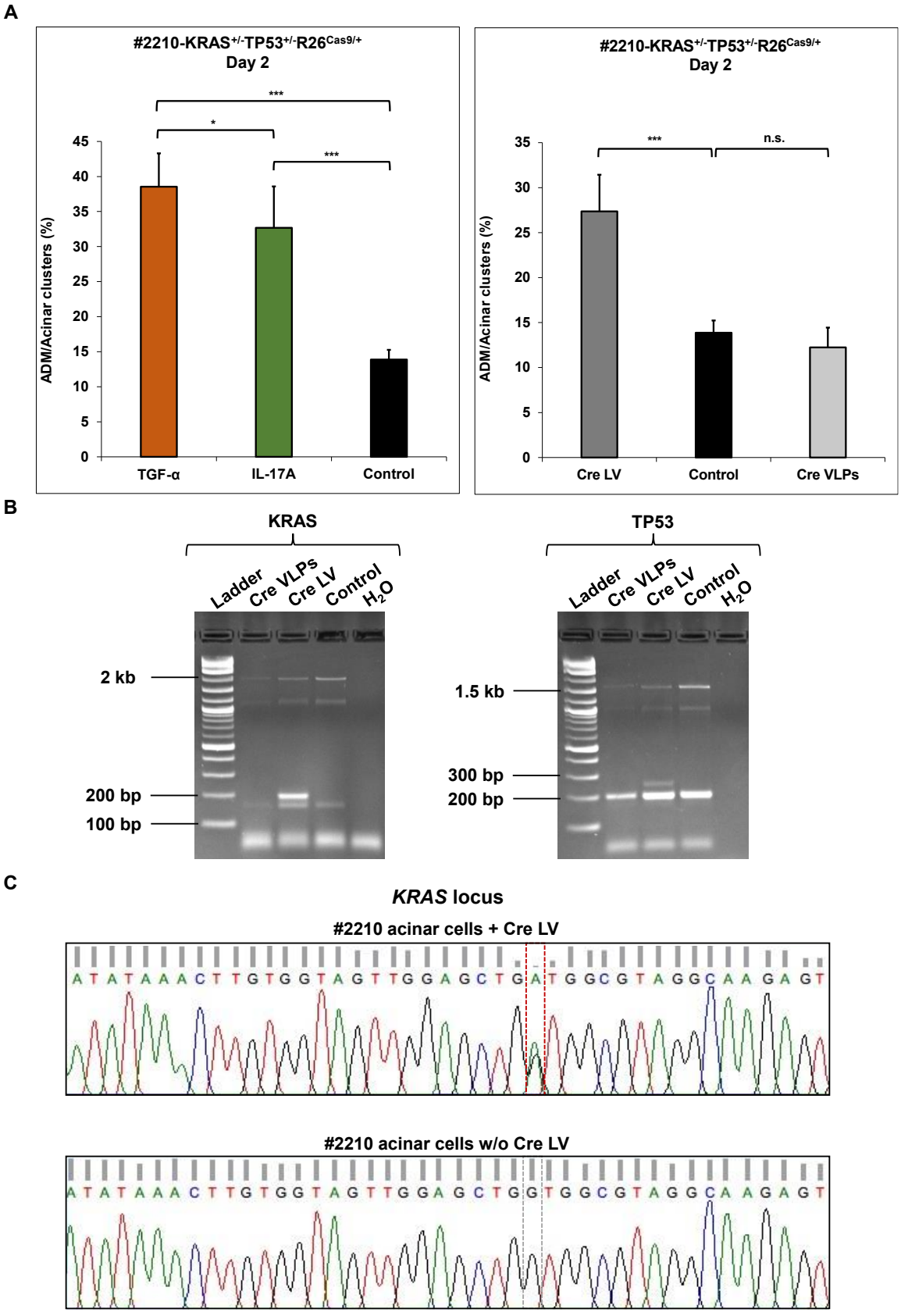

Figure 57. *KRAS*^{G12D} and *TP53*^{R167H} activation in porcine acinar cells. (A) Transdifferentiation rates of two-day-old acinar cells, isolated from 4 weeks old *KRAS*$^{LSLG12D/WT}$*TP53*$^{LSLR167H/WT}$*R26*$^{Cas9/WT}$ piglet, that were either cultured under three different conditions (100 ng/ml TGF-α, 20 ng/ml IL-17A or control) or transduced with Cre LV or Cre VLPs for mutational activation. (B) LSL-excision PCR for *KRAS*^{G12D} and *TP53*^{R167H} activation. (C) Sequencing of *KRAS* using RT-PCR products of Cre LV transduced and untransduced acinar cells from piglet #2210. KRAS$^{+/-}$TP53$^{+/-}$R26$^{Cas9/+}$: *KRAS*$^{WT/LSLG12D}$*TP53*$^{WT/LSLR167H}$*R26*$^{Cas9/WT}$, *p<0.05, **p<0.01, ***p<0.001

Transduction with Cre LV resulted in excision of the LSL cassette of both the *KRAS*^{G12D} and *TP53*^{R167H} alleles, while no recombination was detected after Cre VLP administration to the pancreatic acinar cells (Figure 57B). The lack of recombination for Cre VLP treated acinar cells corresponds to the absence of transdifferentiation shown in Figure 57A (right panel). Since the same Cre VLP preparation was used as before, the slightly increased transdifferentiation rate of the APC/TP53-hom cells in the previous experiment (Figure 56) may not have been due to successful recombination, but rather to the treatment procedure.

In order to verify mutation expression, cDNA was amplified and RT-PCR was performed. Due to the low quantity of available cDNA, only the expression of *KRAS*^{G12D} was assessed. Consistent with the findings shown above, sequencing of the RT-PCR products confirmed the expression of a G→A single base mutation for Cre LV transduced acinar cells at *KRAS* codon 12, resulting in a G→D amino acid substitution and thus expression of *KRAS*^{G12D} (Figure 57C).

As described above, the Cre LV induced activation of *KRAS*^{G12D} and *TP53*^{R167H} mutations resulted in increased transdifferentiation frequency when compared to the non-transduced control sample (Figure 57A). Consequently, it was interesting to investigate if TGF-α and IL-17A treatment of acinar cells carrying activated *KRAS*^{G12D} mutation isolated from *KRAS*$^{G12D/WT}$*PTF1A*$^{5'iCre/WT}$ pig #2242 will lead to higher transdifferentiation rates. As previously demonstrated in section 3.1.3, this pig had an active *KRAS*^{G12D} allele in the pancreas and was diagnosed with ADM and PanIN lesions. After the isolation of acinar cells, they were treated with TGF-α (100 ng/ml) and IL-17A (20 ng/ml) and the transdifferentiation rates were assessed on day 3 after isolation. As expected, the cytokine treatment resulted in high transdifferentiation rates of 51.25% and 65% for TGF-α and IL-17A, respectively, compared to the untreated control sample which revealed an ADM occurrence of 24.25% (Figure 58A). In line with this, microscopy showed the presence of multiple large duct-like spheres evolving from single acinar cell clusters (Figure 58B).

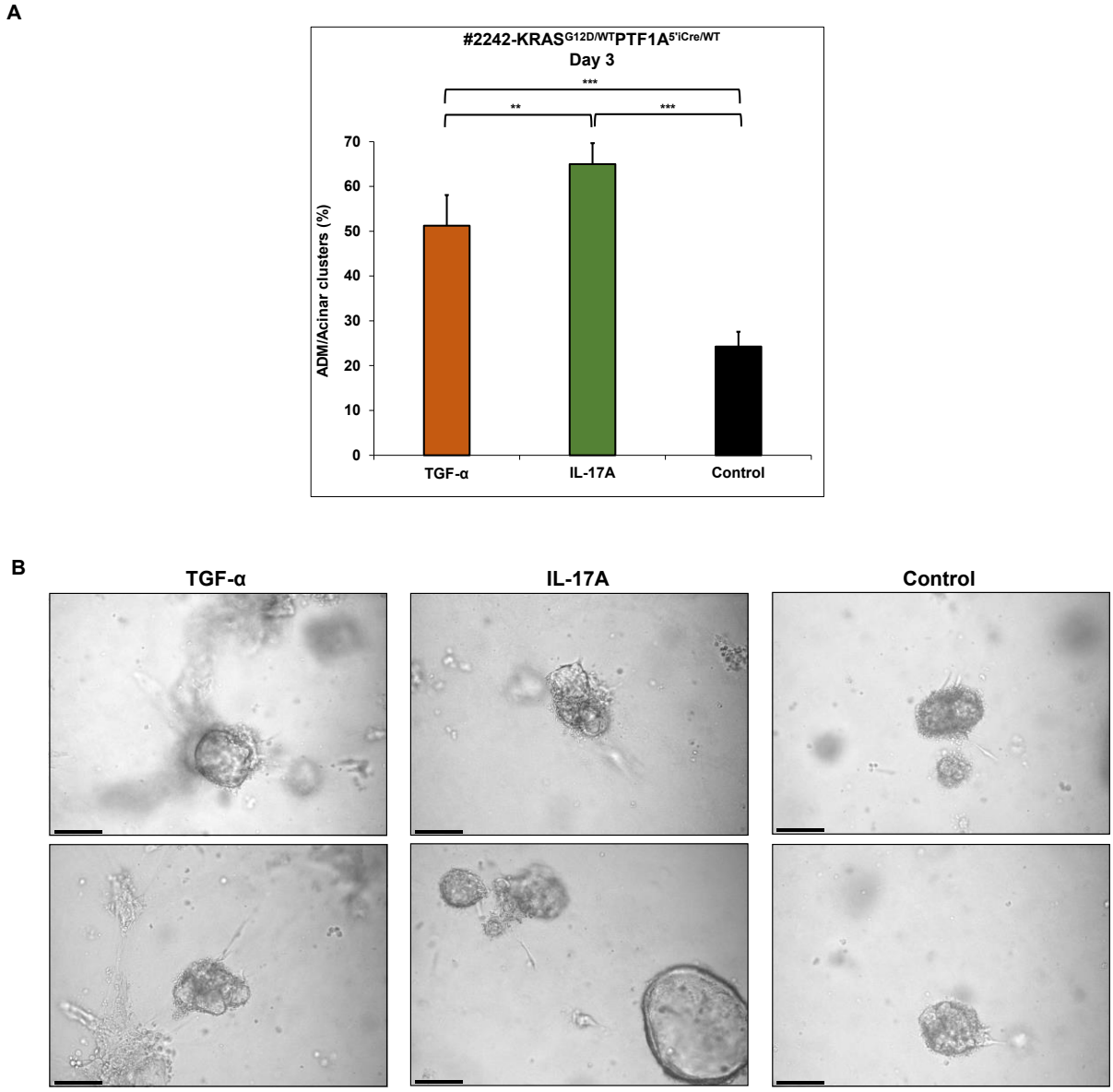

Figure 58. ADM modelling in *KRAS*$^{G12D/WT}$*PTF1A*$^{5'iCre/WT}$ porcine acinar cells. (A) Transdifferentiation rates of a three-day-old acinar cell culture that was isolated from a 5 week old *KRAS*$^{G12D/WT}$*PTF1A*$^{5'iCre/WT}$ piglet and cultured under three different conditions (100 ng/ml TGF-α, 20 ng/ml IL-17A or control). (B) Microscopy of the three-day-old acinar cell culture from piglet #2242. Scale bar represents 100 µm, *p<0.05, **p<0.01, ***p<0.001

The above results show the successful establishment of protocols for ADM induction in porcine pancreatic acinar cells and the comparison of two different cytokines in terms of their transdifferentiation induction capacity. It was also demonstrated that oncogene expression, either by Cre-activation of latent *KRAS*^{G12D} in cultured acinar cells or in the developing piglet, resulted in an increase in ADM.

4 Discussion

Higher life expectancy and the rise of risk factors such as obesity and diabetes are leading to a global increase in cancer incidence. While death rates from lung, breast and colon cancer have declined in recent years, mainly due to prevention and early detection strategies, few improvements have been observed for pancreatic cancer [64, 317-320]. In fact, the incidence and death rates for pancreatic cancer continue to increase [19, 20, 320]. As PDAC is characterised by late diagnosis and thus poor prognosis, improvements in early detection and treatment strategies are urgently needed. Therefore, a porcine model recapitulating the human PDAC phenotype could serve as a translational model allowing validation and complementation of findings obtained from *in vitro* and mouse studies with high predictive value. Based on the work of Hingorani and colleagues with mice, Schnieke et al. have generated pigs that carry latent *KRAS*^{G12D} and *TP53*^{R167H} mutations, which are orthologues of the most common mutations in human PDAC and can be activated by Cre recombination [177, 178]. The major aim of this work was to generate the necessary Cre driver lines to activate the mutations in the porcine pancreas, a final step required to model pancreatic tumour formation. This is discussed in section 4.1. As an alternative to cancer modelling with the help of Cre driver pig lines, section 4.2 addresses the transformation of porcine cells by multiplexed CRISPR/Cas9-mediated gene editing and their retransplantation. Finally, the isolation and transdifferentiation of porcine pancreatic acinar cells to model acinar-to-ductal metaplasia (ADM) *in vitro* is discussed in section 4.3.

4.1 Cre driver pigs for PDAC modelling

As already mentioned, the main objective of this work was to activate the latent *KRAS*^{G12D} and *TP53*^{R167H} mutations in the porcine pancreas to generate a pig model for PDAC. Excision of the LSL cassette and the resulting expression of the mutations can be achieved by Cre recombination. However, mutational activation during early pig development needs to be tissue-restricted as widespread expression of *KRAS*^{G12D} was shown to be embryonically lethal in mice [321, 322]. In the murine PDAC model of Hingorani and colleagues, mutational activation was induced in pancreatic progenitor cells by expression of Cre recombinase from the pancreas-specific gene promoters *Pdx1* and *Ptf1a*, which are active from embryonic days 8.5 and 9.5, respectively [151, 162, 283]. Based on the mouse model, mutational activation was also desired in all pancreatic cell types in the pig. Therefore, the major part of this thesis consisted of generating pigs expressing Cre recombinase from the endogenous *PTF1A* or the murine *Pdx1* promoter. Following characterisation, these Cre driver pigs were then used for breeding with pigs carrying latent *KRAS*^{G12D} and *TP53*^{R167H} mutations to achieve mutational activation in the offspring.

4.1.1 *PTF1A*^{iCre} pigs for PDAC modelling

4.1.1.1 *PTF1A* targeting and generation of *PTF1A*^{iCre} pigs

The *PTF1A*^{iCre} driver pig line was generated by targeting the iCre recombinase gene into the endogenous porcine *PTF1A* locus with the help of the CRISPR/Cas9 system. The first targeting strategy was based on iCre placement into the 5'end of *PTF1A*. In mice, heterozygous inactivation of *Ptf1a* was shown to be associated with decreased gene expression, but had no effect on viability or fertility [323]. In contrast, homozygous knockout led to a lack of the exocrine pancreas, which resulted in a lethal condition shortly after birth [155]. Therefore, it was essential to achieve only heterozygous 5'end targeting and to preserve the integrity of the second *PTF1A* allele. Although no abnormalities in vitality, fertility or body size were observed in mice with heterozygous *Ptf1a* inactivation [323], the effect of reduced *PTF1A* expression in pigs was unknown. Therefore, a second targeting strategy based on *PTF1A* 3'end targeting was carried out in parallel.

As already shown in my master thesis, CRISPR/Cas9-mediated integration of iCre into the 5'end of porcine *PTF1A* was highly efficient, but also associated with unwanted loss of function of the second allele due to InDel mutations [287]. As described in chapter 1.6.3, these InDel mutations are caused by non-homologous end joining (NHEJ), which represents the major pathway of DNA double-strand break (DSB) repair [268]. Consequently, targeting into the 5'end was performed using Cas9 nickase (Cas9n), a Cas9 variant that, unlike conventional Cas9, only generates DNA single-strand breaks (SSBs). DNA SSBs are the most common form of DNA damage and occur mainly due to the attack of reactive oxygen species, as an intermediate in base excision repair or in the case of defective function of cellular enzymes [324]. Steps including DNA break sensing, end processing, DNA polymerase-mediated gap filling and final ligation enable error-free repair of SSBs and thus the preservation of genomic integrity [324, 325]. Therefore, due to the activation of different mechanisms, the repair of SSBs is associated with less mutagenic end joining than DSBs and is thus more suitable for applications where the integrity of the second allele needs to be ensured [288, 289]. Following CRISPR/Cas9-mediated DNA cleavage, the integration of iCre recombinase into the porcine *PTF1A* locus relied on homology-directed repair (HDR). Although HDR is mainly reported on DSBs, homologous recombination has also been shown to occur on DNA nicks [326-328]. As the HDR frequency for SSBs is lower than for DSBs [290, 327], measures were taken to increase the targeting efficiency.

Interestingly, HDR was shown to be more efficient at nicks on the transcribed DNA strand than on the non-transcribed strand [290]. Based on these findings, the Cas9n variant with D10A mutation, which renders the RuvC domain inactive, was chosen for *PTF1A* 5'end targeting.

The active HNH domain of this Cas9n variant thus cleaved the transcribed strand as it was complementary to the selected gRNA. In addition, a further increase in HDR efficiency should be achieved by using a nicked double-stranded DNA (dsDNA) donor as a repair template, since the parallel generation of SSBs in donor and target DNA has been shown to promote HDR [290, 329]. Indeed, the application of Cas9n together with a nicked dsDNA donor resulted in high targeting efficiencies, even higher than those reported for the use of conventional Cas9 nuclease in unsynchronized cells [328, 330, 331].

Although the *PTF1A* 5'end targeting strategy was highly efficient and no abnormalities were reported in mice with heterozygous *Ptf1a* inactivation [323], the effect of reduced *PTF1A* expression in pigs was unclear. Therefore, a second strategy based on the placement of iCre into the 3'UTR of *PTF1A*, thus maintaining the endogenous function of the targeted allele, was carried out in parallel. Successful expression from the porcine *PTF1A* promoter required the removal of the endogenous stop codon and the introduction of a "self-cleaving" peptide from thosea asigna virus 2A (T2A) upstream of the iCre sequence [292]. Several viral 2A sequences are known to enable co-expression of genes and have already been used to generate multitransgenic pigs [332, 333]. During translation, 2A sequences induce self-cleavage of the polyprotein in a process called "ribosome skipping", resulting in the co-expression of equal amounts of proteins [334, 335]. This equimolar expression from the same open reading frame makes 2A sequences best suited for the simultaneous expression of multiple genes compared to the use of an internal ribosomal entry site (IRES), which is often associated with lower expression of the downstream genes [336, 337]. Interestingly, despite the use of conventional Cas9 nuclease in combination with a double cut donor template for increased knock-in probability [291], the HDR efficiency for *PTF1A* 3'end targeting was lower than for Cas9n-mediated 5'end integration. However, this could be due to the fact that different cell types were used for the two targeting strategies.

4.1.1.2 *PTF1A*^{iCre} founders and *PTF1A*^{iCre} progeny

Both cell isolates used for *PTF1A* 5' and 3' targeting proved to be suitable for the generation of transgenic pigs by somatic cell nuclear transfer (SCNT). Among the nine born *PTF1A*^{iCre} piglets, the stillbirth rate for the 5'end targeted piglets was higher than for the 3'end targeted animals. However, a reliable correlation between an increased stillbirth rate and reduced *PTF1A* expression, due to the disruption of one endogenous allele, would require the examination of multiple litters and the quantitative determination of *PTF1A* expression levels for both genotypes.

As shown in section 3.1.1.4, *PTF1A*$^{5'iCre}$ pigs carried only one copy of iCre, while *PTF1A*$^{3'iCre}$ pigs had between two and seven iCre copies. Nevertheless, there was no correlation detectable between stillbirth and iCre copy number in the *PTF1A*$^{3'iCre}$ pigs. In fact, despite its high value for genome engineering, disadvantages have been reported regarding the use of Cre recombinase in the past. For example, *in vitro* expression of Cre recombinase in mammalian cells was shown to be associated with DNA damage, defective proliferation and genome instability [338, 339]. In line with this, several groups reported toxicity of Cre expression in cardiomyocytes and neurons *in vivo*, leading to cardiomyopathy and brain developing defects, respectively [340, 341]. However, the generated *PTF1A*^{iCre} founder animals showed no signs of toxicity by Cre expression, regardless of the number of iCre copies. Since the probability of a toxic effect of iCre also depends on the expression level, it can be assumed that the additional iCre copies in *PTF1A*$^{3'iCre}$ pigs were non-functional due to random integration in the absence of a promoter and thus did not lead to overexpression of iCre recombinase.

The generation of Cre driver lines by *PTF1A* targeting was successful, as all born founder pigs expressed iCre recombinase in the pancreas. In addition, mRNA analysis of the stillborn *PTF1A*$^{5'iCre}$ and *PTF1A*$^{3'iCre}$ piglets also revealed iCre expression in the testicles and stomach and, in the case of *PTF1A* 5'end targeting, also in the brain. This RNA expression pattern was largely consistent with the expression of porcine wild type *PTF1A*, which in turn corresponded to the human *PTF1A* expression profile, as shown by ProteomicsDB and The Human Protein Atlas [342, 343]. Interestingly, the tissue-specific RNA expression detected for the stillborn piglets diverged slightly from the RNA expression profile of founder animals #1964 and #1962 which were sacrificed at 6.5 weeks and 9 months of age, respectively. Despite the age difference at the time of execution, #1962 and #1964 showed the same iCre expression pattern which was restricted to stomach and pancreas. In line with this, expression of *PTF1A* was detected in the pancreas, stomach and weakly in the cerebellum in both *PTF1A*^{iCre} driver lines as well as in the wild type porcine control. Immunohistochemistry (IHC) of pancreas samples from *PTF1A*^{iCre} pigs showed that expression of Cre recombinase was restricted to acinar cells while it was absent in other pancreatic cell types. In contrast, the green fluorescence pattern in pancreatic tissues of *Reporter-PTF1A*^{iCre} pigs revealed widespread recombination throughout the organ. This is consistent with the literature, which reports that *PTF1A* is expressed in all pancreatic progenitors during embryogenesis, but is later restricted to acinar cells in the mature pancreas [151-153, 158]. As a consequence, Cre recombination occurred in all pancreatic cell types during early embryogenesis, leading to a switch from red to green fluorescence in the pancreata of *Reporter-PTF1A*^{iCre} pigs.

In addition, fluorescence analysis showed extensive recombination in the cerebellum of *Reporter-PTF1A*^{iCre} pigs while IHC did not detect Cre protein in cerebellar samples of *PTF1A*^{iCre} pigs. According to the literature, *Ptf1a* is expressed in the neural tube during early murine embryogenesis (E9-10), and later extends to the cerebellum, where it determines the cell fate of neuronal precursors [151, 344, 345]. Furthermore, *PTF1A* plays an indispensable role in neurogenesis as homozygous mutation was reported to result in pancreatic and cerebellar agenesis associated with a lethal condition in humans and mice [157]. Thus, it is assumed that iCre-mediated recombination in the porcine cerebellum was restricted to prenatal development and that Cre recombinase was no longer expressed in the mature pig brain, as *PTF1A* RNA was only weakly detectable in the cerebellum of founder animals #1964 and #1962. Stomach samples from both *PTF1A*^{iCre} and *Reporter-PTF1A*^{iCre} pigs revealed isolated iCre expression and recombination, regardless of the age of the animals. Therefore, *PTF1A* expression in the stomach seems to extend into late adulthood, whereas the exact onset of expression is unknown. These results are consistent with the findings of Busslinger and colleagues, who reported the expression of *PTF1A* in enterochromaffin-like cells, which are neuroendocrine cells in the oxyntic stomach mucosa, of adult humans aged 45-65 years [346].

The recombination pattern found in the fluorescence analysis of tissues from *Reporter-PTF1A*^{iCre} pigs was also confirmed by LSL-excision PCR and pyrosequencing of tissue samples from other *PTF1A*^{iCre} progeny, which detected efficient recombination and thus mutational activation in cerebellum and pancreas of *KRAS*$^{LSLG12D/WT}$*PTF1A*^{iCre} and *TP53*$^{LSLR167H/WT}$*PTF1A*^{iCre} pigs. There was no recombination detectable in the stomach using these two methods, mainly due to the low recombination rate based on the scattered iCre expression in this tissue. In summary, there was no difference in iCre expression and recombination detectable between 5'end and 3'end *PTF1A* targeted pigs. This leads to the assumption that placement into the 3'UTR of *PTF1A* resulted in equally efficient expression from the endogenous *PTF1A* promoter as upon 5'end targeting, but without the destruction of one *PTF1A* allele. However, further analysis would be required to clearly exclude an influence of 3'UTR targeting on endogenous *PTF1A* expression.

When only *TP53*^{R167H} was activated in the porcine pancreas, no histological changes were observed until the end of my studies. This is in line with the findings of Hingorani and colleagues, who showed that Cre-mediated pancreatic activation of *Trp53*^{R172H}, the murine orthologue of human *TP53*^{R175H}, had no effect on the survival rates compared to wild type animals [163]. Although *TP53*^{R175H} is one of the most common mutations in human PDAC disease, it also represents one of the major germline mutations found in Li Fraumeni syndrome, a hereditary disorder which predisposes to cancer development [347-349].

Indeed, mice with widespread activation of *Trp53*^{R172H} developed a variety of tumours, with osteosarcomas and carcinomas being the most common [350]. Since mutational activation in *TP53*$^{LSLR167H/WT}$*PTF1A*^{iCre} pigs was tissue-specific, it is unlikely that activated *TP53*^{R167H} mutation is causative for tumours in organs other than the pancreas and cerebellum, and it also remains to be seen whether tumours will develop in the pancreas over time. However, as pigs carrying the non-activated *TP53*^{LSLR167H} allele were shown to spontaneously develop osteosarcoma due to the inactivation of one endogenous *TP53* allele [351], it could be that the *TP53*$^{LSLR167H/WT}$*PTF1A*^{iCre} animals will develop such tumours at later age.

The activation of *KRAS*^{G12D} in porcine pancreatic progenitor cells during embryogenesis was associated with the presence of widespread ADM lesions as early as postnatal day one. At five weeks of age, *KRAS*$^{G12D/WT}$*PTF1A*^{iCre} pigs showed ADM and PanIN lesions with increased extracellular matrix deposition. Oncogenic *KRAS* mutation is found in more than 90 % of PDAC patients and already occurs in PanIN-1 lesions, making oncogenic *KRAS* the initiating event in pancreatic tumourigenesis and the main driver of PanIN formation [85, 352]. My results are consistent with the findings from Hingorani and colleagues, who reported that Cre-dependent activation of endogenous *Kras*^{G12D} in murine pancreatic progenitor cells was sufficient to induce PanIN formation [162]. However, it took an average of 9 months for widespread PanIN lesions to form in mice and these were mainly low-grade and only rarely developed into invasive and metastatic PDAC [162]. Furthermore, Guerra et al. showed that activation of oncogenic *Kras*, in this case *Kras*^{G12V}, in pancreatic acinar cells during late embryogenesis led to the formation of ADM lesions until three months of age, which developed into extensive PanINs within the first year of life [133]. Simultaneous activation of *KRAS*^{G12D} and *TP53*^{R167H} in pigs resulted in the presence of PanIN lesions at postnatal day one. *KRAS*$^{G12D/WT}$*TP53*$^{R167H/WT}$*PTF1A*^{iCre} pigs up to 10 weeks of age already showed severely altered pancreata ranging from ADM and PanIN lesions to widespread carcinoma with severe tissue fibrosis. This highly fibrotic environment is a common feature of PDAC tumours and has been shown to protect cancer cells from being accessed and eliminated by immune cells, thereby evading an antitumour immune response [353, 354]. Interestingly, it was reported that the presence of *TP53* missense mutations in PDAC tumours is linked to increased expression of fibrosis-related genes and decreased infiltration of cytotoxic T cells into the tumour [355]. In mice, simultaneous expression of *Kras*^{G12D} and *Trp53*^{R172H} mutation resulted in the formation of invasive and metastatic PDAC [163]. These mice had an extremely shortened life expectancy of five months on average and all succumbed within 12 months, although young animals still had normal pancreatic tissue at 4-6 weeks of age [163].

In summary, the porcine *KRAS*$^{G12D/WT}$*PTF1A*^{iCre} and *KRAS*$^{G12D/WT}$*TP53*$^{R167H/WT}$*PTF1A*^{iCre} models recapitulated the findings reported in the mouse model of Hingorani and colleagues [162, 163]. However, with regard to the timeline, the pigs often show first pancreatic changes already after birth. Furthermore, the ADM process appears to be more pronounced than in the mouse model, thus mirroring the human disease development, which progresses from ADM over PanINs to PDAC. At this point it should be mentioned that the reports of Hingorani and colleagues mainly focused on PanIN and PDAC development in *Kras*$^{LSLG12D/WT}$*Pdx1*$^{Cre/WT}$ and *Kras*$^{LSLG12D/WT}$*Trp53*$^{LSLR172H/WT}$*Pdx1*$^{Cre/WT}$ mice, although they initially also used the *Ptf1a* promoter for mutational activation in early murine pancreatic progenitor cells [162, 163]. In fact, they reported that PanIN frequency of *Kras*$^{LSLG12D/WT}$*Pdx1*$^{Cre/WT}$ mice was similar to those of *Kras*$^{LSLG12D/WT}$*Ptf1a*$^{Cre/WT}$ mice, but they also described that *Kras*$^{LSLG12D/WT}$*Ptf1a*$^{Cre/WT}$ mice were characterised with a higher proliferative index of PanINs and acinar cells and higher pancreatic levels of Kras^{G12D} and Ras-GTP, when compared to *Kras*$^{LSLG12D/WT}$*Pdx1*$^{Cre/WT}$ mice [162]. The higher protein levels were mainly due to the uniform expression of the mutant *Kras* allele throughout the pancreas of *Kras*$^{LSLG12D/WT}$*Ptf1a*$^{Cre/WT}$ mice, while *Pdx1*$^{Cre/WT}$ mice only showed stochastic expression of Cre recombinase [162]. Thus, the temporal deviations and the strong metaplasia of acinar cells in the pig model could also be based on the use of the *PTF1A* promoter.

4.1.2 *mPdx1-iCre* pigs for PDAC modelling

Besides *Ptf1a*, the murine PDAC model also used the *Pdx1* promoter to drive expression of Cre recombinase in the mouse pancreas [162, 163]. Studies in mice have shown that Pdx1 is expressed in the developing pancreatic buds from embryonic day 8.5 [283]. Thus, the use of the *Pdx1* promoter enables earlier Cre recombination in all pancreatic cells than *Ptf1a* [151]. However, as heterozygous mutation of *PDX1* was reported to result in maturity-onset diabetes of the young (MODY) in humans and mice, it was not possible to target iCre recombinase into the porcine endogenous *PDX1* locus [297-300]. Consequently, as for the mice the iCre expression vector was integrated as a transgene.

Matsunari et al. showed that the murine *Pdx1* (mPdx1) promoter and its fusion with the rabbit β-globin gene enabled highly tissue-specific expression of Venus, a green fluorescent protein, in pigs [302]. Analysis of porcine fetuses isolated at 47-65 days of gestation revealed pancreas-specific expression that was localized to acinar cells [302]. This expression later became restricted to pancreatic islets, as shown in 27 day old piglets [302]. The functionality was further proven by Berthelsen and colleagues, who used the *mPdx1* promoter for activating and overexpressing an oncogene cassette in pigs in order to generate a porcine PDAC model [181].

Based on these results regarding efficiency and tissue specificity, the *mPdx1* promoter in combination with the rabbit β-globin gene was used in this work to generate pigs expressing iCre recombinase in the pancreas. Three different strategies were pursued for the integration of the *mPdx1-iCre* transgene into the porcine genome, which are discussed below.

4.1.2.1 *mPdx1-iCre* pig generation by *ROSA26* targeting

The first strategy was based on gene targeting into the porcine *ROSA26* locus. Gene targeting into *ROSA26* is often the method of choice as this gene locus is ubiquitously expressed in a variety of tissues and transgene integration has no effect on animal viability or fertility. In mice, targeting into *Rosa26* is associated with a high homologous recombination (HR) rate and thus led to the generation of numerous knock-in strains [304-306]. Consistent with this, the identified porcine *ROSA26* locus has also proven to be a safe haven for efficient transgene integration, leading to expression in many tissues without adverse effects [295]. Indeed, successful gene targeting in pig cells has been reported in the past, albeit with varying targeting efficiencies [295, 356, 357].

In this work it was not possible to generate positive cell clones for gene targeting into porcine *ROSA26*. However, it has to be mentioned that gene targeting in mice was mainly performed in embryonic stem (ES) cells [190, 305, 306], which express HR-associated proteins throughout the cell cycle and, unlike somatic cells, respond mainly with HR to genomic instability [199, 358, 359]. Therefore, due to the absence of ES cells in pigs, gene targeting is less efficient in pig than in mouse experiments. An attempt to increase the targeting efficiency using CRISPR/Cas9 systems resulted in positive cell clones, but these were only positive for 5'junction PCR. Another reason for the inefficient targeting could be the large plasmid size, which may affect transfection as well as correct integration, since the *mPdx1-iCre* sequence already spans more than 8 kb. Especially with regard to conventional gene targeting, where longer homology arms are needed, this leads to a total targeting vector length of over 19 kb.

4.1.2.2 *mPdx1-iCre* pig generation by random integration

Since screening for positive cell clones with correct *ROSA26* targeting was very time-consuming, a second strategy based on random integration of the *mPdx1-iCre* transgene was used. This strategy relied on transfection of porcine cells using a linearized transgene construct, which consisted of the *mPdx1-iCre* sequence and a neomycin resistance gene. Compared to *ROSA26* targeting, this approach was simpler and less time-consuming, as the unpredictability of the integration site did not allow for specific screening. Stable transgene integration was achieved by prolonged G418 selection and the remaining surviving cell clones were analysed for iCre copy numbers.

Since it was unclear whether the *mPdx1* promoter was active in kidney cells, porcine kidney fibroblast cells derived from a dual-fluorescent reporter pig (pig #270) were used for transfection. This would allow promoter activity to be detected by a switch from red to green fluorescence due to iCre recombination. To my knowledge, expression of *PDX1* was not reported in kidney tissue so far. However, expression has been described for numerous other tissues than the pancreas. During early embryogenesis, *Pdx1* expression starts in the foregut endoderm and persists in the evolving pancreatic buds and the developing duodenum [360]. This early expression pattern already indicates a role for *Pdx1* expression in tissues other than the pancreas. In line with this, Stoffers et al. generated transgenic mice expressing lacZ under the control of the *Pdx1* promoter [361]. In addition to the pancreas, they also detected lacZ expression in stomach und duodenal glands, as well as in bile and cystic ducts and in the spleen [361]. Using *Pdx1-Cre* transgenic mice, another group reported Cre recombination in the developing central nervous system and inner ear [309]. In adult mice, expression of *Pdx1* was detected in pancreatic β-cells and weakly in some acinar cells, but also in the stomach and duodenum [310, 311].

In this work, a switch from red to green fluorescence was indeed observed in the majority of kidney fibroblasts that survived antibiotic selection, thus confirming a promoter activity. As the functionality of the *mPdx1* promoter was proven in the green fluorescent cells, only these were then used for SCNT. However, the detected *mPdx1* promoter activity in the cells does not necessarily indicate a general *PDX1* expression in porcine kidney tissue. When isolating fibroblast cells from porcine kidney, a piece from the whole organ was used. As no specific selection for fibroblast cells was performed during isolation, the cell fraction obtained was likely to be a mixture of different cell types. Niemann and colleagues have shown that porcine derived kidney fibroblast cells can be transdifferentiated into hepatocyte-like cells *in vitro* [362]. Although they have used hepatic transcription factors to induce cell conversion [362], it could be that porcine fibroblast cells possess a certain transdifferentiation potential, which enables them to change their cell fate in the course of cultivation. In fact, despite the absence of promoter activity, the red fluorescent cell clones also revealed the presence of iCre copy numbers. It remains unclear whether this was caused by incomplete transfer of the transgene, damage to the promoter sequence or transfection of a different or altered cell type in which the *mPdx1* promoter was not active.

The use of the modified #270 cells for SCNT resulted in two births with a total of five *mPdx1-iCre* piglets, one of which was stillborn. Although cell clones carrying three and 18 iCre copies were used for SCNT, all piglets carried only three copies of iCre recombinase. This one-sided distribution can indicate that the cell clones with 18 copies were not nuclear transfer competent. Alternatively, the high copy number could have led to Cre induced cytotoxicity.

Despite its ease of application, random transgene insertion is also associated with significant drawbacks. For example, random integration into the host genome can damage the function of endogenous genes (insertion mutagenesis), which can have severe effects on development, viability or fertility. In addition, the expression of the transgene is strongly dependent on the host regulatory regions and chromatin structure at the integration site (position effect), thus leading to varying expression patterns among different animals which in turn prevents the comparability of results [185, 363].

Unfortunately, all generated piglets did not survive longer than two days, as they showed severe physiological defects, such as enlarged tongue and splay legs. Such malformations are typically observed in connection with the SCNT procedure for generating transgenic animals [200]. In line with this, Whitworth and Prather described that the occurrence of constant phenotypes when using a certain cell type for SCNT, is probably caused by structural nuclear changes of the cell donor, thus leading to incorrect chromatin remodelling and nuclear reprogramming [202]. As the abnormalities occurred repeatedly with the use of #270 PKF cells, these cells were found to be incompatible for SCNT and were therefore no longer used for the generation of transgenic pigs.

Nevertheless, tissues from the dead piglets were analysed for expression of iCre recombinase. The pancreatic tissues indeed showed widespread expression, which was detectable in different cell types. The expression varied in strength and ranged from a very weak appearance in ductal cells to strong expression in a few isolated cells scattered among the acinar tissue. As already mentioned above, *Pdx1* is expressed from murine embryonic day 8.5 in all cells of the developing pancreas and later becomes restricted to pancreatic islet cells [283, 364, 365]. Histological analysis of the developing mouse pancreas showed that first islets can be detected as an accumulation of endocrine cells as early as day 12 of pregnancy [366]. In humans, the appearance of islet-like cell clusters can be observed from week 11 after conception, with the formation of mature islets being completed in the third trimester of pregnancy [367]. However, no islets were found in the pancreata of the newborn *mPdx1-iCre* pigs and thus an assignment of the detected iCre expression to this cell type was not possible. Interestingly, mature islets do not yet appear to be present in the pancreas of newborn pigs, as Korbutt et al. reported that endocrine cells in the neonatal pancreas were randomly scattered throughout the tissue rather than being arranged in compact cell clusters [368]. Indeed, the isolation of neonatal porcine islets revealed only 7% endocrine cells, while the vast majority of the cell fraction was of exocrine origin [368]. Consistent with this, Nagaya and colleagues showed that islets were absent in the pancreatic tissues of newborn piglets and only formed in juvenile pigs from 21 days of age [369].

While expression of iCre recombinase was restricted to the pancreas, analysis for porcine endogenous PDX1 showed protein expression in pancreas, liver and muscle. Since the *PDX1* gene was reported to be highly conserved between different species [370, 371], an antibody was used which was produced based on the human residues and also shows cross reactivity for the mouse and rat protein. As pronounced *PDX1* expression in liver and muscle has not been reported so far, the detected strong expression in these porcine tissues could be caused by non-specific binding of the utilised antibody. Thus, the generation of reliable PDX1 expression data requires further optimisation for the use of this antibody or the evaluation of other PDX1 binding antibodies.

4.1.2.3 *mPdx1-iCre* pig generation by piggyBac-mediated transposition

A third strategy for integrating the *mPdx1-iCre* transgene into the porcine genome was based on transposon-mediated integration. In order to avoid poor efficiencies and animal defects associated with the SCNT procedure, transposon-mediated integration of *mPdx1-iCre* was performed by microinjection into fertilized porcine oocytes, which were then transferred into a surrogate mother.

DNA transposons are advantageous over viral-based methods due to their ease of use and low-risk application and are therefore widely used for non-viral gene delivery. As already described in chapter 1.6.2, several transposon systems exist for the modification of genomes, with *piggyBac* (PB) and *Sleeping Beauty* (SB) being the most commonly used. Although popular, the SB transposon system has some disadvantageous properties, which led to the use of the PB system for the current study.

In comparison to PB, SB is characterised by pronounced local hopping and leaves footprints at the excision sites [251, 372-376]. Furthermore, the SB system is affected by overproduction inhibition (OPI), which describes the decrease in transposition efficiency with increasing transposase concentrations, a phenomenon that could not be observed with PB transposase [245, 376]. Gene delivery experiments have shown that PB is generally more efficient than SB for transposition in mammalian cells [260, 373, 377]. Especially with regard to the delivery of large transgenes, SB has proven to be unsuitable, as transposition efficiency drops by 50% with a transposon length of 6 kb [245]. In contrast, PB was shown to integrate transgenes of up to 9.1 kb without impact on transposition efficiency [250]. Li and colleagues even reported successful integration of 100 kb into the murine genome using PB transposase [248]. Consequently, since the *mPdx1-iCre* transgene is about 8.3 kb, the PB system was better suited to achieve efficient integration.

In addition to numerous transgenic mouse strains, the PB transposon system has also been used in the past to generate transgenic livestock. In line with this, Yum et al. successfully generated transgenic cattle by microinjection of PB after showing that this transposon system is more efficient than SB in bovine cells [378]. Wu et al. and Li reported the generation of PB-mediated transgenic pigs via SCNT and cytoplasmic microinjection, respectively [379, 380].

Transposon-mediated integration usually requires co-transfection with a transposon plasmid containing the transgene and a helper plasmid encoding the transposase. Although it is the most convenient strategy, delivery of the transposase as DNA plasmid can have strong negative effects on the experimental outcome. It can cause genomic integration of the transposase sequence and prolonged transposase activity, which in turn lead to continuous transposon remobilization [381, 382]. These repeated transposition cycles can then result in chromosomal mutagenesis [381, 382], which can have severe consequences, especially in the generation of transgenic animals. In contrast, delivery of transposase as messenger RNA (mRNA) prevents integration into the host genome and enables temporary and thus limited expression decreasing the risk for chromosomal damage [382]. Therefore, cytoplasmic microinjection into porcine oocytes was performed using mRNA of hyperactive PB transposase and plasmid DNA of the *mPdx1-iCre* transposon. Co-injection of 100 *in vitro* produced zygotes did not reveal any toxicity of the PB transposon system. As the transposase gene was linked to a red fluorescence marker, functional expression of PB was verified by the detection of red fluorescent oocytes 24 h after injection.

4.1.2.4 *mPdx1-iCre* founders and *mPdx1-iCre* progeny

Embryo transfer of injected oocytes into a recipient sow resulted in the birth of ten piglets, of which three female piglets (#2017, #2022 and #2024) carried the *mPdx1-iCre* transgene. However, piglet #2024 showed only a weak band in the PCRs for transgene detection and an iCre copy number close to zero, which led to the assumption that this animal was mosaic. The genetic state of mosaicism was first discovered by Palmiter et al., who found disturbed transgene inheritance in the pedigree of a transgenic mouse [383]. Mosaicism in the context of microinjection occurs when the transgene integrates at different stages of embryonic development, resulting in transgenic animals that do not carry the transgene in all cells [384]. As a consequence, the mosaic transgenic animals are characterised by uneven transgene expression patterns and failure to inherit the transgene [383, 385]. In the past, this genetic condition was described by many groups in the generation of transgenic animals [385-387].

In addition to making genotype analysis more difficult, mosaicism is a major obstacle, especially in livestock, as elimination by outcrossing or the generation of new animals is very time-consuming and cost-intensive [384, 388, 389]. For this reason, it was decided to not use pig #2024 for breeding. Genotype analysis of piglets #2017 and #2022 revealed iCre copies of eleven and four, respectively. These copies were almost exclusively due to PB-mediated insertion rather than random plasmid integration, as only in animal #2017 a single plasmid backbone copy could be detected. Wu and colleagues reported the presence of eight transgene copies on average, when generating transgenic pigs by PB-mediated integration followed by SCNT [379]. Apart from this, the transgenic pigs that were generated by Li et al. via cytoplasmic oocyte injection carried between one and fourteen transgene copies [380]. Hence, the verified iCre copies of the *mPdx1-iCre* pigs are in agreement with the copy numbers reported by the groups of Wu and Li. Pancreatic expression of iCre recombinase in founder sows #2017 and #2022 was analysed at 14 and 12 months of age, respectively. IHC analysis revealed specific iCre expression, which was located in pancreatic islets. This is in line with the Pdx1 expression pattern in the pancreata of adult mice, where expression is mainly restricted to islet cells [310, 311]. However, as already described in section 4.1.2.2, newborn *mPdx1-iCre* piglets generated by random transgene integration showed widespread pancreatic iCre expression with a parallel absence of islet cell clusters. Taken together, these results are consistent with the literature reporting the absence of mature pancreatic islets in newborn pigs and their development in early juvenile age [368, 369].

The functionality of *mPdx1-iCre* was proven by analysing tissues from a 4-day-old *KRAS*$^{LSLG12D/WT}$*mPdx1*^{iCre} piglet. LSL-excision PCR showed efficient recombination in the pancreas and duodenum. As already mentioned above, expression of Pdx1 is detected in the developing pancreas and duodenum of mice, but is later also found in other tissues, e.g. in the stomach [360, 361]. Thus, the recombination distribution found in the *KRAS*$^{LSLG12D/WT}$*mPdx1*^{iCre} piglet showed that the *mPdx1* promoter in the pig follows the same tissue-specific expression pattern as known from mice. However, Matsunari et al., who generated the *mPdx1-Venus* transgenic pigs, reported that transgene expression was only restricted to the pancreas [302]. Expression of *Venus* was located in pancreatic acinar cells of 47-65 day old fetuses, while 27 day old pigs showed fluorescence in β-cells of the pancreatic islets [302]. Additional studies would have to be undertaken to see if these transgenic pigs also expressed *Venus* in the duodenum earlier in development.

In fact, consistent with the known expression pattern of *Pdx1* in the gastric region of mice, Hingorani and colleagues reported that *Kras*$^{LSLG12D/WT}$*Pdx1*$^{Cre/WT}$ mice showed recombination in the stomach and small intestine in addition to the pancreas [162].

Indeed, these mice also sporadically developed other tumours such as cutaneous papillomas or gastrointestinal lesions affecting the stomach and duodenum, a condition that was generally not observed in *Kras*$^{LSLG12D/WT}$*Ptf1a*$^{Cre/WT}$ mice [162].

The analysed 4-day-old *KRAS*$^{LSLG12D/WT}$*mPdx1*^{iCre} piglet already showed widespread ADM and PanIN lesions. Interestingly, a strong expression of iCre recombinase was localised in these areas. This is in line with the findings of Roy et al., who detected a strong expression of *Pdx1* in ADM and PanIN lesions of mice [390]. In addition, *PDX1* was shown to be expressed in various human pancreatic precursor lesions, thus indicating a role of *PDX1* in pancreatic tumourigenesis [391].

In summary, it was shown that transposon-mediated integration via cytoplasmic oocyte injection is an efficient strategy for developing transgenic pigs and that the *mPdx1* promoter successfully drives expression of iCre recombinase in porcine cells. The generated *mPdx1-iCre* pigs have demonstrated to be as suitable for the induction of precancerous pancreatic lesions as the *PTF1A*^{iCre} animals, as they also showed widespread lesions at neonatal age. It remains to be seen, how the preneoplastic lesions will progress, also in the presence of activated *TP53*^{R167H} mutation, and whether tumours will also develop in other tissues.

4.2 CRISPR/Cas9-mediated mutagenesis in porcine cells

The discovery of the CRISPR/Cas9 system as part of the bacterial immune system and its use for specific DNA cleavage has revolutionized genome editing [273]. Its ease of adaptation to individual experimental requirements, as well as its applicability in different species and cost effectiveness have made CRISPR/Cas9 the tool of choice for gene modifications.
The initial aim of this work was to activate porcine *KRAS*^{G12D} and *TP53*^{R167H} mutations by conventional breeding with pigs expressing Cre recombinase in the pancreas. Since previous experiments to generate porcine Cre driver lines by this group and others had not been successful, due to cytotoxicity and non-viable animals, the outcome of generating pancreas-specific Cre driver lines was uncertain. A backup strategy was designed, using a multiplexed CRISPR/Cas9 approach for mutational activation or for induction of TSG mutations.
Multiplexing of gRNAs was performed according to the protocol by Xie et al., who reported the generation of a synthetic polycistronic tRNA-gRNA gene (PTG) construct consisting of tandemly arrayed tRNA-gRNA repeats, that are transcribed as a single transcript which is then cleaved by the endogenous tRNA-processing machinery for the release of the individual gRNAs [279]. They have shown that genome editing using the multiplexed PTG strategy is highly efficient in plant and human cells and that the tRNA sequence probably acts as enhancer of Polymerase III (Pol III) transcription [279, 392].

The PTG multiplexing strategy for genome editing offers several advantages over conventional CRISPR/Cas9-mediated editing with one or more gRNA-expressing cassettes in a single vector.

The transcription of several gRNAs from a single PTG construct only requires the presence of one Pol III promoter and one Pol III terminator, thus reducing the size from 420 bp to ~174 bp per each additionally added gRNA. Therefore, the multiplexed CRISPR/Cas9 editing system is suitable for applications associated with limited packaging capacity, e.g. when using viral vectors for *in vivo* delivery [393]. Furthermore, transcription by Pol III promoters requires the presence of a specific nucleotide at the beginning of the RNA, e.g. “G” for U6 promoters, a circumstance that is omitted in multiplexing due to the preceding tRNA sequence [279, 392].

To remove parts of the LSL cassette, three PTG constructs were generated and tested for activation of $KRAS^{G12D}$ and $TP53^{R167H}$ in porcine cells. Each PTG construct harboured two gRNAs, one binding at the upstream loxP site and the second binding at the end of the splice acceptor (SA) or in the neomycin resistance cassette located downstream of the SA. Transfection with the PTG constructs led to efficient excision of the SA and transcription of the G→A mutation at *KRAS* codon 12 in 17-26% of the cells. The generated constructs are thus suitable for simultaneous activation of both mutations or activation of $KRAS^{G12D}$ alone, the latter when using the neomycin-binding gRNA, as an alternative selectable marker gene was used for targeting *TP53*. In general, CRISPR/Cas9-mediated activation of $KRAS^{G12D}$ and $TP53^{R167H}$ is characterised by several advantages over conventional breeding with Cre driver pigs. Mutational activation by breeding is expensive and time-consuming. It requires the generation of Cre driver pigs, waiting for sexual maturity, complex breeding to obtain triple mutant genetically engineered pigs, resulting in animals with unwanted genotype and considerable costs for animal husbandry.

As the development of PDAC is associated with additional genetic alterations, the next step was to generate and evaluate PTG constructs for the simultaneous inactivation of TSGs, such as *TP53*, *p16*, *SMAD4* and *BRCA2*. Porcine cells transfected with PTG constructs containing three or four arrayed gRNAs showed high InDel frequencies for all TSGs. Interestingly, Xie and colleagues reported an occasional reduction in efficiency depending on the number of gRNAs in the array [279]. However, this was not observed in this work, as the highest InDel abundance was found for *SMAD4*, although this gRNA was located in the second or third position in the PTG constructs, respectively. The highest drop in efficiency was found for *BRCA2* with 40-50% when the gRNA was part of the multiplex and 80% when tested as a single gRNA (Table 42+43).

Cells with *BRCA2* knockout were affected by a significantly increased mortality rate compared to the inactivation of other TSGs, e.g. of *p16*. As already mentioned in chapter 1.1.3, BRCA2 plays an essential role in homologous recombination during DNA DSB repair [118].
It was reported that loss of BRCA2 in non-transformed human cells results in replication stress and defective proliferation with G1 phase arrest, both leading to cell senescence and apoptosis [394]. This leads to the assumption that disruption of porcine *BRCA2* led to cell cycle arrest and that BRCA2 deficient cells might have been overgrown by cells carrying only p16 or SMAD4 inactivation. This might provide an alternative explanation for the lower InDel frequency for *BRCA2* during multiplexed gene editing.

Although the establishment of the PTG multiplex system led to high mutation frequencies in porcine cells, the simultaneous mutation of the aforementioned genes does not reflect the natural situation in PDAC development as activating mutation of *KRAS* and inactivation of the TSGs *p16*, *TP53*, *SMAD4* and *BRCA2* occur at different stages during PanIN progression and PDAC development [95, 113, 114, 124, 352]. Recapitulation of the human disease genotype requires first the activation of $KRAS^{G12D}$ and then the accumulation of the TSG mutations. This could be achieved by first activating $KRAS^{G12D}$ with either Cre or genome editing followed by applying the CRISPR/Cas9 multiplex TSG knockout strategy at a later time point.

Another important point to consider, however, is the delivery strategy of the PTG multiplex system. As already mentioned in chapter 4.1, widespread expression of $Kras^{G12D}$ during embryogenesis leads to lethality in mice [321, 322]. Consistent with this, homozygous knockout of *Brca2* and *Smad4* genes is also embryonically lethal, whereas mice with heterozygous *Brca2* and *Smad4* knockout have been reported to be viable [395, 396]. In contrast, mice carrying homozygous inactivation of *Trp53* or *p16* are viable but prone to early formation of spontaneous tumours [397-399]. Consequently, due to the impact on embryonic development, it is not possible to generate pigs with germline modifications of the above-mentioned genes. The CRISPR/Cas9 system can be used instead to introduce the mutations locally or in a tissue-restricted manner. And as the CRISPR/Cas9 multiplex system is not limited to the pancreas like Cre driver lines, it can also be used to model other tumours. This can be achieved by *in vivo* delivery of the CRISPR/Cas9 components, e.g. using viral vectors, lipid nanoparticles or VLPs [400, 401]. Another option to induce tumour formation in the pig is the transplantation of cells that have been transformed *in vitro*. For example, subcutaneous injection of a human pancreatic cancer cell line was reported to result in tumour formation in immunocompromised pigs [402]. Even more interesting, Schachtschneider and colleagues showed that injection of *in vitro* transformed porcine hepatocytes into subcutaneous and hepatic tissue of immunodeficient mice led to tumour development [403].

Furthermore, subcutaneous injection of the cells into pigs also caused tumours, and when these were transplanted into fibrotic pig livers, intrahepatic tumours developed that recapitulated the human hepatocellular carcinoma genotype [403, 404].
Based on the findings of Schachtschneider and Gaba et al., this work investigated whether the subcutaneous injection of modified porcine ear fibroblast (PEF) cells leads to tumour formation in the pig. Therefore, PEF cells isolated from two *KRAS*$^{LSLG12D/WT}$*TP53*$^{LSLR167H/WT}$ piglets were used for inactivation of the TSGs *TP53*, *p16*, *SMAD4* and *BRCA2* and activation of *KRAS*^{G12D} and *TP53*^{R167H} mutations. In order to avoid the need for autologous transplantation or immune suppression to reduce the risk of an allograft rejection, porcine Beta-2-microglobulin (B2M) was inactivated. Knockout of B2M leads to a loss of the porcine major histocompatibility complex class I (MHCI), which in turn results in a prevention of T cell activation due to a lack of antigen presentation. The cells were additionally transfected with a LEA29Y overexpression vector encoding a variant of the T cell co-stimulation inhibitor called cytotoxic T-lymphocyte antigen 4 (CTLA4-Ig) to inhibit T cell activation.

Pentaplexed gene editing of the TSGs plus B2M resulted in high editing efficiencies. Consistent with the results discussed above, the InDel frequencies were lowest for *BRCA2*, with only 5-8%, which suggests a loss of *BRCA2* mutated cells, possibly due to a proliferative defect [394]. Successful activation of *KRAS*^{G12D} and *TP53*^{R167H} by Cre protein transduction was proven by LSL-excision PCR, which showed a much stronger band for the recombined *KRAS* allele than for the wild type allele in both cell isolates. This result suggests a loss of the wild type *KRAS* allele due to activation of *KRAS*^{G12D} mutation [405], a phenomenon that is described in more detail in section 4.3.2.

Sequencing of PCR products from reverse transcribed PEF cell mRNA confirmed the expression of a G→A mutation at *KRAS* codon 12, with guanine and adenine showing the same peak height, thus not indicating a loss of the wild type *KRAS* allele. This contradiction might be explained by the fact that the reverse transcription was performed with nucleic acids isolated from an earlier cell passage than those used for LSL-excision PCR. This allows the assumption that the wild type *KRAS* allele was still present in earlier cell passages, while it was lost during further cell divisions.

The modified PEF cells were autologously retransplanted by subcutaneous injection into regions of the ear and flank, but no tumour was detected after an observation period of 3.5 months. In contrast, Schachtschneider and Gaba et al. reported successful tumour isolation from subcutaneously injected pigs within the first two months post injection.

Interestingly, while sites injected with low, medium and high cell doses initially showed palpable bulges, only the sites injected with high doses of 10 million cells showed tumour growth at the end [403].

In this work, the pigs were injected with two or five million cells and showed no tumour growth, which is similar to the results of Schachtschneider et al. for the transplantation with low cell numbers [403]. Furthermore, it would be important to examine the mutated PEF cells for transformation, e.g. via proliferation or cell migration assays. The tumourigenic potential of the cells can be tested using the chicken chorioallantoic membrane (CAM) assay, which allows implantation of a xenograft without the risk for rejection, due to the absence of a competent immune system in the first days after egg laying [406, 407].
Another cause for the absence of tumour growth in the pigs after PEF injection could have been immunogenicity of the transplanted cells which could have led to rejection. Rejection of autologous grafts has been reported only very rarely, and mostly in the context of induced pluripotent stem cells which expressed new antigen epitopes due to the reprogramming process [408, 409]. This might have also occurred after inactivating numerous TSGs with concomitant *KRAS*^{G12D} and *TP53*^{R167H} activation. In addition, the abolishment of porcine MHCI by B2M inactivation and the suppression of T cell activation by LEA29Y may not have been sufficient to avoid rejection. Deuse and colleagues have reported the generation of hypoimmunogenic cells by deletion of MHCI and MHCII followed by overexpression of CD47, the latter preventing phagocytosis by macrophages [410]. This strategy could be transferred to porcine cells and thus avoid recognition by the immune system, even in the case of allotransplantation.

4.3 *In vitro* modelling of porcine acinar-to-ductal metaplasia

Adult pancreatic acinar cells possess a high degree of plasticity, which enables them to regenerate in response to tissue damage. Pancreatic regeneration is characterised by dedifferentiation and transdifferentiation of acinar cells into a duct-like phenotype, a process known as acinar-to-ductal metaplasia (ADM) [128]. In a healthy context, dedifferentiation of acinar cells upon inflammation or tissue injury is a reversible process leading to repopulation of the pancreas [411, 412]. However, in the presence of oncogenic *KRAS* signalling, the cells are maintained in a dedifferentiated progenitor state, which irreversibly prevents cell redifferentiation and thus acinar cell regeneration, and can lead to the progression of ADM to PanIN lesions [133, 413, 414].

As ADM is involved in pancreatic regeneration and transformation processes, its study is of important relevance for PDAC research. Indeed, the development of numerous two-dimensional (2D) and three-dimensional (3D) *in vitro* models has demonstrated the ability of murine and human pancreatic acinar cells to transdifferentiate into a duct-like phenotype [139, 142, 314, 415, 416]. The data obtained from mouse and human ADM studies could be validated and complemented by the development of a porcine ADM model, which would then allow for cross-species comparison, e.g. regarding molecular drivers of the ADM process.

4.3.1 Establishment of porcine pancreatic acinar cell culture

Therefore, the first aim of this subproject was to establish the isolation and culture of porcine pancreatic acinar cells. The first approach carried out was the isolation of cells from the porcine pancreatic head and their cultivation in a 2D culture according to the protocols described by De Waele et al. and Akanuma et al. [314, 315] (data not shown). However, despite their ease of use, 2D cultures often do not properly mimic the properties that cells exhibit *in vivo*. Three-dimensional cultivation has significant advantages compared to 2D cultures, e.g. with regard to cell shape, proliferation, gene expression or drug response [417, 418]. Particularly in view of pancreatic acinar cells, 3D cultivation creates a more realistic environment by preserving the grape-like structure of the acinar cell clusters and also allows the formation of multilayer duct-like spheres. As a consequence, all other isolations were established as a 3D culture consisting of three layers, a bottom and top collagen layer with a cell collagen layer in between (Figure 53). Establishment of the 3D porcine acinar cell culture was very time-consuming and required numerous adaptations to the modified protocol for the isolation of murine acinar cells [282], which was kindly provided by Thorsten Neuß (Klinikum rechts der Isar, TUM, Munich).

At the beginning of the work, it was unclear which age of pig was most suitable for the isolation of acinar cells. In mice, the best results are obtained when acinar cells are isolated at 4-7 weeks of age [282, 419-421]. In pigs, the best yield of acinar cells was obtained when using 4-5 week old pigs. Older pigs already showed more pancreatic fat deposits, which impeded cell isolation and led to a lower yield of viable acinar cells, an observation that is most likely related to lipotoxicity [422]. This assumption is supported by the findings of Navina et al., who reported lipolysis-mediated acinar cell necrosis when coculturing human pancreatic acinar cells with adipocytes [423].

In addition, as the porcine organ size is considerably larger than in mice, the utilized pancreatic piece size, volumes of the individual solutions and centrifugation speed had to be adjusted for successful isolation. However, the most significant step in the establishment process was adjusting the time span between sacrificing the pig and start of the isolation. As time is a critical factor to obtain a high yield of viable acinar cells [282, 424], precise planning, preparation and handling was required.

4.3.2 *In vitro* induction and characterisation of porcine ADM

The occurrence of ADM during pancreatitis and its link to pancreatic cancer development has been known for a long time [425-427]. Pancreatitis is characterised by increased inflammatory signalling with a high release of cytokines, some of which have been shown to induce ADM in murine and human pancreatic acinar cells, e.g. TGF-α, TGF-β or interleukins 17 and 22 [137, 139, 141, 316, 428]. Thus, some of the cytokines were selected to test their ability to induce ADM in the porcine acinar cell culture model.

TGF-α is a growth factor that belongs to the epidermal growth factor (EGF) family. Its binding to the EGF receptor (EGFR) leads to the activation of several downstream signalling pathways, which in turn stimulate cell proliferation, differentiation and survival, mechanisms that also play a major role in carcinogenesis [429]. Indeed, elevated expression levels of TGF-α and EGFR are found in chronic pancreatitis and human PDAC [430, 431]. Furthermore, it has also been reported that overexpression of TGF-α in mice led to transdifferentiation of acinar cells *in vivo*, while administration of TGF-α to acinar cells resulted in ADM in *vitro* [137, 138, 142].

Another important cytokine is TGF-β1, a growth factor which is involved in regulating cell growth, immune responses or tissue homeostasis, but also plays a role in tissue fibrosis and carcinogenesis [432-434]. With regard to chronic pancreatitis, increased expression levels of TGF-β1 and its receptors were found in the pancreata of human patients [435]. In addition, TGF-β1 has been found to promote pancreatic fibrosis in the course of pancreatitis, e.g. by stimulating pancreatic stellate cells to produce extracellular matrix components [435-438]. Akanuma and colleagues have reported the induction of ADM by TGF-β1 in human pancreatic acinar cells *in vitro* [141, 315]. Transdifferentiation of acinar cells was induced either by paracrine secretion of TGF-β1 by ductal cells [315], or by manual administration of TGF-β1 [141].

In this work the first porcine acinar culture was performed as a 2D monolayer culture system according to the protocol described by De Waele et al. [314] and ADM was successfully induced using TGF-α and TGF-β1 (data not shown). However, according to the cultivation protocol of De Waele and colleagues [314], foetal bovine serum was included in the cultivation medium, which in turn can induce ADM in a TGF-β1-independent manner, as shown by Akanuma et al. [315]. Thus, the results obtained from this first approach did not allow a reliable assessment of the ADM-inducing effect of TGF-α and TGF-β1. Further cultivation approaches using serum-free medium indeed showed an ADM induction ability for both TGF-α and TGF-β1, but treatment with TGF-β1 was associated with lower ADM rates as well as lower cell viability, which led to TGF-β1 not being included in subsequent experiments.

Interestingly, Akanuma and colleagues reported that TGF-β1 induced ADM in human cells but not in murine acinar cells, while human acinar cells remained unresponsive to TGF-α and other common murine ADM inducers, leading to the assumption of substantial differences between the two species [141, 315]. Although not shown here, the preliminary results on the ability of the two cytokines to induce ADM in porcine acinar cells, albeit with different efficiencies, demonstrate the suitability of the pig as a model for cross-species comparison.

In the established 3D porcine acinar cell culture, TGF-α and Interleukin-17A (IL-17A) were used for the induction of ADM. IL-17A is a proinflammatory cytokine mainly produced by T helper 17 (Th17) cells, which represent a subset of $CD4^+$ T cells [439]. IL-17A plays an essential role in host defence and inflammatory immune response but is also involved in autoimmune diseases such as multiple sclerosis [440-442]. During pancreatitis, high levels of IL-17A are released leading to an increase of the proinflammatory response, which in turn can result in acinar cell damage and worsen the course of the disease [443, 444]. With regard to pancreatic cancer, infiltrations of IL-17 producing T cells and overexpression of IL17 receptor A (IL17RA) were detected in human pancreata close to ADM and PanIN regions, indicating an involvement of IL-17A in the ADM process [316].

Administration of TGF-α and IL-17A led to efficient transdifferentiation of porcine pancreatic acinar cells in all genotypes tested, with a significant increase compared to cells not treated with the cytokines. In addition, no significant difference in the induction capacity was detected between TGF-α and IL-17A. However, administration of IL-17A was associated with a faster growth of the evolving duct-like spheres in terms of sphere diameter. The underlying mechanism remains unclear, but could be due to the activation of different signalling pathways mediated by the two cytokines. Interestingly, transdifferentiation was also observed in porcine pancreatic acinar cells that were not treated with cytokines, but to a much lower extent. As mentioned earlier, ADM represents a protective mechanism of acinar cells against tissue damage [135, 420]. Thus, negative environmental stimuli can affect acinar cells, e.g. by inducing an endoplasmic reticulum (ER) stress response which is closely linked to pancreatitis-mediated apoptosis and inflammation [445, 446]. Therefore, acinar cells may undergo ADM even without cytokine administration, as the cell stress caused by the isolation procedure may have led to the activation of certain signalling pathways for cell survival and regeneration.

One aim was to activate $KRAS^{G12D}$ and $TP53^{R167H}$ mutations to investigate the effect of mutational activation on acinar cell transdifferentiation. Therefore, two different approaches were evaluated for the delivery of Cre recombinase to porcine pancreatic acinar cells, involving the use of either Cre lentivirus (LV) or Cre virus-like particles (VLPs).

The use of lentiviral vectors for gene transfer is characterised by numerous advantages, such as stable integration and large packaging capacity, but they also enable gene delivery into cells that are difficult to transfect, e.g. non-dividing cells [447, 448]. Non-integrating LVs are associated with a lower safety risk and are thus suitable for applications where transient transgene expression is desired, making them an attractive tool for gene therapy [449].
In contrast, VLPs are particles which form by self-assembly of viral structural proteins but do not contain viral genetic material and can be designed to deliver biologically active proteins such as Cre or Cas9 to the cell cytoplasm [401, 450, 451].

Various methods of gene delivery into the exocrine pancreas have been reported in the past. For *in vivo* gene transfer into the pancreas of mouse and rat, adenoviruses and adeno-associated viruses have been described as efficient [452-454]. *In vitro*, successful gene delivery into acinar cell lines can be achieved by transfection using Lipofectamine 2000 [415]. However, this method proved to be highly inefficient in primary acinar cells [454]. Thus, Houbracken and colleagues have tested adenovirus and two different lentiviral vectors for *in vitro* transduction of rat pancreatic exocrine cells, with all viral vectors expressing enhanced green fluorescent protein (EGFP) under the control of the cytomegalovirus (CMV) promoter [454]. They reported that administration of adenovirus resulted in higher transduction rates than LV, but severely impaired cell survival [454]. In summary, vesicular stomatitis virus-glycoprotein (VSV-G) pseudotyped LV turned out to be the best option for *in vitro* transduction of acinar cells as this method was characterised by a high transduction efficiency resulting in stable expression of the EGFP transgene and survival rates comparable to non-transduced acinar cells [454].
While the use of LVs for pancreatic transduction has been described in the literature, at least to my knowledge, the use of VLPs in primary pancreatic acinar cells has not yet been reported. However, efficient VLP-mediated delivery of gene editing proteins such as Cas9 to primary cells other than acinar cells has been demonstrated in mice and humans [401, 455]. In addition, VLPs and their use as vaccines are currently subject to research on cancer prevention and therapy [456].

Here, mutational activation by Cre LV and Cre VLPs was evaluated in porcine acinar cells derived from three different genotypes. As activation of $KRAS^{G12D}$ and $TP53^{R167H}$ only required transient expression of Cre recombinase, a non-integrating Cre LV was used for transduction. Compared to the untransduced cells, transduction with Cre LV increased the transdifferentiation rates of acinar cells regardless of the culture condition (TGF-α, IL-17A and control). Especially in the control sample, which was not treated with cytokines, activation of $KRAS^{G12D}$ and $TP53^{R167H}$ at least doubled the transdifferentiation rate for all three genotypes.

In contrast, transduction with Cre VLPs only slightly increased the transdifferentiation rate of *APC*$^{1311/WT}$*TP53*$^{LSLR167H/LSLR167H}$ cells, while there was no significant increase detectable in *KRAS*$^{LSLG12D/WT}$*TP53*$^{LSLR167H/WT}$*R26*$^{Cas9/WT}$ acinar cells. Consistent with these results, LSL-excision PCR showed efficient excision of the LSL cassette for *KRAS*^{G12D} and *TP53*^{R167H} mutant alleles in Cre LV transduced *KRAS*$^{LSLG12D/WT}$*TP53*$^{LSLR167H/WT}$*R26*$^{Cas9/WT}$ acinar cells, while there was no excision detectable for Cre VLP treated samples.
These results showed that the use of Cre LV is more suitable than VLPs for mutational activation in porcine acinar cells. Interestingly, the PCR band for the *KRAS* recombined allele was characterised by a stronger intensity when compared to the wild type band, a phenomenon that was already described in chapter 3.3.3. In addition, sequencing of PCR products using reverse transcribed mRNA from Cre LV transduced acinar cells confirmed the expression of a G→A single base mutation at *KRAS* codon 12, with increased peak height for adenine when compared to guanine (Figure 57C). In fact, it was reported that PDAC is often characterised by allelic imbalance, thus leading to an increase in oncogenic *KRAS* gene dosage which is associated with loss of wild type *KRAS* [405]. This loss of heterozygosity (LOH) with concomitant oncogenic *KRAS* dosage gain was shown to correlate with highly aggressive phenotypes of PDAC and poor outcome [405, 457]. However, the basis of emerging LOH in Cre LV transduced *KRAS*$^{LSLG12D/WT}$*TP53*$^{LSLR167H/WT}$*R26*$^{Cas9/WT}$ acinar cells remains unclear and would require further analysis, e.g. by pyrosequencing, fluorescence *in situ* hybridization (FISH) or whole-exome sequencing (WES).

In addition, it was of great interest to verify whether the administration of TGF-α and IL-17A also increased the transdifferentiation rate of acinar cells isolated from the pancreas of a *KRAS*$^{G12D/WT}$*PTF1A*$^{5'iCre/WT}$ pig. Due to *PTF1A*^{iCre}-driven activation of the *KRAS*^{G12D} mutation in the pancreas during embryogenesis, this pig already showed ADM and PanIN lesions when the pancreas was isolated at 5 weeks of age (see section 3.1.3). Therefore, the acinar control sample, which was not treated with cytokines, already showed a relatively high transdifferentiation frequency of more than 24%. Nevertheless, administration of cytokines increased the transdifferentiation rates to 51% and 65% for TGF-α and IL-17A, respectively.
It was reported that activation of *Kras*^{G12D} induces the expression of IL17RA on murine ADM and PanIN cells and that IL17RA signalling in turn leads to expression of REG3β, an inflammatory mediator which promotes the transition from pancreatic inflammation to cancer via the JAK2-STAT3 pathway [316, 458]. This *KRAS*^{G12D}-IL-17A relationship leads to the assumption that the higher transdifferentiation rate for IL-17A treated porcine acinar cells compared to TGF-α treatment, is possibly caused by an enhanced responsiveness through increased expression of IL17RA on the acinar cell surface due to oncogenic *KRAS* activation.

In summary, the porcine ADM culture recapitulates substantial key aspects of human and murine ADM cultures and thus has proven to be a promising model for cross-species comparison.

Although a major first step has been taken with its successful establishment, this porcine cultural model still requires additional characterization to confirm its validity. Besides the assessment of transdifferentiation rates by manual counting, other methods of tracking ADM development should be implemented, e.g. labelling acinar cells with fluorescein conjugated Ulex Europaeus Agglutinin I (UEA I). This lectin binds to α-linked fucose residues on cells and was shown to specifically stain human and mouse pancreatic acinar cells with a detection time of up to 7 days [314, 415, 459], allowing evaluation of the origin of the evolving duct-like spheres.
At the molecular level, transdifferentiation of acinar cells was shown to be accompanied by a loss of acinar gene expression with a concomitant increase in the expression of ductal cell markers [139, 460]. Therefore, determining the expression profiles of acinar and ductal markers, such as *Amylase* and *PTF1A* or *Sox9* and *Cytokeratin-19* respectively, would be an important step in characterising and validating the porcine ADM process. It is also essential to further optimise the isolation procedure for the isolation of high quality and quantitative RNA from porcine acinar cells. Besides analysis by PCR, the expression of acinar and duct-specific markers can also be determined by immunohistochemistry (IHC). Especially with regard to a change in the expression profile over time, RNA sequencing (RNA-seq) or fluorescence-activated cell sorting (FACS) are the better methods for quantitatively determining transdifferentiation, although the latter requires careful dissociation of the acinar clusters to avoid cell damage.

Once these new characterisation methods have been established for porcine acinar cells, a larger number of pigs, especially of the $KRAS^{G12D}$ and $PTF1A^{iCre}$ genotypes, should be used for acinar cell isolation. Increasing the number of samples and including other possible ADM inducers, such as RANTES, tumor necrosis factor α (TNF-α) or interleukin 6 [139, 461], will help to generate reliable data trends.

5 Concluding remarks and outlook

In this work, a porcine model for human PDAC was generated. Activation of latent *KRAS*^{G12D} and *TP53*^{R167H} mutations in the pig required breeding with porcine Cre driver lines, which were successfully generated using different strategies. It was demonstrated, that the porcine *PTF1A* and the murine *Pdx1* promoter were both equally capable of driving tissue-specific iCre expression, which in turn activated the *KRAS* and *TP53* mutations and thus resulted in early tumour formation in the porcine pancreas. In the near future, these tumours will be analysed in more detail, both molecularly and histologically, to map further similarities to PDAC tumour formation and progression in humans.

The first approach for Cre driver pig generation, which based on CRISPR/Cas9-mediated integration of iCre into the porcine endogenous *PTF1A* locus revealed that disruption of one endogenous allele had no significant effect on the development of viable and healthy animals and that transgene placement into the 3'UTR using a T2A linker sequence also enabled efficient expression from the endogenous promoter. In summary, transgene placement into the 5'end and 3'end of *PTF1A* resulted in equal iCre expression patterns and tumourigenesis upon breeding with *KRAS*$^{LSLG12D/WT}$ and *TP53*$^{LSLR167H/WT}$ pigs. However, it would be interesting to quantify the *PTF1A* expression levels of 5'end and 3'end targeted pigs and compare them with the wild type profile to evaluate the effects of the respective transgene position. As it preserves both endogenous *PTF1A* alleles, the strategy of expressing iCre from the 3'UTR using a T2A linker enables breeding of *PTF1A*$^{3'iCre/3'iCre}$ animals. These homozygous pigs will help breeding of *KRAS*$^{LSLG12D/WT}$*TP53*$^{LSLR167H/WT}$*PTF1A*$^{3'iCre/WT}$ pigs, as this results in fewer unwanted genotypes and is therefore better for animal welfare.
In addition, expressing a transgene from the 3'UTR using a linker sequence also represents a suitable approach for other projects where the maintenance of both endogenous alleles is required while simultaneous expression from the endogenous promoter is needed. This method can be used to obtain transgenic animals with a natural transgene expression profile without laborious cloning of endogenous promoter regions or inefficient transgene placements into "safe haven" loci such as *ROSA26*.

A Cre driver pig line was also generated by transposon-mediated integration of *mPdx1-iCre* into the porcine genome. It was demonstrated that the piggyBac transposon system is an efficient tool for genome modifications, which can be used for cytoplasmic injection of porcine oocytes as it did not lead to embryo toxicity or detrimental effects on pig development. In this case, application of PB transposase as mRNA can substantially reduce the risk of undesired side effects such as chromosomal mutagenesis, which is often caused by genomic integration of the transposase gene as a result of plasmid delivery.

The generation of transgenic pigs by cytoplasmic oocyte injection represents a promising alternative approach to the SCNT-based procedure as it is less time-consuming and more cost-effective. This is based on the fact, that successful generation of pigs by SCNT usually requires numerous rounds and that these animals are often affected by physiological defects which are caused by incomplete nuclear reprogramming. However, transposon-mediated transgene delivery into porcine oocytes only enables random integration. Besides transposon systems, CRISPR/Cas9 system is also used for the generation of transgenic animals by cytoplasmic oocyte injection, albeit mainly for gene inactivation. It would be a major gain for the creation of transgenic livestock, if the CRISPR/Cas9 system could be optimized for HDR-mediated targeted transgene integration in porcine oocytes, thus replacing the costly and inefficient SCNT procedure.
Regarding gene editing, this work also described the establishment of a highly efficient multiplexed CRISPR/Cas9 system for the inactivation of tumour suppressor genes, which are commonly mutated in the course of human PDAC progression. Gene editing using a CRISPR/Cas9 PTG construct offers the opportunity for simultaneous modification of several genes and significantly reduces the vector size in comparison to the conventional CRISPR/Cas9 editing system. Consequently, this strategy is suitable for applications with limited packaging capacity such as viral delivery and thus avoids the co-transmission of several plasmids or viral vectors, which would have led to unequal transcription levels of the respective gRNAs.

While the generation of Cre driver pig lines enabled PDAC modelling *in vivo*, an alternative approach in this work focused on the establishment and optimization of an *in vitro* system for the induction of ADM, the earliest PDAC precursor state found in the human pancreas. Upon cytokine treatment or activation of $KRAS^{G12D}$ and $TP53^{R167H}$, the porcine acinar cell model showed typical characteristics of ADM. Although this porcine *in vitro* model needs further characterisation and the generation of larger datasets, its development is a great success in terms of cross-species comparison and could serve as a clinical *in vitro* model for the identification of early biomarkers or drug testing.

The applied methods in this work enabled the generation of a porcine PDAC model, which represents a major achievement in preclinical PDAC research. Due to their similarity to humans in terms of organ size, physiology or drug metabolism, the generated PDAC pig represents a valuable translational model that will allow cross-species comparison and validation of preclinical data obtained from mouse studies, hopefully advancing research for early detection and treatment of the devastating PDAC disease.

6 Abbreviations

Abbreviation	Definition
2D	Two-dimensional
3D	Three-dimensional
4-OHT	4-hydroxytamoxifen
AdCre	Adenovirus encoding Cre recombinase
ADM	Acinar-to-ductal metaplasia
AMY2B	Amylase alpha 2B
APC	Adenomatous polyposis coli
ATM	Ataxia-telangiectasia mutated
B2M	Beta-2-microglobulin
bHLH protein	Basic helix-loop-helix protein
BPE	Bovine pituitary extract
BRCA1/2	Breast cancer 1/2
BSA	Bovine serum albumin
CAM	Chorioallantoic membrane
Cas9	CRISPR-associated protein 9
Cas9n	Cas9 nickase
CDKN2A	Cyclin-dependent kinase inhibitor 2A
CDS	Coding DNA sequence
CHEK2	Checkpoint kinase 2
CK19	Cytokeratin 19
CMV	Cytomegalovirus
c-MYC	Cellular myelocytomatosis
Cre	Causes recombination
Cre-ER^{T}	Cre fused to mutant binding domain of the human oestrogen receptor
Cre-ER^{T2}	Cre fused to triple mutant binding domain of the human oestrogen receptor
CRISPR	Clustered Regularly Interspaced Short Palindromic Repeats
crRNA	CRISPR RNA
CTLA4-Ig	T cell co-stimulation inhibitor cytotoxic T-lymphocyte antigen 4
CVD	Cardiovascular disease
ddPCR	Droplet digital PCR
DNA-PK	DNA-dependent protein kinase
DNA-PK$_{CS}$	DNA-PK catalytic subunit
dNTP	Deoxynucleotide
DMEM	Dulbecco's Modified Eagle Medium
Dox	Doxycycline
DSB	Double-strand break
dsDNA	Double-stranded DNA
E.coli	*Escherichia coli*
EGF	Epidermal growth factor
EGFP	Enhanced green fluorescent protein
EGFR	Epidermal growth factor receptor
EMT	Epithelial-mesenchymal transition
ER	Endoplasmic reticulum
ES cells	Embryonic stem cells
EtOH	Ethanol
FAMMM	Familial atypical multiple mole melanoma
FACS	Fluorescence activated cell sorting
FBS	Fetal bovine serum

FISH	Fluorescence in situ hybridization
G12D	G to D amino acid substitution at codon 12
GAPs	GTPase-activating proteins
gDNA	Genomic DNA
GEFs	Guanine nucleotide exchange-factors
GEMMs	Genetically engineered mouse models
Globocan	Global Cancer Observatory
GOI	Gene of interest
gRNA	Guide RNA
h	Hour
HCl	Hydrochloric acid
HDR	Homology-directed repair
H&E	Hematoxylin and Eosin
HR	Homologous recombination
HSP90	Heat shock protein 90
iCre	Improved Cre
IHC	Immunohistochemistry
IL-17A	Interleukin-17A
IL17RA	Interleukin 17 receptor A
InDels	Insertion or deletion mutations
IOPN	Intraductal oncocytic papillary neoplasm
IPMN	Intraductal papillary mucinous neoplasm
iPS cells	Induced pluripotent stem cells
IRES	Internal ribosomal entry site
ITPN	Intraductal tubulopapillary neoplasm
ITR	Inverted terminal repeat
ITS	Insulin-Transferrin-Selenium
KCl	Potassium chloride
KRAS	Kirsten rat sarcoma viral oncogene homologue
l	Litre
LBD	Ligand binding domain
LEA29Y	High affinity variant of CTLA4-Ig
LINEs	Long interspersed nucleotide elements
LOH	Loss of heterozygosity
LoxP	Locus of crossing-over in P1
LSL	Lox-stop-lox
LV	Lentivirus
M	Molar
MII	Metaphase II
MCN	Mucinous cystic neoplasm
mGFP	Membrane-targeted GFP fluorescence cassette
MHCI	Major histocompatibility complex class I
MHCII	Major histocompatibility complex class II
min	Minute
mM	Millimolar
MODY	Maturity-onset diabetes of the young
mPdx1	Murine Pdx1 promoter
mRNA	Messenger RNA
mTomato	Membrane-targeted Tomato fluorescence cassette
NaCl	Sodium chloride
$NaHCO_3$	Sodium bicarbonate
NaOH	Sodium hydroxide
NEAA	Non-essential amino acids

NHEJ	Non-homologous end joining
OPI	Overproduction inhibition
ORF	Open reading frame
PACC	Pancreatic acinar cell carcinoma
PADMSCs	Porcine adipose-derived mesenchymal stem cells
PALB2	Partner and localizer of BRCA2
PAM	Protospacer adjacent motif
PanIN	Pancreatic intraepithelial neoplasia
PB	piggyBac
PBS	Dulbecco's Phosphate Buffered Saline
PCR	Polymerase chain reaction
PDAC	Pancreatic ductal adenocarcinoma
Pdx1	Pancreatic and duodenal homeobox 1
PEFs	Porcine ear fibroblasts
PKFs	Porcine kidney fibroblasts
PNET	Pancreatic neuroendocrine tumour
Pol III	Polymerase III
Pre-crRNA	Precursor CRISPR RNA
P/S	Penicillin-Streptomycin
PTF1A	Pancreas associated transcription factor 1a
PTG	Polycistronic tRNA-gRNA gene
R26	*ROSA26*
Rb	Retinoblastoma
RBP-J/RBP-L	Recombining binding protein suppressor of hairless
RMCE	Recombinase-mediated cassette exchange
RNA-seq	RNA sequencing
RNP	Ribonucleoprotein particle
ROSA26	Reverse orientation splice acceptor β-geo 26
Rpm	Revolutions per minute
RPS28	40S ribosomal protein S28
RT	Room temperature
RT-PCR	Reverse transcription-polymerase chain reaction
rtTa	Reversed tetracycline transactivator
s	Second
SA	Splice acceptor
SB	Sleeping beauty
SCNT	Somatic cell nuclear transfer
SDS	Sodium dodecyl sulfate
sgRNA	Single guide RNA
SINEs	Short interspersed nucleotide elements
SMAD4	Mothers against decapentaplegic homolog 4
SNP	Single nucleotide polymorphism
SOX9	SRY-Box Transcription Factor 9
SFFV	spleen focus forming virus
SPN	Solid pseudopapillary neoplasm
SSB	DNA single-strand break
ssDNA	Single-stranded DNA
SV40LT	Simian virus 40 large T antigen
T2A	Thosea asigna virus self-cleaving peptide
TALEN	Transcription Activator-like Effector Nuclease
TE	Transposable element
Tet	Tetracycline
TF	Transcription factor

TGF-α	Transforming growth factor beta
TGF-β	Transforming growth factor beta
Th17	T helper 17 cells
TNF	Tumor necrosis factor
TNF-α	Tumor necrosis factor alpha
TP53	Tumour protein p53
tracrRNA	Transactivating crRNA
TSG	Tumour suppressor gene
tTa	Tetracycline transactivator
UEA I	Ulex Europaeus Agglutinin I
UTR	Untranslated region
V	Volt
VLPs	Virus-like particles
Vol	Volume
VSV-G	Vesicular stomatitis virus-glycoprotein
WES	whole-exome sequencing
x g	gravity
ZFN	Zinc Finger Nuclease

7 List of tables

8 List of figures

9 List of supplementary figures

10 Literature

1. Jaul, E. and J. Barron, *Age-Related Diseases and Clinical and Public Health Implications for the 85 Years Old and Over Population.* Front Public Health, 2017. **5**: p. 335.
2. Destatis, S.B. *Causes of death by type of disease, 2021*. 2021 [cited 2023 23.01.2023]; Available from: https://www.destatis.de/DE/Themen/Gesellschaft-Umwelt/Gesundheit/Todesursachen/_inhalt.html#sprg229156.
3. Destatis, S.B. *Total deaths from cancer, 2021* 2022 [cited 2023 23.01.2023]; Available from: https://www.destatis.de/DE/Themen/Gesellschaft-Umwelt/Gesundheit/Todesursachen/Tabellen/sterbefaelle-krebs-insgesamt.html.
4. Wilkins E, W.L., Wickramasinghe K, Bhatnagar P, Leal J, Luengo-Fernandez R, Burns R, Rayner M, Townsend N *European Cardiovascular Disease Statistics* European Cardiovascular Disease Statistics 2017 edition 2017; Available from: http://www.ehnheart.org/cvd-statistics.html.
5. Virani, S.S., et al., *Heart Disease and Stroke Statistics-2020 Update: A Report From the American Heart Association.* Circulation, 2020. **141**(9): p. e139-e596.
6. Bhatnagar, P., et al., *Trends in the epidemiology of cardiovascular disease in the UK.* Heart, 2016. **102**(24): p. 1945-1952.
7. Mensah, G.A., et al., *Decline in Cardiovascular Mortality: Possible Causes and Implications.* Circ Res, 2017. **120**(2): p. 366-380.
8. Hay, M., et al., *Clinical development success rates for investigational drugs.* Nature Biotechnology, 2014. **32**(1): p. 40-51.
9. Wong, C.H., K.W. Siah, and A.W. Lo, *Estimation of clinical trial success rates and related parameters.* Biostatistics, 2018. **20**(2): p. 273-286.
10. Fitzmaurice, C., et al., *Global, Regional, and National Cancer Incidence, Mortality, Years of Life Lost, Years Lived With Disability, and Disability-Adjusted Life-Years for 29 Cancer Groups, 1990 to 2016: A Systematic Analysis for the Global Burden of Disease Study.* JAMA Oncol, 2018. **4**(11): p. 1553-1568.
11. Dagenais, G.R., et al., *Variations in common diseases, hospital admissions, and deaths in middle-aged adults in 21 countries from five continents (PURE): a prospective cohort study.* Lancet, 2020. **395**(10226): p. 785-794.
12. Harding, M.C., et al., *Transitions From Heart Disease to Cancer as the Leading Cause of Death in US States, 1999-2016.* Prev Chronic Dis, 2018. **15**: p. E158.
13. Bray, F., et al., *Global cancer statistics 2018: GLOBOCAN estimates of incidence and mortality worldwide for 36 cancers in 185 countries.* CA: A Cancer Journal for Clinicians, 2018. **68**(6): p. 394-424.
14. Sung, H., et al., *Global Cancer Statistics 2020: GLOBOCAN Estimates of Incidence and Mortality Worldwide for 36 Cancers in 185 Countries.* CA: A Cancer Journal for Clinicians, 2021. **71**(3): p. 209-249.
15. Ferlay, J., et al., *Cancer incidence and mortality patterns in Europe: Estimates for 40 countries and 25 major cancers in 2018.* Eur J Cancer, 2018. **103**: p. 356-387.
16. Malvezzi, M., et al., *European cancer mortality predictions for the year 2019 with focus on breast cancer.* Ann Oncol, 2019. **30**(5): p. 781-787.
17. Siegel, R.L., K.D. Miller, and A. Jemal, *Cancer statistics, 2020.* CA Cancer J Clin, 2020. **70**(1): p. 7-30.
18. Siegel, R.L., et al., *Cancer statistics, 2022.* CA: A Cancer Journal for Clinicians, 2022. **72**(1): p. 7-33.
19. Collaborators, G.P.C., *The global, regional, and national burden of pancreatic cancer and its attributable risk factors in 195 countries and territories, 1990-2017: a systematic analysis for the Global Burden of Disease Study 2017.* Lancet Gastroenterol Hepatol, 2019. **4**(12): p. 934-947.
20. Huang, J., et al., *Worldwide Burden of, Risk Factors for, and Trends in Pancreatic Cancer.* Gastroenterology, 2021. **160**(3): p. 744-754.

21. Quante, A.S., et al., *Projections of cancer incidence and cancer-related deaths in Germany by 2020 and 2030.* Cancer Medicine, 2016. **5**(9): p. 2649-2656.
22. Rahib, L., et al., *Projecting Cancer Incidence and Deaths to 2030: The Unexpected Burden of Thyroid, Liver, and Pancreas Cancers in the United States.* Cancer Research, 2014. **74**(11): p. 2913-2921.
23. Henry, B.M., et al., *Development of the human pancreas and its vasculature - An integrated review covering anatomical, embryological, histological, and molecular aspects.* Ann Anat, 2019. **221**: p. 115-124.
24. Hans G. Beger, A.L.W., Ralph H. Hruban, Markus W. Buchler, Markus M. Lerch, John P. Neoptolemos, Tooru Shimosegawa, David C. Whitcomb, *Section 2: Anatomy, Histology, and Fine Structure of the Pancreas*, in *The Pancreas: An Integrated Textbook of Basic Science, Medicine, and Surgery*. 2018, John Wiley & Sons Ltd. p. 10-15.
25. Pandol, S., *The Exocrine Pancreas.*, in *NCBI Bookshelf*. 2010, San Rafael (CA): Morgan & Claypool Life Sciences.
26. Whitcomb, D.C. and M.E. Lowe, *Human pancreatic digestive enzymes.* Dig Dis Sci, 2007. **52**(1): p. 1-17.
27. Avisse, C., J.B. Flament, and J.F. Delattre, *Ampulla of Vater. Anatomic, embryologic, and surgical aspects.* Surg Clin North Am, 2000. **80**(1): p. 201-12.
28. Allescher, H.D., *Papilla of Vater: structure and function.* Endoscopy, 1989. **21 Suppl 1**: p. 324-9.
29. Garber, A., et al., *Mechanisms and Management of Acute Pancreatitis.* Gastroenterol Res Pract, 2018. **2018**: p. 6218798.
30. Huggett, M.T. and S.P. Pereira, *Diagnosing and managing pancreatic cancer.* Practitioner, 2011. **255**(1742): p. 21-5, 2-3.
31. In't Veld, P. and M. Marichal, *Microscopic anatomy of the human islet of Langerhans.* Adv Exp Med Biol, 2010. **654**: p. 1-19.
32. Zhou, Q. and D.A. Melton, *Pancreas regeneration.* Nature, 2018. **557**(7705): p. 351-358.
33. Moldovan, S. and F.C. Brunicardi, *Endocrine Pancreas: Summary of Observations Generated by Surgical Fellows.* World Journal of Surgery, 2001. **25**(4): p. 468-473.
34. Brissova, M., et al., *Assessment of Human Pancreatic Islet Architecture and Composition by Laser Scanning Confocal Microscopy.* Journal of Histochemistry & Cytochemistry, 2005. **53**(9): p. 1087-1097.
35. Cabrera, O., et al., *The unique cytoarchitecture of human pancreatic islets has implications for islet cell function.* Proc Natl Acad Sci U S A, 2006. **103**(7): p. 2334-9.
36. Del Prato, S. and P. Marchetti, *Beta- and alpha-cell dysfunction in type 2 diabetes.* Horm Metab Res, 2004. **36**(11-12): p. 775-81.
37. Gromada, J., P. Chabosseau, and G.A. Rutter, *The alpha-cell in diabetes mellitus.* Nat Rev Endocrinol, 2018. **14**(12): p. 694-704.
38. Masini, M., et al., *Ultrastructural alterations of pancreatic beta cells in human diabetes mellitus.* Diabetes Metab Res Rev, 2017. **33**(6).
39. McGuigan, A., et al., *Pancreatic cancer: A review of clinical diagnosis, epidemiology, treatment and outcomes.* World J Gastroenterol, 2018. **24**(43): p. 4846-4861.
40. Sarantis, P., et al., *Pancreatic ductal adenocarcinoma: Treatment hurdles, tumor microenvironment and immunotherapy.* World J Gastrointest Oncol, 2020. **12**(2): p. 173-181.
41. Lowery, M.A., et al., *Acinar cell carcinoma of the pancreas: new genetic and treatment insights into a rare malignancy.* Oncologist, 2011. **16**(12): p. 1714-20.
42. Chaudhary, P., *Acinar Cell Carcinoma of the Pancreas: A Literature Review and Update.* Indian J Surg, 2015. **77**(3): p. 226-31.
43. Morikawa, M., et al., *Acinar cell carcinoma of the pancreas in childhood.* Int Cancer Conf J, 2016. **5**(3): p. 140-145.
44. Illyés, G., et al., *Cushing's Syndrome in a Child with Pancreatic Acinar Cell Carcinoma.* Endocrine Pathology, 2007. **18**(2): p. 95-102.

45. Ellerkamp, V., et al., *Exocrine pancreatic tumors in childhood in Germany.* Pediatric Blood & Cancer, 2012. **58**(3): p. 366-371.
46. Holen, K.D., et al., *Clinical characteristics and outcomes from an institutional series of acinar cell carcinoma of the pancreas and related tumors.* J Clin Oncol, 2002. **20**(24): p. 4673-8.
47. Wisnoski, N.C., et al., *672 patients with acinar cell carcinoma of the pancreas: a population-based comparison to pancreatic adenocarcinoma.* Surgery, 2008. **144**(2): p. 141-8.
48. Wang, Y., et al., *Acinar cell carcinoma: a report of 19 cases with a brief review of the literature.* World Journal of Surgical Oncology, 2016. **14**(1): p. 172.
49. Klimstra, D.S., et al., *Acinar cell carcinoma of the pancreas. A clinicopathologic study of 28 cases.* Am J Surg Pathol, 1992. **16**(9): p. 815-37.
50. Vossen, S., et al., *Therapeutic Management of Rare Malignant Pancreatic Tumors in Children.* World Journal of Surgery, 1998. **22**(8): p. 879-882.
51. Perez, E.A., et al., *Malignant pancreatic tumors: incidence and outcome in 58 pediatric patients.* Journal of Pediatric Surgery, 2009. **44**(1): p. 197-203.
52. Glick, R.D., et al., *Management of pancreatoblastoma in children and young adults.* J Pediatr Hematol Oncol, 2012. **34 Suppl 2**: p. S47-50.
53. Cavallini, A., et al., *Pancreatoblastoma in adults: a review of the literature.* Pancreatology, 2009. **9**(1-2): p. 73-80.
54. Coleman, K.M., M.C. Doherty, and S.A. Bigler, *Solid-Pseudopapillary Tumor of the Pancreas.* RadioGraphics, 2003. **23**(6): p. 1644-1648.
55. Dinarvand, P. and J. Lai, *Solid Pseudopapillary Neoplasm of the Pancreas: A Rare Entity With Unique Features.* Arch Pathol Lab Med, 2017. **141**(7): p. 990-995.
56. Guo, N., et al., *Diagnosis and surgical treatment of solid pseudopapillary neoplasm of the pancreas: analysis of 24 cases.* Can J Surg, 2011. **54**(6): p. 368-74.
57. Grant, T.J., K. Hua, and A. Singh, *Molecular Pathogenesis of Pancreatic Cancer.* Prog Mol Biol Transl Sci, 2016. **144**: p. 241-275.
58. Dromain, C., et al., *Imaging of neuroendocrine tumors of the pancreas.* Diagnostic and Interventional Imaging, 2016. **97**(12): p. 1241-1257.
59. Wong, K.P., J.S. Tsang, and B.H. Lang, *Role of surgery in pancreatic neuroendocrine tumor.* Gland Surg, 2018. **7**(1): p. 36-41.
60. Perri, G., L.R. Prakash, and M.H.G. Katz, *Pancreatic neuroendocrine tumors.* Curr Opin Gastroenterol, 2019. **35**(5): p. 468-477.
61. Ro, C., et al., *Pancreatic neuroendocrine tumors: biology, diagnosis,and treatment.* Chin J Cancer, 2013. **32**(6): p. 312-24.
62. Sun, J., *Pancreatic neuroendocrine tumors.* Intractable Rare Dis Res, 2017. **6**(1): p. 21-28.
63. Scott, A.T. and J.R. Howe, *Evaluation and Management of Neuroendocrine Tumors of the Pancreas.* Surgical Clinics of North America, 2019. **99**(4): p. 793-814.
64. Rawla, P., T. Sunkara, and V. Gaduputi, *Epidemiology of Pancreatic Cancer: Global Trends, Etiology and Risk Factors.* World J Oncol, 2019. **10**(1): p. 10-27.
65. Yu, J., et al., *Time to progression of pancreatic ductal adenocarcinoma from low-to-high tumour stages.* Gut, 2015. **64**(11): p. 1783-9.
66. Werner, J., et al., *Advanced-stage pancreatic cancer: therapy options.* Nature Reviews Clinical Oncology, 2013. **10**(6): p. 323-333.
67. ACS, *Cancer Facts & Figures 2020*. 2020, American Cancer Society, Atlanta.
68. Yokota, T., et al., *Successful treatment of a locally advanced unresectable pancreatic cancer patient with interstitial pneumonitis by conversion surgery following gemcitabine plus nab-paclitaxel chemotherapy: A case report.* Mol Clin Oncol, 2019. **10**(4): p. 419-424.
69. Peng, J., et al., *Single-cell RNA-seq highlights intra-tumoral heterogeneity and malignant progression in pancreatic ductal adenocarcinoma.* Cell Research, 2019. **29**(9): p. 725-738.
70. Pedersen, K., et al., *Pancreatic cancer heterogeneity and response to Mek inhibition.* Oncogene, 2017. **36**(40): p. 5639-5647.

71. Biancur, D.E. and A.C. Kimmelman, *The plasticity of pancreatic cancer metabolism in tumor progression and therapeutic resistance.* Biochimica et Biophysica Acta (BBA) - Reviews on Cancer, 2018. **1870**(1): p. 67-75.
72. Kim, J.Y. and S.M. Hong, *Precursor Lesions of Pancreatic Cancer.* Oncol Res Treat, 2018. **41**(10): p. 603-610.
73. Brugge, W.R., *Diagnosis and management of cystic lesions of the pancreas.* Journal of Gastrointestinal Oncology, 2015. **6**(4): p. 375-388.
74. Shi, C. and R.H. Hruban, *Intraductal papillary mucinous neoplasm.* Human Pathology, 2012. **43**(1): p. 1-16.
75. Campbell, F. and B. Azadeh, *Cystic neoplasms of the exocrine pancreas.* Histopathology, 2008. **52**(5): p. 539-551.
76. Nilsson, L.N., et al., *Nature and management of pancreatic mucinous cystic neoplasm (MCN): A systematic review of the literature.* Pancreatology, 2016. **16**(6): p. 1028-1036.
77. Ren, B., X. Liu, and A.A. Suriawinata, *Pancreatic Ductal Adenocarcinoma and Its Precursor Lesions: Histopathology, Cytopathology, and Molecular Pathology.* The American Journal of Pathology, 2019. **189**(1): p. 9-21.
78. Basturk, O., et al., *Pancreatic intraductal tubulopapillary neoplasm is genetically distinct from intraductal papillary mucinous neoplasm and ductal adenocarcinoma.* Modern Pathology, 2017. **30**(12): p. 1760-1772.
79. Noë, M. and L.A.A. Brosens, *Pathology of Pancreatic Cancer Precursor Lesions.* Surgical Pathology Clinics, 2016. **9**(4): p. 561-580.
80. Guo, J., K. Xie, and S. Zheng, *Molecular Biomarkers of Pancreatic Intraepithelial Neoplasia and Their Implications in Early Diagnosis and Therapeutic Intervention of Pancreatic Cancer.* Int J Biol Sci, 2016. **12**(3): p. 292-301.
81. Yu, D.Y., et al., *Clinical significance of pancreatic intraepithelial neoplasia in resectable pancreatic cancer on survivals.* Ann Surg Treat Res, 2018. **94**(5): p. 247-253.
82. Cornish, T.C. and R.H. Hruban, *Pancreatic Intraepithelial Neoplasia.* Surg Pathol Clin, 2011. **4**(2): p. 523-35.
83. Murphy, S.J., et al., *Genetic alterations associated with progression from pancreatic intraepithelial neoplasia to invasive pancreatic tumor.* Gastroenterology, 2013. **145**(5): p. 1098-1109.e1.
84. Hruban, R.H., et al., *Pancreatic intraepithelial neoplasia: a new nomenclature and classification system for pancreatic duct lesions.* Am J Surg Pathol, 2001. **25**(5): p. 579-86.
85. Witkiewicz, A.K., et al., *Whole-exome sequencing of pancreatic cancer defines genetic diversity and therapeutic targets.* Nat Commun, 2015. **6**: p. 6744.
86. Hruban, R.H., et al., *Progression Model for Pancreatic Cancer.* Clinical Cancer Research, 2000. **6**(8): p. 2969-2972.
87. Murtaugh, L.C., *Pathogenesis of Pancreatic Cancer: Lessons from Animal Models.* Toxicologic Pathology, 2013. **42**(1): p. 217-228.
88. Haigis, K.M., *KRAS Alleles: The Devil Is in the Detail.* Trends Cancer, 2017. **3**(10): p. 686-697.
89. Simanshu, D.K., D.V. Nissley, and F. McCormick, *RAS Proteins and Their Regulators in Human Disease.* Cell, 2017. **170**(1): p. 17-33.
90. Raphael, B.J., et al., *Integrated Genomic Characterization of Pancreatic Ductal Adenocarcinoma.* Cancer Cell, 2017. **32**(2): p. 185-203.e13.
91. Waters, A.M. and C.J. Der, *KRAS: The Critical Driver and Therapeutic Target for Pancreatic Cancer.* Cold Spring Harb Perspect Med, 2018. **8**(9).
92. Vatansever, S., B. Erman, and Z.H. Gümüş, *Oncogenic G12D mutation alters local conformations and dynamics of K-Ras.* Scientific Reports, 2019. **9**(1): p. 11730.
93. Schutte, M., et al., *Abrogation of the Rb/p16 tumor-suppressive pathway in virtually all pancreatic carcinomas.* Cancer Res, 1997. **57**(15): p. 3126-30.
94. Yachida, S., et al., *Clinical significance of the genetic landscape of pancreatic cancer and implications for identification of potential long-term survivors.* Clin Cancer Res, 2012. **18**(22): p. 6339-47.

95. Furukawa, T., et al., *Distinct progression pathways involving the dysfunction of DUSP6/MKP-3 in pancreatic intraepithelial neoplasia and intraductal papillary-mucinous neoplasms of the pancreas.* Modern Pathology, 2005. **18**(8): p. 1034-1042.
96. Sharpless, N.E., *INK4a/ARF: A multifunctional tumor suppressor locus.* Mutation Research/Fundamental and Molecular Mechanisms of Mutagenesis, 2005. **576**(1): p. 22-38.
97. Ozenne, P., et al., *The ARF tumor suppressor: structure, functions and status in cancer.* Int J Cancer, 2010. **127**(10): p. 2239-47.
98. Romagosa, C., et al., *p16Ink4a overexpression in cancer: a tumor suppressor gene associated with senescence and high-grade tumors.* Oncogene, 2011. **30**(18): p. 2087-2097.
99. Zhao, R., et al., *Implications of Genetic and Epigenetic Alterations of CDKN2A (p16(INK4a)) in Cancer.* EBioMedicine, 2016. **8**: p. 30-39.
100. Hainaut, P. and G.P. Pfeifer, *Somatic TP53 Mutations in the Era of Genome Sequencing.* Cold Spring Harb Perspect Med, 2016. **6**(11).
101. Aubrey, B.J., A. Strasser, and G.L. Kelly, *Tumor-Suppressor Functions of the TP53 Pathway.* Cold Spring Harb Perspect Med, 2016. **6**(5).
102. Kotler, E., et al., *A Systematic p53 Mutation Library Links Differential Functional Impact to Cancer Mutation Pattern and Evolutionary Conservation.* Molecular Cell, 2018. **71**(1): p. 178-190.e8.
103. Cicenas, J., et al., *KRAS, TP53, CDKN2A, SMAD4, BRCA1, and BRCA2 Mutations in Pancreatic Cancer.* Cancers (Basel), 2017. **9**(5).
104. Lu, L. and J. Zeng, *Evaluation of K-ras and p53 expression in pancreatic adenocarcinoma using the cancer genome atlas.* PLoS One, 2017. **12**(7): p. e0181532.
105. Suenaga, M., et al., *Pancreatic Juice Mutation Concentrations Can Help Predict the Grade of Dysplasia in Patients Undergoing Pancreatic Surveillance.* Clin Cancer Res, 2018. **24**(12): p. 2963-2974.
106. Wilentz, R.E., et al., *Immunohistochemical labeling for dpc4 mirrors genetic status in pancreatic adenocarcinomas : a new marker of DPC4 inactivation.* Am J Pathol, 2000. **156**(1): p. 37-43.
107. Xu, J.-Z., et al., *The Loss of SMAD4/DPC4 Expression Associated with a Strongly Activated Hedgehog Signaling Pathway Predicts Poor Prognosis in Resected Pancreatic Cancer.* Journal of Cancer, 2019. **10**(17): p. 4123-4131.
108. Hahn, S.A., et al., *DPC4, A Candidate Tumor Suppressor Gene at Human Chromosome 18q21.1.* Science, 1996. **271**(5247): p. 350-353.
109. Schutte, M., et al., *DPC4 Gene in Various Tumor Types.* Cancer Research, 1996. **56**(11): p. 2527-2530.
110. Ahmed, S., et al., *The TGF-β/Smad4 Signaling Pathway in Pancreatic Carcinogenesis and Its Clinical Significance.* J Clin Med, 2017. **6**(1).
111. Shi, Y. and J. Massagué, *Mechanisms of TGF-β Signaling from Cell Membrane to the Nucleus.* Cell, 2003. **113**(6): p. 685-700.
112. Zhao, M., L. Mishra, and C.X. Deng, *The role of TGF-β/SMAD4 signaling in cancer.* Int J Biol Sci, 2018. **14**(2): p. 111-123.
113. Wilentz, R.E., et al., *Loss of Expression of Dpc4 in Pancreatic Intraepithelial Neoplasia: Evidence That DPC4 Inactivation Occurs Late in Neoplastic Progression.* Cancer Research, 2000. **60**(7): p. 2002-2006.
114. Lüttges, J., et al., *Allelic loss is often the first hit in the biallelic inactivation of the p53 and DPC4 genes during pancreatic carcinogenesis.* Am J Pathol, 2001. **158**(5): p. 1677-83.
115. Drabsch, Y. and P. ten Dijke, *TGF-β signalling and its role in cancer progression and metastasis.* Cancer and Metastasis Reviews, 2012. **31**(3): p. 553-568.
116. Lamouille, S. and R. Derynck, *Cell size and invasion in TGF-beta-induced epithelial to mesenchymal transition is regulated by activation of the mTOR pathway.* J Cell Biol, 2007. **178**(3): p. 437-51.

117. Bardeesy, N., et al., *Smad4 is dispensable for normal pancreas development yet critical in progression and tumor biology of pancreas cancer.* Genes Dev, 2006. **20**(22): p. 3130-46.
118. Zhao, W., et al., *The BRCA Tumor Suppressor Network in Chromosome Damage Repair by Homologous Recombination.* Annu Rev Biochem, 2019. **88**: p. 221-245.
119. Castéra, L., et al., *Landscape of pathogenic variations in a panel of 34 genes and cancer risk estimation from 5131 HBOC families.* Genetics in Medicine, 2018. **20**(12): p. 1677-1686.
120. Consortium, T.B.C.L., *Cancer Risks in BRCA2 Mutation Carriers.* JNCI: Journal of the National Cancer Institute, 1999. **91**(15): p. 1310-1316.
121. Thompson, D., D.F. Easton, and t.B.C.L. Consortium, *Cancer Incidence in BRCA1 Mutation Carriers.* JNCI: Journal of the National Cancer Institute, 2002. **94**(18): p. 1358-1365.
122. Waddell, N., et al., *Whole genomes redefine the mutational landscape of pancreatic cancer.* Nature, 2015. **518**(7540): p. 495-501.
123. Alexandrov, L.B., et al., *Signatures of mutational processes in human cancer.* Nature, 2013. **500**(7463): p. 415-21.
124. Goggins, M., R.H. Hruban, and S.E. Kern, *BRCA2 Is Inactivated Late in the Development of Pancreatic Intraepithelial Neoplasia: Evidence and Implications.* The American Journal of Pathology, 2000. **156**(5): p. 1767-1771.
125. Chaffee, K.G., et al., *Prevalence of germ-line mutations in cancer genes among pancreatic cancer patients with a positive family history.* Genetics in Medicine, 2018. **20**(1): p. 119-127.
126. de Snoo, F.A., et al., *Increased Risk of Cancer Other Than Melanoma in CDKN2A Founder Mutation (p16-Leiden)-Positive Melanoma Families.* Clinical Cancer Research, 2008. **14**(21): p. 7151-7157.
127. McWilliams, R.R., et al., *Prevalence of CDKN2A mutations in pancreatic cancer patients: implications for genetic counseling.* Eur J Hum Genet, 2011. **19**(4): p. 472-8.
128. Storz, P., *Acinar cell plasticity and development of pancreatic ductal adenocarcinoma.* Nat Rev Gastroenterol Hepatol, 2017. **14**(5): p. 296-304.
129. Yamaguchi, J., et al., *Cells of origin of pancreatic neoplasms.* Surgery Today, 2018. **48**(1): p. 9-17.
130. Ferreira, R.M.M., et al., *Duct- and Acinar-Derived Pancreatic Ductal Adenocarcinomas Show Distinct Tumor Progression and Marker Expression.* Cell Reports, 2017. **21**(4): p. 966-978.
131. Kopp, J.L., et al., *Identification of Sox9-dependent acinar-to-ductal reprogramming as the principal mechanism for initiation of pancreatic ductal adenocarcinoma.* Cancer Cell, 2012. **22**(6): p. 737-50.
132. Wei, D., et al., *KLF4 Is Essential for Induction of Cellular Identity Change and Acinar-to-Ductal Reprogramming during Early Pancreatic Carcinogenesis.* Cancer Cell, 2016. **29**(3): p. 324-338.
133. Guerra, C., et al., *Chronic pancreatitis is essential for induction of pancreatic ductal adenocarcinoma by K-Ras oncogenes in adult mice.* Cancer Cell, 2007. **11**(3): p. 291-302.
134. Guerra, C., et al., *Pancreatitis-induced inflammation contributes to pancreatic cancer by inhibiting oncogene-induced senescence.* Cancer Cell, 2011. **19**(6): p. 728-39.
135. Murtaugh, L.C. and M.D. Keefe, *Regeneration and Repair of the Exocrine Pancreas.* Annual Review of Physiology, 2015. **77**(1): p. 229-249.
136. Padoan, A., M. Plebani, and D. Basso, *Inflammation and Pancreatic Cancer: Focus on Metabolism, Cytokines, and Immunity.* Int J Mol Sci, 2019. **20**(3).
137. Sandgren, E.P., et al., *Overexpression of TGF alpha in transgenic mice: induction of epithelial hyperplasia, pancreatic metaplasia, and carcinoma of the breast.* Cell, 1990. **61**(6): p. 1121-35.
138. Wagner, M., et al., *Malignant transformation of duct-like cells originating from acini in transforming growth factor α transgenic mice.* Gastroenterology, 1998. **115**(5): p. 1254-1262.

139. Liou, G.Y., et al., *Macrophage-secreted cytokines drive pancreatic acinar-to-ductal metaplasia through NF-κB and MMPs.* J Cell Biol, 2013. **202**(3): p. 563-77.
140. Liou, G.Y., et al., *Mutant KRas-Induced Mitochondrial Oxidative Stress in Acinar Cells Upregulates EGFR Signaling to Drive Formation of Pancreatic Precancerous Lesions.* Cell Rep, 2016. **14**(10): p. 2325-36.
141. Liu, J., et al., *TGF-β1 promotes acinar to ductal metaplasia of human pancreatic acinar cells.* Scientific Reports, 2016. **6**(1): p. 30904.
142. Means, A.L., et al., *Pancreatic epithelial plasticity mediated by acinar cell transdifferentiation and generation of nestin-positive intermediates.* Development, 2005. **132**(16): p. 3767-3776.
143. Fleming Martinez, A.K. and P. Storz, *Mimicking and Manipulating Pancreatic Acinar-to-Ductal Metaplasia in 3-dimensional Cell Culture.* J Vis Exp, 2019(144).
144. Krah, N.M., et al., *The acinar differentiation determinant PTF1A inhibits initiation of pancreatic ductal adenocarcinoma.* Elife, 2015. **4**.
145. Krah, N.M., et al., *Prevention and reversion of pancreatic tumorigenesis through a differentiation-based mechanism.* bioRxiv, 2017: p. 221986.
146. NCBI, *PTF1A pancreas associated transcription factor 1a [Sus scrofa (pig)]*.
147. NCBI, *PTF1A pancreas associated transcription factor 1a [Homo sapiens (human)]*.
148. NCBI, *Ptf1a pancreas specific transcription factor, 1a [Mus musculus (house mouse)]*.
149. NCBI, *Nucleotide and Protein BLAST*.
150. Krapp, A., et al., *The p48 DNA-binding subunit of transcription factor PTF1 is a new exocrine pancreas-specific basic helix-loop-helix protein.* Embo j, 1996. **15**(16): p. 4317-29.
151. Obata, J., et al., *p48 subunit of mouse PTF1 binds to RBP-Jκ/CBF-1, the intracellular mediator of Notch signalling, and is expressed in the neural tube of early stage embryos.* Genes to Cells, 2001. **6**(4): p. 345-360.
152. Masui, T., et al., *Transcriptional Autoregulation Controls Pancreatic Ptf1a Expression during Development and Adulthood.* Molecular and Cellular Biology, 2008. **28**(17): p. 5458-5468.
153. Beres, T.M., et al., *PTF1 is an organ-specific and Notch-independent basic helix-loop-helix complex containing the mammalian Suppressor of Hairless (RBP-J) or its paralogue, RBP-L.* Mol Cell Biol, 2006. **26**(1): p. 117-30.
154. Kawaguchi, Y., et al., *The role of the transcriptional regulator Ptf1a in converting intestinal to pancreatic progenitors.* Nat Genet, 2002. **32**(1): p. 128-34.
155. Krapp, A., et al., *The bHLH protein PTF1-p48 is essential for the formation of the exocrine and the correct spatial organization of the endocrine pancreas.* Genes Dev, 1998. **12**(23): p. 3752-63.
156. Iskusnykh, I.Y., E.Y. Steshina, and V.V. Chizhikov, *Loss of Ptf1a Leads to a Widespread Cell-Fate Misspecification in the Brainstem, Affecting the Development of Somatosensory and Viscerosensory Nuclei.* J Neurosci, 2016. **36**(9): p. 2691-710.
157. Sellick, G.S., et al., *Mutations in PTF1A cause pancreatic and cerebellar agenesis.* Nat Genet, 2004. **36**(12): p. 1301-5.
158. Masui, T., et al., *Replacement of Rbpj with Rbpjl in the PTF1 complex controls the final maturation of pancreatic acinar cells.* Gastroenterology, 2010. **139**(1): p. 270-80.
159. Hoang, C.Q., et al., *Transcriptional Maintenance of Pancreatic Acinar Identity, Differentiation, and Homeostasis by PTF1A.* Molecular and Cellular Biology, 2016. **36**(24): p. 3033-3047.
160. Sakikubo, M., et al., *Ptf1a inactivation in adult pancreatic acinar cells causes apoptosis through activation of the endoplasmic reticulum stress pathway.* Scientific Reports, 2018. **8**(1): p. 15812.
161. Jakubison, B.L., et al., *Induced PTF1a expression in pancreatic ductal adenocarcinoma cells activates acinar gene networks, reduces tumorigenic properties, and sensitizes cells to gemcitabine treatment.* Mol Oncol, 2018. **12**(7): p. 1104-1124.
162. Hingorani, S.R., et al., *Preinvasive and invasive ductal pancreatic cancer and its early detection in the mouse.* Cancer Cell, 2003. **4**(6): p. 437-50.

163. Hingorani, S.R., et al., *Trp53R172H and KrasG12D cooperate to promote chromosomal instability and widely metastatic pancreatic ductal adenocarcinoma in mice.* Cancer Cell, 2005. **7**(5): p. 469-83.
164. Aguirre, A.J., et al., *Activated Kras and Ink4a/Arf deficiency cooperate to produce metastatic pancreatic ductal adenocarcinoma.* Genes Dev, 2003. **17**(24): p. 3112-26.
165. Dolenšek, J., M.S. Rupnik, and A. Stožer, *Structural similarities and differences between the human and the mouse pancreas.* Islets, 2015. **7**(1): p. e1024405.
166. Steiniger, B.S., *Human spleen microanatomy: why mice do not suffice.* Immunology, 2015. **145**(3): p. 334-46.
167. Mestas, J. and C.C. Hughes, *Of mice and not men: differences between mouse and human immunology.* J Immunol, 2004. **172**(5): p. 2731-8.
168. Holliday, R., *Neoplastic transformation: the contrasting stability of human and mouse cells.* Cancer Surv, 1996. **28**: p. 103-15.
169. Rangarajan, A. and R.A. Weinberg, *Opinion: Comparative biology of mouse versus human cells: modelling human cancer in mice.* Nat Rev Cancer, 2003. **3**(12): p. 952-9.
170. Watson, A.L., et al., *Engineered Swine Models of Cancer.* Front Genet, 2016. **7**: p. 78.
171. Perleberg, C., A. Kind, and A. Schnieke, *Genetically engineered pigs as models for human disease.* Disease Models & Mechanisms, 2018. **11**(1).
172. Flisikowska, T., A. Kind, and A. Schnieke, *Genetically modified pigs to model human diseases.* Journal of Applied Genetics, 2014. **55**(1): p. 53-64.
173. Myers, M.J., et al., *Identification of Multiple Constitutive and Inducible Hepatic Cytochrome P450 Enzymes in Market Weight Swine.* Drug Metabolism and Disposition, 2001. **29**(6): p. 908-915.
174. Skaanild, M.T., *Porcine cytochrome P450 and metabolism.* Curr Pharm Des, 2006. **12**(11): p. 1421-7.
175. Hoffe, B. and M.R. Holahan, *The Use of Pigs as a Translational Model for Studying Neurodegenerative Diseases.* Frontiers in Physiology, 2019. **10**(838).
176. Kalla, D., A. Kind, and A. Schnieke, *Genetically Engineered Pigs to Study Cancer.* International Journal of Molecular Sciences, 2020. **21**(2): p. 488.
177. Li, S., et al., *Viable pigs with a conditionally-activated oncogenic KRAS mutation.* Transgenic Research, 2015. **24**(3): p. 509-517.
178. Leuchs, S., et al., *Inactivation and Inducible Oncogenic Mutation of p53 in Gene Targeted Pigs.* PLOS ONE, 2012. **7**(10): p. e43323.
179. Schook, L.B., et al., *A Genetic Porcine Model of Cancer.* PLOS ONE, 2015. **10**(7): p. e0128864.
180. Principe, D.R., et al., *KRAS(G12D) and TP53(R167H) Cooperate to Induce Pancreatic Ductal Adenocarcinoma in Sus scrofa Pigs.* Sci Rep, 2018. **8**(1): p. 12548.
181. Berthelsen, M.F., et al., *Pancreas specific expression of oncogenes in a porcine model.* Transgenic Res, 2017. **26**(5): p. 603-612.
182. Gordon, J.W., et al., *Genetic transformation of mouse embryos by microinjection of purified DNA.* Proc Natl Acad Sci U S A, 1980. **77**(12): p. 7380-4.
183. Hammer, R.E., et al., *Production of transgenic rabbits, sheep and pigs by microinjection.* Nature, 1985. **315**(6021): p. 680-3.
184. Tian, X., et al., *AANAT transgenic sheep generated via OPS vitrified-microinjected pronuclear embryos and reproduction efficiency of the transgenic offspring.* PeerJ, 2018. **6**: p. e5420.
185. Wilson, C., H.J. Bellen, and W.J. Gehring, *Position Effects on Eukaryotic Gene Expression.* Annual Review of Cell Biology, 1990. **6**(1): p. 679-714.
186. Kikuchi, K., et al., *Morphological features of lipid droplet transition during porcine oocyte fertilisation and early embryonic development to blastocyst in vivo and in vitro.* Zygote, 2002. **10**(4): p. 355-66.
187. Petersen, B., et al., *Efficient production of biallelic GGTA1 knockout pigs by cytoplasmic microinjection of CRISPR/Cas9 into zygotes.* Xenotransplantation, 2016. **23**(5): p. 338-46.
188. Wang, Y., et al., *Efficient generation of gene-modified pigs via injection of zygote with Cas9/sgRNA.* Scientific Reports, 2015. **5**(1): p. 8256.

189. Evans, M.J. and M.H. Kaufman, *Establishment in culture of pluripotential cells from mouse embryos.* Nature, 1981. **292**(5819): p. 154-156.
190. Thomas, K.R. and M.R. Capecchi, *Site-directed mutagenesis by gene targeting in mouse embryo-derived stem cells.* Cell, 1987. **51**(3): p. 503-512.
191. Hooper, M., et al., *HPRT-deficient (Lesch-Nyhan) mouse embryos derived from germline colonization by cultured cells.* Nature, 1987. **326**(6110): p. 292-5.
192. Blomberg, L.A. and B.P. Telugu, *Twenty years of embryonic stem cell research in farm animals.* Reprod Domest Anim, 2012. **47 Suppl 4**: p. 80-5.
193. Campbell, K.H.S., et al., *Sheep cloned by nuclear transfer from a cultured cell line.* Nature, 1996. **380**(6569): p. 64-66.
194. Wilmut, I., et al., *Viable offspring derived from fetal and adult mammalian cells.* Nature, 1997. **385**(6619): p. 810-813.
195. Schnieke, A.E., et al., *Human factor IX transgenic sheep produced by transfer of nuclei from transfected fetal fibroblasts.* Science, 1997. **278**(5346): p. 2130-3.
196. McCreath, K.J., et al., *Production of gene-targeted sheep by nuclear transfer from cultured somatic cells.* Nature, 2000. **405**(6790): p. 1066-1069.
197. Park, K.W., et al., *Production of nuclear transfer-derived swine that express the enhanced green fluorescent protein.* Anim Biotechnol, 2001. **12**(2): p. 173-81.
198. Dai, Y., et al., *Targeted disruption of the alpha1,3-galactosyltransferase gene in cloned pigs.* Nat Biotechnol, 2002. **20**(3): p. 251-5.
199. Tichy, E.D., et al., *Mouse embryonic stem cells, but not somatic cells, predominantly use homologous recombination to repair double-strand DNA breaks.* Stem Cells Dev, 2010. **19**(11): p. 1699-711.
200. Kurome, M., et al., *Factors influencing the efficiency of generating genetically engineered pigs by nuclear transfer: multi-factorial analysis of a large data set.* BMC Biotechnology, 2013. **13**(1): p. 43.
201. Solter, D., *Mammalian cloning: advances and limitations.* Nat Rev Genet, 2000. **1**(3): p. 199-207.
202. Whitworth, K.M. and R.S. Prather, *Somatic cell nuclear transfer efficiency: how can it be improved through nuclear remodeling and reprogramming?* Mol Reprod Dev, 2010. **77**(12): p. 1001-15.
203. Sternberg, N. and D. Hamilton, *Bacteriophage P1 site-specific recombination: I. Recombination between loxP sites.* Journal of Molecular Biology, 1981. **150**(4): p. 467-486.
204. Sternberg, N., et al., *Bacteriophage P1 cre gene and its regulatory region: Evidence for multiple promoters and for regulation by DNA methylation.* Journal of Molecular Biology, 1986. **187**(2): p. 197-212.
205. Austin, S., M. Ziese, and N. Sternberg, *A novel role for site-specific recombination in maintenance of bacterial replicons.* Cell, 1981. **25**(3): p. 729-36.
206. Hoess, R.H., M. Ziese, and N. Sternberg, *P1 site-specific recombination: nucleotide sequence of the recombining sites.* Proc Natl Acad Sci U S A, 1982. **79**(11): p. 3398-402.
207. Hoess, R.H. and K. Abremski, *Interaction of the bacteriophage P1 recombinase Cre with the recombining site loxP.* Proceedings of the National Academy of Sciences, 1984. **81**(4): p. 1026-1029.
208. Mack, A., et al., *Stoichiometry of the Cre recombinase bound to the lox recombining site.* Nucleic Acids Res, 1992. **20**(17): p. 4451-5.
209. Guo, F., D.N. Gopaul, and G.D. Van Duyne, *Structure of Cre recombinase complexed with DNA in a site-specific recombination synapse.* Nature, 1997. **389**(6646): p. 40-46.
210. Ghosh, K. and G.D. Van Duyne, *Cre–loxP biochemistry.* Methods, 2002. **28**(3): p. 374-383.
211. Albert, H., et al., *Site-specific integration of DNA into wild-type and mutant lox sites placed in the plant genome.* The Plant Journal, 1995. **7**(4): p. 649-659.
212. Oberdoerffer, P., et al., *Unidirectional Cre-mediated genetic inversion in mice using the mutant loxP pair lox66/lox71.* Nucleic Acids Res, 2003. **31**(22): p. e140.

213. Hoess, R.H. and K. Abremski, *Mechanism of strand cleavage and exchange in the Cre-lox site-specific recombination system.* Journal of Molecular Biology, 1985. **181**(3): p. 351-362.
214. Hoess, R.H., A. Wierzbicki, and K. Abremski, *The role of the loxP spacer region in P1 site-specific recombination.* Nucleic Acids Res, 1986. **14**(5): p. 2287-300.
215. Bouhassira, E.E., K. Westerman, and P. Leboulch, *Transcriptional Behavior of LCR Enhancer Elements Integrated at the Same Chromosomal Locus by Recombinase-Mediated Cassette Exchange.* Blood, 1997. **90**(9): p. 3332-3344.
216. Brocard, J., et al., *Spatio-temporally controlled site-specific somatic mutagenesis in the mouse.* Proceedings of the National Academy of Sciences of the United States of America, 1997. **94**(26): p. 14559-14563.
217. Metzger, D. and P. Chambon, *Site- and Time-Specific Gene Targeting in the Mouse.* Methods, 2001. **24**(1): p. 71-80.
218. Kim, H., et al., *Mouse Cre-LoxP system: general principles to determine tissue-specific roles of target genes.* Lab Anim Res, 2018. **34**(4): p. 147-159.
219. Feil, R., et al., *Regulation of Cre recombinase activity by mutated estrogen receptor ligand-binding domains.* Biochem Biophys Res Commun, 1997. **237**(3): p. 752-7.
220. Indra, A.K., et al., *Temporally-controlled site-specific mutagenesis in the basal layer of the epidermis: comparison of the recombinase activity of the tamoxifen-inducible Cre-ER(T) and Cre-ER(T2) recombinases.* Nucleic Acids Res, 1999. **27**(22): p. 4324-7.
221. Gossen, M. and H. Bujard, *Tight control of gene expression in mammalian cells by tetracycline-responsive promoters.* Proc Natl Acad Sci U S A, 1992. **89**(12): p. 5547-51.
222. Gossen, M., et al., *Transcriptional activation by tetracyclines in mammalian cells.* Science, 1995. **268**(5218): p. 1766-1769.
223. Shimshek, D.R., et al., *Codon-improved Cre recombinase (iCre) expression in the mouse.* Genesis, 2002. **32**(1): p. 19-26.
224. McClintock, B., *The origin and behavior of mutable loci in maize.* Proceedings of the National Academy of Sciences, 1950. **36**(6): p. 344-355.
225. Muñoz-López, M. and J.L. García-Pérez, *DNA transposons: nature and applications in genomics.* Curr Genomics, 2010. **11**(2): p. 115-28.
226. Lander, E.S., et al., *Initial sequencing and analysis of the human genome.* Nature, 2001. **409**(6822): p. 860-921.
227. Ivics, Z., et al., *Transposon-mediated genome manipulation in vertebrates.* Nat Methods, 2009. **6**(6): p. 415-22.
228. Finnegan, D.J., *Retrotransposons.* Current Biology, 2012. **22**(11): p. R432-R437.
229. Goodier, J.L. and H.H. Kazazian, Jr., *Retrotransposons Revisited: The Restraint and Rehabilitation of Parasites.* Cell, 2008. **135**(1): p. 23-35.
230. Cordaux, R. and M.A. Batzer, *The impact of retrotransposons on human genome evolution.* Nat Rev Genet, 2009. **10**(10): p. 691-703.
231. Han, J.S., *Non-long terminal repeat (non-LTR) retrotransposons: mechanisms, recent developments, and unanswered questions.* Mobile DNA, 2010. **1**(1): p. 15.
232. Kramerov, D.A. and N.S. Vassetzky, *Origin and evolution of SINEs in eukaryotic genomes.* Heredity, 2011. **107**(6): p. 487-495.
233. Elbarbary, R.A., B.A. Lucas, and L.E. Maquat, *Retrotransposons as regulators of gene expression.* Science, 2016. **351**(6274): p. aac7247.
234. Feschotte, C. and E.J. Pritham, *DNA transposons and the evolution of eukaryotic genomes.* Annu Rev Genet, 2007. **41**: p. 331-68.
235. Hickman, A.B. and F. Dyda, *DNA Transposition at Work.* Chem Rev, 2016. **116**(20): p. 12758-12784.
236. Wicker, T., et al., *A unified classification system for eukaryotic transposable elements.* Nature Reviews Genetics, 2007. **8**(12): p. 973-982.
237. Woodard, L.E. and M.H. Wilson, *piggyBac-ing models and new therapeutic strategies.* Trends in Biotechnology, 2015. **33**(9): p. 525-533.
238. Kim, A. and I. Pyykko, *Size matters: versatile use of PiggyBac transposons as a genetic manipulation tool.* Molecular and Cellular Biochemistry, 2011. **354**(1): p. 301-309.

239. Saha, S. and M.H. Wilson, *Transposons for Non-Viral Gene Transfer*. Gene Therapy - Tools and Potential Applications, ed. F.M. Molina. 2013: IntechOpen. 269-285.
240. Yusa, K., et al., *A hyperactive piggyBac transposase for mammalian applications.* Proc Natl Acad Sci U S A, 2011. **108**(4): p. 1531-6.
241. Mátés, L., et al., *Molecular evolution of a novel hyperactive Sleeping Beauty transposase enables robust stable gene transfer in vertebrates.* Nature Genetics, 2009. **41**(6): p. 753-761.
242. Ivics, Z., et al., *Molecular Reconstruction of Sleeping Beauty, a Tc1-like Transposon from Fish, and Its Transposition in Human Cells.* Cell, 1997. **91**(4): p. 501-510.
243. Kebriaei, P., et al., *Phase I trials using Sleeping Beauty to generate CD19-specific CAR T cells.* J Clin Invest, 2016. **126**(9): p. 3363-76.
244. Gao, B., et al., *Changes in Skeletal Muscle and Body Weight on Sleeping Beauty Transposon-Mediated Transgenic Mice Overexpressing Pig mIGF-1.* Biochemical Genetics, 2018. **56**(4): p. 341-355.
245. Geurts, A.M., et al., *Gene transfer into genomes of human cells by the sleeping beauty transposon system.* Mol Ther, 2003. **8**(1): p. 108-17.
246. Cary, L.C., et al., *Transposon mutagenesis of baculoviruses: Analysis of Trichoplusia ni transposon IFP2 insertions within the FP-locus of nuclear polyhedrosis viruses.* Virology, 1989. **172**(1): p. 156-169.
247. Fraser, M.J., et al., *Assay for Movement of Lepidopteran Transposon IFP2 in Insect Cells Using a Baculovirus Genome as a Target DNA.* Virology, 1995. **211**(2): p. 397-407.
248. Li, M.A., et al., *Mobilization of giant piggyBac transposons in the mouse genome.* Nucleic Acids Res, 2011. **39**(22): p. e148.
249. Grabundzija, I., et al., *Comparative analysis of transposable element vector systems in human cells.* Mol Ther, 2010. **18**(6): p. 1200-9.
250. Ding, S., et al., *Efficient Transposition of the piggyBac (PB) Transposon in Mammalian Cells and Mice.* Cell, 2005. **122**(3): p. 473-483.
251. Woltjen, K., et al., *piggyBac transposition reprograms fibroblasts to induced pluripotent stem cells.* Nature, 2009. **458**(7239): p. 766-70.
252. Manuri, P.V., et al., *piggyBac transposon/transposase system to generate CD19-specific T cells for the treatment of B-lineage malignancies.* Hum Gene Ther, 2010. **21**(4): p. 427-37.
253. Koga, A., et al., *Transposable element in fish.* Nature, 1996. **383**(6595): p. 30-30.
254. Kawakami, K., et al., *A Transposon-Mediated Gene Trap Approach Identifies Developmentally Regulated Genes in Zebrafish.* Developmental Cell, 2004. **7**(1): p. 133-144.
255. Chan, S., et al., *Development of enhancer-trapping and -detection vectors mediated by the Tol2 transposon in zebrafish.* PeerJ, 2019. **7**: p. e6862.
256. Urasaki, A., K. Asakawa, and K. Kawakami, *Efficient transposition of the Tol2 transposable element from a single-copy donor in zebrafish.* Proc Natl Acad Sci U S A, 2008. **105**(50): p. 19827-32.
257. Tsukahara, T., et al., *The Tol2 transposon system mediates the genetic engineering of T-cells with CD19-specific chimeric antigen receptors for B-cell malignancies.* Gene Ther, 2015. **22**(2): p. 209-15.
258. Kawakami, K. and T. Noda, *Transposition of the Tol2 element, an Ac-like element from the Japanese medaka fish Oryzias latipes, in mouse embryonic stem cells.* Genetics, 2004. **166**(2): p. 895-9.
259. Suster, M.L., K. Sumiyama, and K. Kawakami, *Transposon-mediated BAC transgenesis in zebrafish and mice.* BMC Genomics, 2009. **10**(1): p. 477.
260. Huang, X., et al., *Gene transfer efficiency and genome-wide integration profiling of Sleeping Beauty, Tol2, and piggyBac transposons in human primary T cells.* Mol Ther, 2010. **18**(10): p. 1803-13.
261. Wang, B. and J. Zhou, *Specific genetic modifications of domestic animals by gene targeting and animal cloning.* Reprod Biol Endocrinol, 2003. **1**: p. 103.

262. Denning, C., et al., *Gene targeting in primary fetal fibroblasts from sheep and pig.* Cloning Stem Cells, 2001. **3**(4): p. 221-31.
263. Sander, J.D. and J.K. Joung, *CRISPR-Cas systems for editing, regulating and targeting genomes.* Nat Biotechnol, 2014. **32**(4): p. 347-55.
264. Chiruvella, K.K., Z. Liang, and T.E. Wilson, *Repair of double-strand breaks by end joining.* Cold Spring Harb Perspect Biol, 2013. **5**(5): p. a012757.
265. Critchlow, S.E. and S.P. Jackson, *DNA end-joining: from yeast to man.* Trends Biochem Sci, 1998. **23**(10): p. 394-8.
266. Chang, H.H.Y., et al., *Non-homologous DNA end joining and alternative pathways to double-strand break repair.* Nat Rev Mol Cell Biol, 2017. **18**(8): p. 495-506.
267. Chen, C.C., et al., *Homology-Directed Repair and the Role of BRCA1, BRCA2, and Related Proteins in Genome Integrity and Cancer.* Annu Rev Cancer Biol, 2018. **2**: p. 313-336.
268. Rothkamm, K., et al., *Pathways of DNA double-strand break repair during the mammalian cell cycle.* Mol Cell Biol, 2003. **23**(16): p. 5706-15.
269. Gaj, T., C.A. Gersbach, and C.F. Barbas, 3rd, *ZFN, TALEN, and CRISPR/Cas-based methods for genome engineering.* Trends Biotechnol, 2013. **31**(7): p. 397-405.
270. Barrangou, R., et al., *CRISPR Provides Acquired Resistance Against Viruses in Prokaryotes.* Science, 2007. **315**(5819): p. 1709-1712.
271. Horvath, P. and R. Barrangou, *CRISPR/Cas, the Immune System of Bacteria and Archaea.* Science, 2010. **327**(5962): p. 167-170.
272. Deltcheva, E., et al., *CRISPR RNA maturation by trans-encoded small RNA and host factor RNase III.* Nature, 2011. **471**(7340): p. 602-7.
273. Jinek, M., et al., *A programmable dual-RNA-guided DNA endonuclease in adaptive bacterial immunity.* Science, 2012. **337**(6096): p. 816-21.
274. Gasiunas, G., et al., *Cas9-crRNA ribonucleoprotein complex mediates specific DNA cleavage for adaptive immunity in bacteria.* Proc Natl Acad Sci U S A, 2012. **109**(39): p. E2579-86.
275. Redman, M., et al., *What is CRISPR/Cas9?* Arch Dis Child Educ Pract Ed, 2016. **101**(4): p. 213-5.
276. Freund, E.C., et al., *Efficient gene knockout in primary human and murine myeloid cells by non-viral delivery of CRISPR-Cas9.* Journal of Experimental Medicine, 2020. **217**(7).
277. Park, S.H., et al., *Highly efficient editing of the β-globin gene in patient-derived hematopoietic stem and progenitor cells to treat sickle cell disease.* Nucleic Acids Res, 2019. **47**(15): p. 7955-7972.
278. Yan, S., et al., *A Huntingtin Knockin Pig Model Recapitulates Features of Selective Neurodegeneration in Huntington's Disease.* Cell, 2018. **173**(4): p. 989-1002.e13.
279. Xie, K., B. Minkenberg, and Y. Yang, *Boosting CRISPR/Cas9 multiplex editing capability with the endogenous tRNA-processing system.* Proceedings of the National Academy of Sciences, 2015. **112**(11): p. 3570-3575.
280. Ran, F.A., et al., *Double nicking by RNA-guided CRISPR Cas9 for enhanced genome editing specificity.* Cell, 2013. **154**(6): p. 1380-9.
281. Brinkman, E.K., et al., *Easy quantitative assessment of genome editing by sequence trace decomposition.* Nucleic Acids Res, 2014. **42**(22): p. e168.
282. Lubeseder-Martellato, C., *Isolation, Culture and Differentiation of Primary Acinar Epithelial Explants from Adult Murine Pancreas.* Bio-protocol, 2013. **3**(13): p. e818.
283. Ahlgren, U., J. Jonsson, and H. Edlund, *The morphogenesis of the pancreatic mesenchyme is uncoupled from that of the pancreatic epithelium in IPF1/PDX1-deficient mice.* Development, 1996. **122**(5): p. 1409-1416.
284. Ijichi, H., *Genetically-engineered mouse models for pancreatic cancer: Advances and current limitations.* World J Clin Oncol, 2011. **2**(5): p. 195-202.
285. Kalla, D., et al., *The Missing Link: Cre Pigs for Cancer Research.* Front Oncol, 2021. **11**: p. 755746.
286. Grodziecki, A., *Delivery of Cre as an integrated transgene or viral vector*, in *Chair of Livestock Biotechnology*. 2017, Technical University of Munich.

287. Kalla, D.C., *Placement of the Cre recombinase gene into porcine PTF1α and R26 loci*, in *Chair of Livestock Biotechnology*. 2018, Technical University of Munich.
288. Ramirez, C.L., et al., *Engineered zinc finger nickases induce homology-directed repair with reduced mutagenic effects.* Nucleic Acids Res, 2012. **40**(12): p. 5560-8.
289. Davis, L. and N. Maizels, *DNA Nicks Promote Efficient and Safe Targeted Gene Correction.* PLOS ONE, 2011. **6**(9): p. e23981.
290. Davis, L. and N. Maizels, *Homology-directed repair of DNA nicks via pathways distinct from canonical double-strand break repair.* Proceedings of the National Academy of Sciences, 2014. **111**(10): p. E924-E932.
291. Zhang, J.-P., et al., *Efficient precise knockin with a double cut HDR donor after CRISPR/Cas9-mediated double-stranded DNA cleavage.* Genome Biology, 2017. **18**(1): p. 35.
292. Liu, Z., et al., *Systematic comparison of 2A peptides for cloning multi-genes in a polycistronic vector.* Scientific Reports, 2017. **7**(1): p. 2193.
293. Kristianto, J., et al., *Spontaneous recombinase activity of Cre-ERT2 in vivo.* Transgenic Res, 2017. **26**(3): p. 411-417.
294. Álvarez-Aznar, A., et al., *Tamoxifen-independent recombination of reporter genes limits lineage tracing and mosaic analysis using CreERT2 lines.* Transgenic Research, 2020. **29**(1): p. 53-68.
295. Li, S., et al., *Dual Fluorescent Reporter Pig for Cre Recombination: Transgene Placement at the ROSA26 Locus.* PLOS ONE, 2014. **9**(7): p. e102455.
296. Muzumdar, M.D., et al., *A global double-fluorescent Cre reporter mouse.* Genesis, 2007. **45**(9): p. 593-605.
297. Staffers, D.A., et al., *Early-onset type-ll diabetes mellitus (MODY4) linked to IPF1.* Nature Genetics, 1997. **17**(2): p. 138-139.
298. Clocquet, A.R., et al., *Impaired insulin secretion and increased insulin sensitivity in familial maturity-onset diabetes of the young 4 (insulin promoter factor 1 gene).* Diabetes, 2000. **49**(11): p. 1856-64.
299. Ahlgren, U., et al., *beta-cell-specific inactivation of the mouse Ipf1/Pdx1 gene results in loss of the beta-cell phenotype and maturity onset diabetes.* Genes Dev, 1998. **12**(12): p. 1763-8.
300. Brissova, M., et al., *Reduction in pancreatic transcription factor PDX-1 impairs glucose-stimulated insulin secretion.* J Biol Chem, 2002. **277**(13): p. 11225-32.
301. Schulze, É., *Cre/loxP-mediated tissue specific activation of oncogene expression in pigs*, in *Chair of Livestock Biotechnology*. 2018, Technical University of Munich.
302. Matsunari, H., et al., *Transgenic pigs with pancreas-specific expression of green fluorescent protein.* J Reprod Dev, 2014. **60**(3): p. 230-7.
303. Friedrich, G. and P. Soriano, *Promoter traps in embryonic stem cells: a genetic screen to identify and mutate developmental genes in mice.* Genes Dev, 1991. **5**(9): p. 1513-23.
304. Zambrowicz, B.P., et al., *Disruption of overlapping transcripts in the ROSA beta geo 26 gene trap strain leads to widespread expression of beta-galactosidase in mouse embryos and hematopoietic cells.* Proc Natl Acad Sci U S A, 1997. **94**(8): p. 3789-94.
305. Soriano, P., *Generalized lacZ expression with the ROSA26 Cre reporter strain.* Nat Genet, 1999. **21**(1): p. 70-1.
306. Srinivas, S., et al., *Cre reporter strains produced by targeted insertion of EYFP and ECFP into the ROSA26 locus.* BMC Developmental Biology, 2001. **1**(1): p. 4.
307. Irion, S., et al., *Identification and targeting of the ROSA26 locus in human embryonic stem cells.* Nature Biotechnology, 2007. **25**(12): p. 1477-1482.
308. Kobayashi, T., et al., *Identification of rat Rosa26 locus enables generation of knock-in rat lines ubiquitously expressing tdTomato.* Stem Cells Dev, 2012. **21**(16): p. 2981-6.
309. Honig, G., et al., *Precise pattern of recombination in serotonergic and hypothalamic neurons in a Pdx1-cre transgenic mouse line.* Journal of Biomedical Science, 2010. **17**(1): p. 82.
310. Wu, K.L., et al., *Hepatocyte nuclear factor 3beta is involved in pancreatic beta-cell-specific transcription of the pdx-1 gene.* Mol Cell Biol, 1997. **17**(10): p. 6002-13.

311. Larsson, L.I., et al., *Pancreatic-duodenal homeobox 1 -role in gastric endocrine patterning.* Mech Dev, 1996. **60**(2): p. 175-84.
312. Morris, J.P., S.C. Wang, and M. Hebrok, *KRAS, Hedgehog, Wnt and the twisted developmental biology of pancreatic ductal adenocarcinoma.* Nature Reviews Cancer, 2010. **10**(10): p. 683-695.
313. Fontana, R., et al., *Dual Role of the Alternative Reading Frame ARF Protein in Cancer.* Biomolecules, 2019. **9**(3): p. 87.
314. De Waele, E., et al., *Conversion of Human Pancreatic Acinar Cells Toward a Ductal-Mesenchymal Phenotype and the Role of Transforming Growth Factor β and Activin Signaling.* Pancreas, 2014. **43**(7).
315. Akanuma, N., et al., *Paracrine Secretion of Transforming Growth Factor β by Ductal Cells Promotes Acinar-to-Ductal Metaplasia in Cultured Human Exocrine Pancreas Tissues.* Pancreas, 2017. **46**(9): p. 1202-1207.
316. McAllister, F., et al., *Oncogenic Kras activates a hematopoietic-to-epithelial IL-17 signaling axis in preinvasive pancreatic neoplasia.* Cancer Cell, 2014. **25**(5): p. 621-37.
317. Howlader, N., et al., *The Effect of Advances in Lung-Cancer Treatment on Population Mortality.* New England Journal of Medicine, 2020. **383**(7): p. 640-649.
318. Giaquinto, A.N., et al., *Breast Cancer Statistics, 2022.* CA: A Cancer Journal for Clinicians, 2022. **72**(6): p. 524-541.
319. Brown, J.J., et al., *Decreased colorectal cancer incidence and mortality in a diverse urban population with increased colonoscopy screening.* BMC Public Health, 2021. **21**(1): p. 1280.
320. Cronin, K.A., et al., *Annual report to the nation on the status of cancer, part 1: National cancer statistics.* Cancer, 2022. **128**(24): p. 4251-4284.
321. Tuveson, D.A., et al., *Endogenous oncogenic K-rasG12D stimulates proliferation and widespread neoplastic and developmental defects.* Cancer Cell, 2004. **5**(4): p. 375-387.
322. Shaw, A.T., et al., *Sprouty-2 regulates oncogenic K-ras in lung development and tumorigenesis.* Genes Dev, 2007. **21**(6): p. 694-707.
323. Fukuda, A., et al., *Reduction of Ptf1a gene dosage causes pancreatic hypoplasia and diabetes in mice.* Diabetes, 2008. **57**(9): p. 2421-31.
324. Caldecott, K.W., *Single-strand break repair and genetic disease.* Nature Reviews Genetics, 2008. **9**(8): p. 619-631.
325. Hegde, M.L., T. Izumi, and S. Mitra, *Oxidized base damage and single-strand break repair in mammalian genomes: role of disordered regions and posttranslational modifications in early enzymes.* Prog Mol Biol Transl Sci, 2012. **110**: p. 123-53.
326. Lee, G.S., et al., *RAG Proteins Shepherd Double-Strand Breaks to a Specific Pathway, Suppressing Error-Prone Repair, but RAG Nicking Initiates Homologous Recombination.* Cell, 2004. **117**(2): p. 171-184.
327. Metzger, M.J., et al., *Single-strand nicks induce homologous recombination with less toxicity than double-strand breaks using an AAV vector template.* Nucleic Acids Research, 2010. **39**(3): p. 926-935.
328. Mali, P., et al., *RNA-guided human genome engineering via Cas9.* Science, 2013. **339**(6121): p. 823-6.
329. Gonçalves, M.A., et al., *Concerted nicking of donor and chromosomal acceptor DNA promotes homology-directed gene targeting in human cells.* Nucleic Acids Res, 2012. **40**(8): p. 3443-55.
330. Lin, S., et al., *Enhanced homology-directed human genome engineering by controlled timing of CRISPR/Cas9 delivery.* Elife, 2014. **3**: p. e04766.
331. Di Stazio, M., et al., *Systematic analysis of factors that improve homologous direct repair (HDR) efficiency in CRISPR/Cas9 technique.* PLoS One, 2021. **16**(3): p. e0247603.
332. Deng, W., et al., *Use of the 2A Peptide for Generation of Multi-Transgenic Pigs through a Single Round of Nuclear Transfer.* PLOS ONE, 2011. **6**(5): p. e19986.
333. Yan, Q., et al., *Production of transgenic pigs over-expressing the antiviral gene Mx1.* Cell Regeneration, 2014. **3**(1): p. 11.

334. Doronina, V.A., et al., *Site-specific release of nascent chains from ribosomes at a sense codon.* Mol Cell Biol, 2008. **28**(13): p. 4227-39.
335. de Felipe, P., et al., *E unum pluribus: multiple proteins from a self-processing polyprotein.* Trends in Biotechnology, 2006. **24**(2): p. 68-75.
336. Hennecke, M., et al., *Composition and arrangement of genes define the strength of IRES-driven translation in bicistronic mRNAs.* Nucleic Acids Res, 2001. **29**(16): p. 3327-34.
337. Mizuguchi, H., et al., *IRES-dependent second gene expression is significantly lower than cap-dependent first gene expression in a bicistronic vector.* Mol Ther, 2000. **1**(4): p. 376-82.
338. Loonstra, A., et al., *Growth inhibition and DNA damage induced by Cre recombinase in mammalian cells.* Proceedings of the National Academy of Sciences, 2001. **98**(16): p. 9209-9214.
339. Janbandhu, V.C., D. Moik, and R. Fässler, *Cre recombinase induces DNA damage and tetraploidy in the absence of loxP sites.* Cell Cycle, 2014. **13**(3): p. 462-70.
340. Buerger, A., et al., *Dilated cardiomyopathy resulting from high-level myocardial expression of Cre-recombinase.* J Card Fail, 2006. **12**(5): p. 392-8.
341. Forni, P.E., et al., *High levels of Cre expression in neuronal progenitors cause defects in brain development leading to microencephaly and hydrocephaly.* J Neurosci, 2006. **26**(37): p. 9593-602.
342. ProteomicsDB. *Pancreas transcription factor 1 subunit alpha - Transcriptomics*. 11.05.2023; Available from: https://www.proteomicsdb.org/protein/68892/expression.
343. TheHumanProteinAtlas. *PTF1A tissue expression*. 11.05.2023; Available from: https://www.proteinatlas.org/ENSG00000168267-PTF1A/tissue.
344. Hoshino, M., et al., *Ptf1a, a bHLH Transcriptional Gene, Defines GABAergic Neuronal Fates in Cerebellum.* Neuron, 2005. **47**(2): p. 201-213.
345. Yamada, M., et al., *Specification of Spatial Identities of Cerebellar Neuron Progenitors by Ptf1a and Atoh1 for Proper Production of GABAergic and Glutamatergic Neurons.* The Journal of Neuroscience, 2014. **34**(14): p. 4786-4800.
346. Busslinger, G.A., et al., *Human gastrointestinal epithelia of the esophagus, stomach, and duodenum resolved at single-cell resolution.* Cell Rep, 2021. **34**(10): p. 108819.
347. Li, F.P., J.F. Fraumeni, Jr., and F.A.C.P. M.D., *Soft-Tissue Sarcomas, Breast Cancer, and Other Neoplasms.* Annals of Internal Medicine, 1969. **71**(4): p. 747-752.
348. Li, F.P., et al., *A cancer family syndrome in twenty-four kindreds.* Cancer Res, 1988. **48**(18): p. 5358-62.
349. Kratz, C.P., et al., *Analysis of the Li-Fraumeni Spectrum Based on an International Germline TP53 Variant Data Set: An International Agency for Research on Cancer TP53 Database Analysis.* JAMA Oncology, 2021. **7**(12): p. 1800-1805.
350. Olive, K.P., et al., *Mutant p53 Gain of Function in Two Mouse Models of Li-Fraumeni Syndrome.* Cell, 2004. **119**(6): p. 847-860.
351. Saalfrank, A., et al., *A porcine model of osteosarcoma.* Oncogenesis, 2016. **5**(3): p. e210-e210.
352. Kanda, M., et al., *Presence of somatic mutations in most early-stage pancreatic intraepithelial neoplasia.* Gastroenterology, 2012. **142**(4): p. 730-733.e9.
353. Ene-Obong, A., et al., *Activated pancreatic stellate cells sequester CD8+ T cells to reduce their infiltration of the juxtatumoral compartment of pancreatic ductal adenocarcinoma.* Gastroenterology, 2013. **145**(5): p. 1121-32.
354. Feig, C., et al., *Targeting CXCL12 from FAP-expressing carcinoma-associated fibroblasts synergizes with anti-PD-L1 immunotherapy in pancreatic cancer.* Proc Natl Acad Sci U S A, 2013. **110**(50): p. 20212-7.
355. Maddalena, M., et al., *TP53 missense mutations in PDAC are associated with enhanced fibrosis and an immunosuppressive microenvironment.* Proceedings of the National Academy of Sciences, 2021. **118**(23): p. e2025631118.
356. Fischer, K., et al., *Efficient production of multi-modified pigs for xenotransplantation by 'combineering', gene stacking and gene editing.* Scientific Reports, 2016. **6**(1): p. 29081.

357. Kong, Q., et al., *Rosa26 locus supports tissue-specific promoter driving transgene expression specifically in pig.* PLoS One, 2014. **9**(9): p. e107945.
358. Choi, E.-H., et al., *The Homologous Recombination Machinery Orchestrates Post-replication DNA Repair During Self-renewal of Mouse Embryonic Stem Cells.* Scientific Reports, 2017. **7**(1): p. 11610.
359. Choi, E.-H., et al., *Maintenance of genome integrity and active homologous recombination in embryonic stem cells.* Experimental & Molecular Medicine, 2020. **52**(8): p. 1220-1229.
360. Guz, Y., et al., *Expression of murine STF-1, a putative insulin gene transcription factor, in β cells of pancreas, duodenal epithelium and pancreatic exocrine and endocrine progenitors during ontogeny.* Development, 1995. **121**(1): p. 11-18.
361. Stoffers, D.A., et al., *Developmental expression of the homeodomain protein IDX-1 in mice transgenic for an IDX-1 promoter/lacZ transcriptional reporter.* Endocrinology, 1999. **140**(11): p. 5374-81.
362. Fráguas-Eggenschwiler, M., et al., *Direct conversion of porcine primary fibroblasts into hepatocyte-like cells.* Scientific Reports, 2021. **11**(1): p. 9334.
363. Clark, A.J., et al., *Chromosomal position effects and the modulation of transgene expression.* Reprod Fertil Dev, 1994. **6**(5): p. 589-98.
364. Ohlsson, H., K. Karlsson, and T. Edlund, *IPF1, a homeodomain-containing transactivator of the insulin gene.* The EMBO Journal, 1993. **12**(11): p. 4251-4259.
365. Serup, P., et al., *The homeodomain protein IPF-1/STF-1 is expressed in a subset of islet cells and promotes rat insulin 1 gene expression dependent on an intact E1 helix-loop-helix factor binding site.* Biochem J, 1995. **310 (Pt 3)**(Pt 3): p. 997-1003.
366. Pictet, R.L., et al., *An ultrastructural analysis of the developing embryonic pancreas.* Dev Biol, 1972. **29**(4): p. 436-67.
367. Anderson, S.J., et al., *Immunohistochemical Characterization of Insulin, Glucagon, PDX1, SOX17 and NGN3 Expression in Human Fetal Pancreatic Development.* Journal of Stem Cell Research & Therapy, 2013. **3**: p. 1-10.
368. Korbutt, G.S., et al., *Large scale isolation, growth, and function of porcine neonatal islet cells.* J Clin Invest, 1996. **97**(9): p. 2119-29.
369. Nagaya, M., et al., *Distributions of endocrine cell clusters during porcine pancreatic development.* PLOS ONE, 2019. **14**(5): p. e0216254.
370. Marshak, S., et al., *Functional conservation of regulatory elements in the pdx-1 gene: PDX-1 and hepatocyte nuclear factor 3beta transcription factors mediate beta-cell-specific expression.* Mol Cell Biol, 2000. **20**(20): p. 7583-90.
371. Gerrish, K., J.C. Van Velkinburgh, and R. Stein, *Conserved transcriptional regulatory domains of the pdx-1 gene.* Mol Endocrinol, 2004. **18**(3): p. 533-48.
372. Lu, B., et al., *Generation of rat mutants using a coat color-tagged Sleeping Beauty transposon system.* Mamm Genome, 2007. **18**(5): p. 338-46.
373. Liang, Q., et al., *Chromosomal mobilization and reintegration of Sleeping Beauty and PiggyBac transposons.* Genesis, 2009. **47**(6): p. 404-8.
374. Luo, G., et al., *Chromosomal transposition of a Tc1/mariner-like element in mouse embryonic stem cells.* Proc Natl Acad Sci U S A, 1998. **95**(18): p. 10769-73.
375. Izsvák, Z., et al., *Healing the Wounds Inflicted by Sleeping Beauty Transposition by Double-Strand Break Repair in Mammalian Somatic Cells.* Molecular Cell, 2004. **13**(2): p. 279-290.
376. Wilson, M.H., C.J. Coates, and A.L. George, Jr., *PiggyBac transposon-mediated gene transfer in human cells.* Mol Ther, 2007. **15**(1): p. 139-45.
377. Wu, S.C.-Y., et al., *piggyBac is a flexible and highly active transposon as compared to Sleeping Beauty, Tol2, and Mos1 in mammalian cells.* Proceedings of the National Academy of Sciences, 2006. **103**(41): p. 15008-15013.
378. Yum, S.-Y., et al., *Efficient generation of transgenic cattle using the DNA transposon and their analysis by next-generation sequencing.* Scientific Reports, 2016. **6**(1): p. 27185.
379. Wu, Z., et al., *Pig transgenesis by piggyBac transposition in combination with somatic cell nuclear transfer.* Transgenic Res, 2013. **22**(6): p. 1107-18.

380. Li, Z., et al., *Generation of transgenic pigs by cytoplasmic injection of piggyBac transposase-based pmGENIE-3 plasmids.* Biol Reprod, 2014. **90**(5): p. 93.
381. Bire, S., et al., *Optimization of the piggyBac transposon using mRNA and insulators: toward a more reliable gene delivery system.* PLoS One, 2013. **8**(12): p. e82559.
382. Sandoval-Villegas, N., et al., *Contemporary Transposon Tools: A Review and Guide through Mechanisms and Applications of Sleeping Beauty, piggyBac and Tol2 for Genome Engineering.* Int J Mol Sci, 2021. **22**(10).
383. Palmiter, R.D., et al., *Transmission distortion and mosaicism in an unusual transgenic mouse pedigree.* Cell, 1984. **36**(4): p. 869-877.
384. Chan, A.W.S., et al., *Timing of DNA integration, transgenic mosaicism, and pronuclear microinjection.* Molecular Reproduction and Development, 1999. **52**(4): p. 406-413.
385. Krimpenfort, P., et al., *Generation of transgenic dairy cattle using 'in vitro' embryo production.* Biotechnology (N Y), 1991. **9**(9): p. 844-7.
386. Burdon, T.G. and R.J. Wall, *Fate of microinjected genes in preimplantation mouse embryos.* Molecular Reproduction and Development, 1992. **33**(4): p. 436-442.
387. Cousens, C., et al., *Use of PCR-based methods for selection of integrated transgenes in preimplantation embryos.* Mol Reprod Dev, 1994. **39**(4): p. 384-91.
388. Wall, R.J. and G.E. Seidel, Jr., *Transgenic farm animals - A critical analysis.* Theriogenology, 1992. **38**(2): p. 337-57.
389. Wall, R.J., *A new lease on life for transgenic livestock.* Nature Biotechnology, 1997. **15**(5): p. 416-417.
390. Roy, N., et al., *PDX1 dynamically regulates pancreatic ductal adenocarcinoma initiation and maintenance.* Genes Dev, 2016. **30**(24): p. 2669-2683.
391. Park, J.Y., et al., *Pdx1 expression in pancreatic precursor lesions and neoplasms.* Appl Immunohistochem Mol Morphol, 2011. **19**(5): p. 444-9.
392. Dong, F., et al., *Polycistronic tRNA and CRISPR guide-RNA enables highly efficient multiplexed genome engineering in human cells.* Biochem Biophys Res Commun, 2017. **482**(4): p. 889-895.
393. Xu, C.L., et al., *Viral Delivery Systems for CRISPR.* Viruses, 2019. **11**(1).
394. Feng, W. and M. Jasin, *BRCA2 suppresses replication stress-induced mitotic and G1 abnormalities through homologous recombination.* Nat Commun, 2017. **8**(1): p. 525.
395. Yang, X., et al., *The tumor suppressor SMAD4/DPC4 is essential for epiblast proliferation and mesoderm induction in mice.* Proceedings of the National Academy of Sciences, 1998. **95**(7): p. 3667-3672.
396. Ludwig, T., et al., *Targeted mutations of breast cancer susceptibility gene homologs in mice: lethal phenotypes of Brca1, Brca2, Brca1/Brca2, Brca1/p53, and Brca2/p53 nullizygous embryos.* Genes Dev, 1997. **11**(10): p. 1226-41.
397. Donehower, L.A., et al., *Mice deficient for p53 are developmentally normal but susceptible to spontaneous tumours.* Nature, 1992. **356**(6366): p. 215-221.
398. Jacks, T., et al., *Tumor spectrum analysis in p53-mutant mice.* Curr Biol, 1994. **4**(1): p. 1-7.
399. Serrano, M., et al., *Role of the INK4a Locus in Tumor Suppression and Cell Mortality.* Cell, 1996. **85**(1): p. 27-37.
400. Behr, M., et al., *In vivo delivery of CRISPR-Cas9 therapeutics: Progress and challenges.* Acta Pharmaceutica Sinica B, 2021. **11**(8): p. 2150-2171.
401. Mangeot, P.E., et al., *Genome editing in primary cells and in vivo using viral-derived Nanoblades loaded with Cas9-sgRNA ribonucleoproteins.* Nature Communications, 2019. **10**(1): p. 45.
402. Hendricks-Wenger, A., et al., *Employing Novel Porcine Models of Subcutaneous Pancreatic Cancer to Evaluate Oncological Therapies.* Methods Mol Biol, 2022. **2394**: p. 883-895.
403. Schachtschneider, K.M., et al., *A validated, transitional and translational porcine model of hepatocellular carcinoma.* Oncotarget, 2017. **8**(38): p. 63620-63634.
404. Gaba, R.C., et al., *Development and comprehensive characterization of porcine hepatocellular carcinoma for translational liver cancer investigation.* Oncotarget, 2020. **11**(28): p. 2686-2701.

405. Mueller, S., et al., *Evolutionary routes and KRAS dosage define pancreatic cancer phenotypes.* Nature, 2018. **554**(7690): p. 62-68.
406. Eckrich, J., et al., *Monitoring of tumor growth and vascularization with repetitive ultrasonography in the chicken chorioallantoic-membrane-assay.* Sci Rep, 2020. **10**(1): p. 18585.
407. Marga Janse, E. and S.H.M. Jeurissen, *Ontogeny and Function of Two Non-Lymphoid Cell Populations in the Chicken Embryo.* Immunobiology, 1991. **182**(5): p. 472-481.
408. Zhao, T., et al., *Humanized Mice Reveal Differential Immunogenicity of Cells Derived from Autologous Induced Pluripotent Stem Cells.* Cell Stem Cell, 2015. **17**(3): p. 353-359.
409. Deuse, T., et al., *De novo mutations in mitochondrial DNA of iPSCs produce immunogenic neoepitopes in mice and humans.* Nature Biotechnology, 2019. **37**(10): p. 1137-1144.
410. Deuse, T., et al., *Hypoimmunogenic derivatives of induced pluripotent stem cells evade immune rejection in fully immunocompetent allogeneic recipients.* Nat Biotechnol, 2019. **37**(3): p. 252-258.
411. Jensen, J.N., et al., *Recapitulation of elements of embryonic development in adult mouse pancreatic regeneration.* Gastroenterology, 2005. **128**(3): p. 728-41.
412. Desai, B.M., et al., *Preexisting pancreatic acinar cells contribute to acinar cell, but not islet beta cell, regeneration.* J Clin Invest, 2007. **117**(4): p. 971-7.
413. Morris, J.P.t., et al., *Beta-catenin blocks Kras-dependent reprogramming of acini into pancreatic cancer precursor lesions in mice.* J Clin Invest, 2010. **120**(2): p. 508-20.
414. Collins, M.A., et al., *MAPK signaling is required for dedifferentiation of acinar cells and development of pancreatic intraepithelial neoplasia in mice.* Gastroenterology, 2014. **146**(3): p. 822-834.e7.
415. Houbracken, I., et al., *Lineage Tracing Evidence for Transdifferentiation of Acinar to Duct Cells and Plasticity of Human Pancreas.* Gastroenterology, 2011. **141**(2): p. 731-741.e4.
416. Baldan, J., et al., *Adult human pancreatic acinar cells dedifferentiate into an embryonic progenitor-like state in 3D suspension culture.* Scientific Reports, 2019. **9**(1): p. 4040.
417. Yamada, K.M. and E. Cukierman, *Modeling Tissue Morphogenesis and Cancer in 3D.* Cell, 2007. **130**(4): p. 601-610.
418. Jensen, C. and Y. Teng, *Is It Time to Start Transitioning From 2D to 3D Cell Culture?* Front Mol Biosci, 2020. **7**: p. 33.
419. Ding, L., et al., *Glycogen synthase kinase-3β ablation limits pancreatitis-induced acinar-to-ductal metaplasia.* The Journal of Pathology, 2017. **243**(1): p. 65-77.
420. Wang, L., D. Xie, and D. Wei, *Pancreatic Acinar-to-Ductal Metaplasia and Pancreatic Cancer*, in *Pancreatic Cancer: Methods and Protocols*, G.H. Su, Editor. 2019, Springer New York: New York, NY. p. 299-308.
421. Qian, W., et al., *Resveratrol slows the tumourigenesis of pancreatic cancer by inhibiting NFκB activation.* Biomedicine & Pharmacotherapy, 2020. **127**: p. 110116.
422. Williams, J.A., *Isolation of rodent pancreatic acinar cells and acini by collagenase digestion*. 2010, Pancreapedia: Exocrine Pancreas Knowledge Base.
423. Navina, S., et al., *Lipotoxicity causes multisystem organ failure and exacerbates acute pancreatitis in obesity.* Sci Transl Med, 2011. **3**(107): p. 107ra110.
424. Gout, J., et al., *Isolation and culture of mouse primary pancreatic acinar cells.* J Vis Exp, 2013(78).
425. Bockman, D.E., et al., *Origin of tubular complexes developing during induction of pancreatic adenocarcinoma by 7,12-dimethylbenz(a)anthracene.* Am J Pathol, 1978. **90**(3): p. 645-58.
426. Bockman, D.E., W.R. Boydston, and M.C. Anderson, *Origin of tubular complexes in human chronic pancreatitis.* Am J Surg, 1982. **144**(2): p. 243-9.
427. Willemer, S. and G. Adler, *Histochemical and ultrastructural characteristics of tubular complexes in human acute pancreatitis.* Dig Dis Sci, 1989. **34**(1): p. 46-55.

428. Perusina Lanfranca, M., et al., *Interleukin 22 Signaling Regulates Acinar Cell Plasticity to Promote Pancreatic Tumor Development in Mice.* Gastroenterology, 2020. **158**(5): p. 1417-1432.e11.
429. Al Moustafa, A.E., A. Achkhar, and A. Yasmeen, *EGF-receptor signaling and epithelial-mesenchymal transition in human carcinomas.* Front Biosci (Schol Ed), 2012. **4**(2): p. 671-84.
430. Korc, M., et al., *Overexpression of the epidermal growth factor receptor in human pancreatic cancer is associated with concomitant increases in the levels of epidermal growth factor and transforming growth factor alpha.* The Journal of Clinical Investigation, 1992. **90**(4): p. 1352-1360.
431. Korc, M., et al., *Chronic pancreatitis is associated with increased concentrations of epidermal growth factor receptor, transforming growth factor alpha, and phospholipase C gamma.* Gut, 1994. **35**(10): p. 1468-1473.
432. Buscemi, L., et al., *The Single-Molecule Mechanics of the Latent TGF-β1 Complex.* Current Biology, 2011. **21**(24): p. 2046-2054.
433. Batlle, E. and J. Massagué, *Transforming Growth Factor-β Signaling in Immunity and Cancer.* Immunity, 2019. **50**(4): p. 924-940.
434. Ikushima, H. and K. Miyazono, *TGFβ signalling: a complex web in cancer progression.* Nature Reviews Cancer, 2010. **10**(6): p. 415-424.
435. di Mola, F.F., et al., *Connective tissue growth factor is a regulator for fibrosis in human chronic pancreatitis.* Ann Surg, 1999. **230**(1): p. 63-71.
436. Van Laethem, J.L., et al., *Transforming growth factor beta promotes development of fibrosis after repeated courses of acute pancreatitis in mice.* Gastroenterology, 1996. **110**(2): p. 576-82.
437. Menke, A., et al., *Extracellular matrix is reduced by inhibition of transforming growth factor beta1 in pancreatitis in the rat.* Gastroenterology, 1997. **113**(1): p. 295-303.
438. Apte, M.V., et al., *Pancreatic stellate cells are activated by proinflammatory cytokines: implications for pancreatic fibrogenesis.* Gut, 1999. **44**(4): p. 534-41.
439. Harrington, L.E., et al., *Interleukin 17–producing CD4+ effector T cells develop via a lineage distinct from the T helper type 1 and 2 lineages.* Nature Immunology, 2005. **6**(11): p. 1123-1132.
440. Gu, C., L. Wu, and X. Li, *IL-17 family: cytokines, receptors and signaling.* Cytokine, 2013. **64**(2): p. 477-85.
441. Kang, Z., et al., *Astrocyte-restricted ablation of interleukin-17-induced Act1-mediated signaling ameliorates autoimmune encephalomyelitis.* Immunity, 2010. **32**(3): p. 414-25.
442. Komiyama, Y., et al., *IL-17 plays an important role in the development of experimental autoimmune encephalomyelitis.* J Immunol, 2006. **177**(1): p. 566-73.
443. Vlachos, S., et al., *Serum profiles of M30, M65 and interleukin-17 compared with C-reactive protein in patients with mild and severe acute pancreatitis.* Journal of hepato-biliary-pancreatic sciences, 2014. **21**(12): p. 911-918.
444. Li, G., et al., *Role of Interleukin-17 in Acute Pancreatitis.* Front Immunol, 2021. **12**: p. 674803.
445. Tan, J.H., et al., *EMC6 regulates acinar apoptosis via APAF1 in acute and chronic pancreatitis.* Cell Death Dis, 2020. **11**(11): p. 966.
446. Kubisch, C.H. and C.D. Logsdon, *Endoplasmic reticulum stress and the pancreatic acinar cell.* Expert Review of Gastroenterology & Hepatology, 2008. **2**(2): p. 249-260.
447. Naldini, L., et al., *In Vivo Gene Delivery and Stable Transduction of Nondividing Cells by a Lentiviral Vector.* Science, 1996. **272**(5259): p. 263-267.
448. Kumar, M., et al., *Systematic determination of the packaging limit of lentiviral vectors.* Hum Gene Ther, 2001. **12**(15): p. 1893-905.
449. Shaw, A. and K. Cornetta, *Design and Potential of Non-Integrating Lentiviral Vectors.* Biomedicines, 2014. **2**(1): p. 14-35.
450. Grgacic, E.V. and D.A. Anderson, *Virus-like particles: passport to immune recognition.* Methods, 2006. **40**(1): p. 60-5.

451. Kaczmarczyk, S.J., et al., *Protein delivery using engineered virus-like particles.* Proc Natl Acad Sci U S A, 2011. **108**(41): p. 16998-7003.
452. Zhou, Q., et al., *In vivo reprogramming of adult pancreatic exocrine cells to beta-cells.* Nature, 2008. **455**(7213): p. 627-32.
453. Wang, A.Y., et al., *Comparison of adenoviral and adeno-associated viral vectors for pancreatic gene delivery in vivo.* Hum Gene Ther, 2004. **15**(4): p. 405-13.
454. Houbracken, I., et al., *Gene delivery to pancreatic exocrine cells in vivo and in vitro.* BMC Biotechnology, 2012. **12**(1): p. 74.
455. Banskota, S., et al., *Engineered virus-like particles for efficient in vivo delivery of therapeutic proteins.* Cell, 2022. **185**(2): p. 250-265.e16.
456. Tornesello, A.L., et al., *Virus-like Particles as Preventive and Therapeutic Cancer Vaccines.* Vaccines (Basel), 2022. **10**(2).
457. Ma, Y., et al., *Loss of Heterozygosity for Kras(G12D) Promotes Malignant Phenotype of Pancreatic Ductal Adenocarcinoma by Activating HIF-2α-c-Myc-Regulated Glutamine Metabolism.* Int J Mol Sci, 2022. **23**(12).
458. Loncle, C., et al., *IL17 Functions through the Novel REG3β-JAK2-STAT3 Inflammatory Pathway to Promote the Transition from Chronic Pancreatitis to Pancreatic Cancer.* Cancer Res, 2015. **75**(22): p. 4852-62.
459. Xiao, X., et al., *PNA lectin for purifying mouse acinar cells from the inflamed pancreas.* Sci Rep, 2016. **6**: p. 21127.
460. Shi, G., et al., *Maintenance of acinar cell organization is critical to preventing Kras-induced acinar-ductal metaplasia.* Oncogene, 2013. **32**(15): p. 1950-8.
461. Corcoran, R.B., et al., *STAT3 plays a critical role in KRAS-induced pancreatic tumorigenesis.* Cancer Res, 2011. **71**(14): p. 5020-9.

11 Supplementary

11.1 Plasmid maps

11.1.1 Cloning vectors

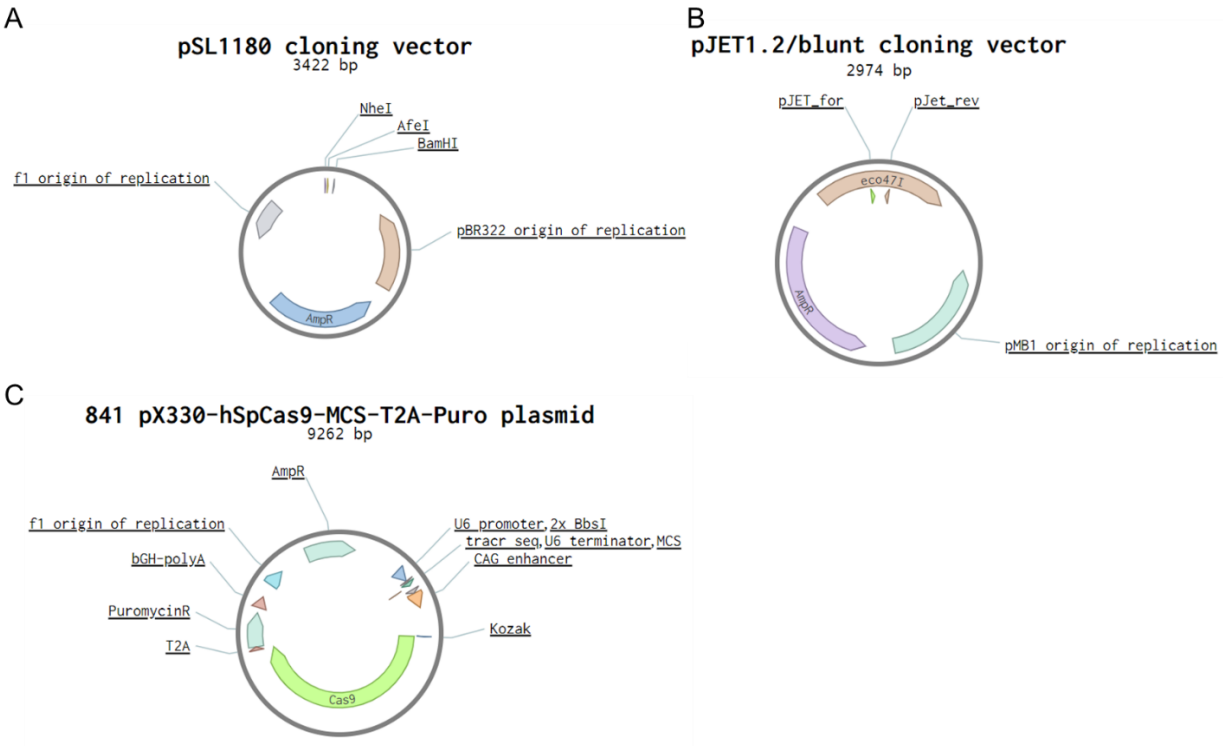

Supplementary figure 1. Utilised cloning vectors. (A) PSL1180 cloning vector for *PTF1A* targeting vector generation. (B) PJet1.2/blunt cloning vector for subcloning. (C) 841 pX330-hSpCas9-MCS-T2A-Puro plasmid for gene editing. The plasmid maps were generated using the Benchling biotechnology software.

11.1.2 Vectors for *PTF1A* 5'end targeting

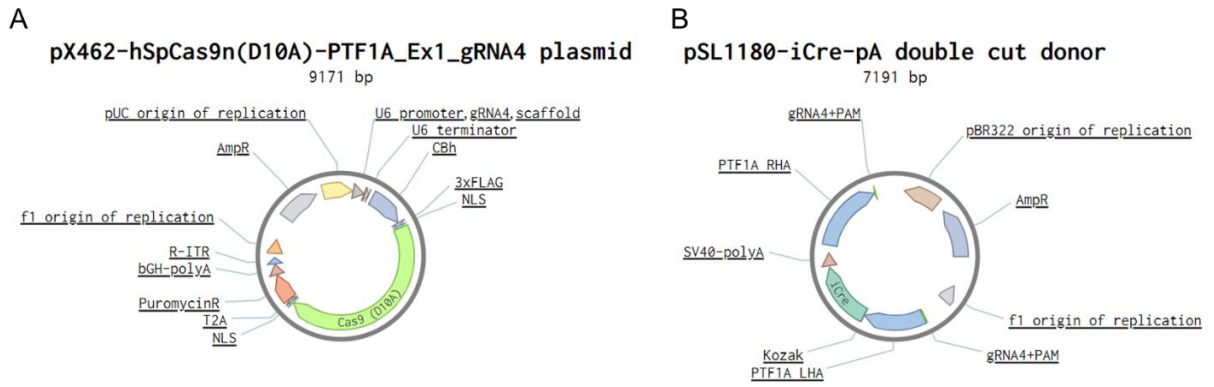

Supplementary figure 2. Plasmids used for *PTF1A* 5'end targeting. (A) PX462-Cas9n vector for targeting *PTF1A* exon 1.(B) Double cut donor for integration of iCre via HDR. The plasmid maps were generated using the Benchling biotechnology software.

11.1.3 Vectors for *PTF1A* 3'end targeting

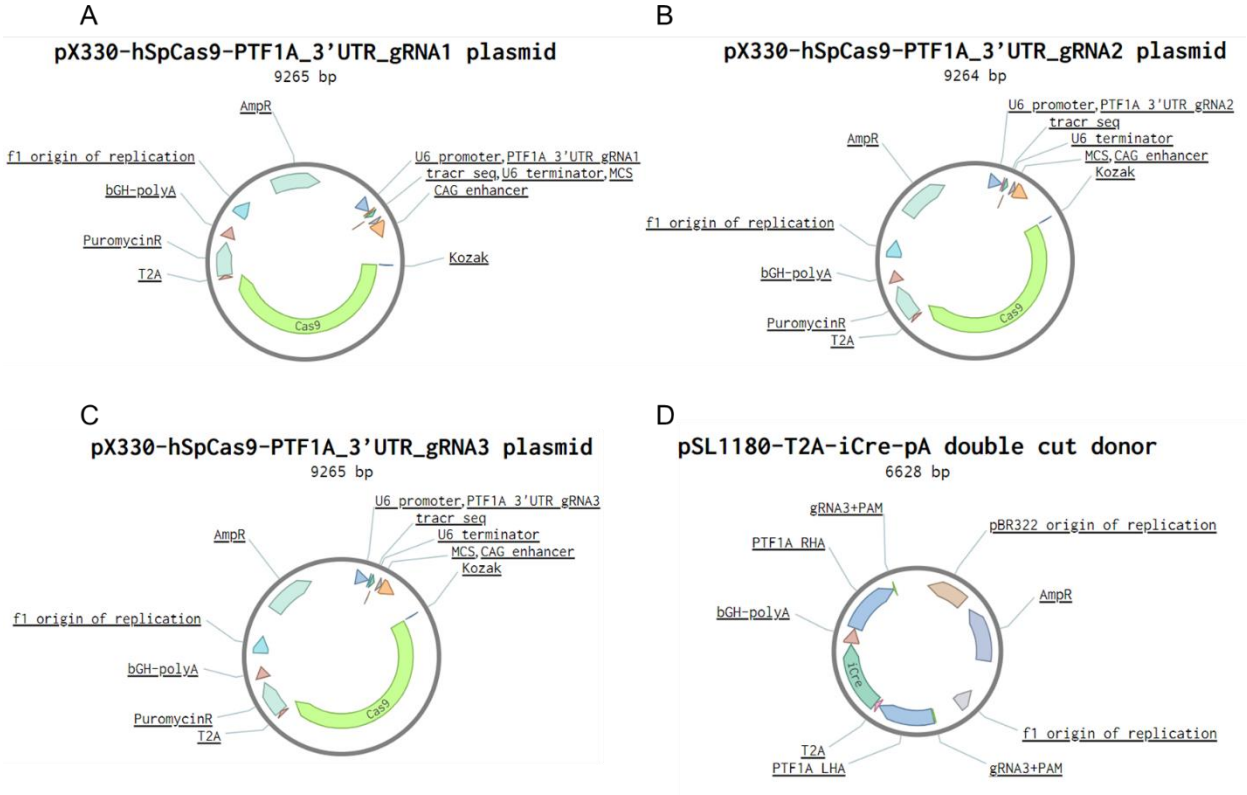

Supplementary figure 3. Plasmids used for PTF1A 3'end targeting. (A-C) pX330-Cas9 plasmids for testing editing efficiencies of *PTF1A* gRNAs 1, 2 or 3. (C+D) pX330-Cas9-gRNA3 vector and double cut donor for integration of T2A-iCre into the 3'UTR of *PTF1A*. The plasmid maps were generated using the Benchling biotechnology software.

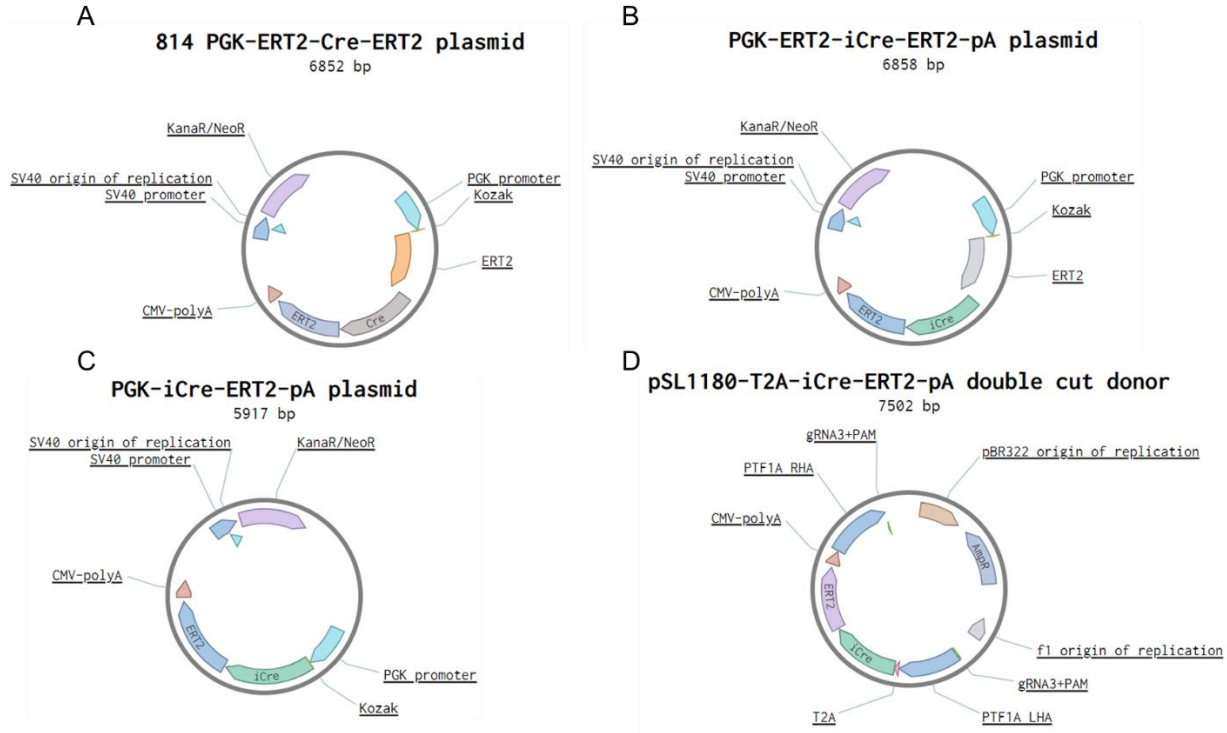

Supplementary figure 4. Plasmids used for inducible Cre driver line generation. (A) Vector used for the generation of plasmids for validating the inducibility of iCre-ER^{T2} and ER^{T2}-iCre-ER^{T2} systems in porcine cells. (B) Plasmid for testing the 4-OHT induction efficiency of ER^{T2}-iCre-ER^{T2} in porcine cells. (C) Plasmid for testing the 4-OHT induction efficiency of the iCre-ER^{T2} system in porcine cells. (D) Double cut donor for the generation of a 4-OHT inducible Cre driver pig line. The plasmid maps were generated using the Benchling biotechnology software.

11.1.4 Vectors for *ROSA26* targeting and random integration of *mPdx1-iCre*

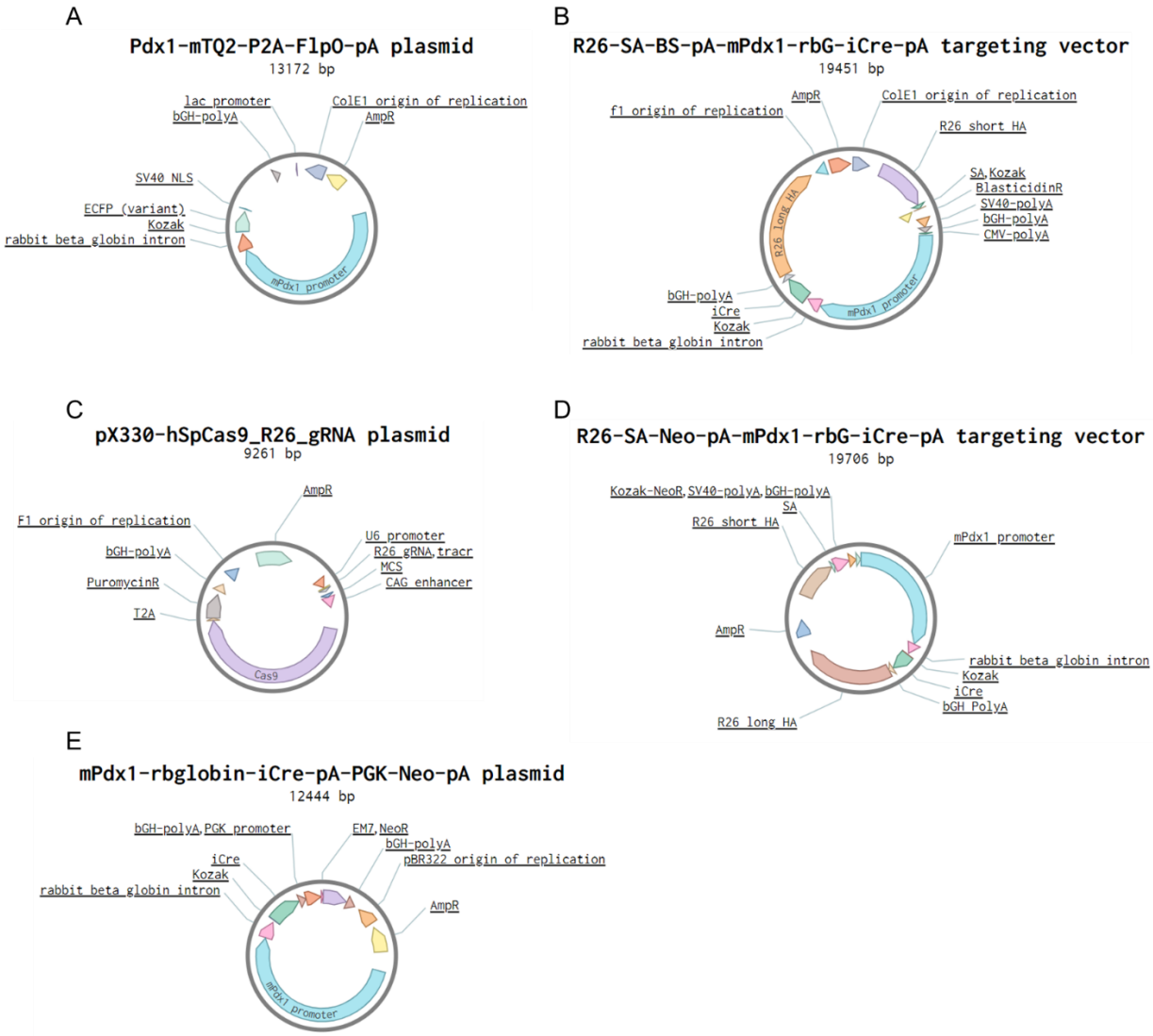

Supplementary figure 5. Plasmids for ROSA26 targeting and random integration. (A) Plasmid used for cloning of the *mPdx1* promoter and rabbit β-globin sequence. (B+D) Targeting vectors for *ROSA26* targeting. (C) PX330-Cas9 vector for CRISPR/Cas9-mediated integration of *mPdx1-iCre* into porcine *ROSA26*. (E) Plasmid for random integration of *mPdx1-iCre* into the porcine genome. The plasmid maps were generated using the Benchling biotechnology software.

11.1.5 Vectors for transposon-mediated integration of *mPdx1-iCre*

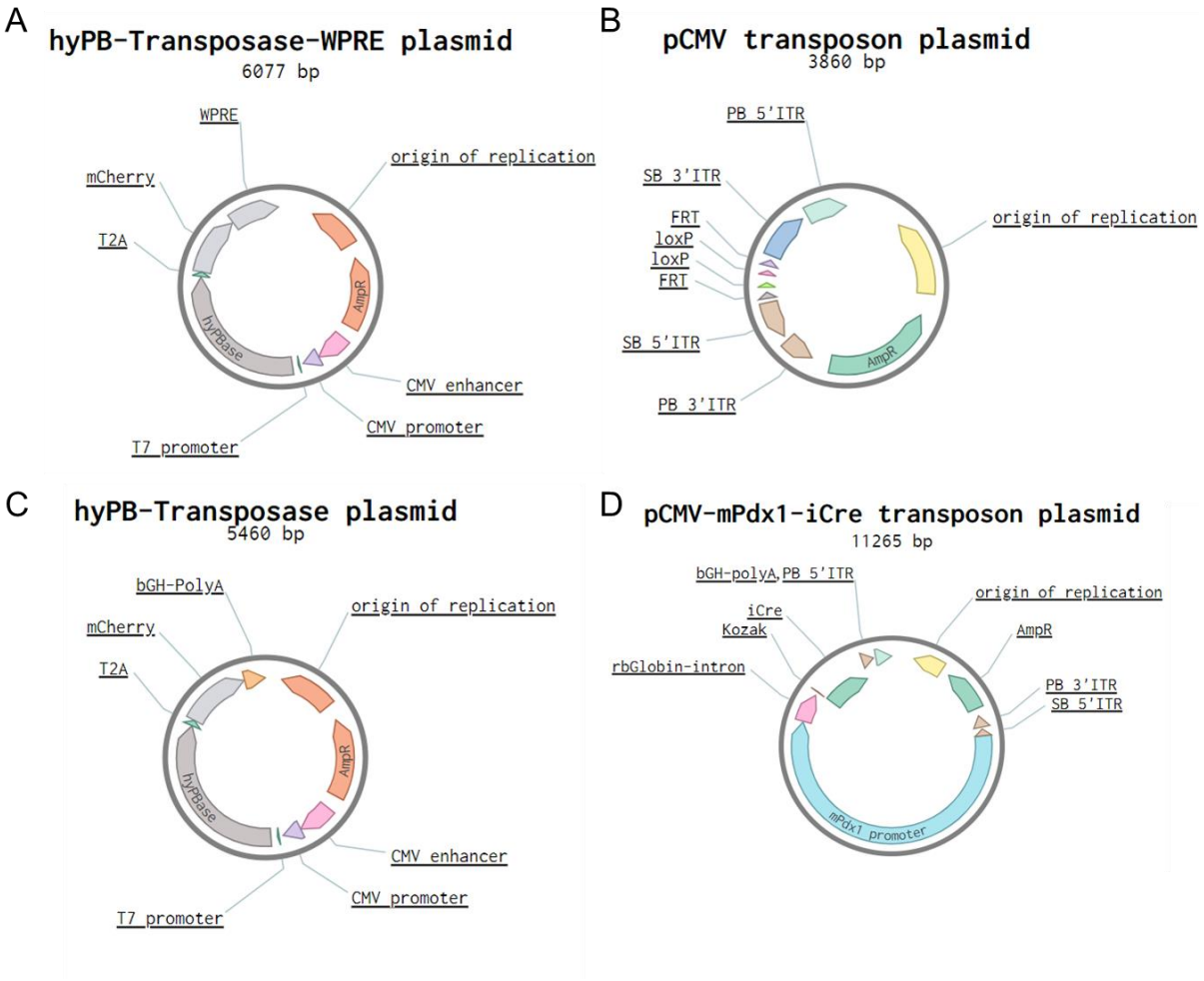

Supplementary figure 6. Plasmids for transposon-mediated integration of *mPdx1-iCre*. (A+B) Hyperactive PB transposase and transposon plasmids kindly provided by Prof. Dr. Roland Rad. (C+D) Hyperactive PB transposase plasmid and *mPdx1-iCre* transposon for PB-mediated integration of the *mPdx1-iCre* sequence into the porcine genome. The plasmid maps were generated using the Benchling biotechnology software.

11.2 Vectors for multiplexed gene editing for mutational activation

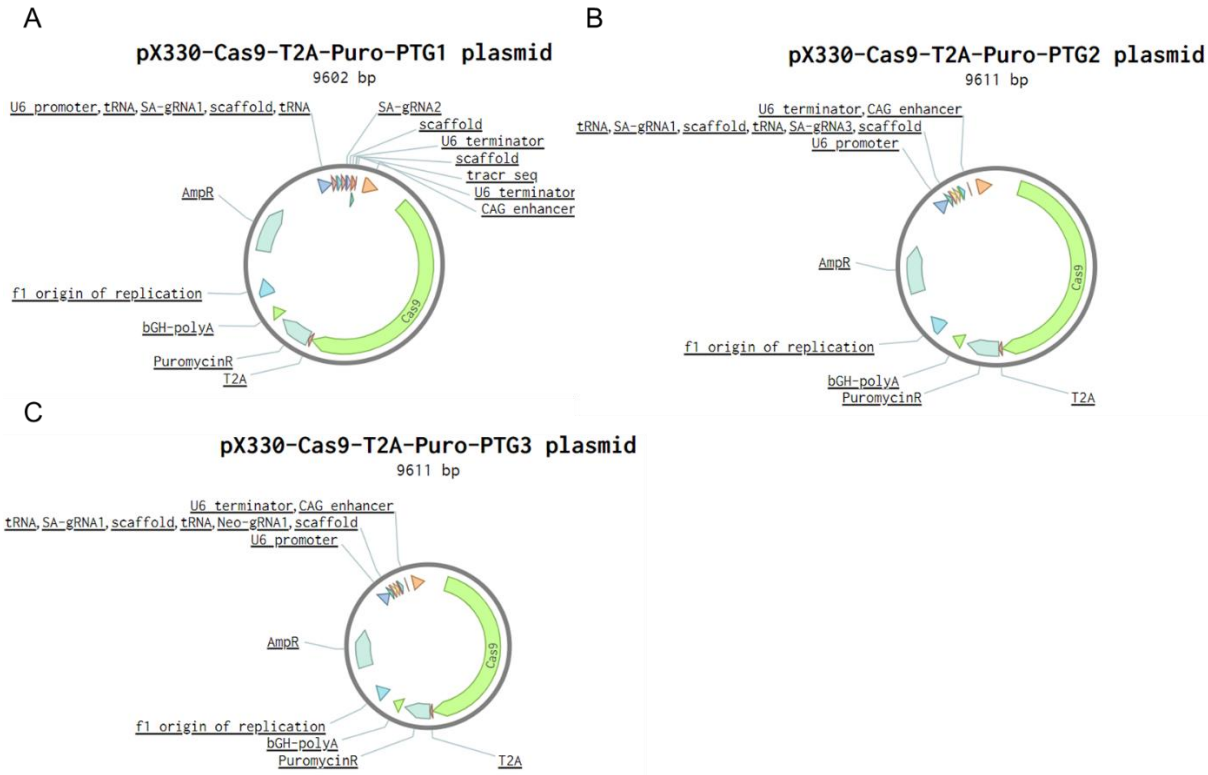

Supplementary figure 7. Plasmids for mutational activation of *KRAS*^{G12D} and *TP53*^{R167H}. (A+B) PTG constructs for activating *KRAS*^{G12D} and *TP53*^{R167H} mutations via multiplexed gene editing. (C) PTG construct for activation of *KRAS*^{G12D}. The plasmid maps were generated using the Benchling biotechnology software.

11.3 Vectors for multiplexed gene editing of TSGs

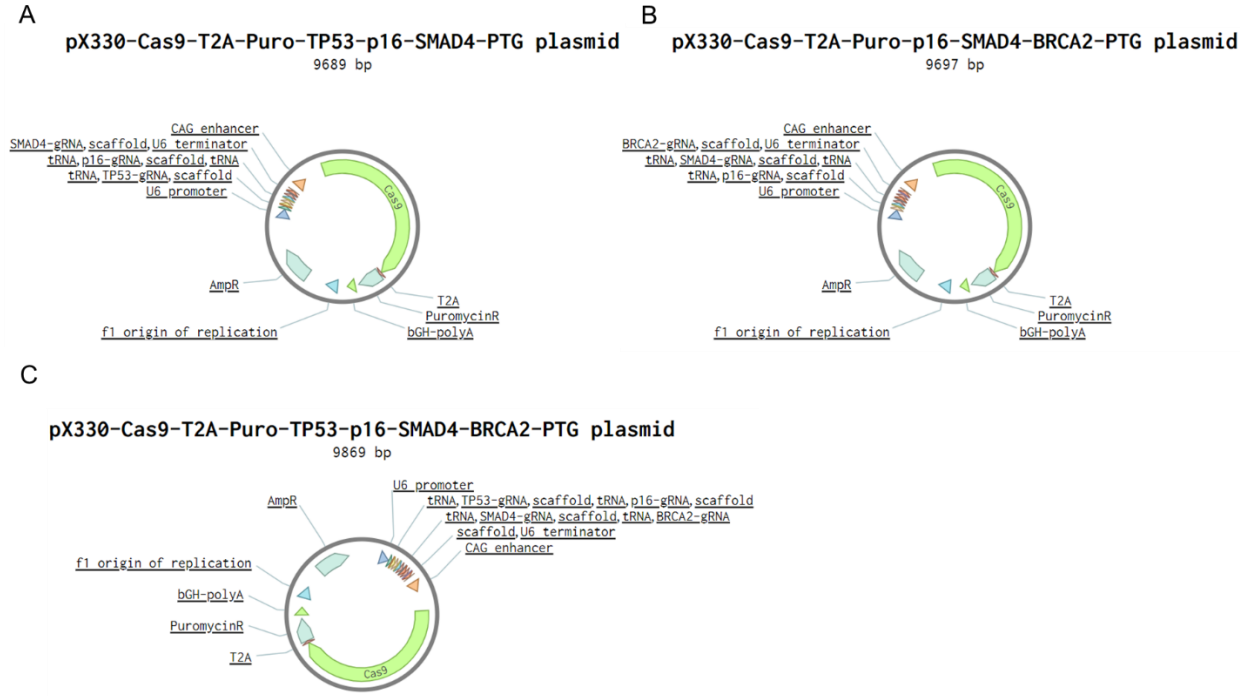

Supplementary figure 8. Plasmids for multiplexed gene editing of TSGs. (A) Plasmid for multiplexed gene editing of porcine *TP53*, *p16* and *SMAD4*. (B) Plasmid for multiplexed gene editing of porcine *p16*, *SMAD4* and *BRCA2*. (C) Plasmid for multiplexed gene editing of porcine *TP53*, *p16*, *SMAD4* and *BRCA2*. The plasmid maps were generated using the Benchling biotechnology software.

11.4 Vectors for transformation and retransplantation of porcine cells

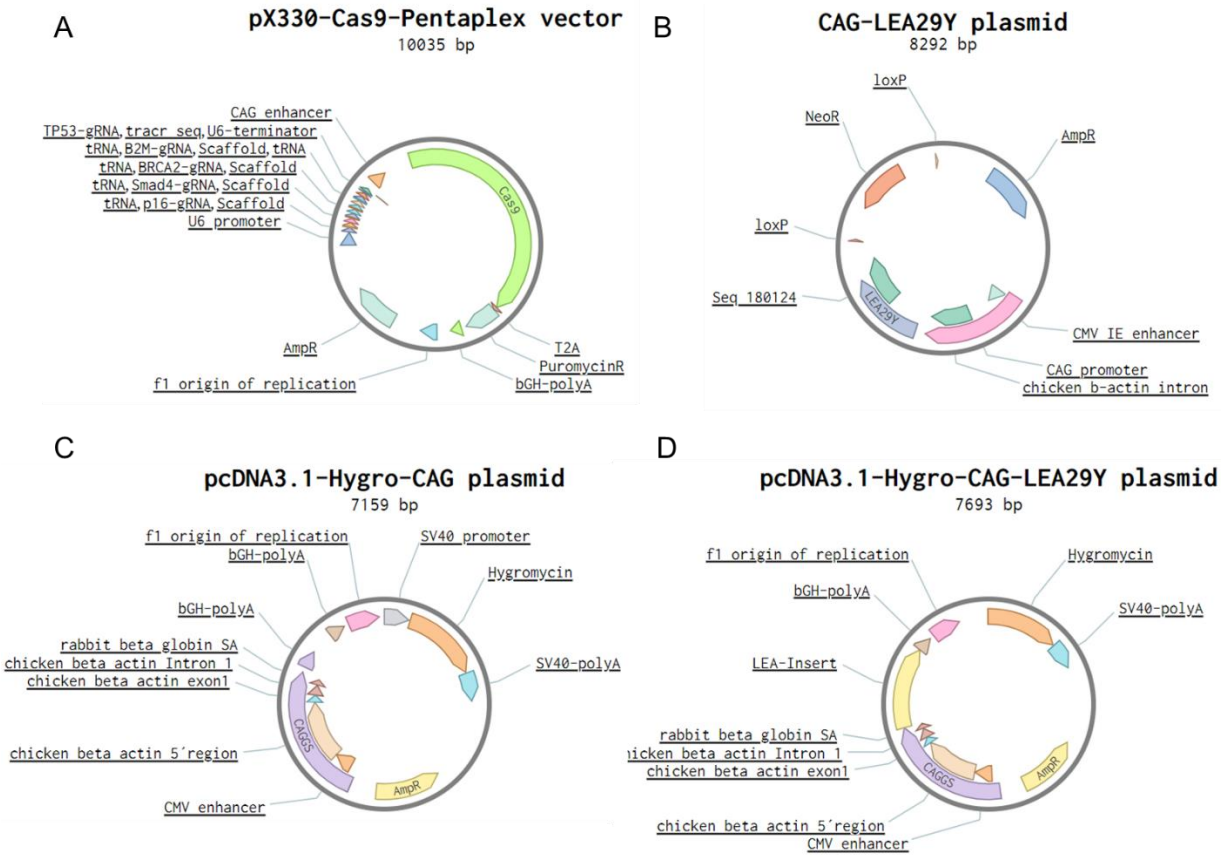

Supplementary figure 9. Plasmids for cell transformation and retransplantation. (A) Plasmid for multiplexed gene editing of *p16*, *SMAD4*, *BRCA2*, *B2M and TP53.* (B+C) Plasmids for cloning the Hygro-CAG-LEA29Y plasmid. (D) Hygro-CAG-LEA29Y plasmid to reduce cell rejection. The plasmid maps were generated using the Benchling biotechnology software.

11.5 Vectors for mutational activation in porcine pancreatic acinar cells

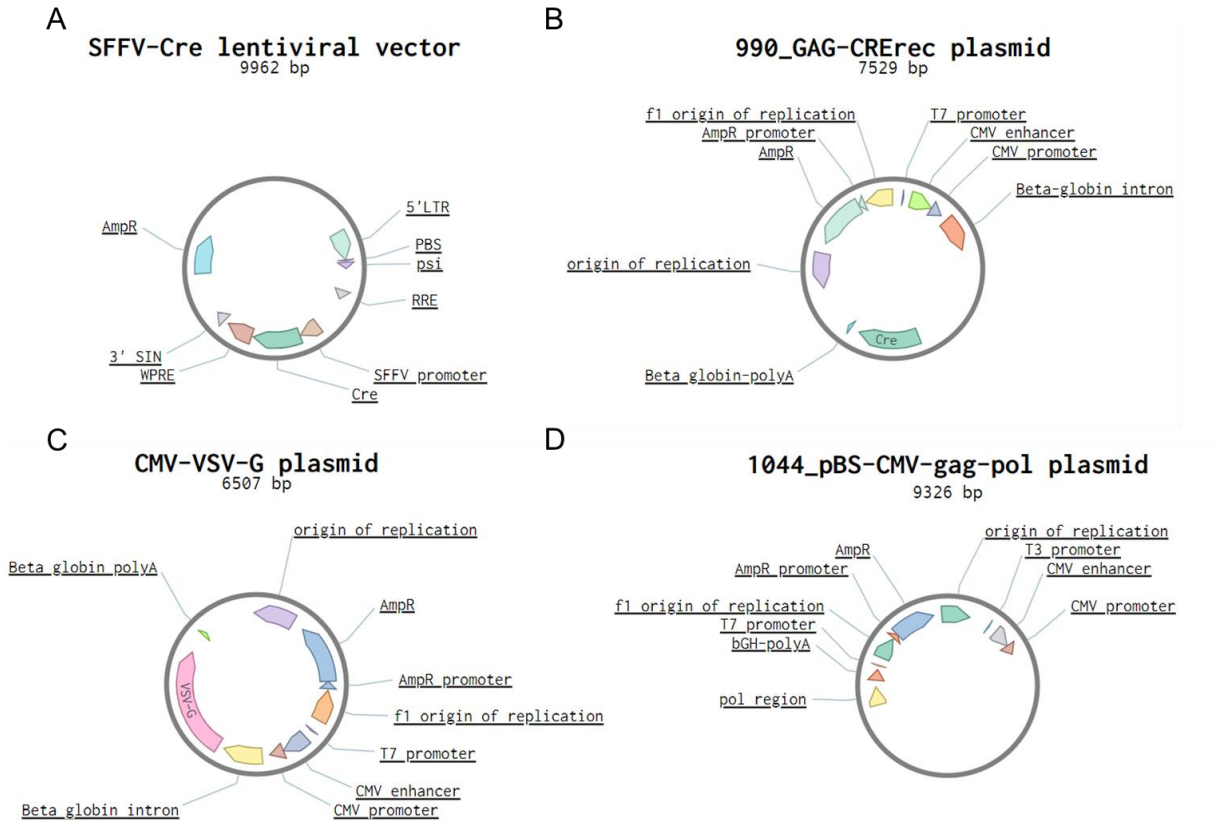

Supplementary figure 10. Plasmids for mutational activation in porcine acinar cells. (A) SFFV-Cre lentiviral vector for activation of *KRAS*^{G12D} and *TP53*^{R167H} in porcine pancreatic acinar cells. (B-D) Plasmids for the production of Cre-VLPs for mutational activation in pancreatic acinar cells. The plasmid maps were generated using the Benchling biotechnology software.

11.6 Characterisation of cell clones for *PTF1A*^{iCre} pig generation

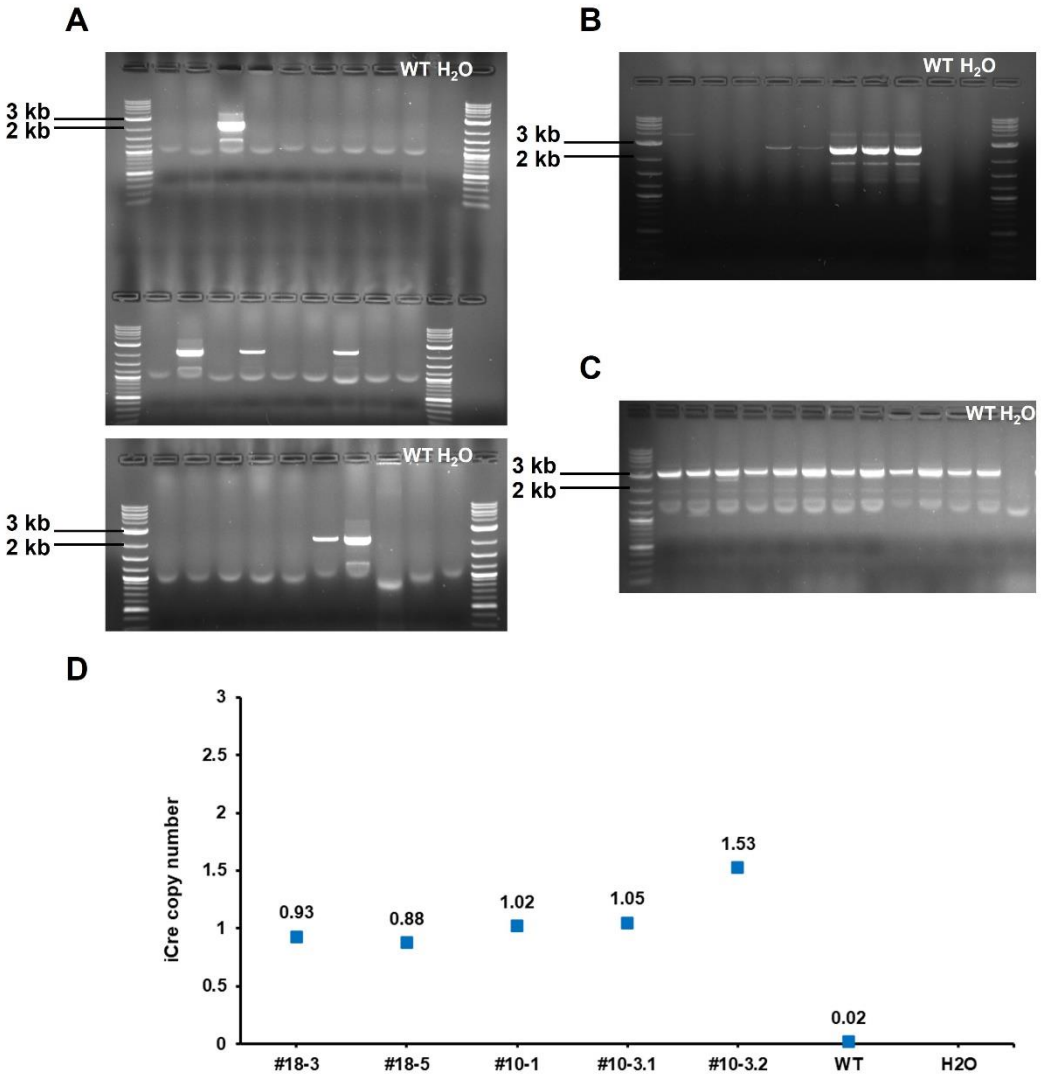

Supplementary figure 11. Analysis of *PTF1A*$^{5'iCre}$ cell clones. (A) 5'screening PCR results in a band of 2233 bp for correctly targeted cell clones. (B) 3'screening PCR shows a band of 2346 bp for correctly targeted cell clones. (C) Endogenous PCR gives a band of 3020 bp for the non-targeted endogenous allele. (D) DdPCR for iCre copy numbers of selected cell clones.

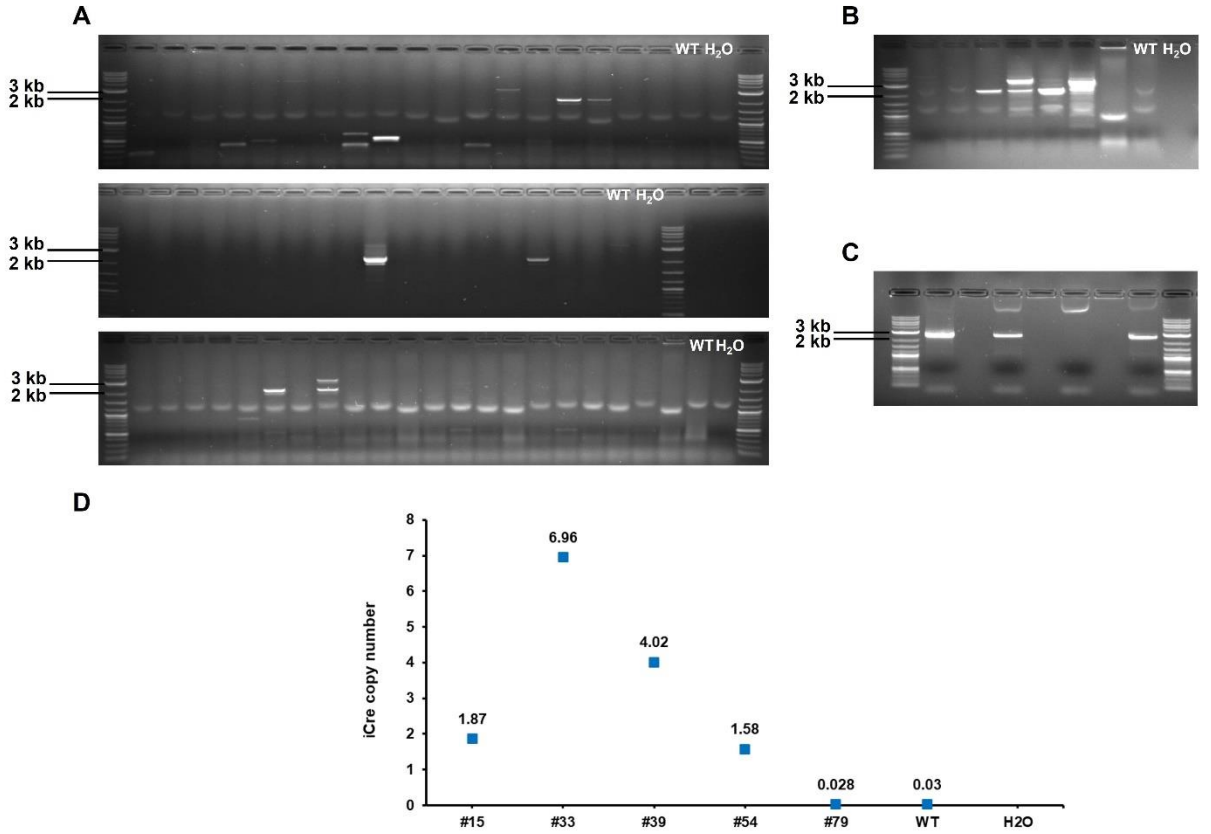

Supplementary figure 12. Analysis of *PTF1A*$^{3'iCre}$ cell clones. (A) 5'screening PCR results in a band of 2127 bp for correctly targeted cell clones: (B) 3'screening PCR shows a band of 2300 bp for correctly targeted cell clones. (C) Endogenous PCR gives a band of 2887 bp for the non-targeted endogenous allele. (D) DdPCR for iCre copy numbers of selected cell clones.

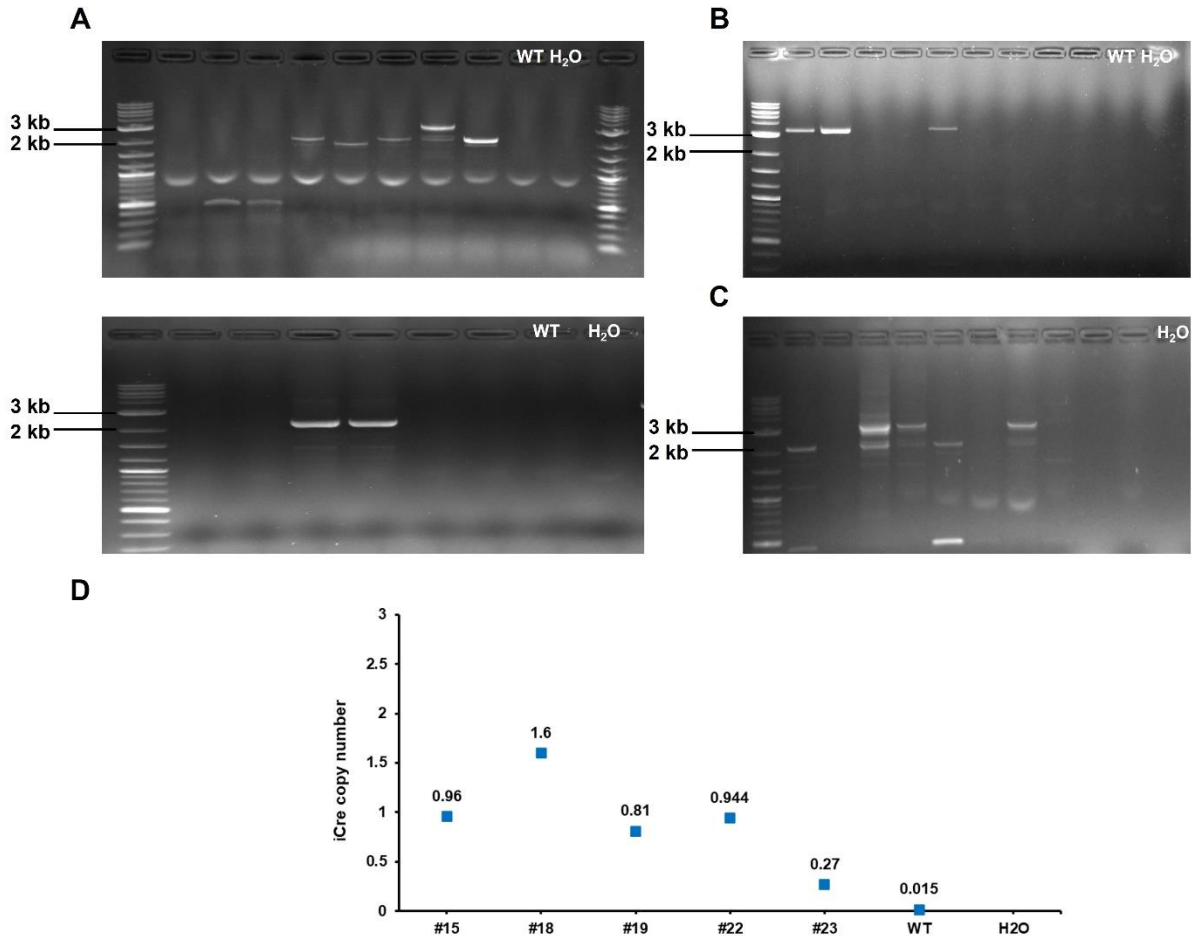

Supplementary figure 13. Analysis of *PTF1A*$^{3'iCre\text{-}ERT2}$ cell clones. (A) 5'screening PCR results in a band of 2127 bp for correctly targeted cell clones. (B) 3'screening PCR shows a band of 3261 bp for correctly targeted cell clones. (C) Endogenous PCR gives a band of 2887 bp for the non-targeted endogenous allele. (D) DdPCR for iCre copy numbers of selected cell clones.

11.7 Pyrosequencing results: *PTF1A^{iCre}* progeny

KRAS:

***KRAS$^{LSLG12D/WT}$PTF1A$^{5'iCre}$* small brain:**
A: 43%
G: 57%

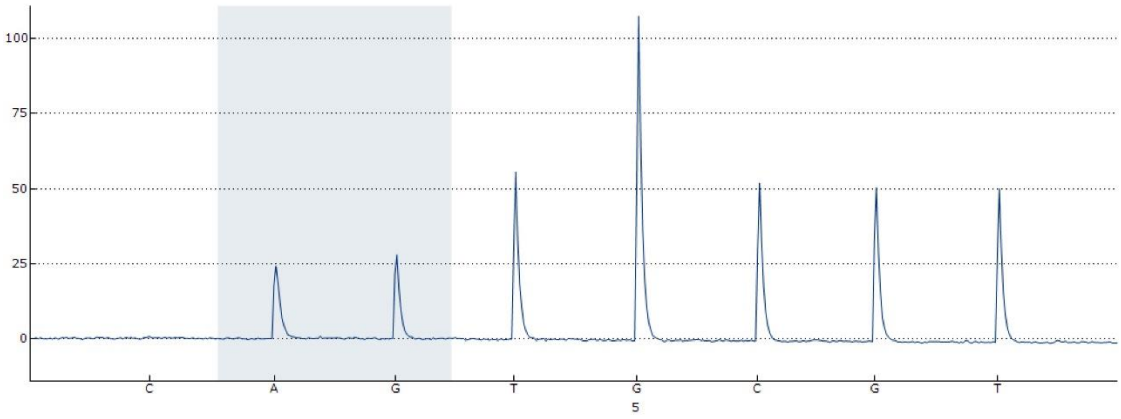

***KRAS$^{LSLG12D/WT}$PTF1A$^{5'iCre}$* pancreas:**
A: 35%
G: 65%

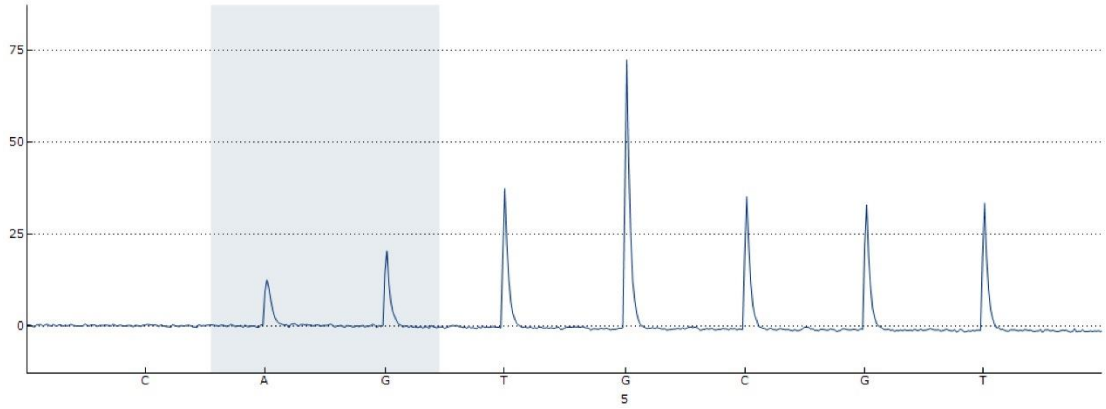

***KRAS$^{LSLG12D/WT}$PTF1A$^{5'iCre}$* stomach:**
A: 6%
G: 94%

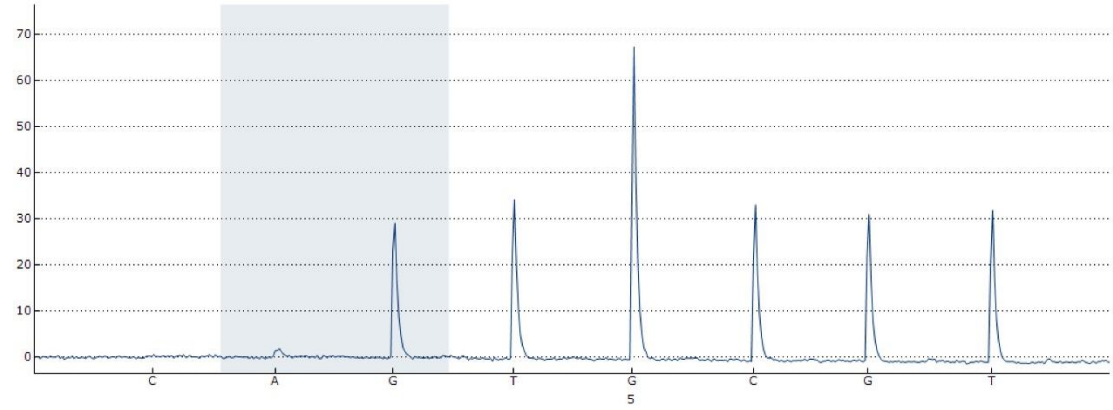

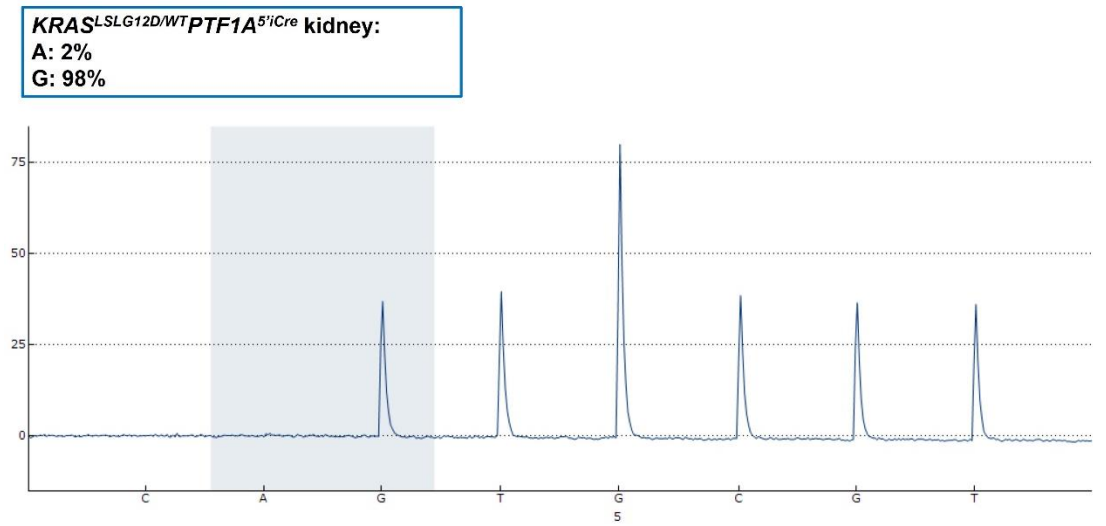

Supplementary figure 14. KRAS Pyrosequencing: *KRAS$^{LSLG12D/WT}$PTF1A$^{5'iCre}$* pig.

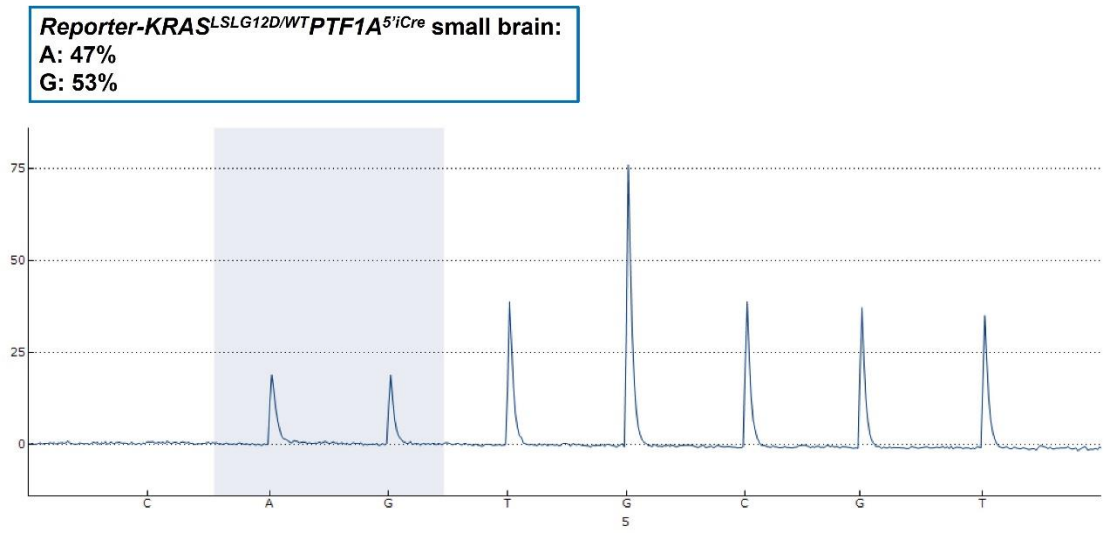

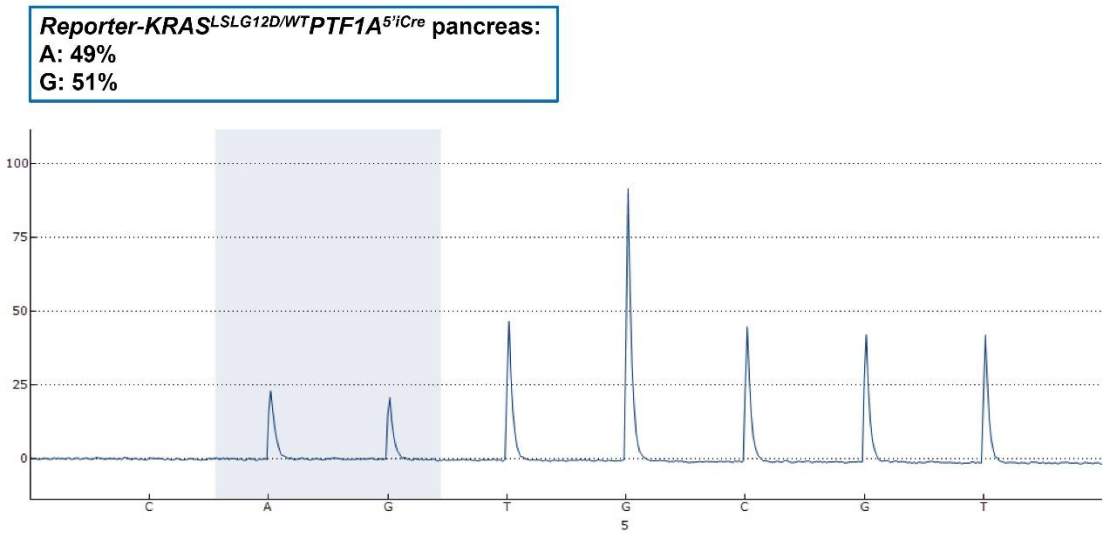

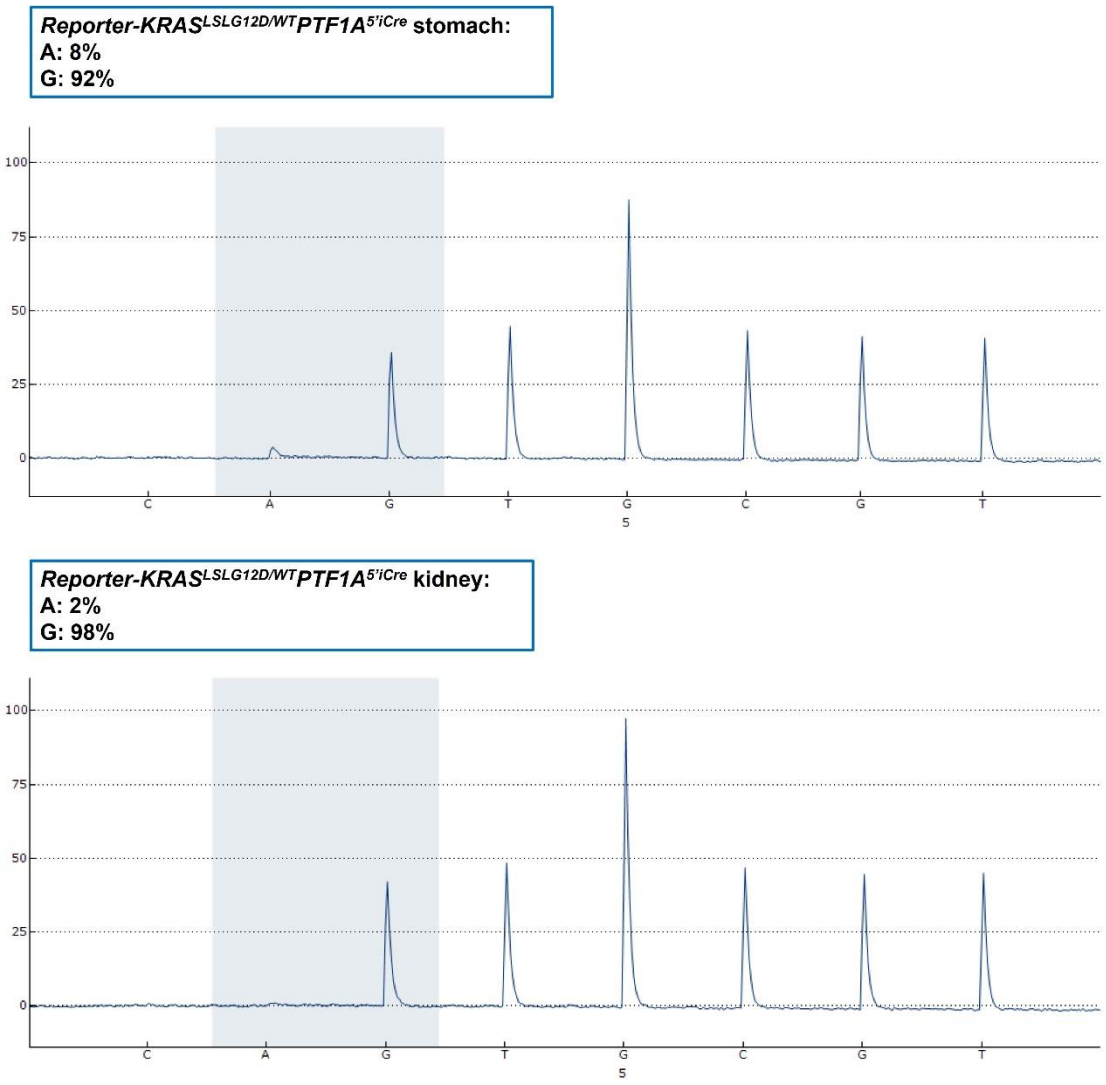

Supplementary figure 15. KRAS pyrosequencing: *Reporter-KRAS$^{LSLG12D/WT}$PTF1A$^{5'iCre}$* pig.

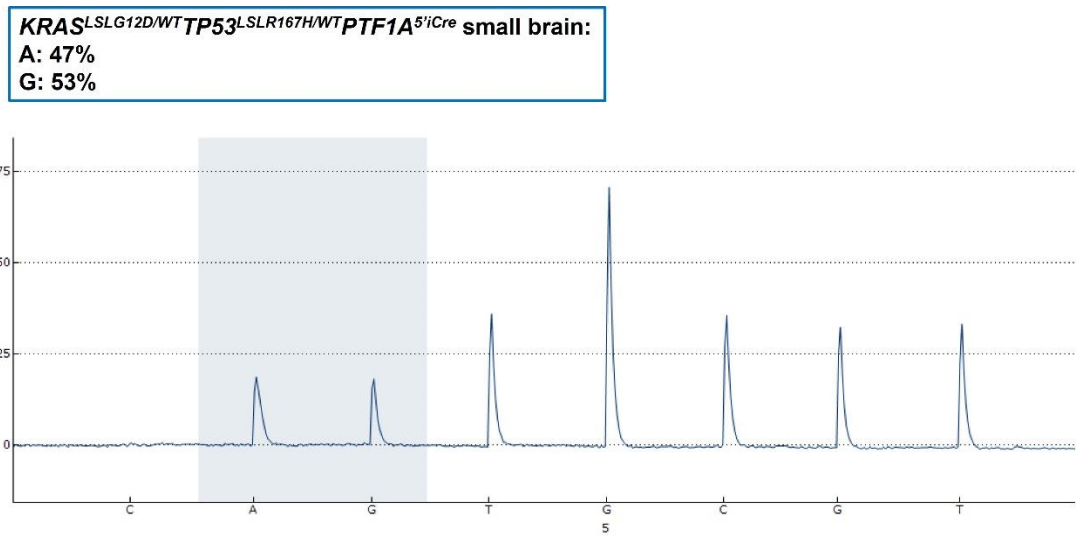

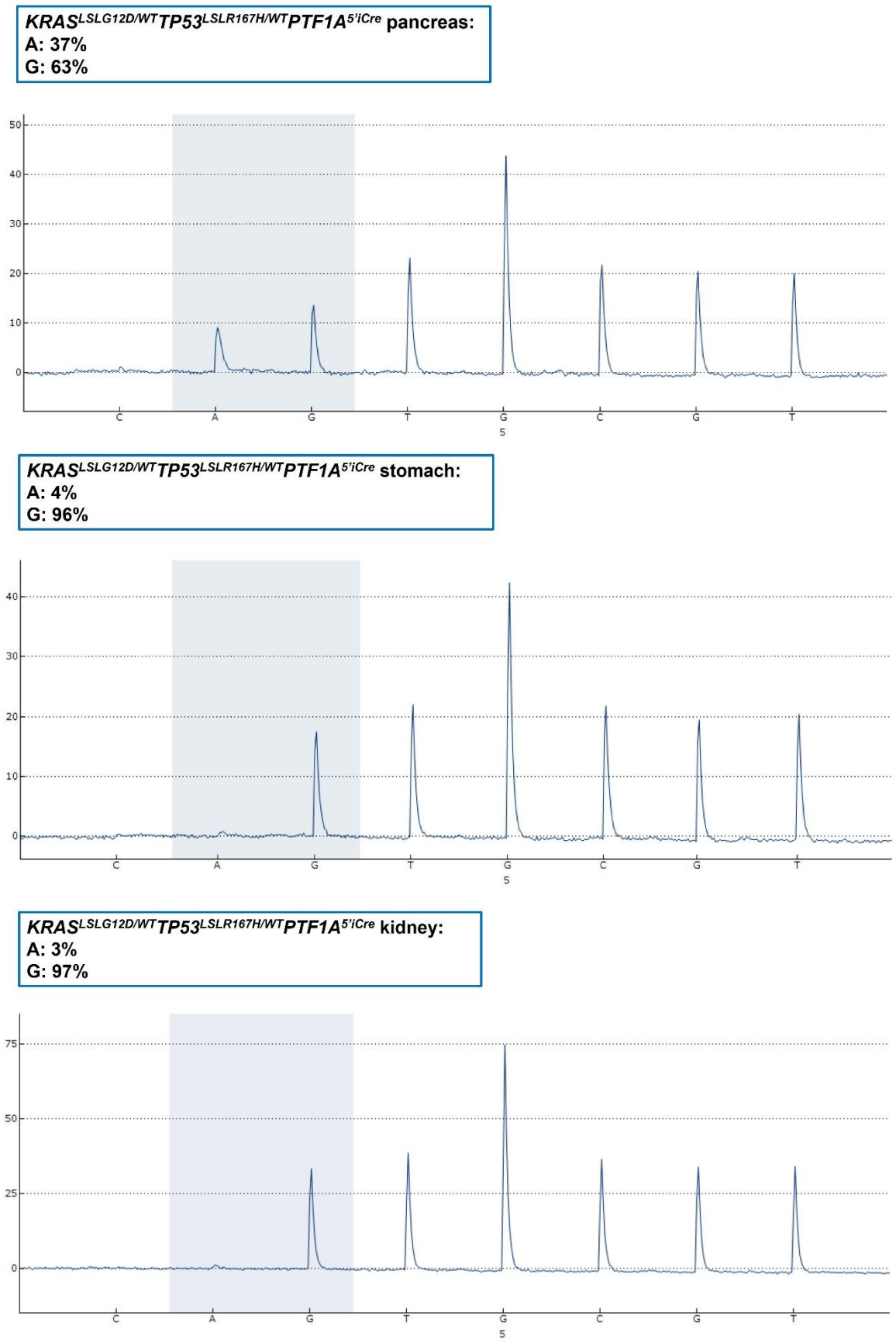

Supplementary figure 16. KRAS pyrosequencing: *KRAS*$^{LSLG12D/WT}$*TP53*$^{LSLR167H/WT}$*PTF1A*$^{5'iCre}$ pig.

***KRAS*$^{LSLG12D/WT}$*PTF1A*$^{3'iCre}$ small brain:**
A: 54%
G: 46%

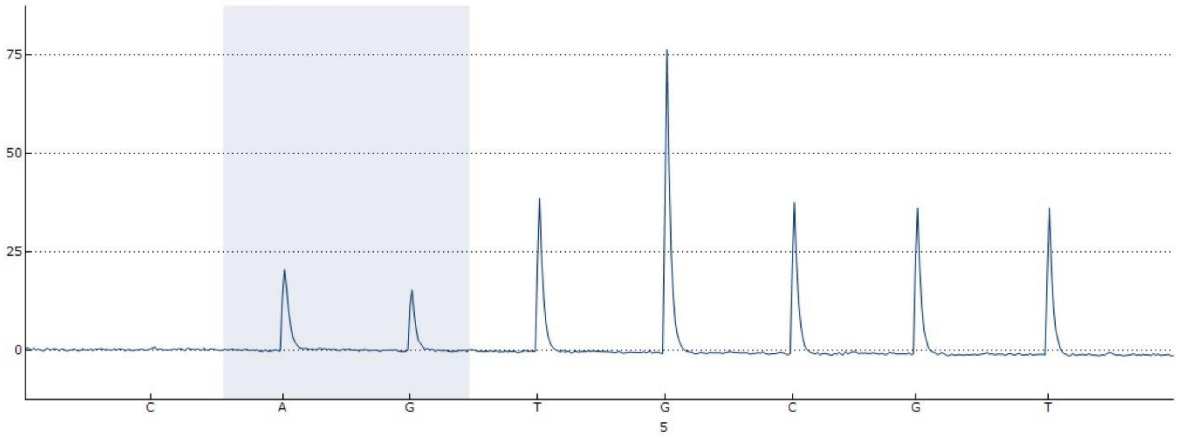

***KRAS*$^{LSLG12D/WT}$*PTF1A*$^{3'iCre}$ pancreas:**
A: 35%
G: 65%

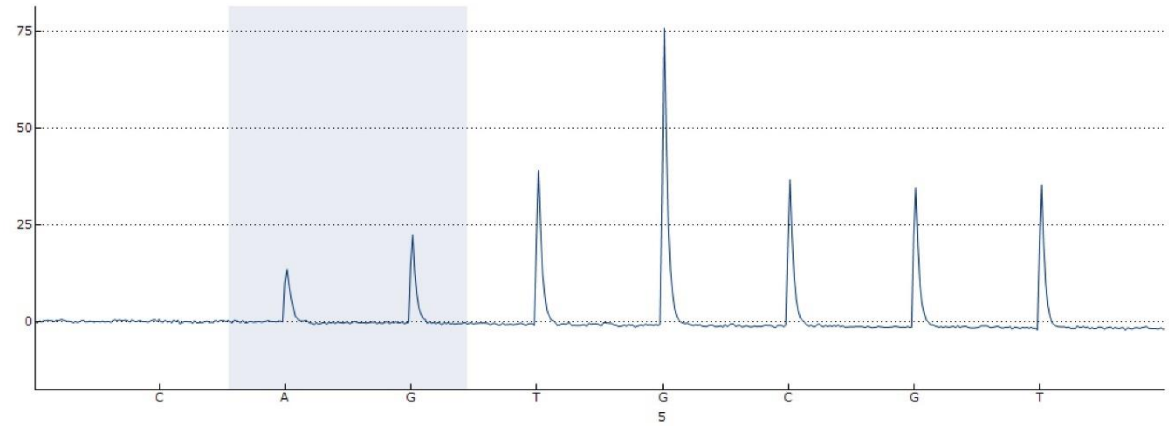

***KRAS*$^{LSLG12D/WT}$*PTF1A*$^{3'iCre}$ stomach:**
A: 4%
G: 96%

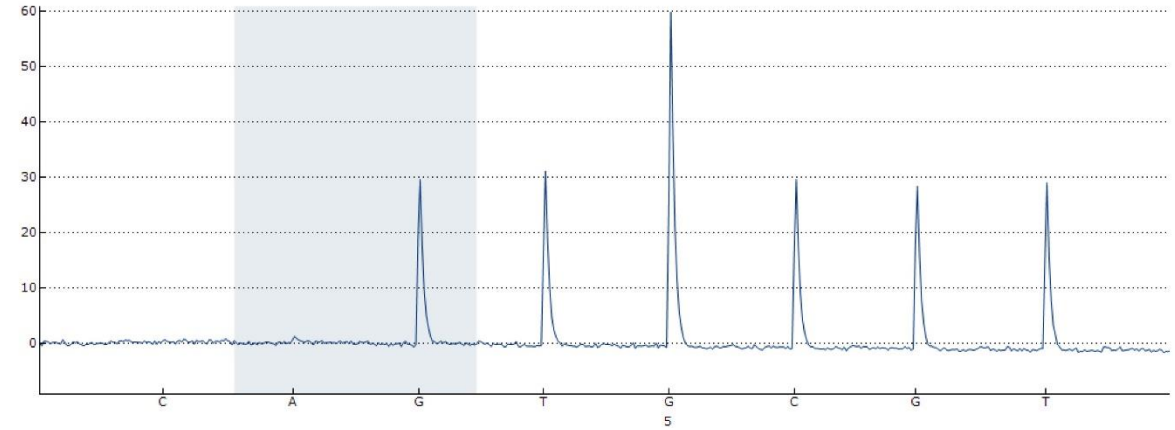

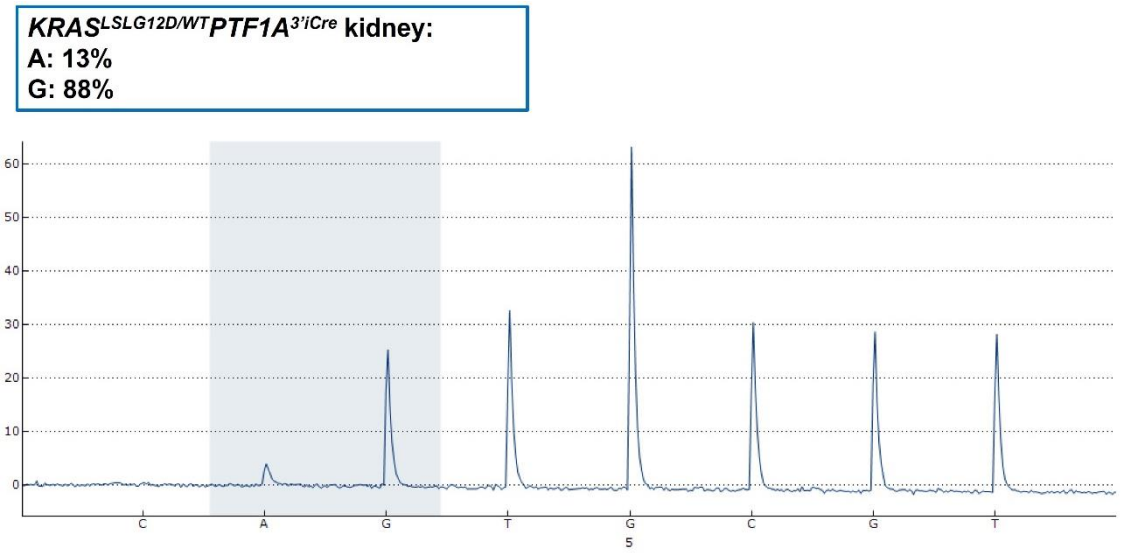

Supplementary figure 17. KRAS pyrosequencing: *KRAS$^{LSLG12D/WT}$PTF1A$^{3'iCre}$* pig.

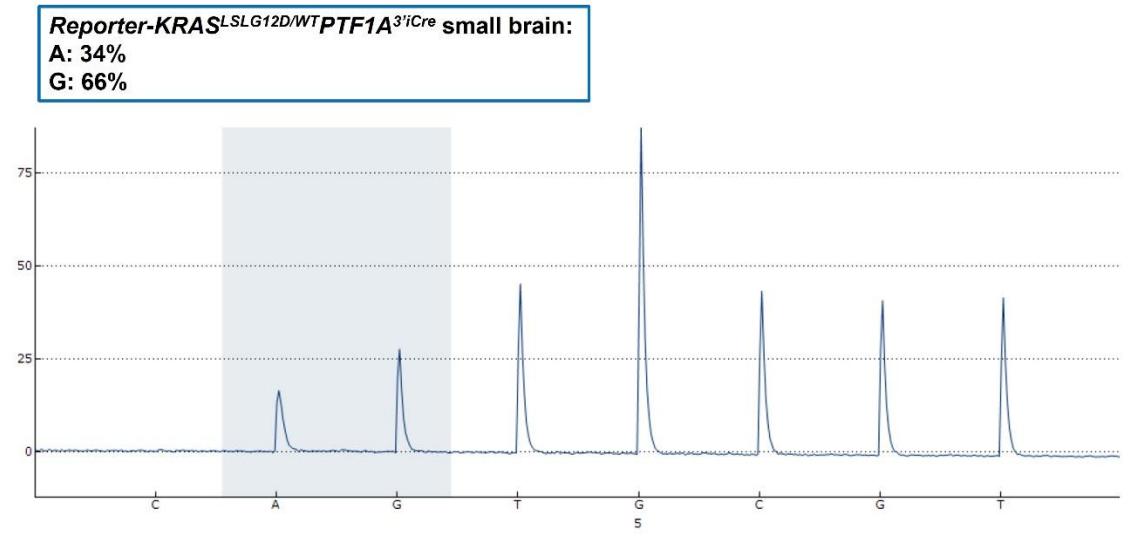

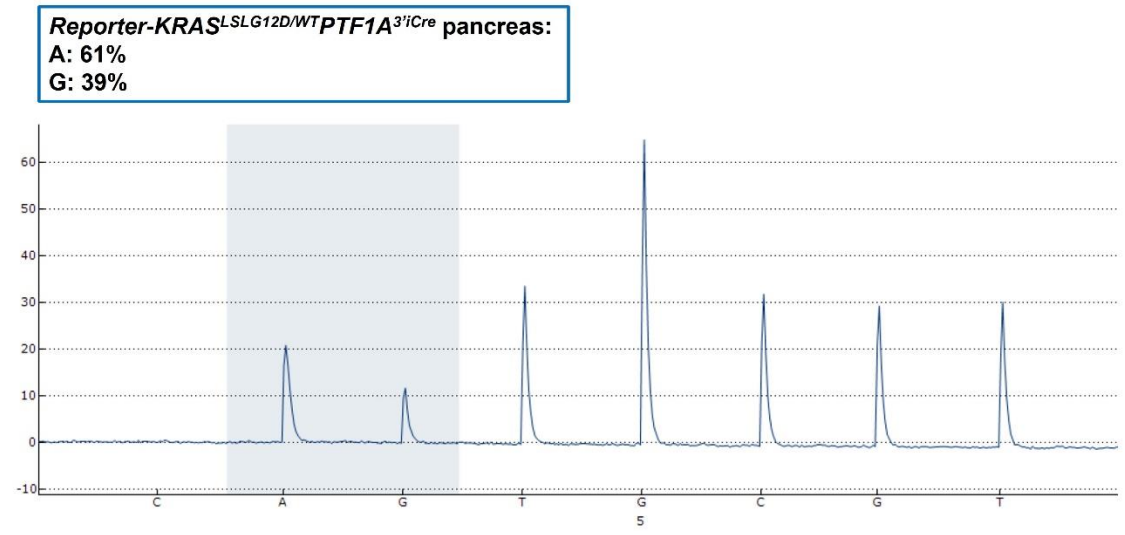

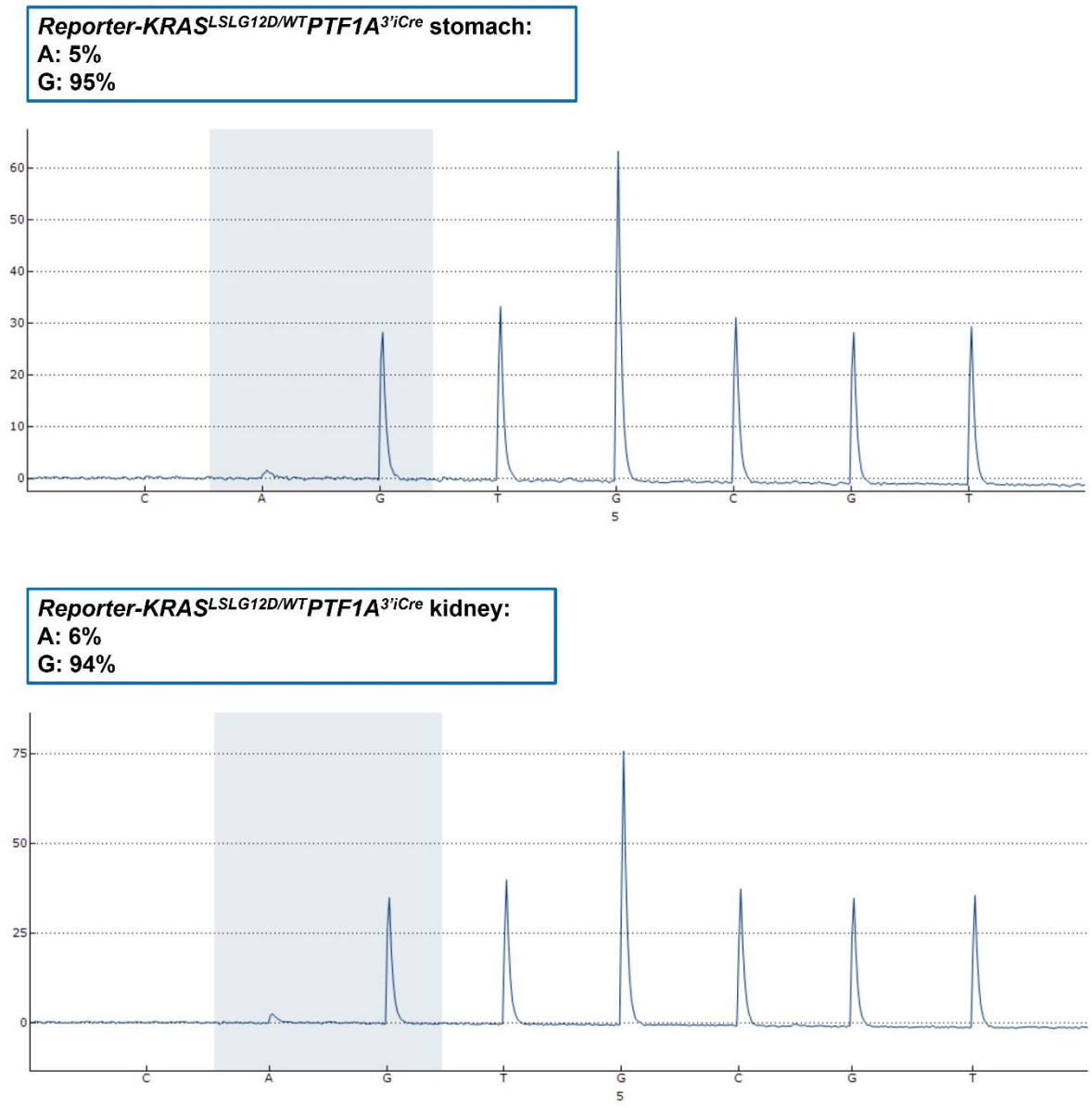

Supplementary figure 18. KRAS pyrosequencing: *Reporter-KRAS$^{LSLG12D/WT}$PTF1A$^{3'iCre}$* pig.

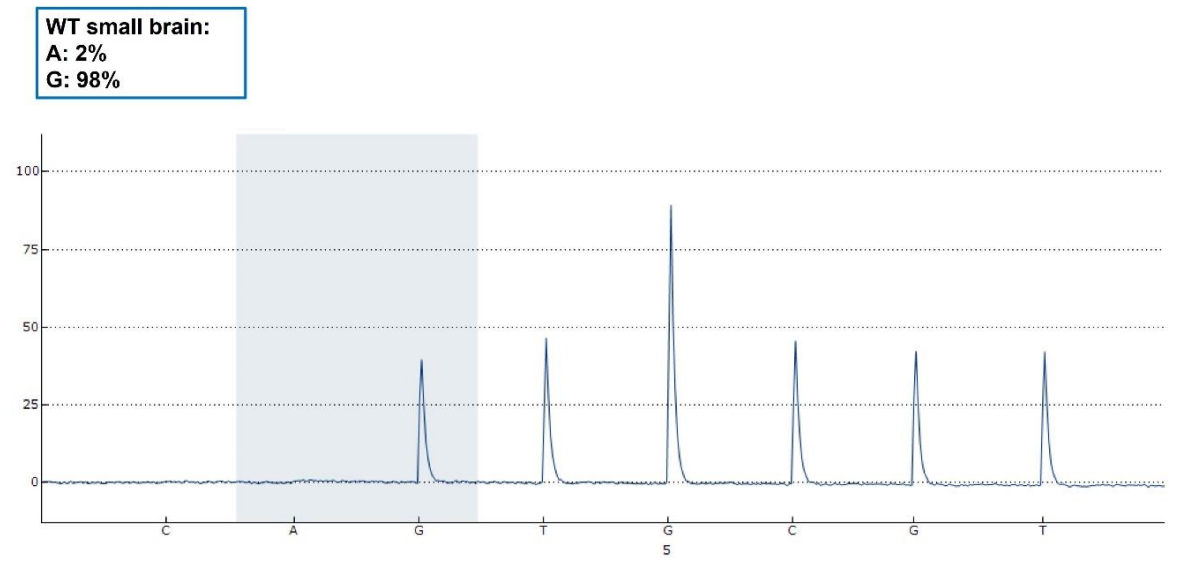

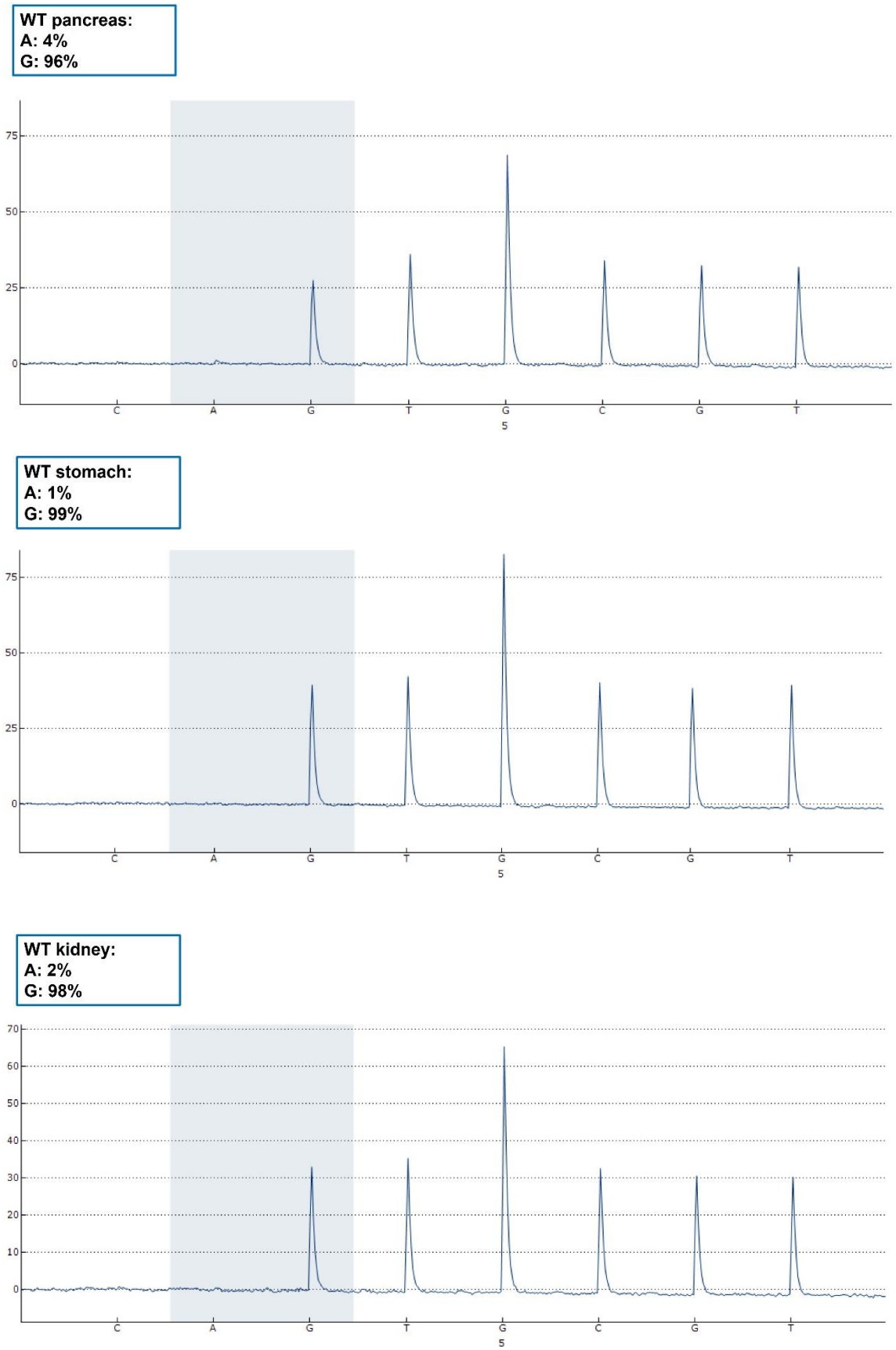

Supplementary figure 19. KRAS pyrosequencing: Wild type pig.

TP53:

***TP53*$^{LSLR167H/WT}$*PTF1A*$^{5'iCre}$ small brain:**
A: 40%
G: 60%

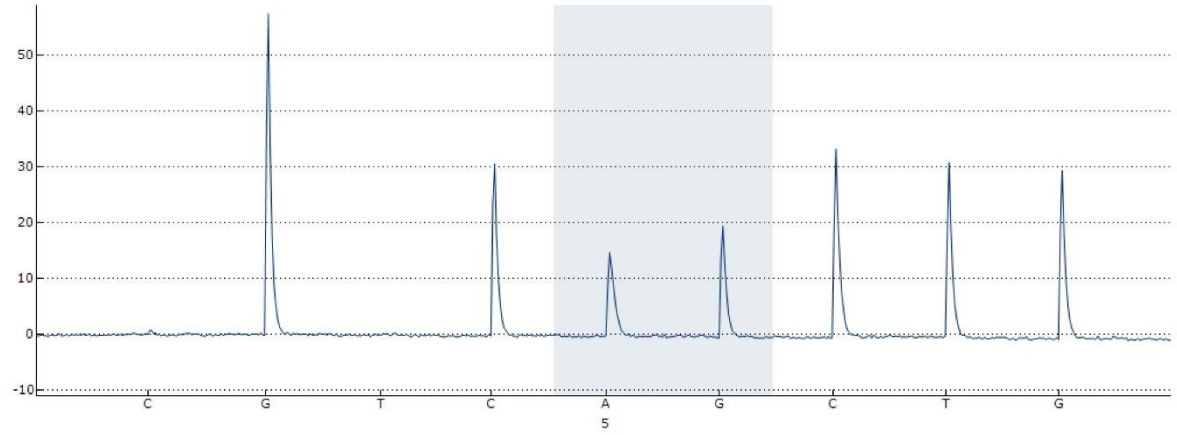

***TP53*$^{LSLR167H/WT}$*PTF1A*$^{5'iCre}$ pancreas:**
A: 15%
G: 85%

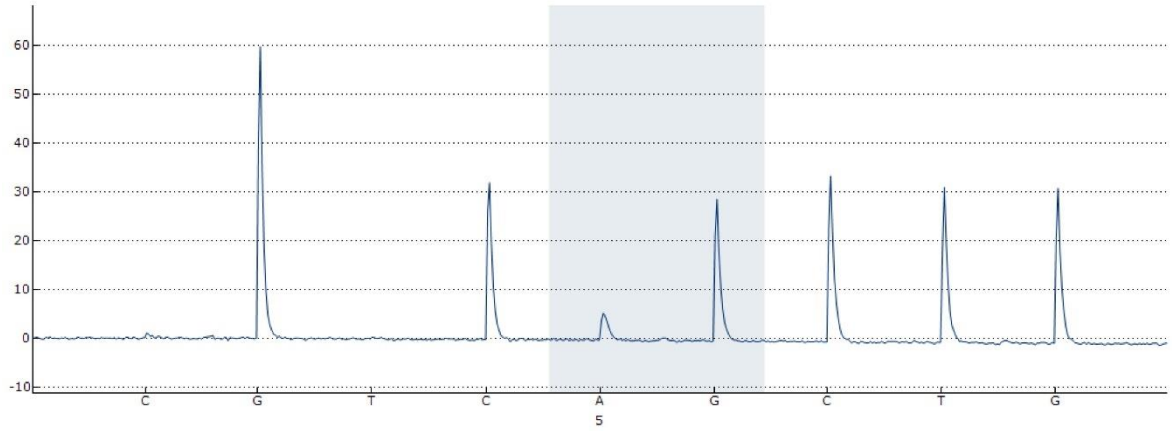

***TP53*$^{LSLR167H/WT}$*PTF1A*$^{5'iCre}$ stomach:**
A: 3%
G: 97%

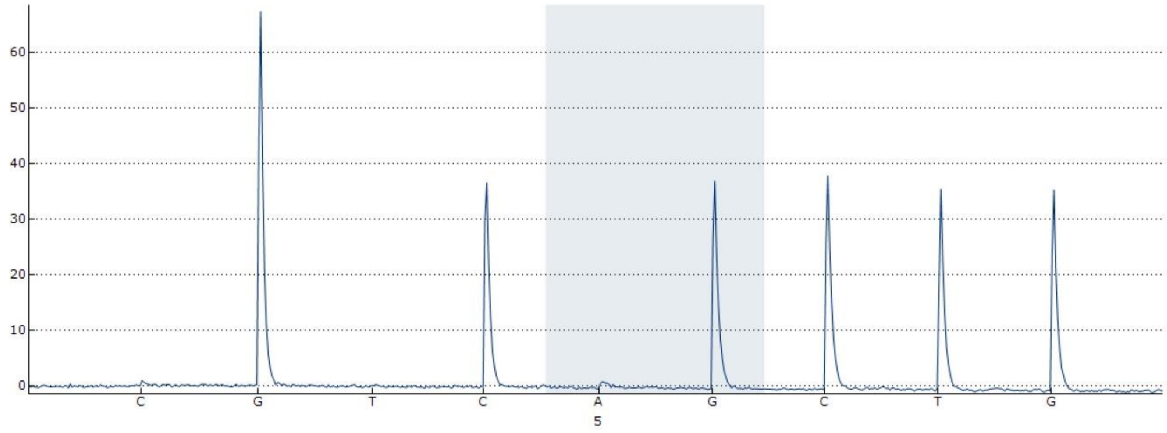

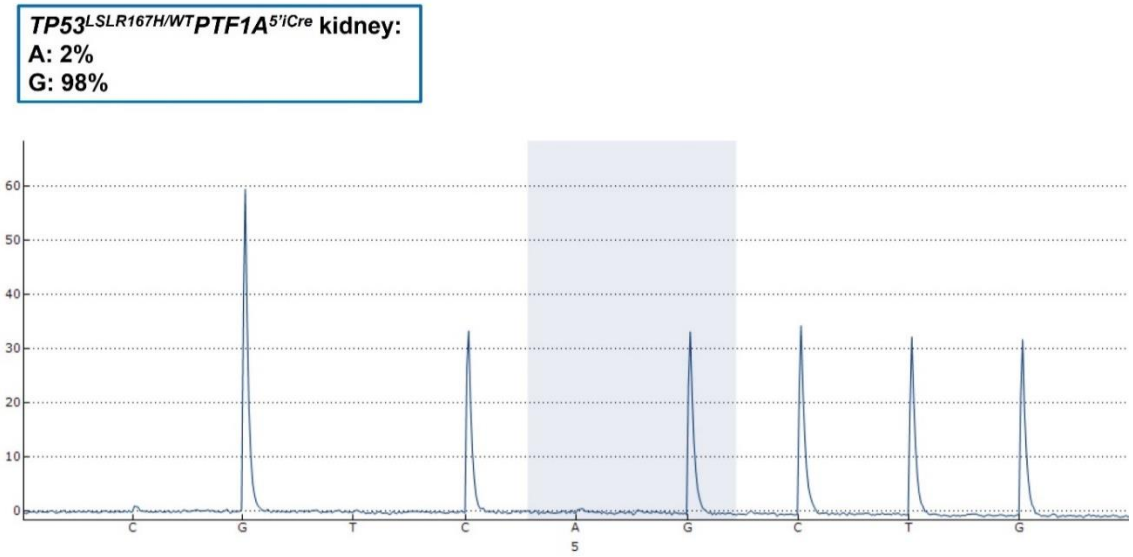

Supplementary figure 20. TP53 pyrosequencing: *TP53*$^{LSLR167H/WT}$*PTF1A*$^{5'iCre}$ pig.

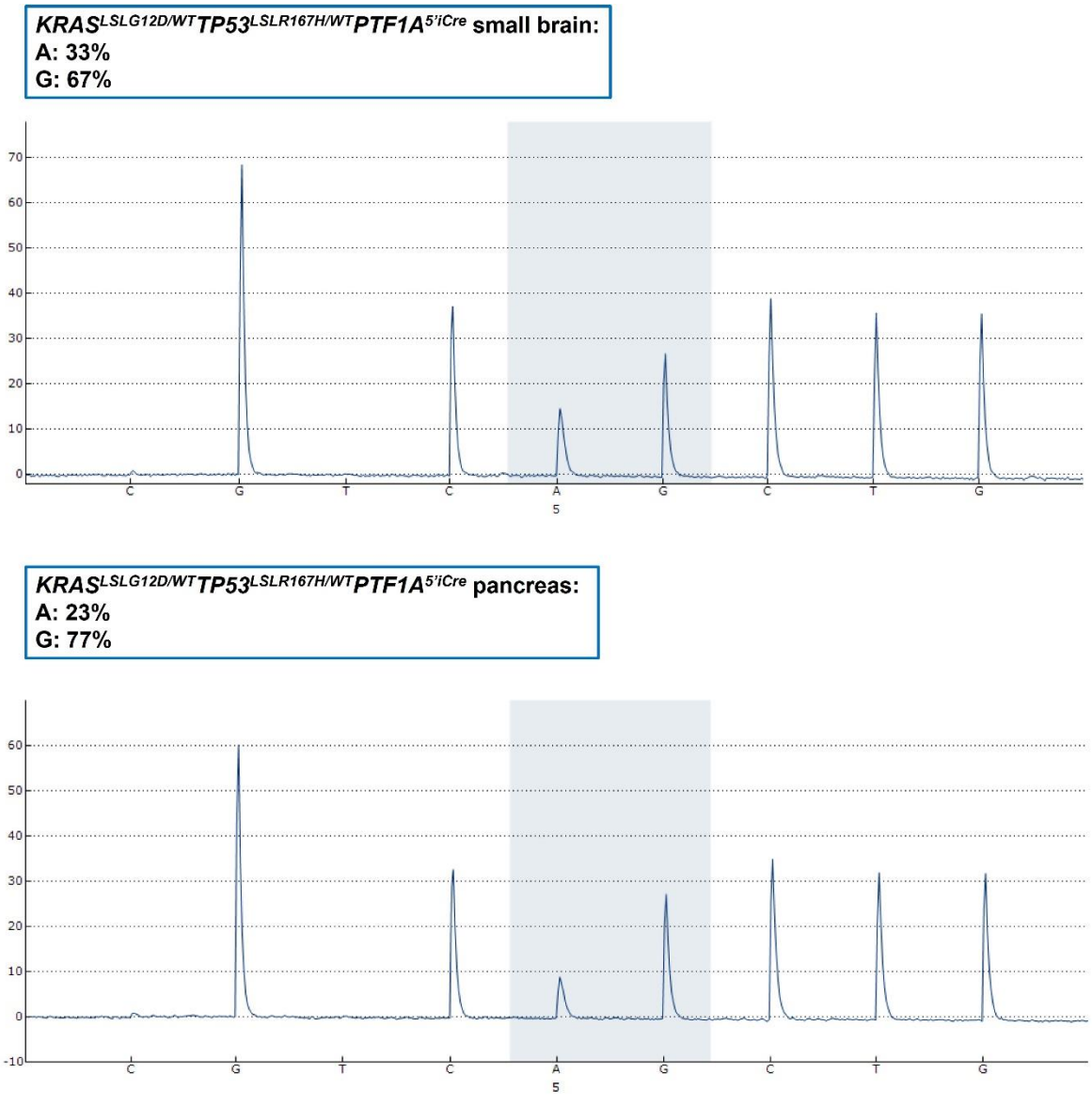

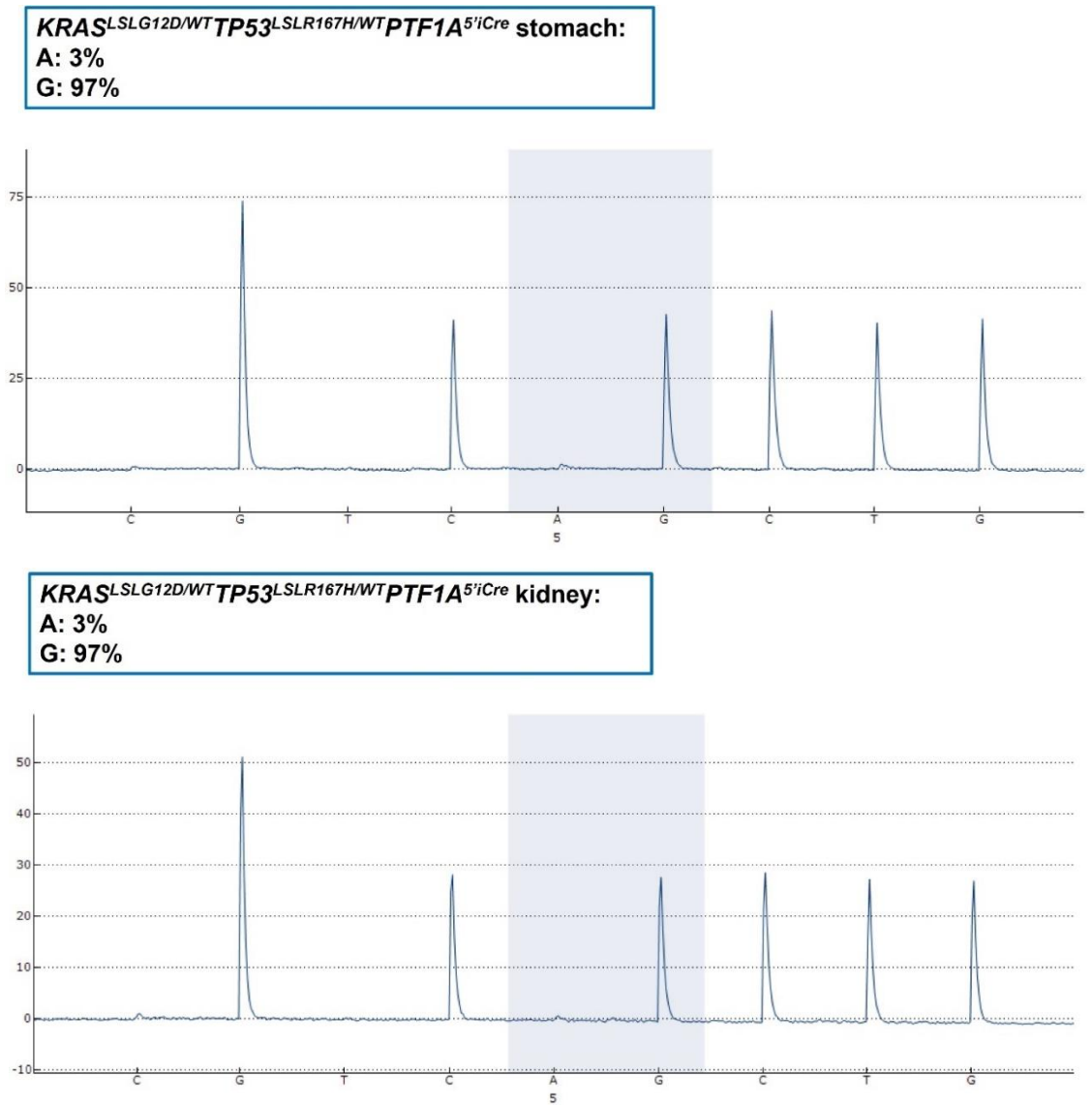

Supplementary figure 21. TP53 pyrosequencing: *KRAS*$^{LSLG12D/WT}$*TP53*$^{LSLR167H/WT}$*PTF1A*$^{5'iCre}$ pig.

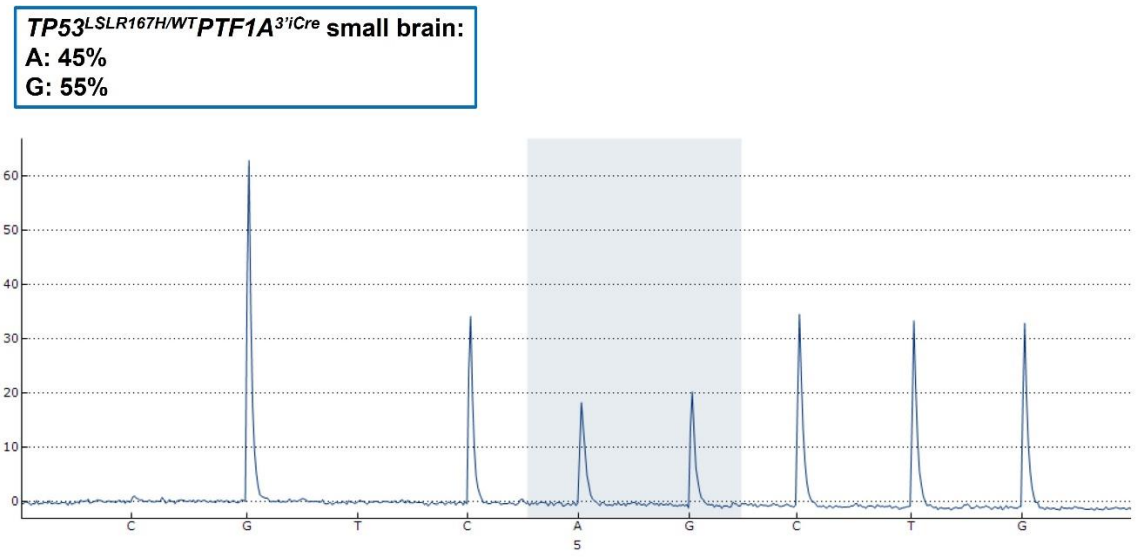

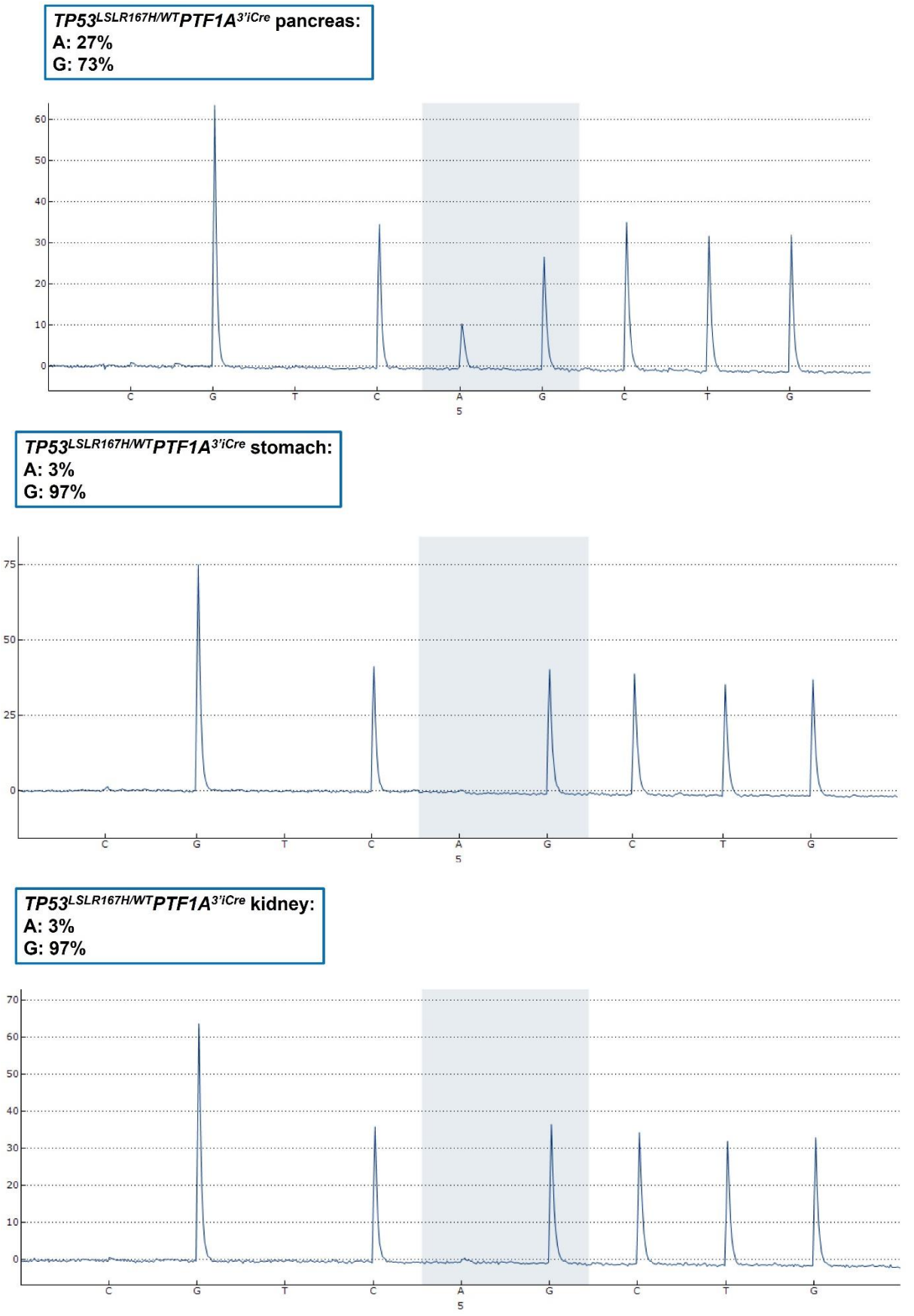

Supplementary figure 22. TP53 pyrosequencing: *TP53*$^{LSLR167H/WT}$*PTF1A*$^{3'iCre}$ pig.

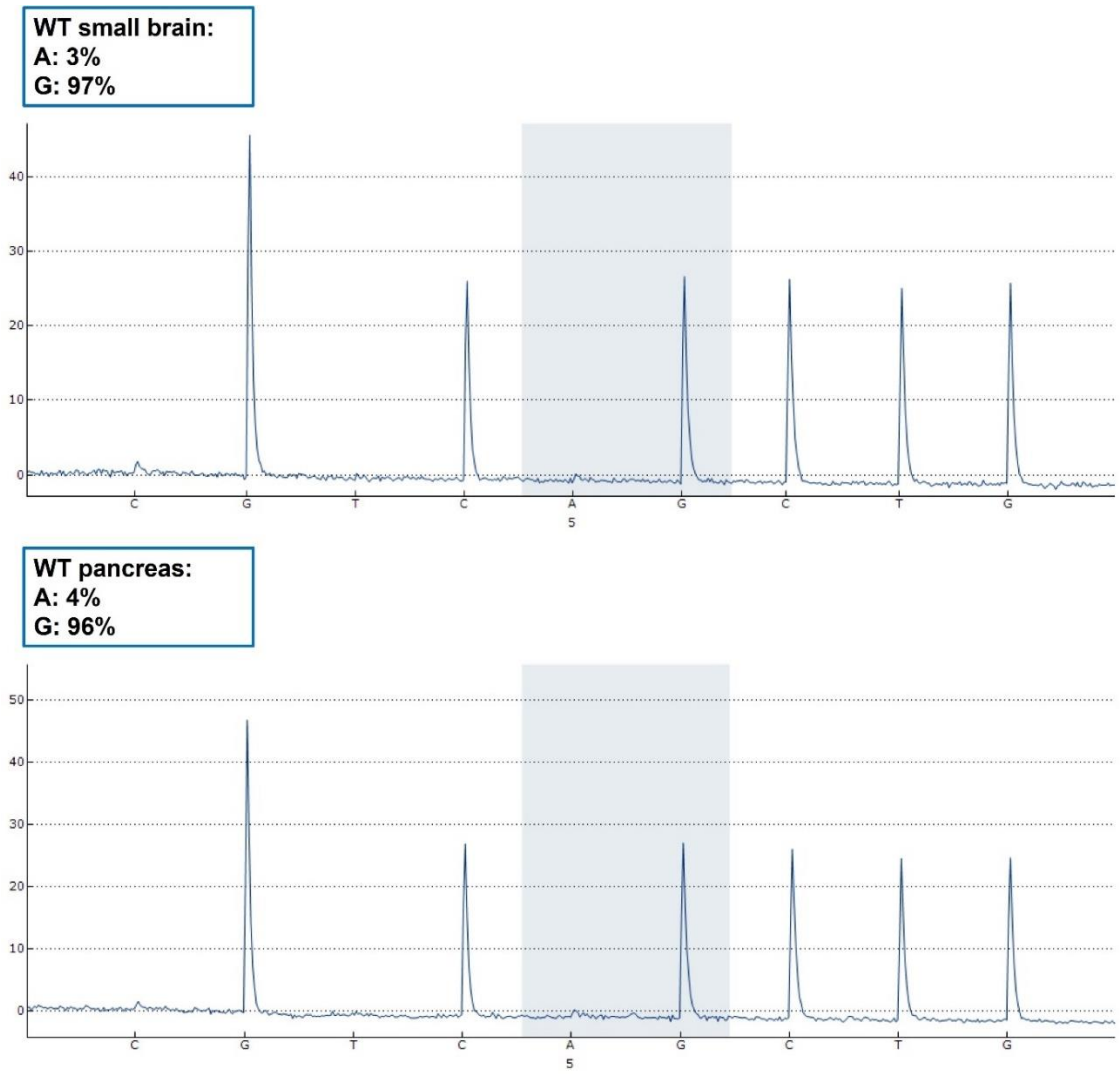
WT small brain:
A: 3%
G: 97%
40
30
20
10
0
C
G
T
C
A
G
C
T
G
5
WT pancreas:
A: 4%
G: 96%
50
40
30
20
10
0
C
G
T
C
A
G
C
T
G
5

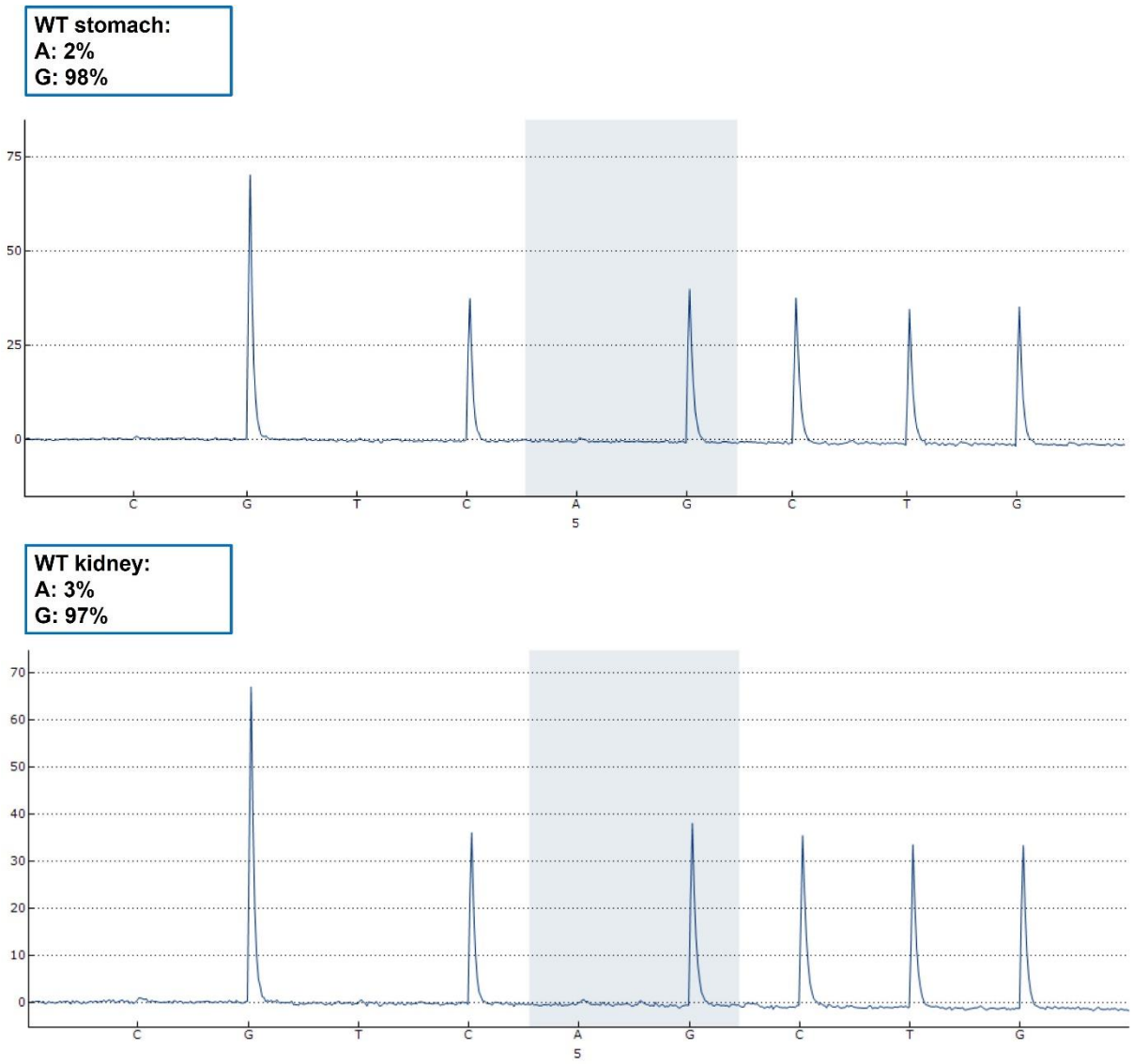

Supplementary figure 23. TP53 pyrosequencing: Wild type pig.

11.8 Results for *ROSA26* targeting

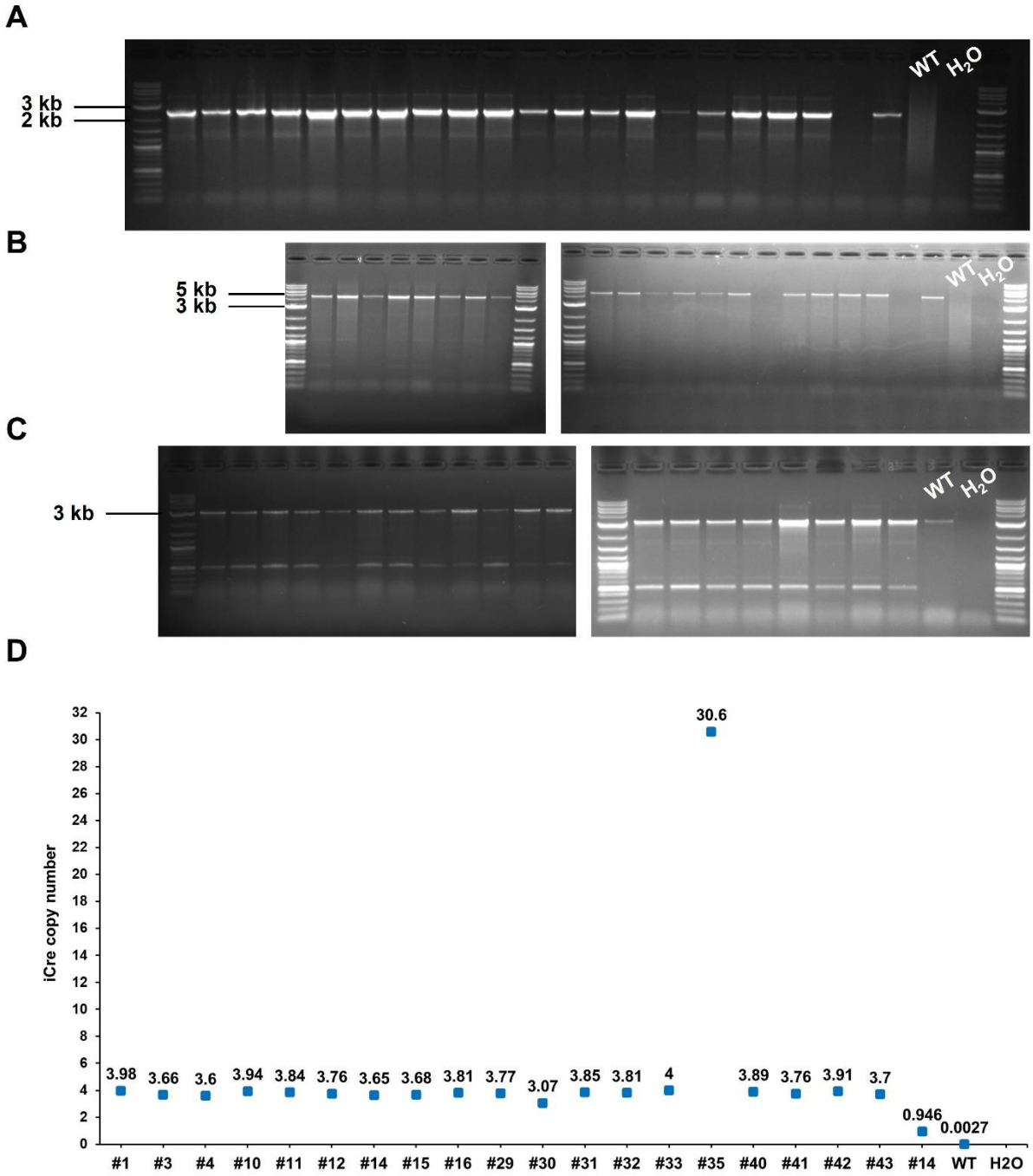

Supplementary figure 24. Results for *ROSA26* targeting. (A) 5'junction PCR from 5'endogenous end into SA shows 2481 bp band for positive cell clones. (B) 5'junction PCR from 5'endogenous end into *mPdx1* promoter reveals 4518 bp and 4266 bp bands for *R26-SA-Neo-mPdx1-iCre* and *R26-SA-BS-mPdx1-iCre*, respectively. (C) R26 endogenous PCR shows a 3105 bp band for the intact second allele. (D) DdPCR results for *R26-mPdx1-iCre* cell clones.

11.9 Pyrosequencing results: mutational activation by gene editing

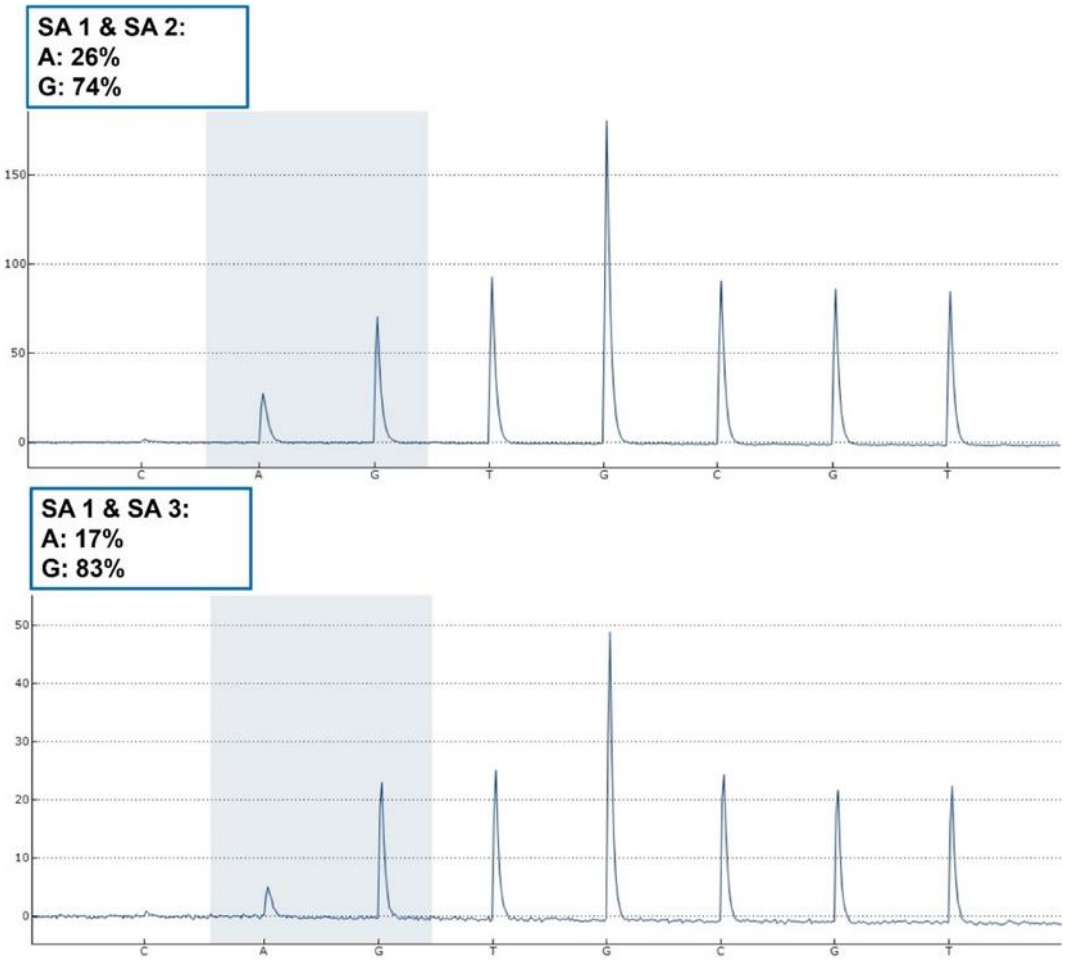

Supplementary figure 25. Pyrosequencing: SA gRNA 1 with SA gRNA 2/SA gRNA 3.

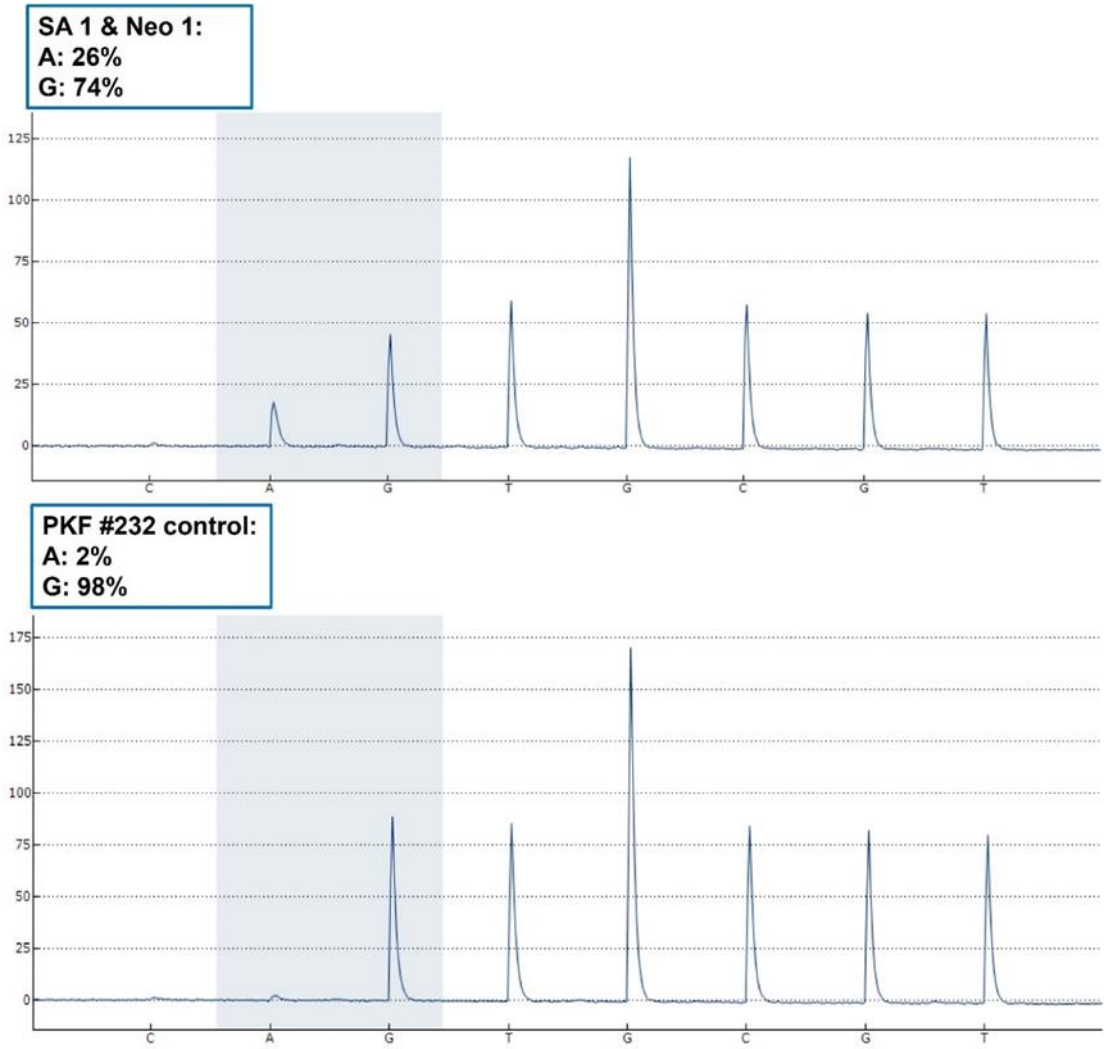

Supplementary figure 26. Pyrosequencing: SA gRNA 1 with Neo gRNA 1 and control.

11.10 Results for porcine ADM modelling

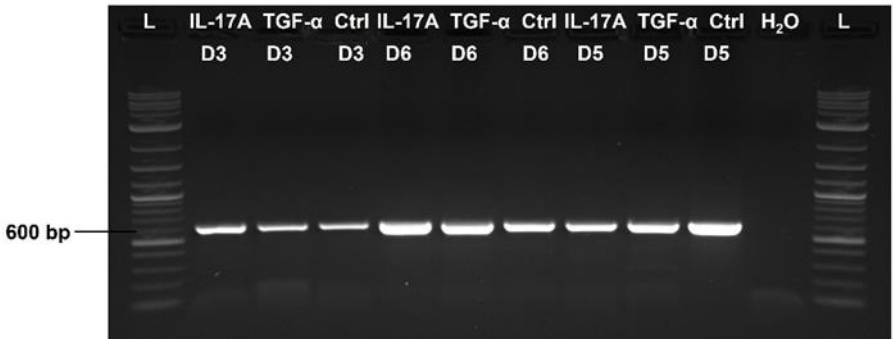

Supplementary figure 27. Preliminary results for further ADM characterisation. RT-PCR for GAPDH expression resulted in a band of 576 bp for day 3 (D3), day 6 (D6) and day 5 (D5) samples isolated from a porcine acinar cell culture.

12 Acknowledgement

Zu allererst möchte ich mich bei meiner Betreuerin Frau Prof. Angelika Schnieke bedanken, dass sie es mir ermöglicht hat, meine Promotion am Lehrstuhl durchzuführen. Ich bedanke mich für die Ermutigung und das Vertrauen in meine Fähigkeiten, welche mir während der Bearbeitung dieses höchst interessanten, wenn auch anspruchsvollen Projektes, entgegengebracht wurden. Vielen Dank für die Wertschätzung und die Motivation zur Teilnahme an zahlreichen Konferenzen, welche mich darin bestärkt haben, meine eigenen Forschungsergebnisse vorzustellen. Zudem danke ich Dr. Alexander Kind für die Korrektur und die nette Zusammenarbeit während der Erstellung meines Review-Artikels.

Ein großer Dank geht an Dr. Tatiana Flisikowska für die Unterstützung bei der Planung und Umsetzung meines PhD-Projektes. Bei dir fand ich immer Zuspruch und ein offenes Ohr, wenn das Cre Driver-Projekt, an welchem sich schon so viele Doktoranden vor mir versucht hatten, mich stellenweise dazu gebracht hat, an mir selbst zu zweifeln. Ich bedanke mich für dein Verständnis sowie für die tollen Gespräche und Treffen und ich hoffe, dass wir weiterhin eine berufliche Zukunft teilen können. Vielen Dank an Dr. Krzysztof Flisikowski für deine lustige Art und deinen Humor, welche so manche Situation aufgelockert haben. Danke, dass du dich um die Tiere gekümmert hast und Proben gesammelt hast und für deine Unterstützung beim ADM-Projekt. Zudem danke ich Dr. Beate Rieblinger und Dr. Konrad Fischer für die konstruktiven Ratschläge. Danke Bea, für die angenehme und strukturierte Zusammenarbeit beim Retransplantations-Projekt.

Ebenso möchte ich mich bei meinen Studentinnen Patricia Zecua, Melissa Thalhammer, Anna Schwaiger und Hannah Thoma bedanken. Ihr wart immer verlässlich und motiviert und ich bedanke mich für euren Beitrag zu meiner Arbeit. Es war sehr angenehm mit euch zu arbeiten und für euren weiteren Weg wünsche ich euch alles Gute.

Ein großer Dank geht an Alexander Carrapeiro für die Hilfsbereitschaft und Unterstützung im Labor sowie für dein offenes Ohr in jeder Situation. Deine lustige und ruhige Art hat die Pankreaszellen-Isolation immer zu einem besonderen Ereignis gemacht. Ich werde dich im Labor vermissen und wünsche dir zeitgleich alles erdenklich Gute für deine Zukunft.

Vielen Dank auch an Peggy Müller-Fliedner, Marlene Stumbaum, Johanna Tebbing, Kristina Mosandl, Lea Radomsky, Sara Robin, Nina Simm und Sulith Christan. Danke, dass ihr mir mit Rat und Tat zur Seite standet und eine so angenehme Arbeitsatmosphäre geschaffen habt. Eure Kompetenz und oft jahrelange Erfahrung wusste ich immer sehr zu schätzen. Zudem wart ihr ein lustiger Haufen, indem man sich einfach nur wohl fühlen konnte. Ein großer Dank gebührt auch Barbara Bauer für die Hilfe bei verwaltungstechnischen Angelegenheiten sowie ihre Zuverlässigkeit und herrlich lustige Art.

Darüber hinaus danke ich meinen aktuellen und ehemaligen Mitstreitern Alessandro Grodziecki, Guanglin Niu, Agnieszka Bak, Laura Beltran Sangüesa, Ying Wang, Thomas

Winogrodzki, Liang Wei, David Preisinger, Theresa Göring, Bernhard Klinger und Andrea Fischer für die tolle Zeit. Mit euch war es immer lustig und ich habe euch stets für eure ruhige und gelassene Art bewundert. Hierbei geht ein besonderer Dank an Alessandro, Lin und Aga, welche ich sehr in mein Herz geschlossen habe. Lieben Dank für euer offenes Ohr, die netten Abende, das herzliche Lachen und die schonungslos ehrlichen Gespräche. Ich wünsche euch für eure Zukunft alles erdenklich Gute und ich hoffe, dass wir irgendwann noch einmal zusammenfinden werden.

Von ganzem Herzen möchte ich meiner Familie danken. Danke Jola und Toni, dass ihr immer an mich geglaubt habt und ich immer auf eure Unterstützung zählen konnte. Ohne euch wäre ich sicher nicht so weit gekommen und ihr habt viel geleistet um uns eine sorgenfreie akademische Laufbahn zu ermöglichen. Danke Daniel, dass du mich auf den Studiengang „Molekulare Biotechnologie“ gebracht hast.
Unendlicher Dank geht an meinen besten Freund und Ehemann Mateusz für die unendliche Unterstützung. Du bist mein Fels und mein Weggefährte und dein nie abreißender Optimismus hat mich sicher durch diese Zeit gebracht und mir immer ein Lachen auf meine Lippen gezaubert. Du musstest viel Rücksicht nehmen in den letzten Monaten und hast dich immer rührend um unsere Kinder gekümmert, wofür ich dir sehr dankbar bin.
Zum Schluss danke ich meinen Kindern, dass ihr mir eine Welt gezeigt habt, die mir vielleicht für immer verborgen geblieben wäre. Ihr seid für mich das größte Wunder dieser Zeit und ich wünsche mir, dass die Sonne immer für euch scheint.